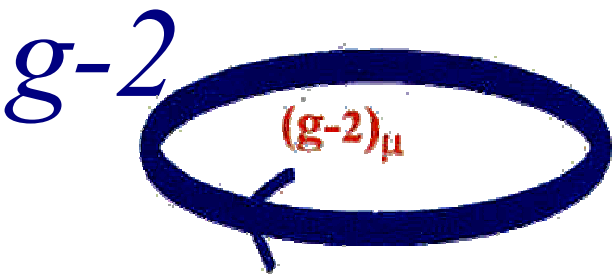

Brookhaven National Laboratory

Brookhaven Science Associates

Upton, New York 11973

Muon g-2 Note No. 423

Title: **G2off Based 2000 ω_α Analysis of g-2**

Author: **Cenap S. Özben**

Date: **October 21, 2002**

G2off Based 2000 w_a Analysis of g-2

Cenap S. Özben
Brookhaven National Laboratory, Department of Physics,
Upton, NY 11973-5000

October 21, 2002

1 Introduction

The third muon injection run of g-2 took place in the winter 2000. That year the muon g-2 experiment ran with positive muons. We collected ≈3.9 billion positrons (t>50μs, and E>2GeV) in 1292 successful runs after filtering the fills with undesired running conditions for ω_a analysis like unstable T0 signal, quad off, no quad readout, fills with laser and quad sparks (1/100000) (Figure 1). That year, using the sweeper magnet allowed us to reduce flashlet level to ≈30 ppm level in the average and switching off the quads at every once out of certain number of fills provided us a very good flashlet systematic study [1].

On the other hand, running with high hardware thresholds and late gate on times in the first side of the ring and CBO frequency close to $2\omega_a$ were the main difficulties of the 2000 ω_a analysis.

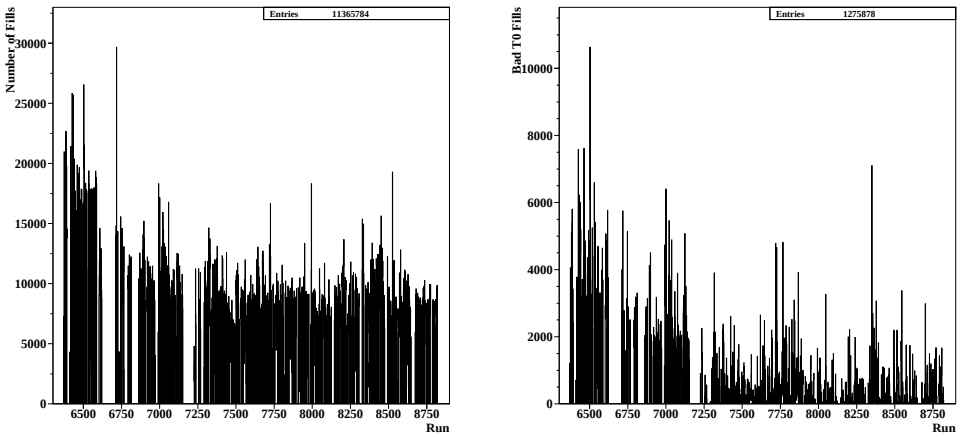

Figure 1 : Number of fills cut during the run. 11% due to unstable T0, 2% due to quad sparks (including the no quad readout), 5% due to quad-off (for flashlet systematics) and 2% due to laser runs were cut over all the fills at all energies.

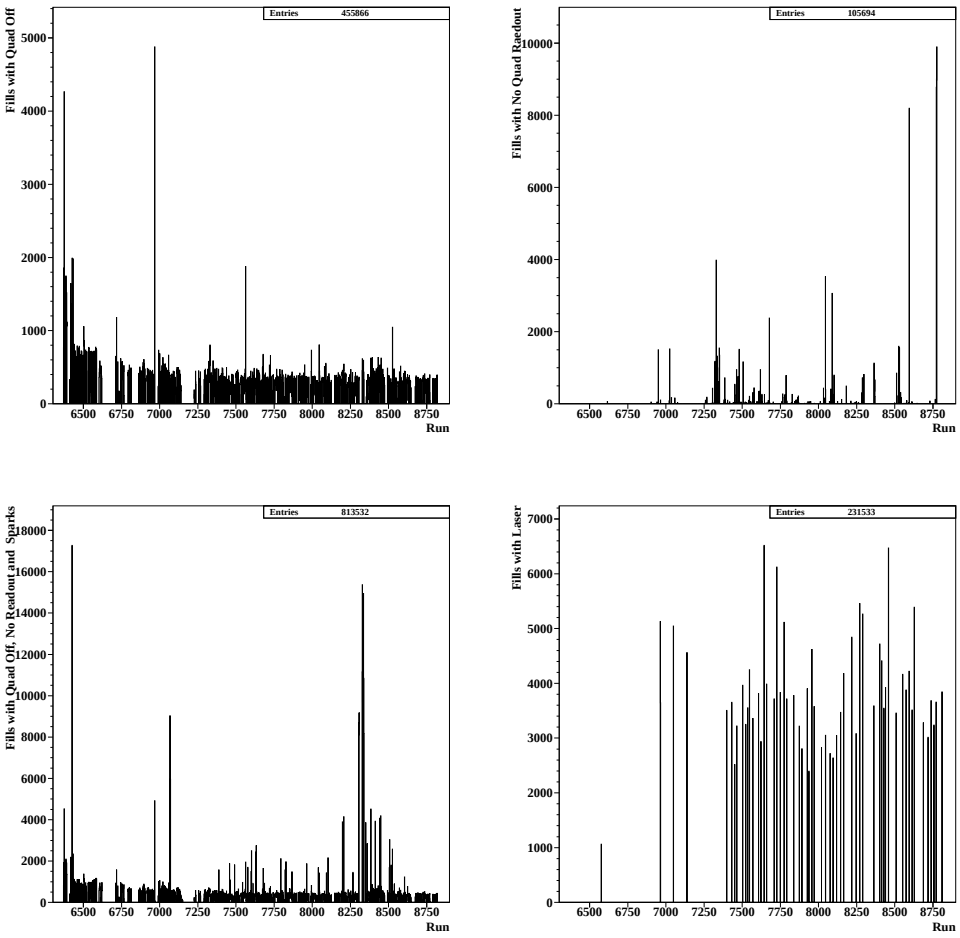

Figure 1 : Continued.

2 Run Selection

In this analysis, selected 1292 runs [2] between 6369 and 8822 were used for comparison purposes between the ω_a analyzers.

A very simple run selection algorithm was also performed by myself based on the fit parameter stability of the individual runs. In this study the detectors were combined and fitted to the traditional five parameter function and the parameter stability between the runs was monitored. It turned out to be this method was very sensitive to determine the runs with, e.g., early quad off, laser, LED runs, fiber harp runs and runs with gate on time changes, etc.. These kind of problematic runs were confirmed with the log book summary of the 2000 [3]. Figure 2 shows this study with selected runs so outliers are already taken out. This is shown to give a feeling of parameter stability during the run. When we look at the parameter distribution of the individual runs only R was a perfect

Gaussian before the run selection. Figure 3 shows these distributions with 1292 accepted runs.

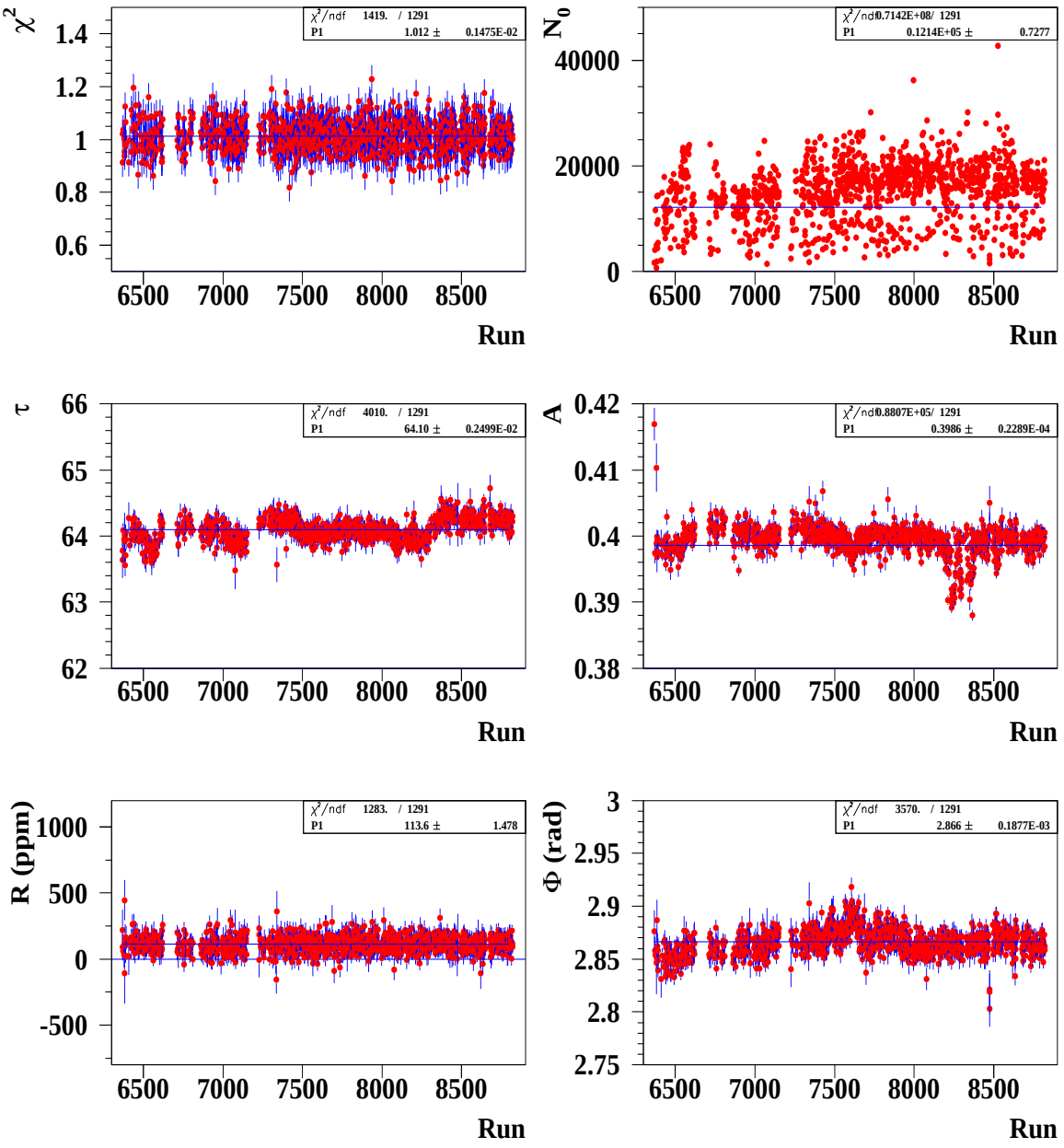

Figure 2 : Parameter stability of the selected runs. The fits were performed between 45μs-150μs . One may notice the lifetime ($\tau\gamma$) gradually gets closer to the nominal value of 64.407μs after the run ≈8200 where the radial field was changed around this point and muon losses were dramatically reduced [4].

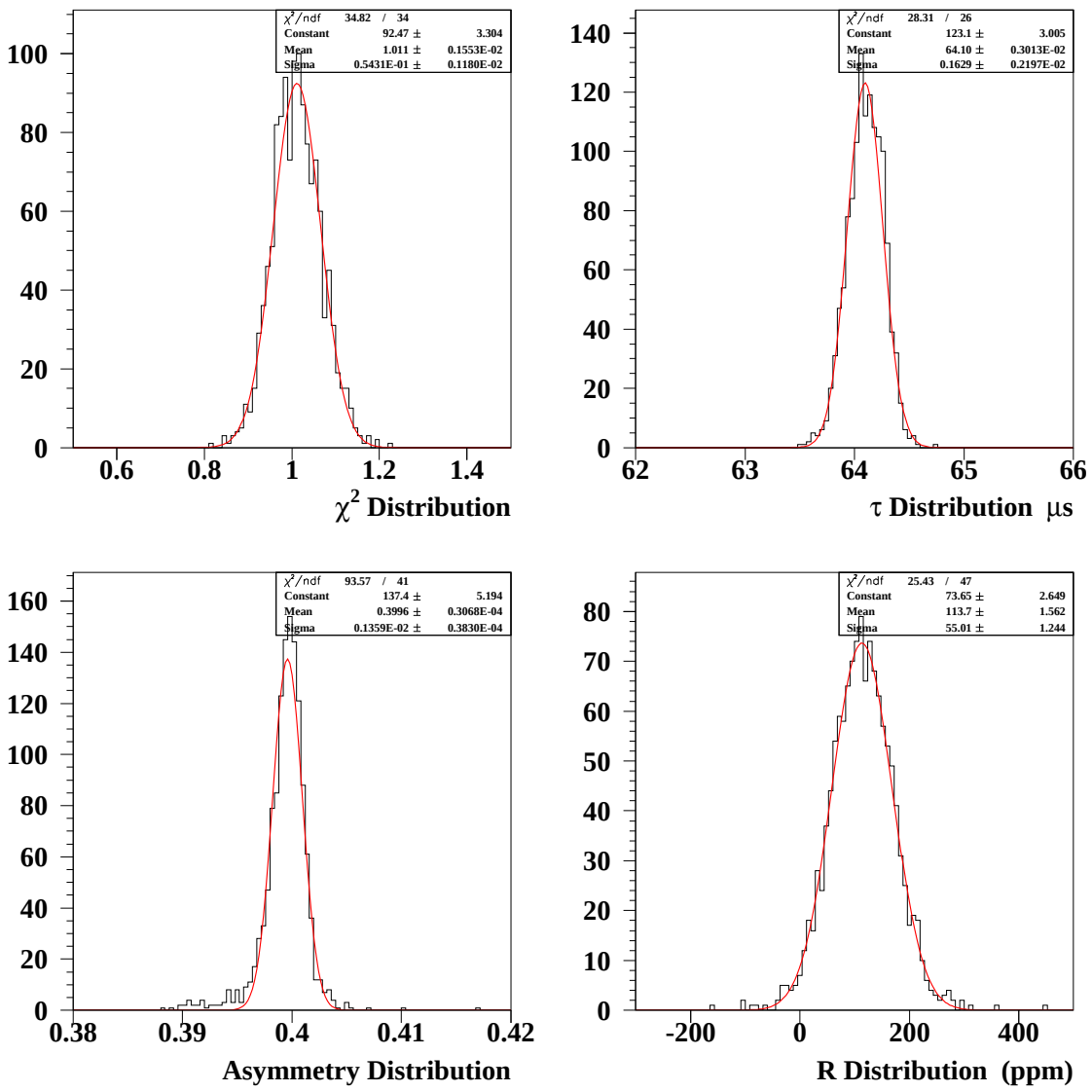

Figure 3 : Parameter distributions of the selected runs.

To assure the quality of the run selection, some parameters were monitored during the run such as fit pedestals and gate on times. The hardware thresholds were also monitored for the missing part correction on the constructed doubles for pileup subtraction which is going to be mentioned later. Figure 4 shows the fit pedestal versus run number for two detectors; detector four ("noisy" side of the ring) and detector 18 ("quiet" side of the ring). These pedestals are the average pedestals determined after 45 μs.

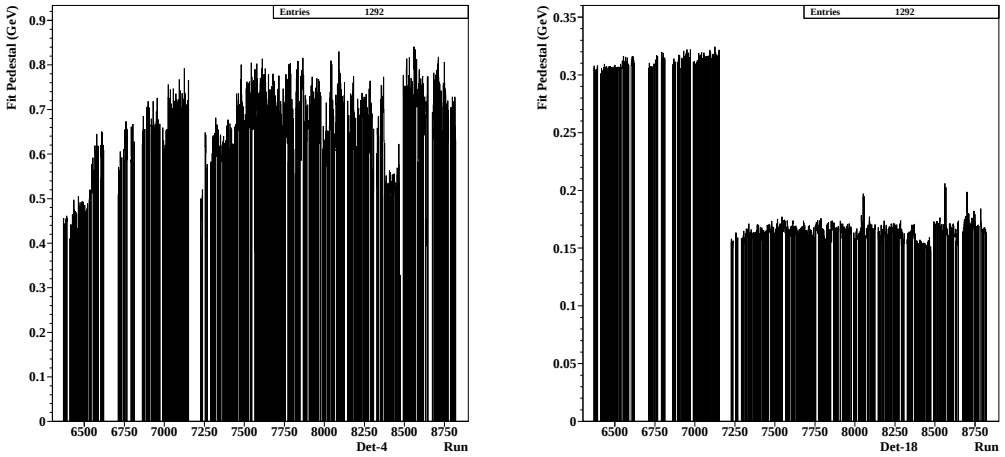

Figure 4 : Stability of the pedestal during 2000 run for detectors 4 and 18.

Four runs were excluded from the original run list (1296 runs) due to some extra requirements (related with the energy calibration determination quality) specific to my analysis and/or problems on some runs during histogram filling which didn't exist before. This year I preferred to use run by run based energy calibration coefficients since there are some intervals that difficult to describe the changes with ordinary functions unless one uses large number of steps or linear functions.

Figure 5 shows the change in the endpoint coefficient for detectors 3 and 17 during the run as an example. We observed continuous decrease in the calibration coefficients for all the detectors which could be due to the aging of the tubes.

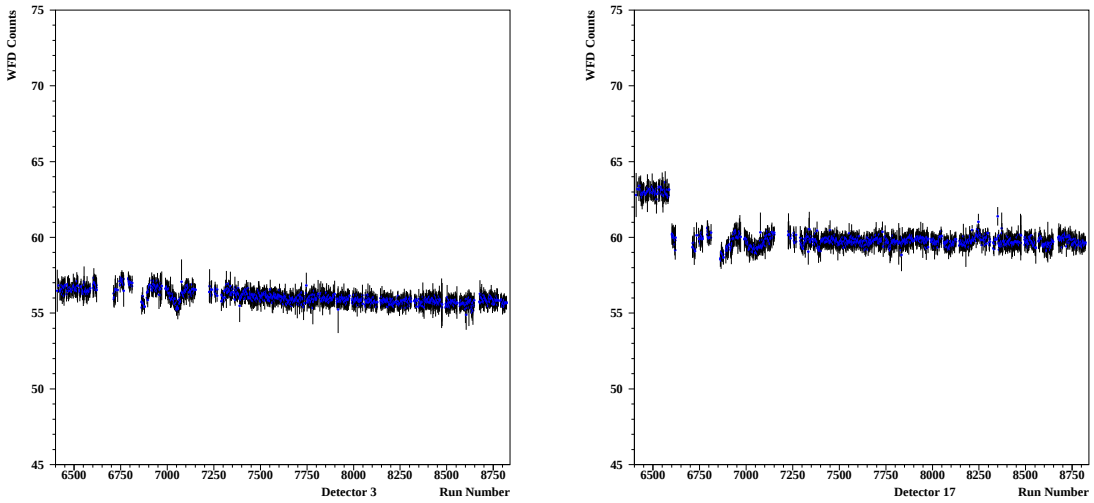

Figure 5 : The change in the endpoint coefficient of detector 3 and 17 during the data taking.

3 Fast Rotation Analysis

The fast rotation analysis of this year was performed with the modified Fourier analysis [5]. The data binned with 5ns and the positrons selected $E > 1.5$ GeV to increase the statistics. Detectors 18-24 were used where common earliest gate on time of 8 μs was present. Figure 6a shows the time spectrum with 5ns bin width where both g-2 and cyclotron oscillations are visible, **6b** shows it after divided to 5 parameter function F(t) and **6c** shows the 1μs interval. Figure 7 shows the muon momentum distribution for 2000.

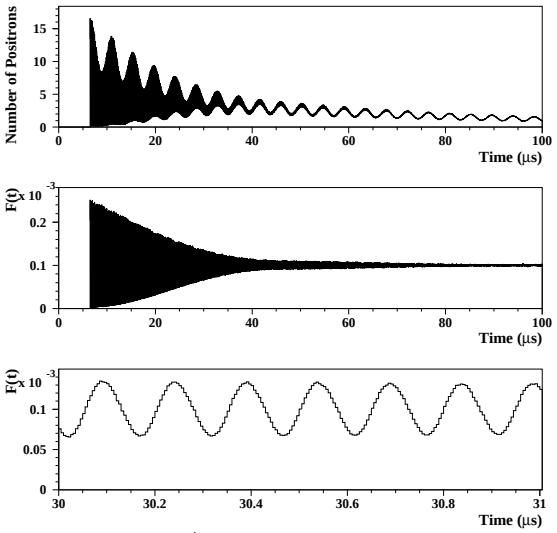

Figure 6 : a) The time spectrum with 5ns bin width, b-c) Time spectrum with 5 ns bin with is divided to 5 parameter function.

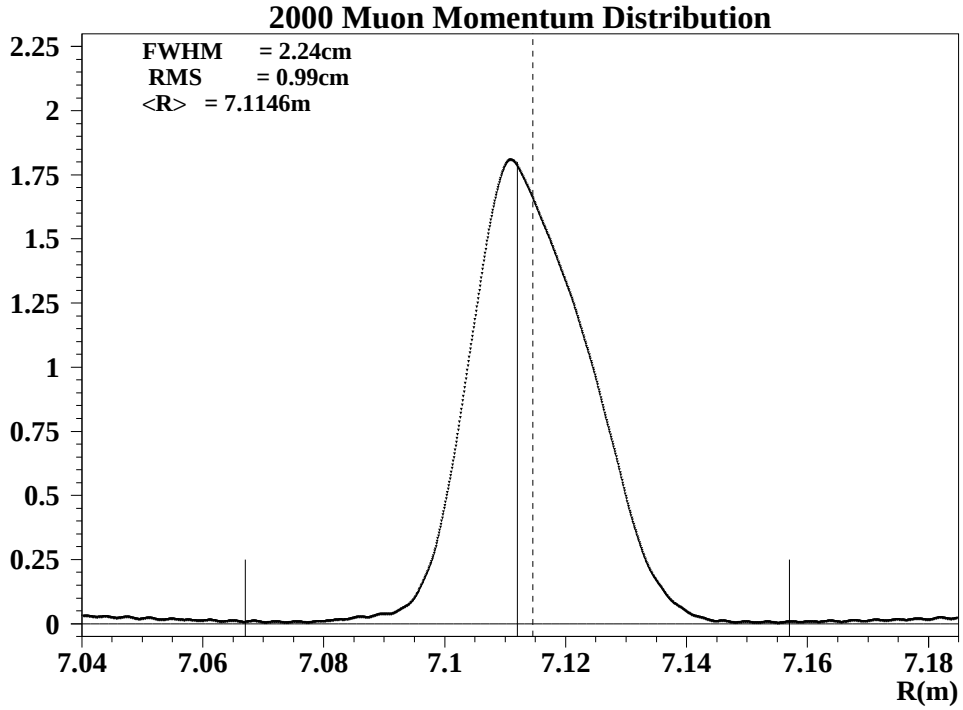

Figure 7 : The momentum distribution of the muons. Two small vertical lines show the boundary of the vacuum chamber, continuous vertical line is 7.112 m and dashed vertical line is the average center of 7.1146 m. This distribution is in good agreement with the fast rotation analysis performed by Boston University using modified CERN method [6].

The envelope of the fast rotation was determined from the Fourier integration of the data (after divided by the 5 parameter function, Figure 6b). This was originally Francis's idea which we had already used in 1999 fast rotation analysis. The basic of this idea was to make Fourier integration for each fast rotation period and determine the amplitude as follows ;

$$a = \frac{2}{n} \sum_{n_i=1}^{n} F(t) \times cos(\frac{2\pi n_i}{30})$$

$$b = \frac{2}{n} \sum_{n_i=1}^{n} F(t) \times sin(\frac{2\pi n_i}{30})$$

$$A = \sqrt{a^2 + b^2}$$

where F(t) stands for time spectrum (after divided by the 5 parameter function), n is number of bins to combine for full fast rotation cycle (n=30 for 5ns bin). We also applied this method to determine the CBO envelope from the data this year. Figure 8 shows the envelope of the fast rotation.

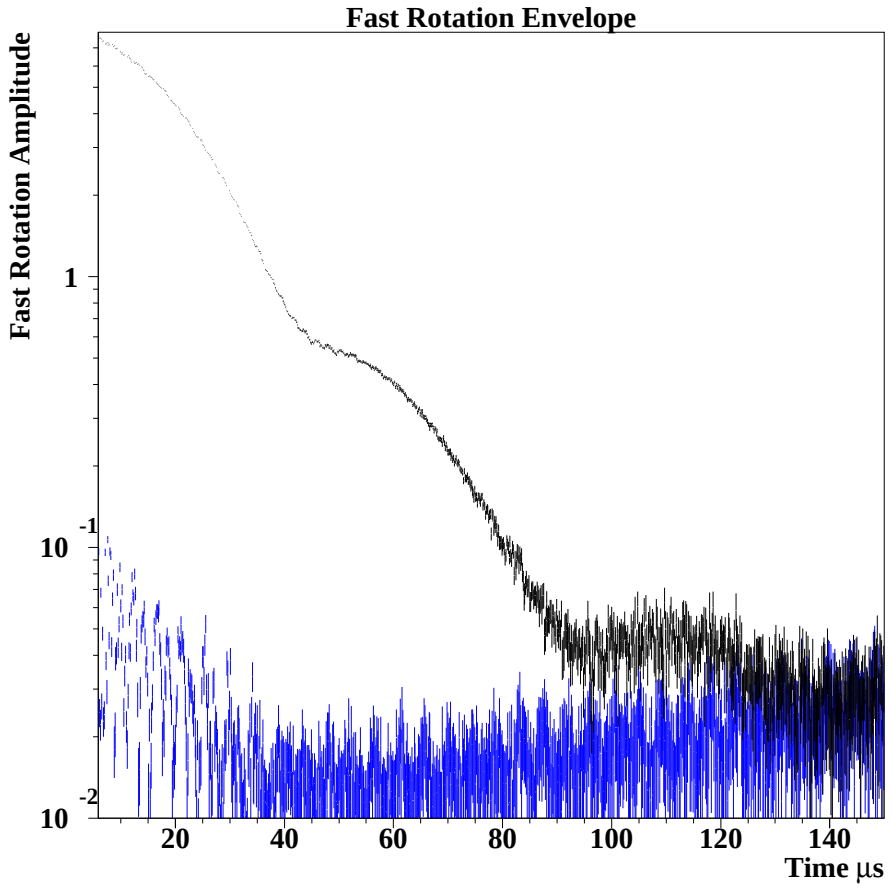

Figure 8 : Fast rotation envelope. After randomization (blue) and before fill randomization (black). The pileup is not subtracted for this study therefore the effect of PU can be seen at early times.

4 The Analysis Strategy

In this report we have tried to address many main issues like CBO, pileup and muon losses on all aspects and many less important issues such as higher harmonics of CBO, CBO frequency change due to decreasing voltage of the quads, etc..

The half ring effect [7] is one of the most important issue known as the whole collaboration took most of the time of this year's analysis. Related to that, the functional form and the envelope of the CBO, g-2 phase and asymmetry modulations due to CBO, gain effect, pileup subtraction efficiency, muon losses and residual slow effects and the uncertainty on the functional forms are also studied in this report.

Even though we ran with higher intensity on 2000 which made the pileup 1.7 times more compared to 1999 run (at 32 μs), we have a reasonable approach to the pileup issue from 1999 analysis [8]. The effect of the high hardware thresholds on pileup reconstruction was already studied in detail [9]. Briefly the hardware thresholds were determined for the individual runs for each detectors and missing parts on constructed pileup doubles (D) were corrected on a run by run basis.

For the first time this year an independent method provided us the muon losses shape [4]. The muon losses provided before and after radial field changes properly added and used in the fits to the data.

5 Coherent Betatron Oscillations (CBO)

The existence of CBO first observed in 1999 data on the residuals. That time we knew that it was an effect that changes the acceptance and modifies the ideal functional form as follows:

$$F(t) \ = F_{id}(t) \ \Big[\ 1 + A_{cbo} \ e^{-0.5 \ (t/\tau_{cbo})^2} \ cos\{2\pi f_{cbo} t + \phi_{cbo}\} \Big] \qquad (1)$$

where F_{id} is the well known ideal 5 parameter function, A_{cbo} is the amplitude, τ_{cbo} is the decay lifetime, f_{cbo} is the frequency and ϕ_{cbo} is the phase of the CBO.

This year because of factor 4.5 larger statistics, the functional form was modified to achieve acceptable parameter stability and fit χ^2 as well as to get rid of the half ring effect [7]. The CBO frequency was determined directly from the fits as 465.70 kHz with 10 Hz accuracy from the minimization of the χ^2 when all the detectors overall the runs were added together.

The first starting point for better CBO analysis was to determine the CBO envelope better.

5.1 CBO Envelope

Coherent betatron oscillations influences the energy spectrum of the detected positrons. Therefore detected positron energy (so the g-2 asymmetry) is modulated by the CBO oscillations. g-2 phase also changes due to the relative beam position caused by CBO and the result of it is time of flight of the positrons changes. Recently a new effect called FBI (Francis, Bill, Ioannis) was also discovered related with the CBO oscillations. This effect is an additional effect to the time of flight caused by the acceptance difference between in/out direction of the decay positron pileup on the average radial postion.

Since CBO modulates the energy spectrum of the detected positrons, one can observe the envelope (the decay of CBO) by looking at the energy spectrum. This study was originally proposed by Yannis. We look at 2001 data for this purpose since the beat frequency between ω_a and ω_{cbo} was much smaller compared to 2000. This makes the observation of the beating process possible before the statistical power vanishes. The recipe of the method is as follows; The energy spectra of the positrons fall into 1 μs window (shown in blue regions in Figure 9) on the top of g-2 cycles were constructed.

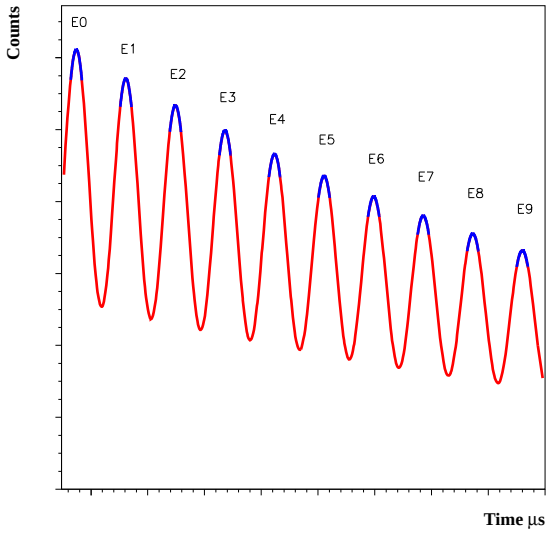

Figure 9 : Schematic representation of the determination of CBO envelope. $E0, .., E_n$ represents the energy spectra at the blue regions.

Then $\frac{E_0}{E_1}$, $\frac{E_0}{E_2}$, $\frac{E_0}{E_3}$, ..., $\frac{E_0}{E_n}$ ratios were fitted, in their linear region, and the slopes of these fits were plotted vs time for each detector. The CBO modulation causes the slope changes. Since there are CBO phase differences between the detectors they were aligned so that their phases match and finally they were summed to get the final envelope (Figure 10). This process was done with 2 different n values separately. The envelopes obtained were fitted to the following function as expected :

$$F_{env}(t) = P_1 \ sin(2\pi t/P_2 + P_3) \ e^{-t/P_4} \tag{2}$$

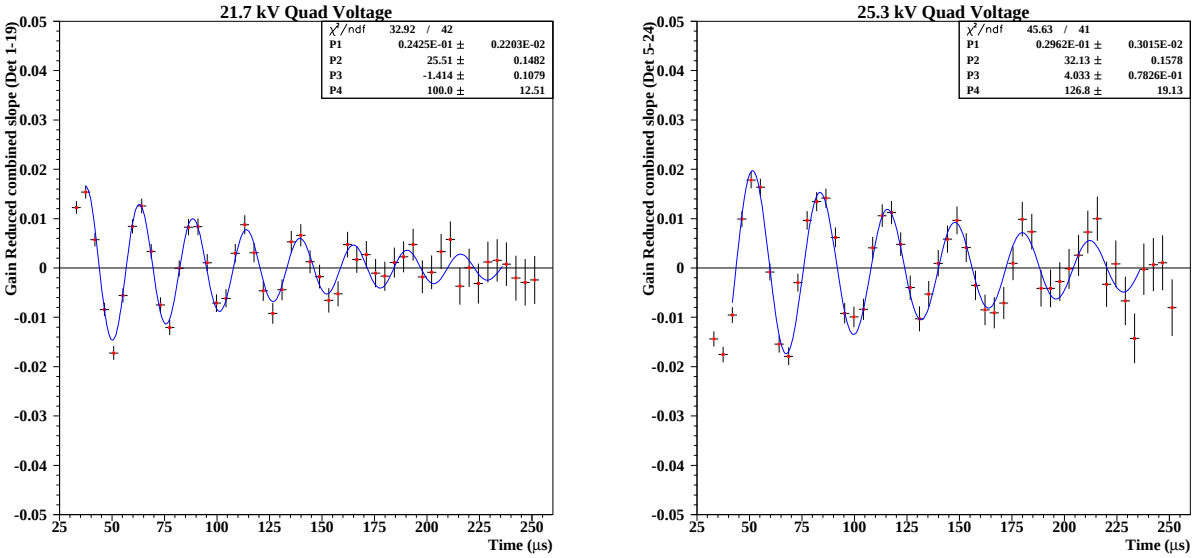

Figure 10 : CBO envelope from 2001 run for two different n values.

This study already showed that CBO envelope is close to exponential rather than a Gaussian. Dima Grigoryev's also did a study long before myself to determine the CBO envelope. Basically he fit the time spectrum to a 8 parameter function and determined all the parameters. Then he fixed all the parameters except the CBO amplitude and fit the data again for each two g-2 cycles which allowed him to get A_{cbo} versus time behavior. That envelope was not a Gaussian either and it was close to an exponential with a small periodical deviations. Today we understood these small deviations were mostly due to the mixture of different n values. This is going to be studied detail in the next chapters. The CBO lifetime for two n values were statistically consistent (100 ± 12 μs and 127 ± 19 μs) for different n-values.

There is also another method to determine CBO envelope very similar to the one we have done for the fast rotation analysis. In 2000 analysis, the functional form is more complicated than 1999 form. For that reason to determine the CBO envelope, in the presence of the g-2 amplitude and the phase modulations due to CBO and the satellites created by the main CBO, the functional form so called "physics form" was used below :

$$F(t) = N_0 e^{-t/\tau_\mu} \left[1 + A' cos(2\pi f_a t + \phi')\right] \left(1 + A_{cbo} e^{-t/\tau_{cbo}} cos(2\pi f_{cbo} t + \phi_{cbo}) \right) \quad (3)$$

where

$$A' = A\{1 + A_1 e^{-t/\tau_{cbo}} cos(2\pi f_{cbo} t + \phi_1)\} \quad (4)$$

$$\phi' = \phi_a + A_2 e^{-t/\tau_{cbo}} cos(2\pi f_{cbo} t + \phi_2) \quad (5)$$

Here A_1 is the amplitude and ϕ_1 is the phase of g-2 asymmetry modulation due to CBO. A_2 is the amplitude and ϕ_2 is the phase of g-2 phase modulation due to CBO.

Each detector were fitted to the physics function above with an exponential CBO lifetime after 45 μs including muon losses and other residual slow effects. After that the CBO residuals (free from all other effects such as g-2 asymmetry and phase modulations) were constructed by determining the ratio of DATA to FIT where A_{cbo} was set to zero in the fit function. Then the residuals from each detector were phase shifted to align the CBO. Later on, the Fourier integration was applied to these phase shifted CBO residuals. Figure 11 shows the residuals and the envelope. The bumpy structure comes from the combination of the different CBO frequencies.

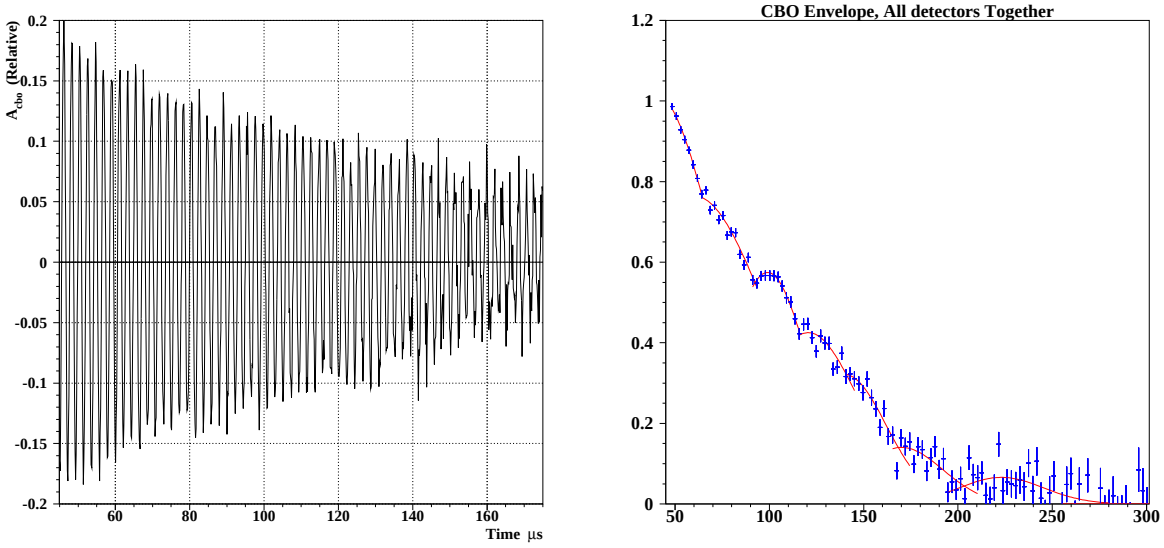

Figure 11 : **a-)** Enhanced CBO residuals, **b-)** 2000 CBO envelope.

The regions were fitted separately to the Gaussian functions ($a_1\ exp[-\frac{1}{2}\ ((t - a_2)/a_3)^2]$) and the parameters are given in Table 1. This work was also repeated for different energy bands ($E < 2.6GeV$, $E > 2.6GeV$) and the envelopes were observed to be the same statistically. Detectors 7,8 and 9 which have the most of the CBO in the ring have no statistically different envelope either.

Table 1: CBO Envelope

Time (μs)	a1	a2	a3
45.0-64.6	1.014	40.	32.3
64.6-92.4	0.765	60.	39.7
92.4-116.5	0.574	99.	22.0
116.5-140.8	0.425	120.6	27.0
140.8-168.4	0.321	140.0	22.0
168.4-203.4	0.140	170.0	22.0
203.4-285.0	0.066	223.0	22.0

6 Some Systematic Studies

In this section we will study some systematics due to some known effects.

6.1 Systematic Due to Early to Late n Value Change

Quad voltages increases to its nominal operation voltage after scraping with ≈ 5 μs lifetime and also decays with another RC time constant of ≈ 200 ms. The time dependence of the CBO frequency was first observed when the CBO frequency left free in the fits. That was the first signature of the droop in the quad voltages to cause n value to change. n value is directly related with the CBO frequency. After that we also saw a large acceptance change at early times ($t < 30\mu$s) by looking at the residuals. The pattern on all detectors were the same and it was due to large increase on n value after scraping which changes the acceptance couple of percent level. To observe the n value (CBO freq.) during the scraping from the Fourier analysis is difficult since the scraping time was only 16 μs. For that reason Ofer's fiber harp measurements played a key role on the determination of CBO frequency during scraping. He gives a value of f_{cbo}=416 kHz for 7 kHz scraping. Our main CBO frequency determined from the fits after 50 μs and found to be 465.7 kHz $\pm$ 10 Hz. This CBO frequency represents the average since the fit interval extends from 50 to 500 μs under the influence of n value change due to quad voltage droop and also the combination of different n-values.

We can calculate the observed n value due to the quad voltage drop after 50 μs as follows :

$$\langle n(t)\rangle = \frac{n_0}{\Delta T}\int_{50}^{500} dt \;\; e^{(t-50)/(2\;\;10^5)} \tag{6}$$

where n_0 is the n value at 50 μs and $\Delta T = 450\ \mu s$. The result of this integration is $\langle n(t)\rangle = 0.99887 n_0$. This result can be interpreted as two different ways. One ; determined CBO frequency is 0.5 kHz smaller than the reality, two; if there is a frequency change due to the RC time constant of the quads that should be no more than 0.5 kHz with in 500 μs. When the frequency left free in the fits, it showed much more (2 kHz within 200 μs) change which can not be explain from the drop itself. Also Ralf's recipe [10] (CBO phase also changes due to this drop) was applied but no considerable improvement observed in the fits. For that reason, to simplify the fitting function, fixing the frequency to the fit value and leaving the phase free with no correction and determining the systematic error due to this droop was preferred in this analysis.

In a Monte Carlo, a time spectrum with 8 parameters (5PAR + CBO) was produced with a variable CBO frequency drop. The size of the input parameters were taken from the real data when all detectors were together. An exponential droop was started from 50 μs (f_{cbo}(50)=465.7 kHz) ended at 500 μs (f_{cbo}(450)=460.7 kHz). This was ten times larger than the expected change. This MC data was first fitted with fixed 465.7 kHz CBO

frequency (Figure 12a). Then just like we do it in the fits to the real data, the effective CBO frequency was determined at 50 μs and fixed all the time (Figure 12b).

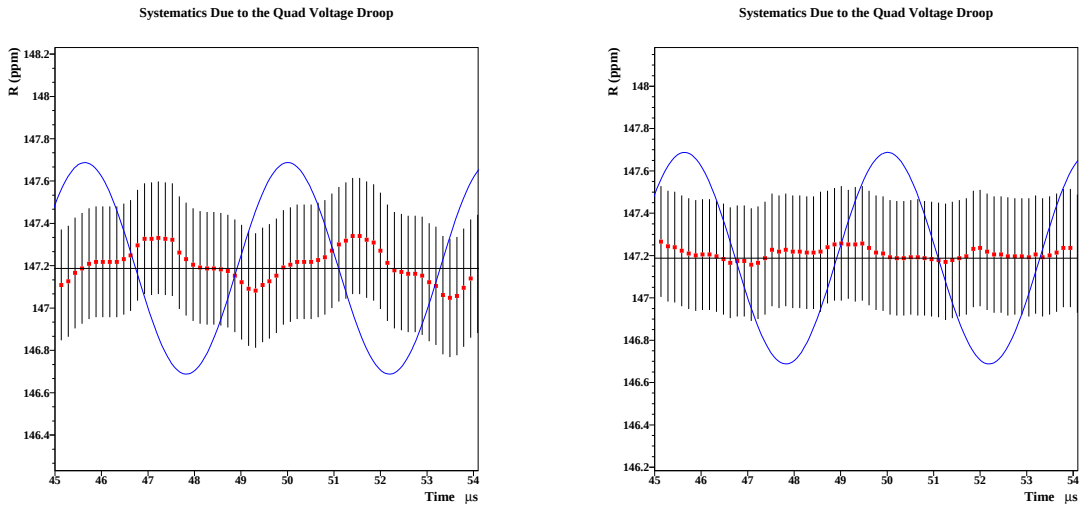

Figure 12 : The systematic due to early to late n value change as a result of quad voltage droop. a) When the frequency is fixed to 465.7 kHz, b) when the effective frequency was determined from the fit at 50μ and fixed all the time to this value. The effect introduced here is 10 times larger than what it should be.

The fit determined the CBO frequency as 463.95 kHz in this case. This value is as expected between 465.7 kHz and 460.7 kHz since the fit represents the average value between 50 μs and 500 μs. The maximum changes on R between 50 μs and 54 μs were 0.29 ppm for the first and 0.11 ppm for the second cases. There is a factor 20 (factor 10 for the real data reduction and factor two for the half of the maximum oscillation amplitude) for the normalization which makes the systematic for the first case 0.015 ppm and the second case **0.01 ppm**. In the second case since the oscillation was not symmetric around the real value, to be conservative, only factor ten reduction was applied. The second case is the one we will use as the systematic on this number for 1999 functional form since this is the exact procedure followed in the data analysis (determining the frequency from the data at the first point of the fit interval and fixing it all the time).

When the functional form gets more complicated, this systematic also changes since more effects including the CBO frequency take place in the fit function. For instance for 1999 form including the g-2 asymmetry modulation this systematic is **0.02 ppm** and for the complete physics form it is **0.05 ppm**.

6.2 Systematic Due to Combination of Different n Values

Our data contains mainly three running regions with different n values even though the regions one and two are not steady constant (Figure 13). These CBO frequencies are 474.09 kHz (6.7%), 468.04 kHz (11.9%) and 465.59 kHz (81.4%). A set of simulated data with the combination of these CBO frequencies and with their statistical weights were

produced and combined. For the envelope standard exponential with 120 μs decay lifetime were used. This data was fitted with 1999, 1999 including g-2 and the complete physics forms respectively. Since the CBO frequencies of these three regions are slightly different from each other, the CBO related parameters were heavily influenced by this effect.

Figure 13 shows the CBO frequency versus run number in 2000 data. This plot is constructed from the individual runs adding the large CBO detectors 7,8 and 9 together. Basically each run was first fitted to the five parameter function and the parameters were determined. Then the data for each detector group was fitted again but this time the CBO with fixed 120 μs lifetime and with free frequency was included in to the fitting function. In this fit all g-2 related parameters were fixed to the previously determined values (from 5 parameter fit) and the fit parameter f_{cbo} was obtained. This method provides much better accuracy on frequency compared to the one determined from the Fourier analysis.

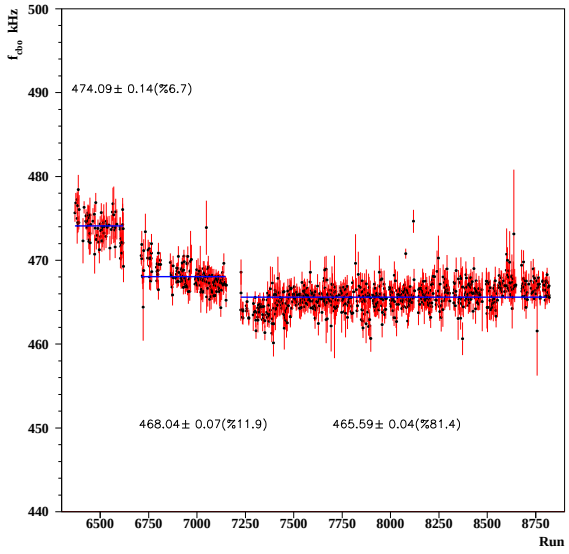

Figure 13 : The CBO frequency vs run.

In the simulations some of the deviations from the input value were statistical. To have a realistic χ^2 all three data set were produced with different random number seeds. In order to remove the contribution from the statistical fluctuations, another set of data with the same random seeds used for generating the previous case (the mixture) but this time a single CBO frequency of (average of three, 465.7kHz) was the input of the MC. Therefore the R results show the differences between these cases. Figure 14 shows the fit result of the MC (mixture of the CBO frequencies) with an exponential lifetime. The first observation is the error propagation on CBO related parameters are not Gaussian and parameter stability in A_{cbo} is unacceptable.

The residual of this simulated data (mixture of the CBO frequencies) is determined from the ratio of the data to the five parameter fitting function. This method is the cleanest way to extract the CBO residual information and free from art effects of the satellites ($\omega_a \pm \omega_{cbo}$). Figure 15 shows this residual.

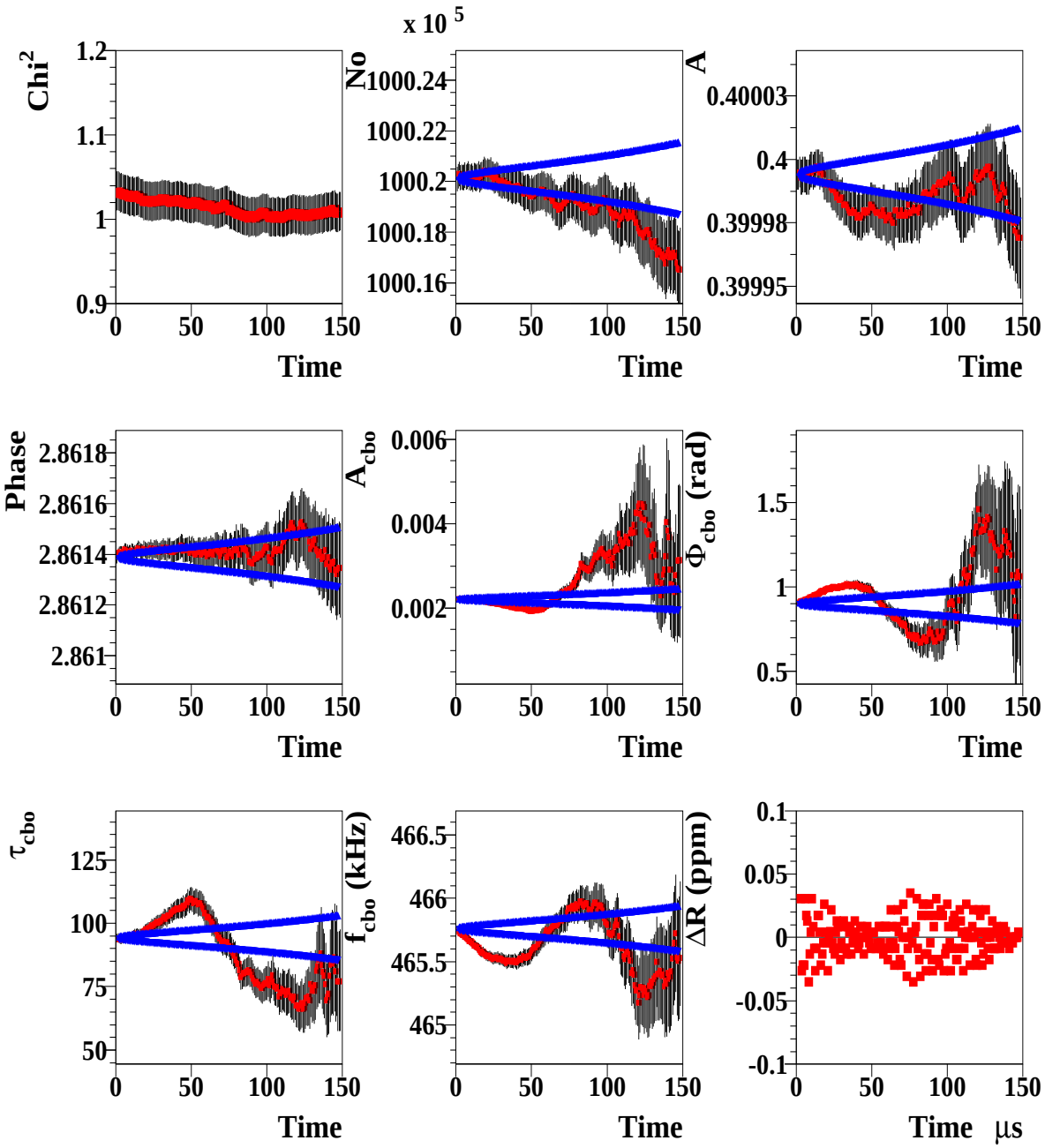

Figure 14 : The change on the fit parameters due to having different CBO frequencies in the data. The weights are realistic and determined from the data. 474.09±0.14 kHz (6.7%), 468.04±0.07 kHz(11.9%) and 465.59±0.04 kHz(81.4%). Dramatic changes in the CBO related parameters are seen. R differs by 0.013 ppm from the original value @50 μs.

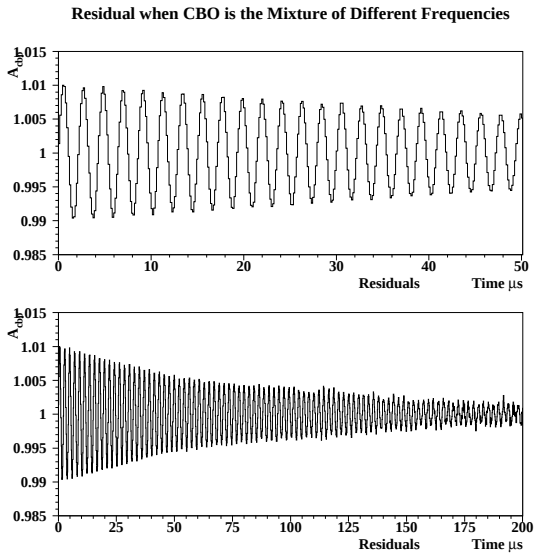

Figure 15 : The residual (Data/5Par) of simulated data. This data is the mixture of different CBO frequencies.

The CBO envelope (Figure 16) was determined from the recipe described in the fast rotation analysis. This method was also used in 1999 fast rotation analysis before and it is very powerful to obtain the envelope of the decaying effects with long lifetime from the data. The striking point here is when the data is mixture of different CBO frequencies, the envelope deviates dramatically from the original exponential one. In the next step, this experimentally determined envelope was put into the fits instead of the exponential envelope. Figure 17 shows the parameter stability with the experimentally determined envelope.

The bad behavior on A_{cbo} was recovered to a high degree. Changes in the CBO frequency and the phase are still exist. The shape of the envelope does not influence the R value. This is the same conclusion one could get from the data itself also. At 50 μs R is different by only 0.013 ppm.

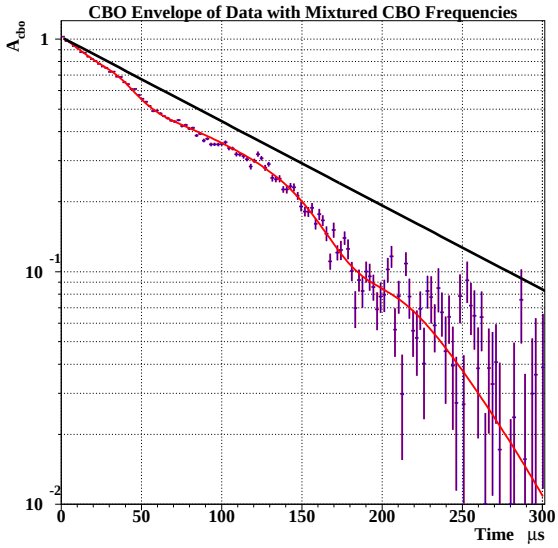

Figure 16 : The CBO envelope of the simulated data produced from the mixture of three different CBO frequencies. The black solid line shows the exponential envelope where those three individual cases were generated in the MC. As a result of these three frequency combination, the final CBO envelope is wavy.

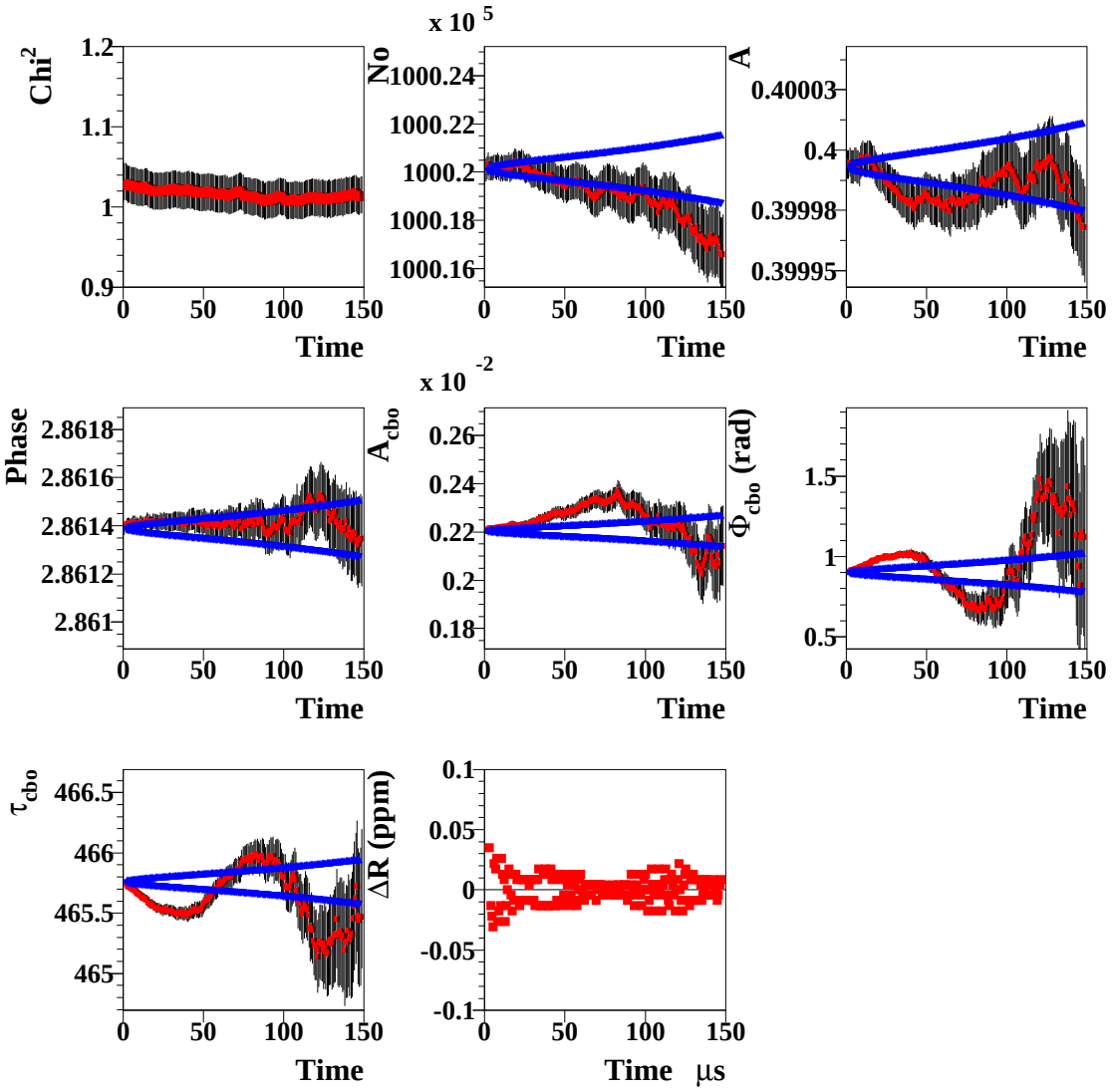

Figure 17 : The parameter stability with experimentally determined CBO envelope. Here, the bad stability of A_{cbo} is highly recovered.

Since the CBO phase and frequency are highly correlated, as it was preferred to fix the CBO frequency to the value obtained from the fits and let the phase float in the real data analysis. Figure 18 shows the parameter stability in this case. This shows that stability on phase gets much better!

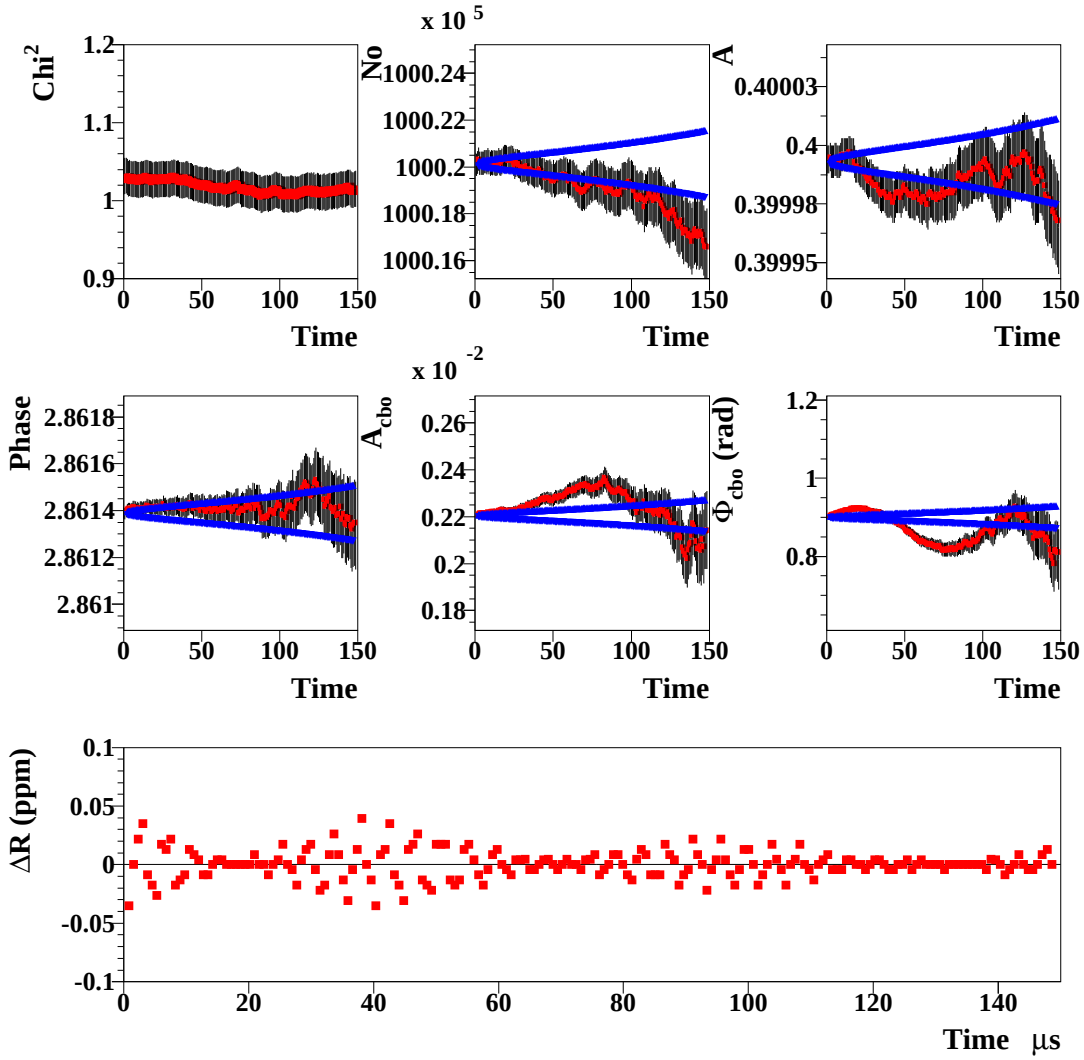

Figure 18 : The parameter stability when f_{cbo} was fixed. Stability on CBO phase is much better now. In this case R differs by 0.03 ppm from the original input value. The error propagation on CBO related parameters is closer to a Gaussian now.

In the data, we don't see any phase pulling (after 50μs). The reason for that may be there are smooth transitions between the regions (Figure 13). Therefore in the reality the systematic effect is actually smaller. However we will **0.03 ppm** systematic due to this effect for 1999 functional form.

This effect also studied for the other functional forms. The influence on 1999 functional form with g-2 asymmetry modulation is shown in Figure 19. The stability of g-2 asymmetry modulation parameters are considered as fair. In this study experimentally determined envelope was used and f_{cbo} was fixed to the value determined from the first point of the fit.

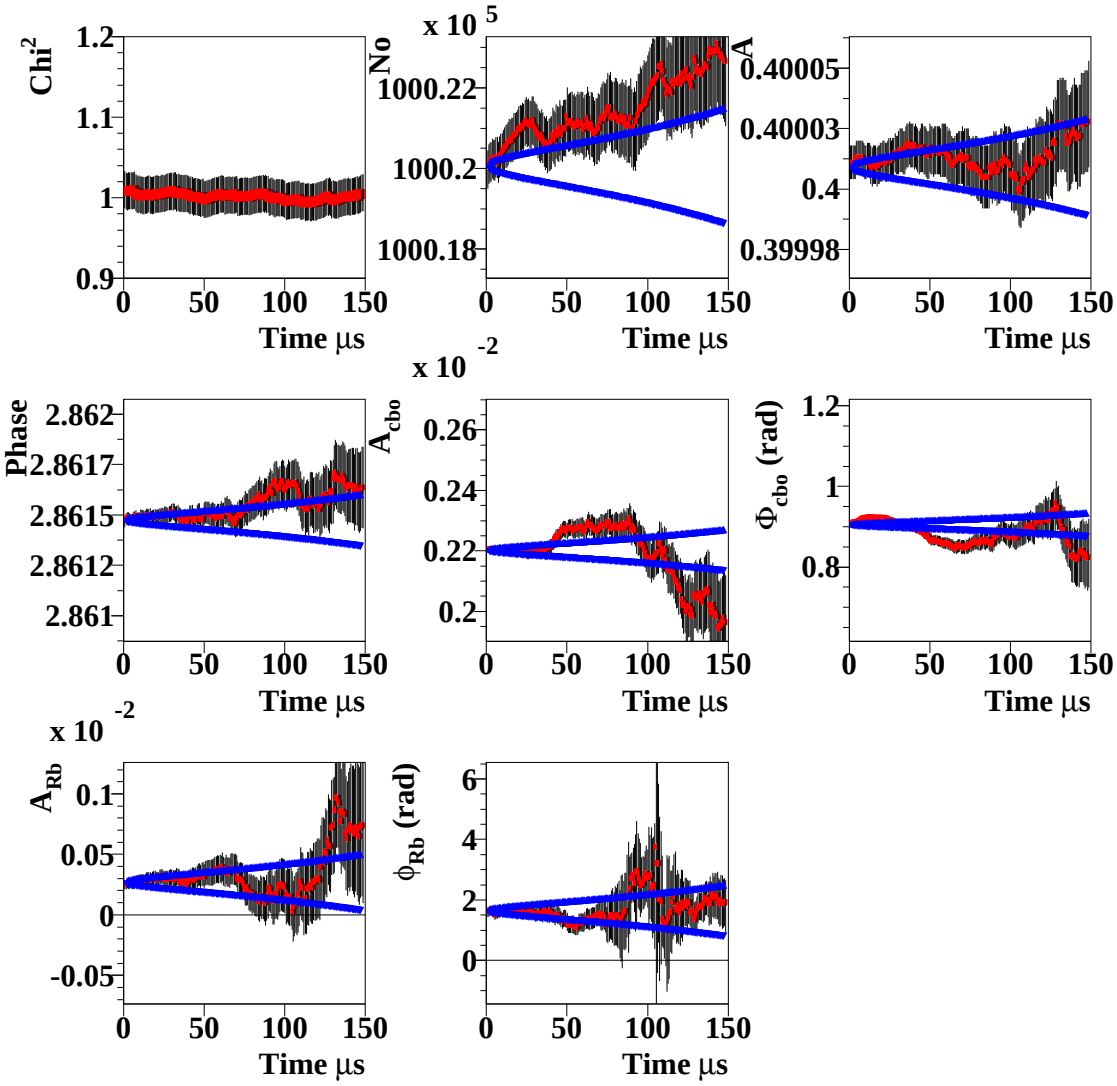

Figure 19 : The parameter stability when 1999 form with g-2 asymmetry modulation was used. Experimentally determined envelope was used and f_{cbo} was determined at 0 μs and fixed all the time.

When the complete physics form was used the things did not changed much except the asymmetry. Somehow the stability on asymmetry got worse (Figure 20). Figure 21 shows the ΔR vs time for this functional form.

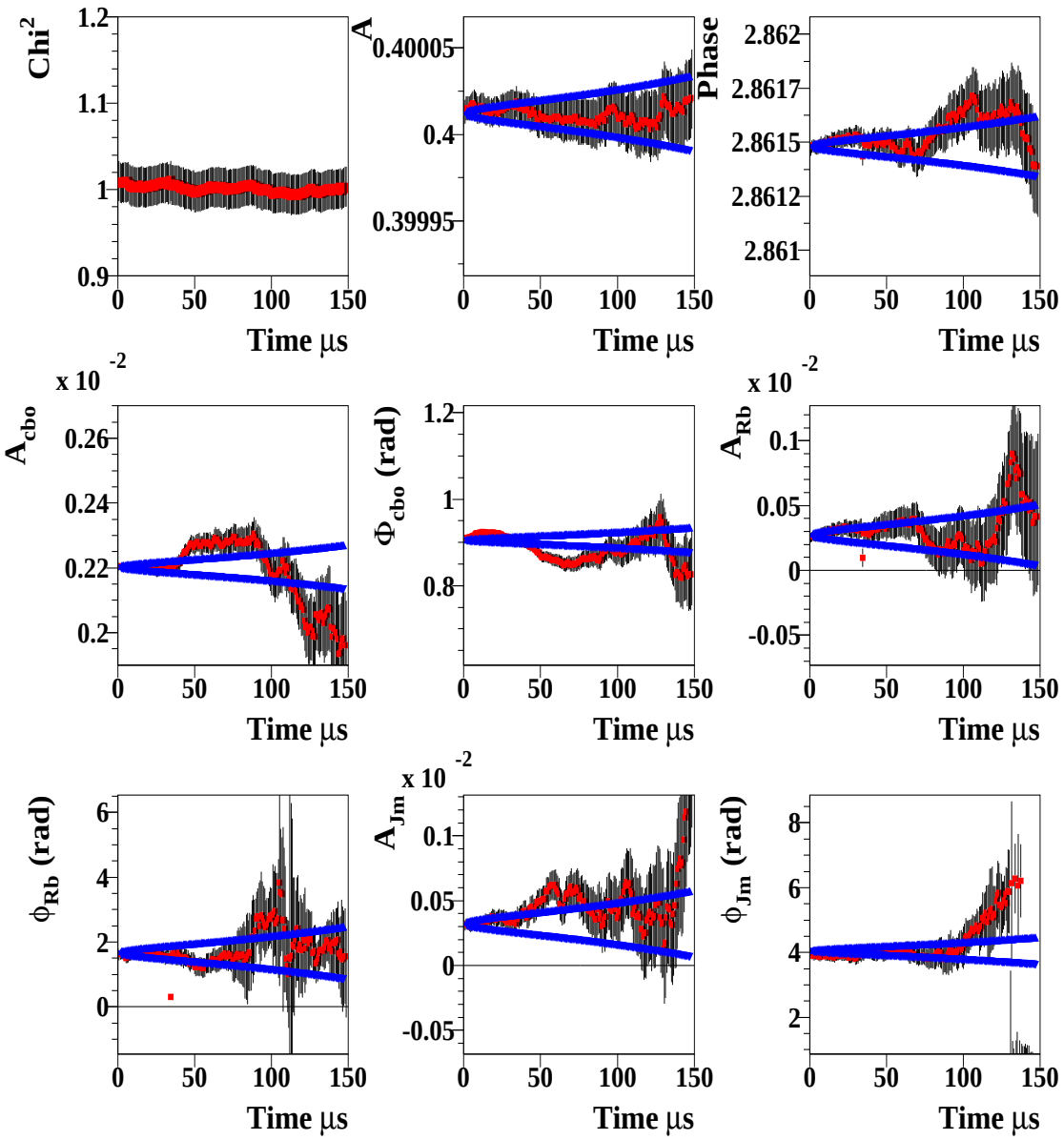

Figure 20 : The parameter stability when the complete functional form was used. Experimentally determined envelope was used and f_{cbo} was determined at 0 μs and fixed all the time. The asymmetry instability is question here!

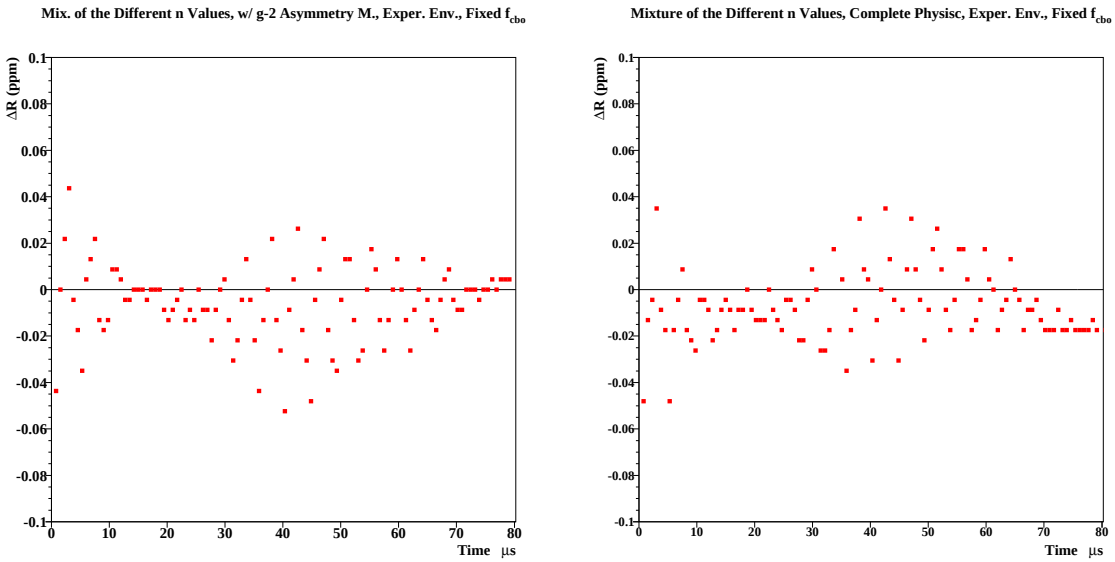

Figure 21 : R vs time stability on 1999 including g-2 asymmetry modulation and the complete physics forms. The phase pulling is **0.04** ppm for the 1999 functional form including the g-2 asymmetry modulation and for the complete physics form.

As a result of this study we assigned following systematics based on the deviations at 50 μs where larger than the size of the phase pullings and conservative.

1999 Functional Form	:	0.03 ppm
1999 Functional form including the g-2 asymmetry modulation	:	0.04 ppm
The complete Physics Form	:	0.04 ppm

6.2.1 CBO Reduction Factor

In the previous subsection, the influence of the mixture of different CBO frequencies in the data was studied. The question of the CBO reduction factor is directly related with the mixture of the CBO frequencies. If the functional form is exact and there is only one n value present, the CBO should be removed completely from the data. However, we know that we have the combination of the different n values in the data and there are also uncertainties due to the envelope. These issues are going to be show up in the reduction factor of CBO.

The reduction factor of the CBO could be determined practically by comparing the strength of the CBO in the data and in the residuals. The red color in Figure 22 shows the strength of the CBO in the simulated data under the mixture of the n value conditions. After the MC data was fitted with the ideal function including the CBO with an exponential envelope and single frequency, the function was subtracted from the data to obtain the residual. The blue color in Figure 22 shows the Fourier analysis of this residual. Comparison of the areas of two peaks with the background correction, one gets factor ≈ 8 in reduction. Using the experimentally determined envelope makes this reduction factor little more than two times better. This also agrees very well with the reduction factor

we have in the real data which is 20. Therefore we can conclude that most of the left over CBO comes from the fact that there is a mixture of CBO frequencies in the data. The maximum systematic error assigned for this study is normalized to 20 to obtain CBO reduction factor related systematic error as **0.05ppm**. The CBO amplitude is one of the most uncorrelated parameter in all type of functional forms we use in this analysis. For that reason there is no need to repeat this study for other functional forms.

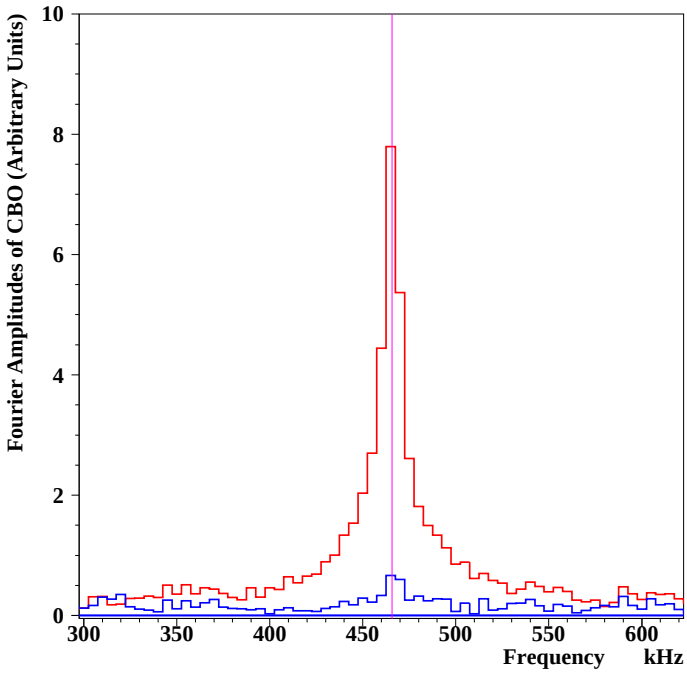

Figure 22 : The CBO residual of the simulated data is Fourier analyzed after 45 μs (red line). The blue color shows the Fourier analysis of the residuals after fit to the function of $F(t) = A_1\ e^{-t/A_2}\ cos(2\pi f_{cbo} t + \phi)$ known as CBO functional form.

6.3 Systematics due to Fourier Outcome

Looking at the Fourier analysis of the residuals one can identify the remnants of the fitting procedure. In this section we concentrated on the conventional Fourier analysis (not normalized χ) to assign conservative systematics. The size of the effects on the regular Fourier spectrum are much more enhanced (due to more weight at early times) than the normalized χ method [11]. On the other hand normalized χ spectrum is very useful to determine the contribution to χ^2 from the effects seen in the Fourier Spectrum. Figures 23-25 show the enhanced conventional Fourier spectra on both first, second halves and all detectors.

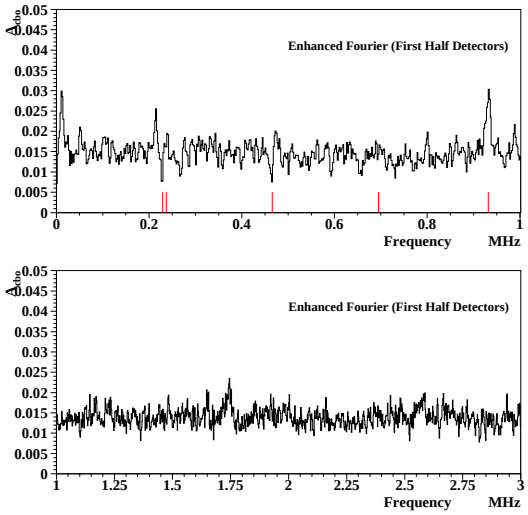

Figure 23 : Fourier, the first half.

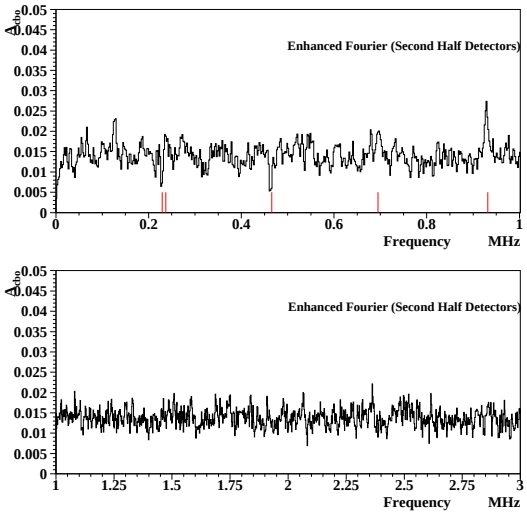

Figure 24 : Fourier , the second half.

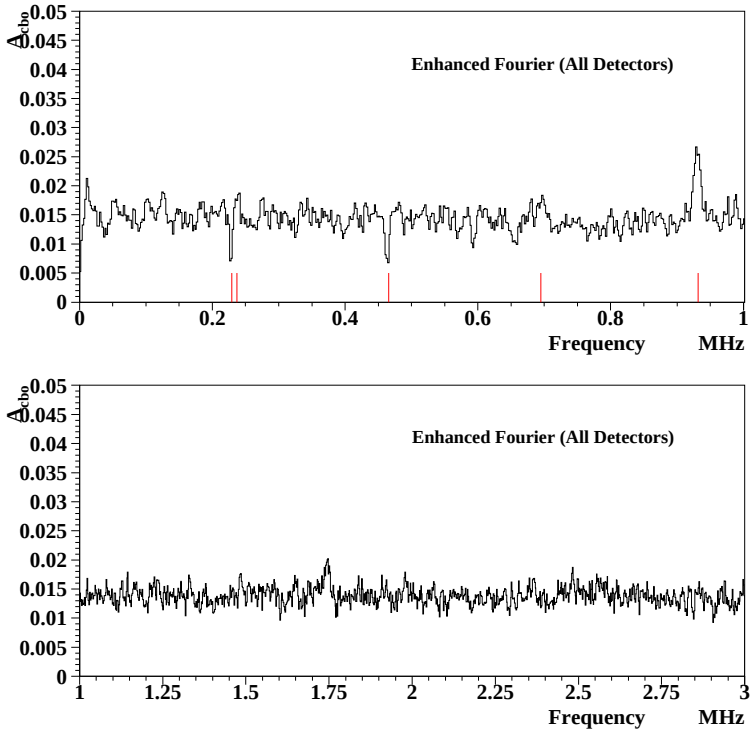

Figure 25 : Enhanced Fourier spectrum of all detectors.

The enhanced Fourier spectrum was constructed by adding the Fourier spectra from the residuals of the individual detectors. In the reality, since the phase of those effects change between zero to 2π around the ring, when the detectors are added they cancel to a high order (such as CBO $\approx$ 4 times). For that reason in the average we can say that these affects we see in the enhanced Fourier spectrum are 4 times greater than what we have in the data.

6.3.1 Systematics Due to Double CBO and Vertical Waist

Double horizontal betatron oscillation ($2f_c(1-\sqrt{1-n})$ and Vertical waist ($2f_c(1-2\sqrt{n}$, where f_c is cyclotron frequency) peaks are visible in the enhanced Fourier spectrum of the data after 45 μs. Both of these effects have relatively short lifetime and small. Lack of the knowledge of the functional form of those effects (especially Vertical Waist), instead of fitting them, determining the systematics due to those small effects on ω_a was preferred. In a Monte Carlo program 20 billion positrons were generated with DCBO and Vertical Waist. The strength of these affect were estimated from the relative amplitude compared to the main CBO peak in the Fourier spectrum of the real data.

The relative ratios of the DCBO and VW peaks to the main CBO peak at zero time (with decay time correction) were determined to be 28 and 21 consecutively. The lifetimes of those effects were assigned from Jim Miller's detailed study [12] but frequencies are taken from what Fourier analysis were provided.

Two sets of MC data were produced with DCBO and VW and they were fitted with 1999, 1999 with g-2 asymmetry modulation and the complete physics forms without DCBO. Table 2 gives the results for 1999 functional form.

Table 2: Decay of the systematics shifts on R from DCBO and VW.

Time(μs)	Double CBO		Vertical Waist	
	$\Delta\chi^2$	ΔR(ppm)	$\Delta\chi^2$	ΔR(ppm)
0-15	0.022	0.027	0.036	0.015
15-30	0.011	0.020	0.010	0.006
30-45	0.006	0.016	0.003	0.005

The table proves that short lived VW has more influence to χ^2 at very early times than DCBO. Figure 26 shows the R difference between the fits with and without the Vertical Waist of the simulated data. g-2 phase pulling is higher at early times and quickly decays with VW lifetime of 27 μs. Similar plot for DCBO don't show this kind of regular g-2 phase pulling rather it shows irregular fluctuations.

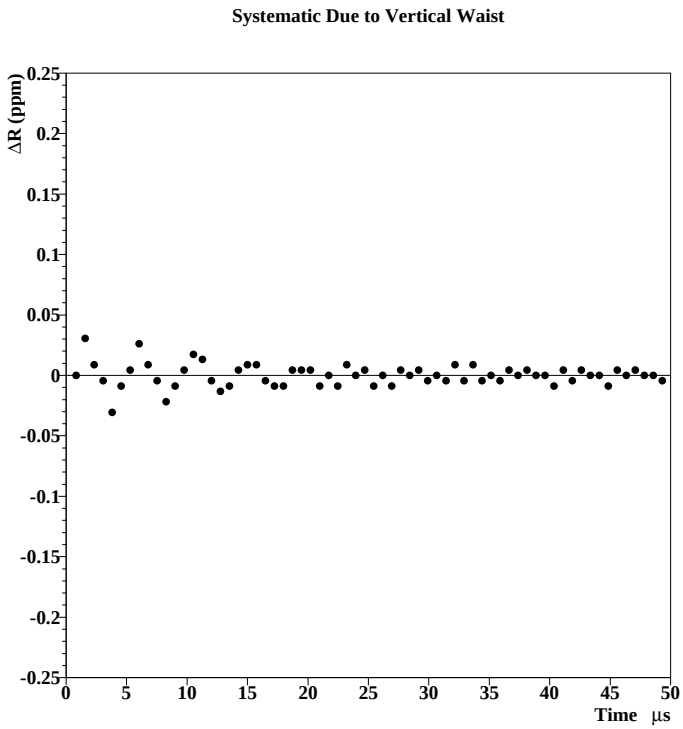

Figure 26 : The systematic error due to the Vertical Waits.

The initial phases of DCBO and VW are important. The initial phase of these effects were changed from 0 to 2π and corresponding R value change at 50 μs was studied. Table 3 shows the maximum effect of the initial phase on R value for different functional forms.

Table 3: Systematics table of DCBO and Vertical Waist for different functional forms. These numbers were obtained at 49.9 μs.

Functional Form	ΔR(ppm) Double CBO	ΔR(ppm) Vertical Waist
1999 Type	0.009	0.004
Incl. g-2 asymmetry mod.	0.004	0.004
The complete physics form	0.004	0.000

From this table we will assign a conservative **0.01 ppm** systematic error due to double CBO and vertical waist same for all the functional forms.

6.4 Systematics Due to Energy Scale Changes

Observed positron energy spectrum on the peak of the g-2 cycle and on the trough of the g-2 cycle are different as the nature of g-2 experiment (Figure 27). For that reason, to look at the gain stability from average energies, one needs to look at the average energy versus time for g-2 cycles unless one wants to correct for g-2.

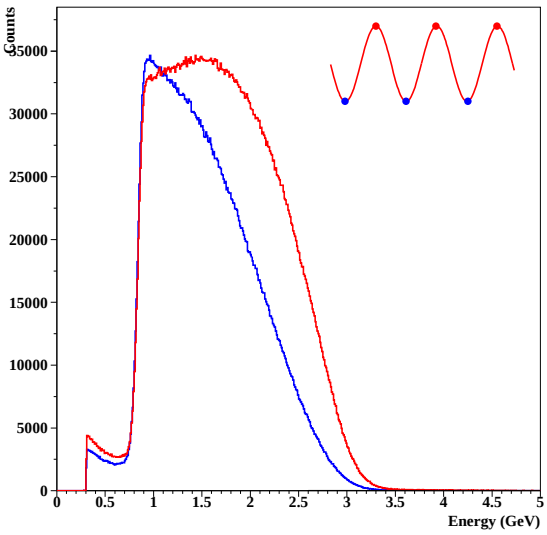

Figure 27 : g-2 energy spectrum at the peak and the through of g-2 cycles.

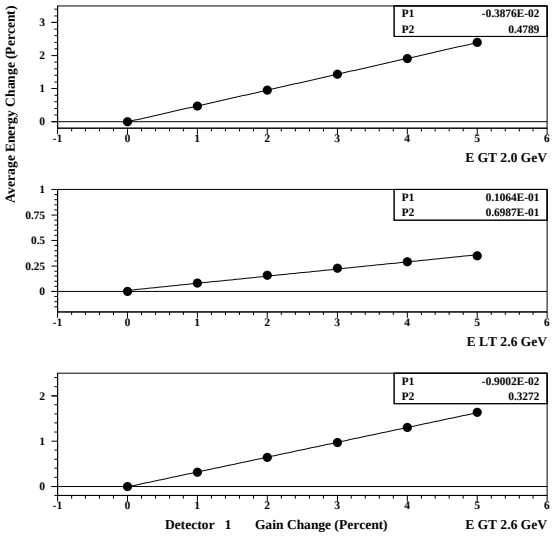

Figure 28 : The relations between the gain changes (ΔG) and the average energy ($\Delta\overline{E}$) for different energy regions.

The average energy of the detected positrons also changes with the gain effects. The relation between the average energy and the gain was determined from Axel's method. The energy of the positrons scaled (increased) by 1%, 2%,.. and 5% and corresponding average energy change determined. This relation is very linear. Figure 28 shows this relation for 2 GeV, 2-2.6 GeV and above 2.6 GeV for detector one as an example. The relations between gain and $\overline{E}$ is shown in the following Table 4 for different energy regions. Sensitivity to the gain change from average energies increases with the energy (compare E>2.0 and E>2.6GeV).

Table 4: The relations between average energies and the gain changes.

Det.	$\frac{\Delta\overline{E}}{\Delta G}$ (E>2)	$\frac{\Delta\overline{E}}{\Delta G}$ (2<E<2.6)	$\frac{\Delta\overline{E}}{\Delta G}$ (E>2.6)
1	0.480	0.070	0.327
3	0.462	0.062	0.325
4	0.471	0.060	0.339
5	0.465	0.064	0.329
6	0.451	0.063	0.323
7	0.417	0.047	0.305
8	0.400	0.041	0.301
9	0.419	0.044	0.311
10	0.453	0.072	0.314
11	0.456	0.077	0.312
12	0.448	0.068	0.308
13	0.470	0.070	0.321
14	0.464	0.063	0.324
15	0.471	0.064	0.323
16	0.448	0.065	0.322
17	0.472	0.067	0.339
18	0.453	0.067	0.316
19	0.460	0.065	0.314
21	0.461	0.068	0.320
22	0.448	0.065	0.326
23	0.455	0.065	0.315
24	0.446	0.067	0.312

The gain effects usually take place at early times after the detectors gated on and they last sometimes tens of μ seconds. We also know that $\overline{E}(t)$ should also be influenced by CBO since CBO oscillations modulates the positron energy spectrum (remember this is

how we obtained the CBO envelope from 2001 run). Pileup leftover/over-subtraction is also another one to influence the $\overline{E}(t)$ which mostly important at early times where the pileup is dominated. Besides to those facts gain behavior may not be the same in each quadrant of the calorimeters. To check this, one can look at the discriminator pattern in the ntuple structure. The discriminator bit pattern allowed us to distinguish the events in the quadrants and described as :

$$k = jbit[disc(j), n] \tag{7}$$

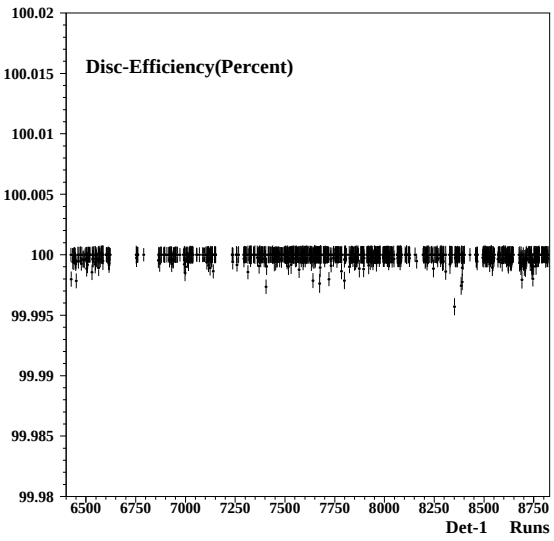

Figure 29 : Disc. efficiency versus run.

where n represents the quadrant (n=7 quadrant 1, n=1 quadrant 2, n=2 quadrant 3, n=3 quadrant 4), j is the pulse. k is the logic value and equals to 1 if there is any hit in the related quadrant. The efficiency of the discriminator bit is very good and Figure 29 shows it versus run number.

After determining the discriminator bit efficiency (Fig. 29) is very close to 100%, one can check the average energy versus time for each segments. At early part of the ring the discriminator bit thresholds were set rather high in order to prevent continuous digitization.

Figure 30 shows the average energies for up and down segments in addition to for the events occurs in both up and down segments at the same time and for without any discriminator bit selection. When the pedestal was high at early times and above the discriminator bit threshold, disc. pattern selects more low energy pulses at early times than the late times. Hence one can see an increasing trend in average energies which is non real (Figure 30 detector 6). When the hardware threshold was high enough (lets say 2.6 GeV) this behavior was gone. The effect of the pileup can be seen clearly from all the segments in detector 19 where there is no issue about discriminator bit thresholds since this detector is located in the quiet side of the ring.

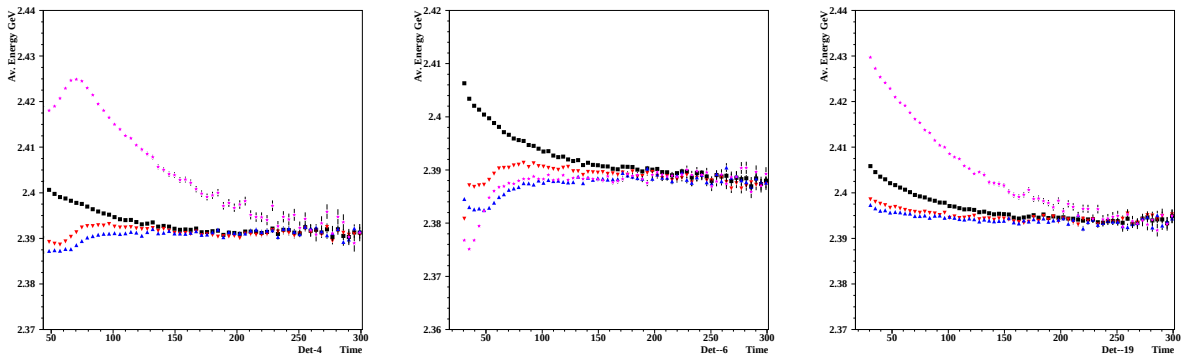

Figure 30 : Average energy versus time for no discriminator bit selection (black), for top segments (red), for bottom segments (blue), for the events occurs in both halves (purple). There is no pileup subtraction applied for this study.

The gain behavior may change also during the run. For instance we know that detector 7 was not bad all the time. In the presence of all, the energy scale correction based on the average energy is not preferable unless one makes sure that average energy represents only the pure gain changes. Therefore energy scale correction was not applied this year. Not to mention, also from 1999 analysis we had the experience of worse χ^2 and parameter instability problems after the energy scale corrections. On the other hand it is still a good tool to check the pileup subtraction qualitatively. Figure 31 shows $\overline{E}(t)$ of all detectors. In the insets the average energies are translated to the gain changes by taking into account the conversion coefficients shown in Table 4.

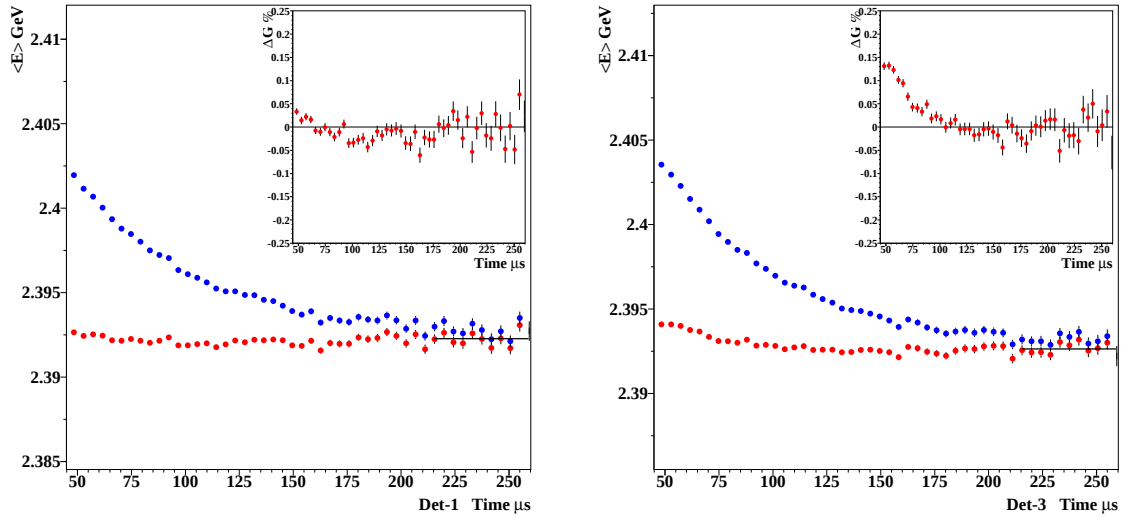

Figure 31 : The average energy and the gain (ΔG in %, insets) for detectors.

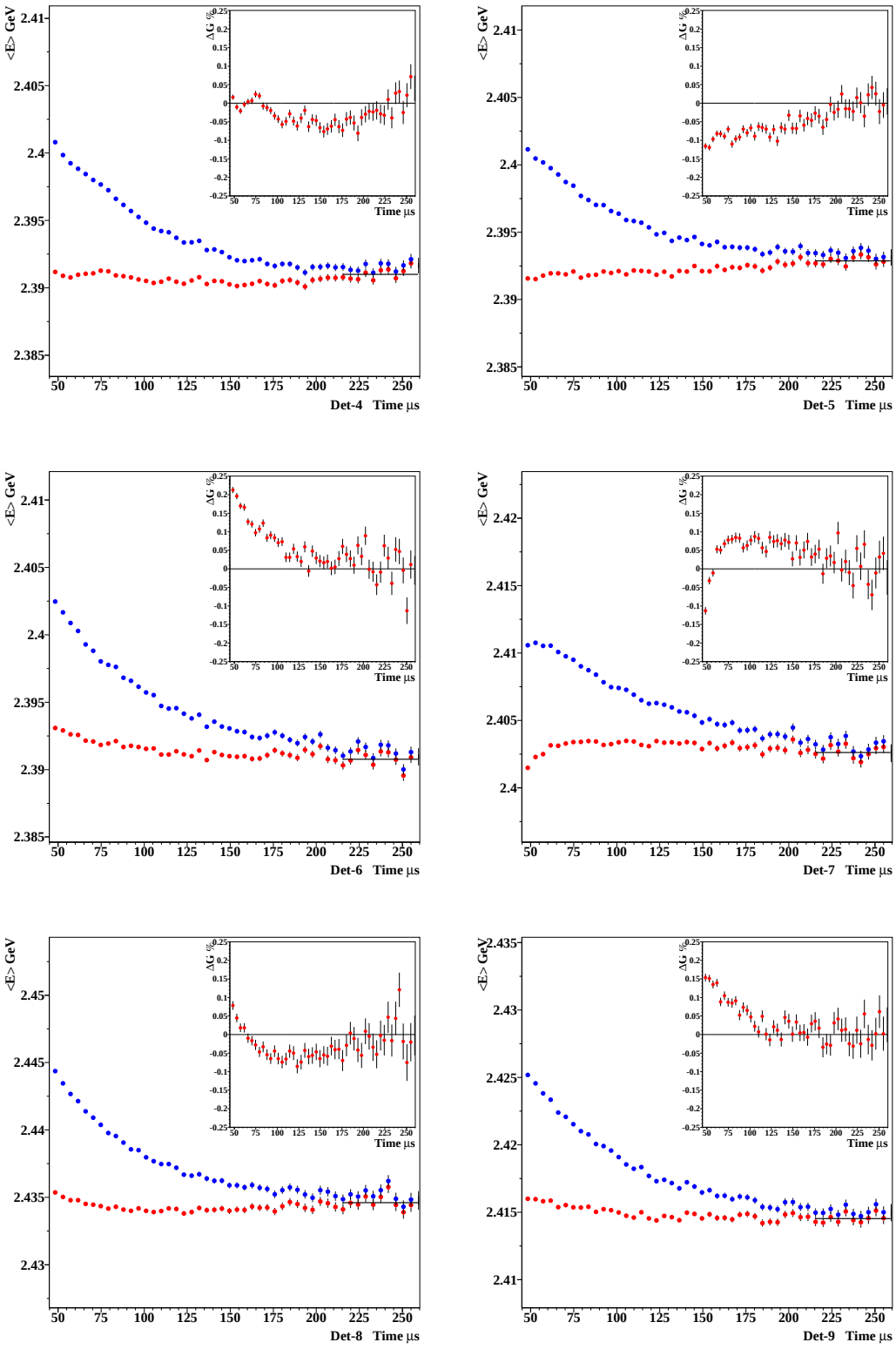

Figure 31 : continued,

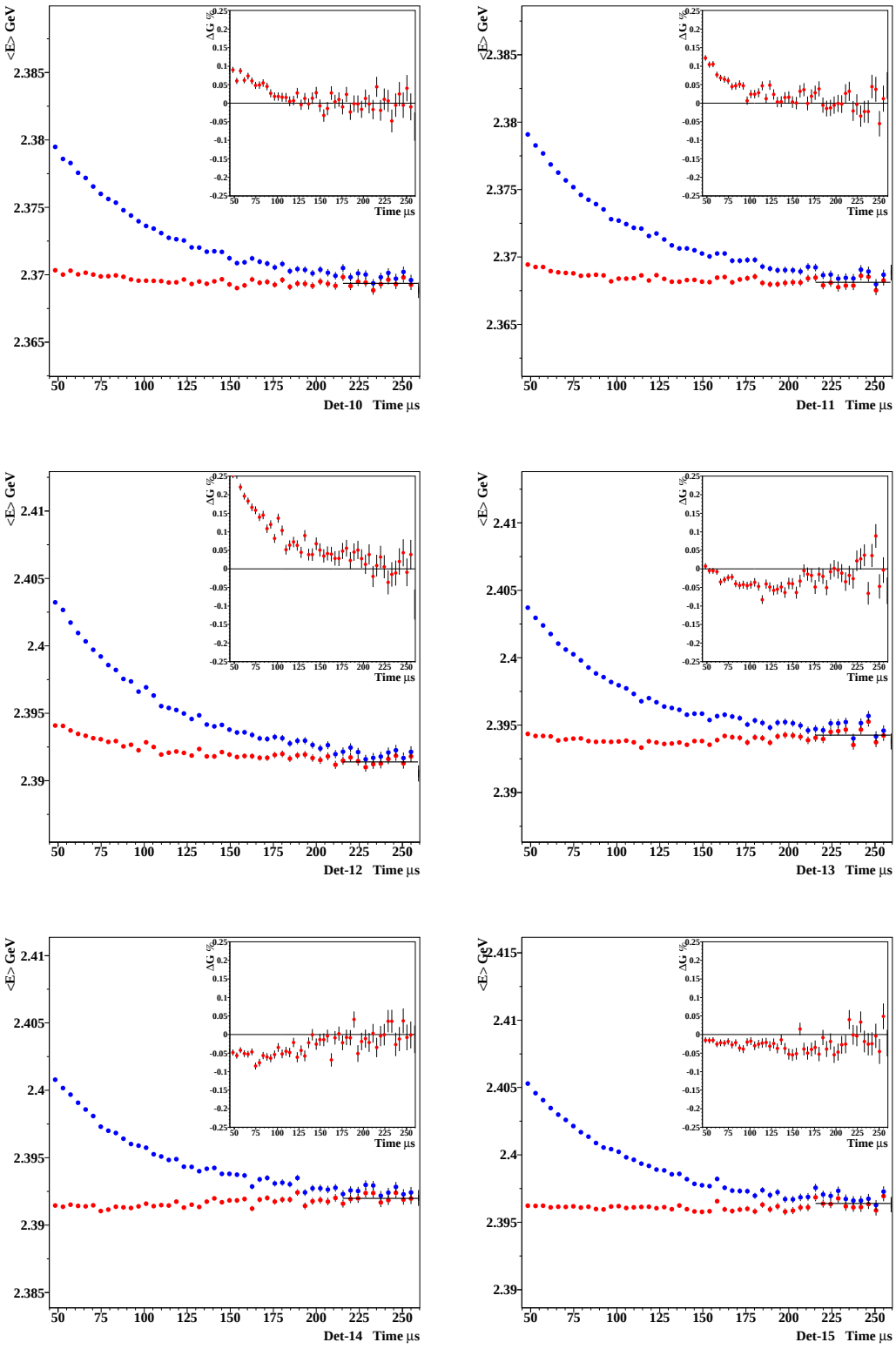

Figure 31 : continued,

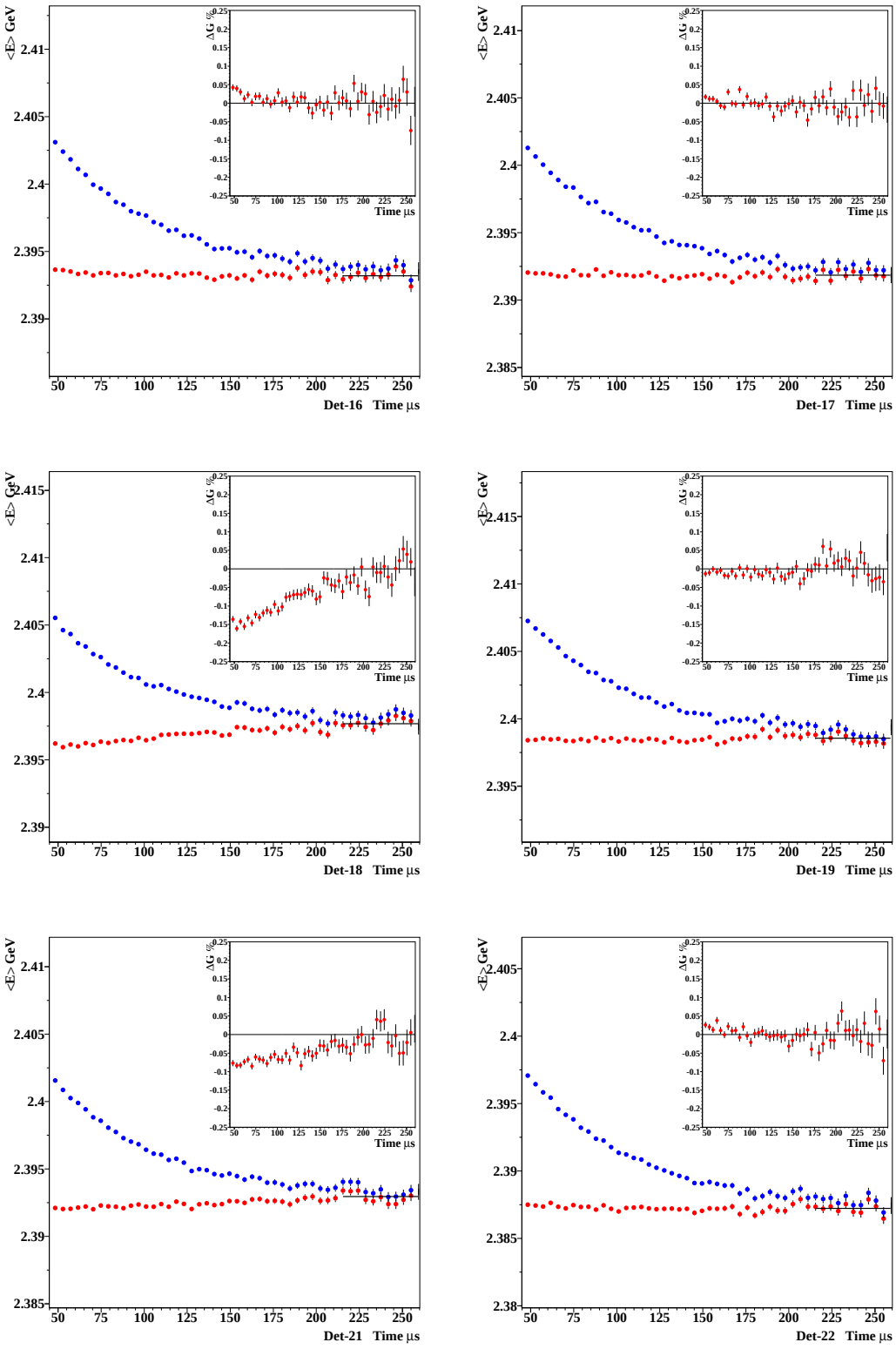

Figure 31 : continued,

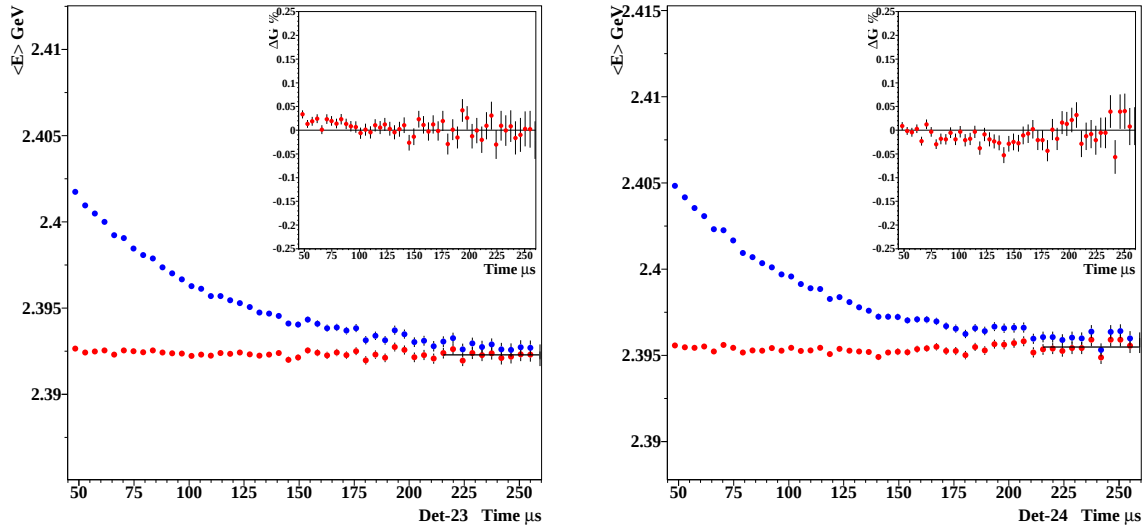

Figure 31 : continued.

The result of the average energies show that most of the detectors in the first half show gain effects larger than 0.1%. In the second half detectors 13, 14, 18 and 21 show little large effect but in generally they are fair. When we look at the first and the second halves (Figure 32) the picture is clear. The second half is roughly 5 times better (@ 50 μs) than the first half.

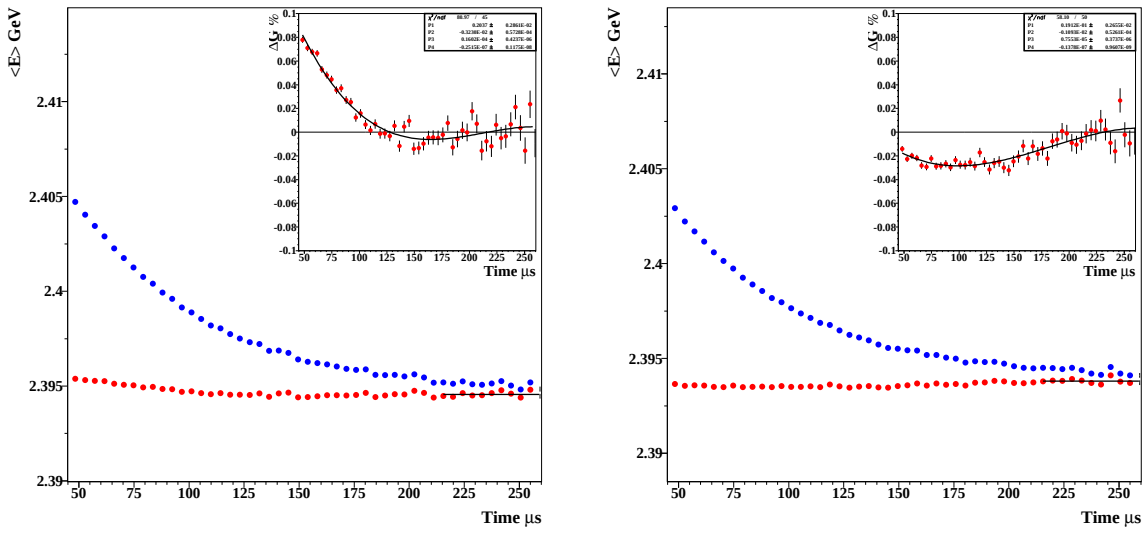

Figure 32 : Average Energy and Gain for the first and the second halves of the ring.

When all the detectors were combined (Figure 33), gain becomes smaller 0.04% at 50 μs.

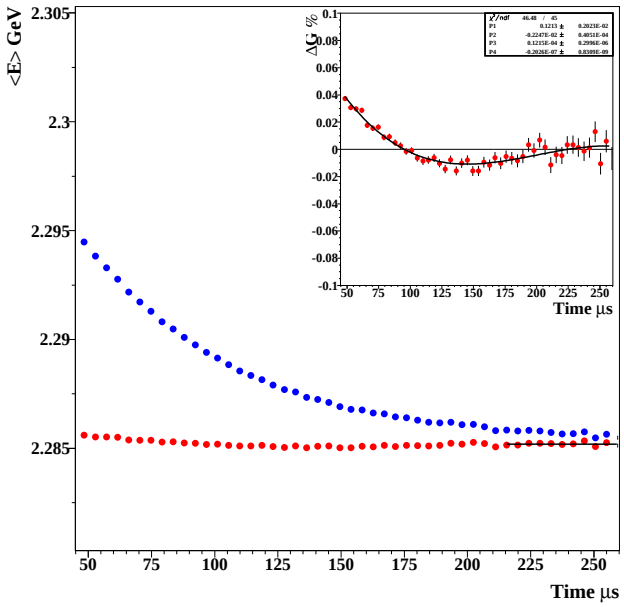

Figure 33 : $\overline{E}$ and Gain (All detectors together.)

To study the influence of the gain changes on ω_a, an artificial gain was introduced into the data. Each individual detectors were exposed to a 1% linear gain change between zero to 100 μs. The most important observation was when we fit the gain enhanced data with the complete physics form, the influence on R was the largest. This is due both the amplitude and the phase of the g-2 asymmetry and phase modulations are greatly influenced by the gain changes.

First lets look at the influence of the 1% gain change (@ 0 μs) on the fit parameters. For this study even one detector was enough to determine the systematics but in order to increase the statistics the second half detectors were used together. On the average, the second half have less gain problem and is free from some other problems that first half detectors have, like high hardware thresholds, flashes, etc..

The gain systematics were determined for three functional forms. These functional forms are 1999 functional form, 1999 functional form including the g-2 asymmetry modulation due to CBO and the complete physics form. The data was fitted to each functional form between the start time and 600 μs. For the start time sweep, the fit start time was changed between 49.9 μs and 150 μs. Parameters related with the residual slow term determined from the very first point (49.9μs) and were fixed all the time. Figures 34-36 show the fit parameter stability of the regular and the gain enhanced data in the case of 1999, 1999 form with g-2 asymmetry modulation and the complete physics functional forms were used.

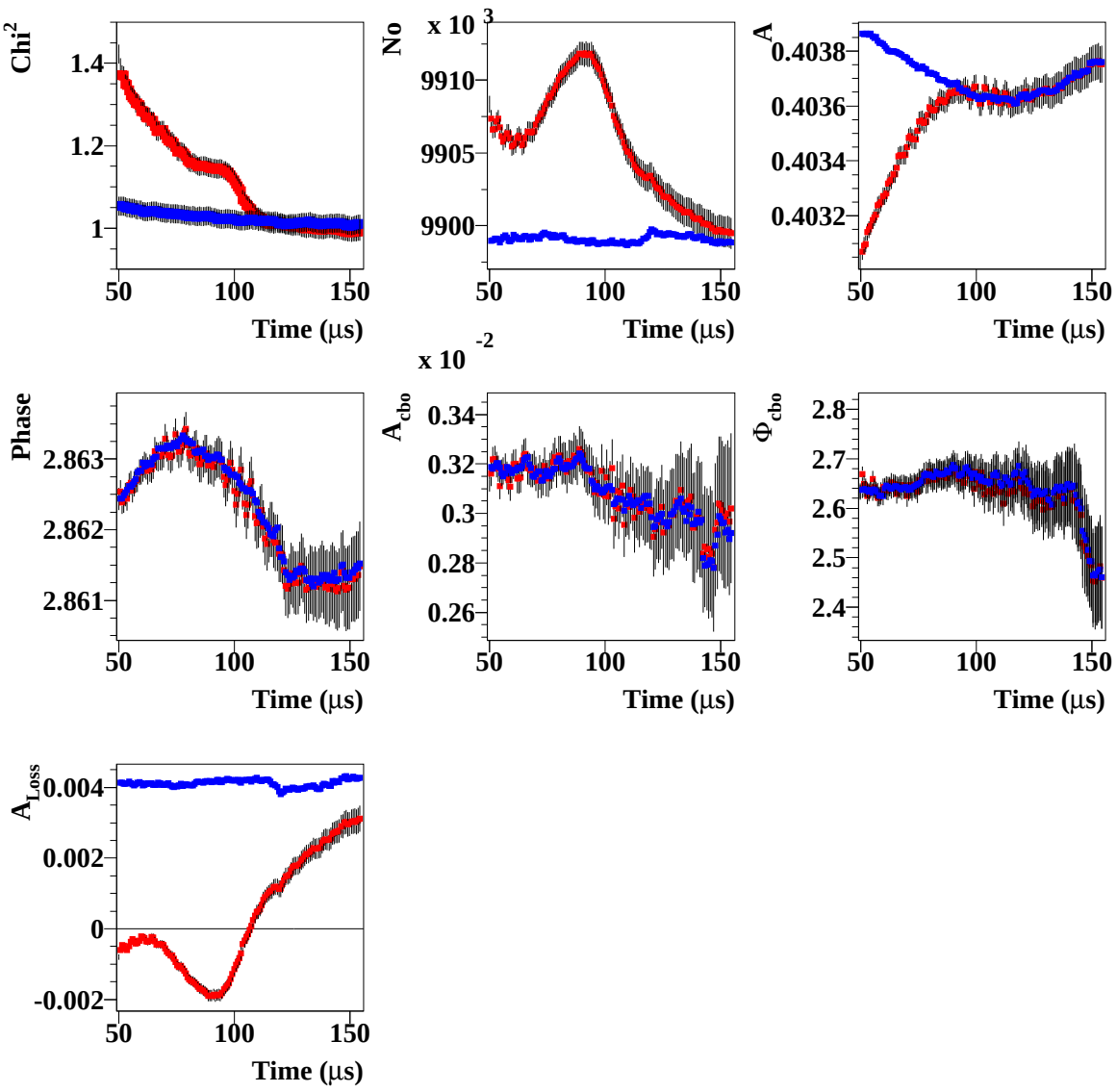

Figure 34 : Fit stability of the gain enhanced data for the 1999 functional form including the g-2 asymmetry modulation. Blue is the regular data and red is the gain enhanced data (1% at zero time and linearly vanishes at 100 μs).

Here are some useful numbers. For 1999 functional form, 0.5% (@ 50 μs) gain change causes to change the asymmetry by 0.21% and N_0 by 0.1%. The CBO related parameters A_{cbo} and ϕ_{cbo} are the least gain influenced parameters (only with a small phase pulling around the true value). As expected, the losses amplitude is influenced dramatically by the gain change. The phase pulling on g-2 phase, asymmetry and CBO phase becomes the largest around 100 μs where the artificial gain effect is about to vanish.

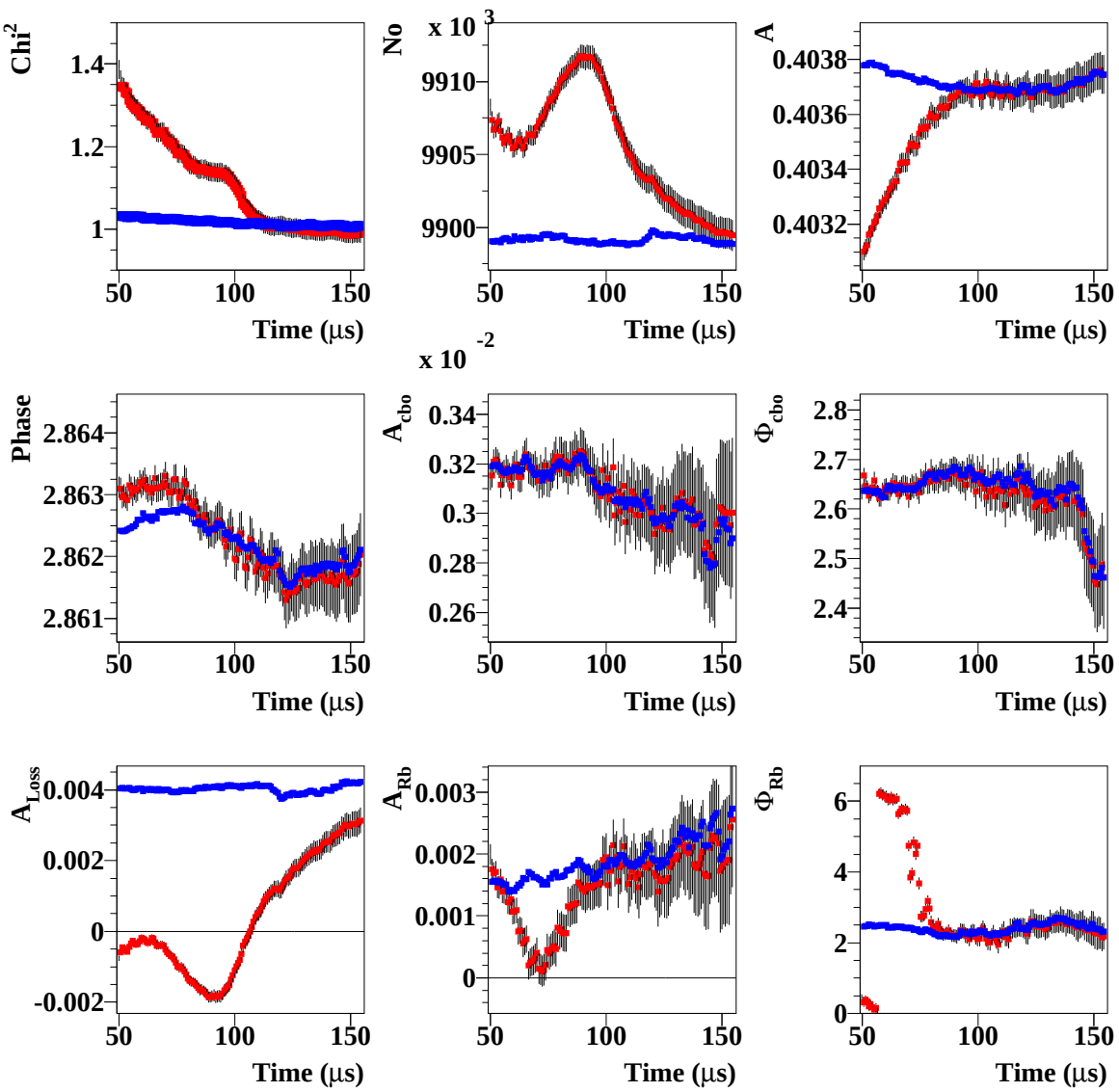

Figure 35 : Fit stability of gain enhanced data for 1999 functional form. Blue is the regular data and red is the gain enhanced data.

For this functional form 0.5% (@ 50 μs) gain change causes to change the asymmetry by 0.18%. The g-2 asymmetry modulation amplitude starts near the correct value at 50 μs but it quickly goes to zero around 75 μs where this is almost the middle of the gain enhanced region (take into account that the fit starts from 50 μs). The phase of the g-2 asymmetry modulation gradually decreases and only after 75-80 μs it converges to the correct value. The difference between the g-2 asymmetry modulation amplitudes for the regular and the gain enhanced data is 26% at 50 μs.

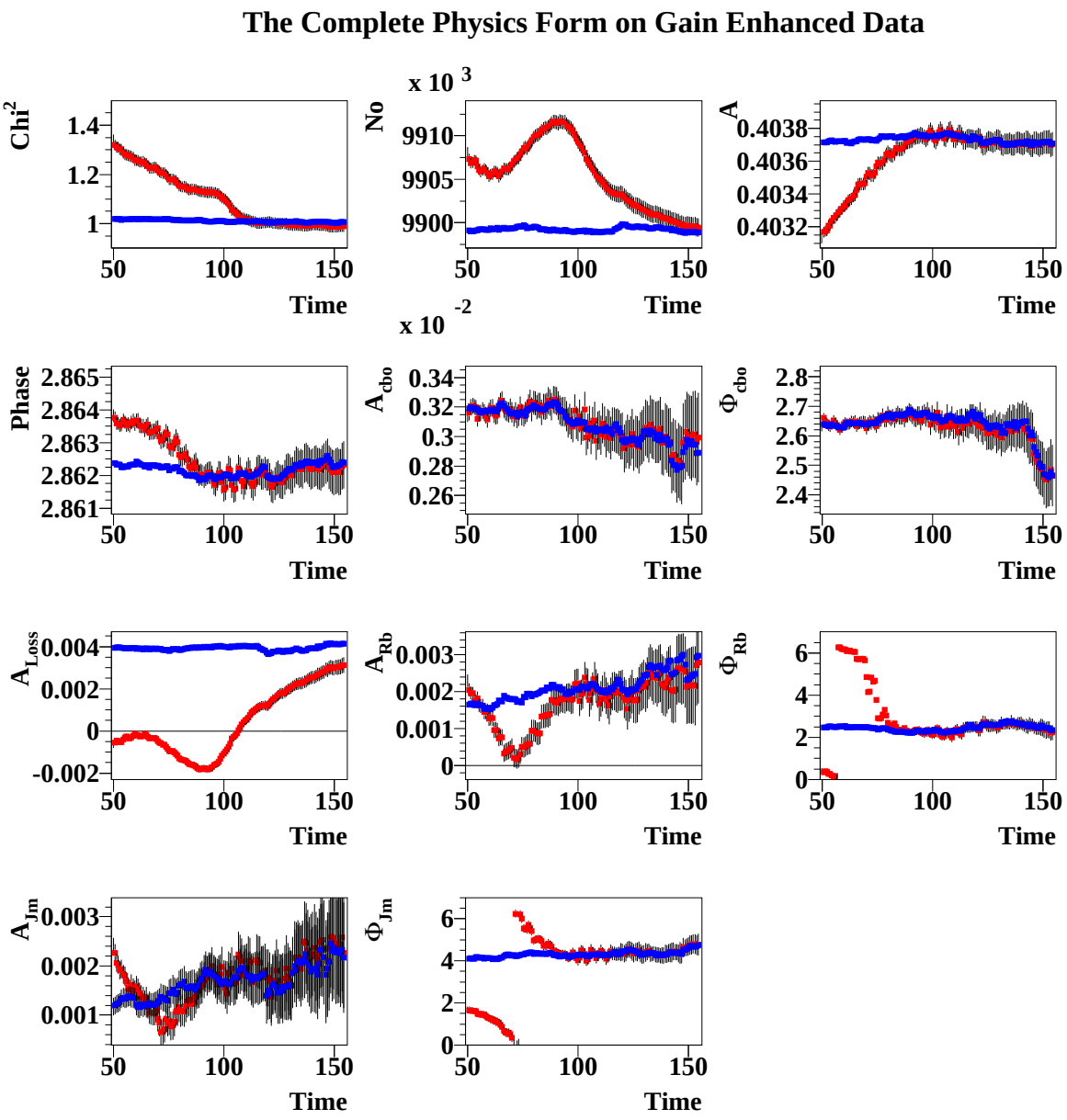

Figure 36 : Fit stability of gain enhanced data for the complete physics function. Blue is the regular data and red is the gain enhanced data.

For the complete physics form 0.5% (@ 50 μs) gain change causes to change the asymmetry by 0.14%. In addtion to the g-2 asymmetry modulation, g-2 phase modulation parameters behave the similar way under the influence of the enhanced gain. However g-2 phase modulation amplitude becomes 103% higher than the one for non-enhanced at 50 μs.

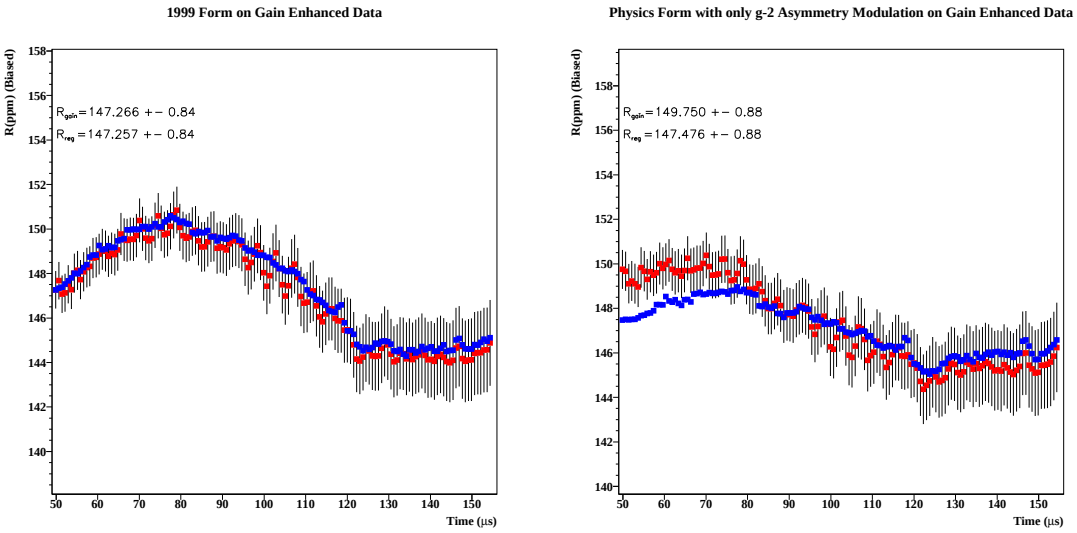

Figure 37 : The influence of 1% gain change (@ 0 μs) on R for 1999 functional form and for the 1999 functional form including the g-2 asymmetry modulation. Gain changes introduces g-2 phase pulling on R. Even though the steps are coarse g-2 phase pulling can be seen.

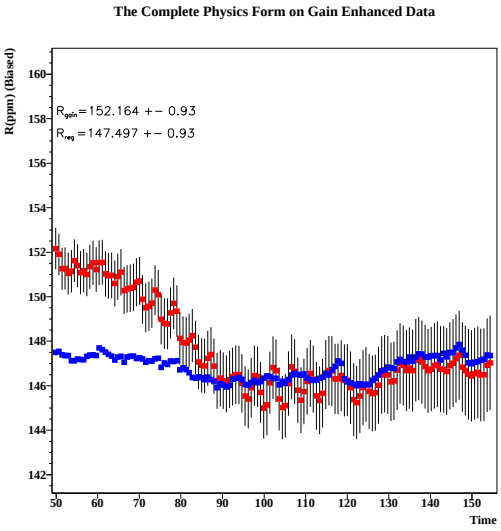

Figure 38 : The influence of 1% (@ 0 μs) gain change on R for the complete physics form.

These figures show that the influence of the gain changes on ω_a is small in 99 form and is much larger in the complete physics form. Let's remember that the artificial gain introduced to the data was 1% (within 100 μs) at zero time. Number of positrons effected from the gain changes should be taken into account. This could be done by integrating the Gain function in the influence of the exponential decay. The ratio below gives the conversion from artificial gain to the observed gain.

$$\frac{\int_{50}^{100} |G^{artificial}(t)| e^{-t/64} dt}{\int_{50}^{t_m} |G^{observed}(t)| e^{-t/64} dt} \tag{8}$$

Here G is the gain function obtained from the fit of gain versus time plots to the polynomial functions for the first and the second halves and when all the detectors together. For the artificial gain enhance data G can be determined from $G = g - \frac{g}{\Delta t} \times (t - 50)$ where Δt is the integration interval of (450 μs) g=0.5% at 50 μs and t is the time where t_m is the

time that the gain vanishes. It turned out to be the first half has 0.078% gain change at 50 μs and the gain effect vanishes around t_m=215 μs. The second half has 0.018 % gain change at 50 μs and the gain vanishes around 225 μs. When all the detectors together, gain is 0.037% (@ 50μs) and it lasts until t_m=230 μs. The normalization ratios between the artificially enhanced data and the regular data were determined to be 5.5 for the first half, 7.0 for the second half and 12.6 for all the detectors together case. To be conservative in the numbers, absolute values of the G(t) were integrated as showed in the formula 8.

Table 5 gives the comparisons and the assigned systematics due to the gain for different functional forms. These numbers were determined at 49.9μs.

Table 5: Systematics table of the gain. The first number is determined at 50 μs and the second number is the maximum deviation between 50 μs and 60 μs. The gain systematic is almost zero for 1999 functional form around the zero crossing whereas for the other functional forms they are maximum.

Detectors	1999 Form	Only Asymmetry Modulation	Physics Form
First half	0.002-0.10 ppm	0.41-0.41 ppm	0.85-0.85 ppm
Second half	0.001-0.08 ppm	0.33-0.33 ppm	0.67-0.67 ppm
All of them	**0.002-0.04** ppm	**0.18-0.18 ppm**	**0.37-0.37 ppm**

By looking at these results one can conclude that the more complicated the functional form is the more systematic error due to the gain. As we proposed from the beginning, combining all the detectors together definitely brings an advantage for reducing the systematics from the gain. The gain changes have opposite signs in the first and in the second halves. This helps to reduce the gain systematic when the detectors from both halves were added. @ 50 μs the first half almost have 5 times more gain than the second half.

6.5 Systematic From the Bin Width

The systematic from the bin width was studied in 1999 analysis by many different groups. We knew that it was a small effect however in order to complete the systematic studies for this year, we studied this effect again. In this study, fifteen different time spectra were constructed using 120 ns, 125 ns, 130 ns,...,190 ns bins. The time spectra from each detector was added together and the grand total time spectra were obtained for each bin set. These spectra were fitted to 1999 function, 1999 function including the g-2 asymmetry modulation and the complete physics functions. There is no considerable difference observed due to fitting function differences on this effect as expected. For the starting point of the fit, the closest bin to 50 μs was chosen for each set. The muon losses had to be re-binned for each set by interpolating the data between the consecutive points. The figure 39 shows the R vs time plots for 15 different bin widths, and the errors are plain statistical errors.

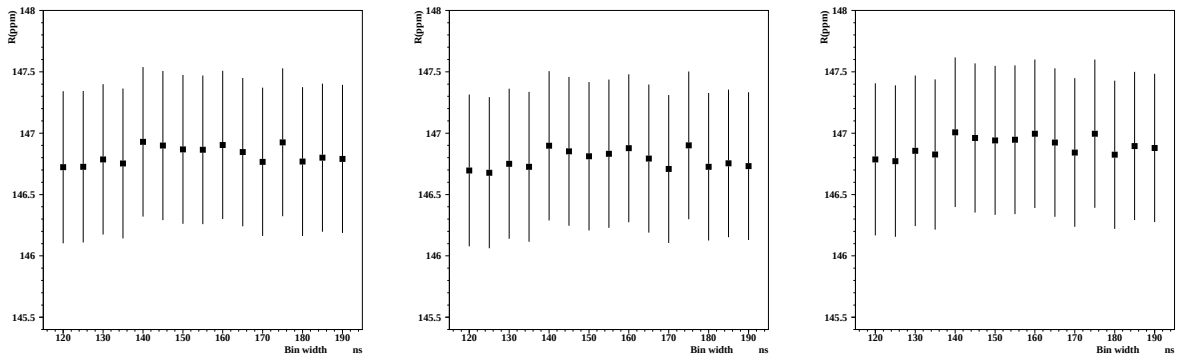

Figure 39 : The influence of the bin width. Since the starting time is slightly different for each case, in order to find out the size of the effect of the starting time, the R values at one bin earlier than 50 μs and one bin later than 50μs were also determined.

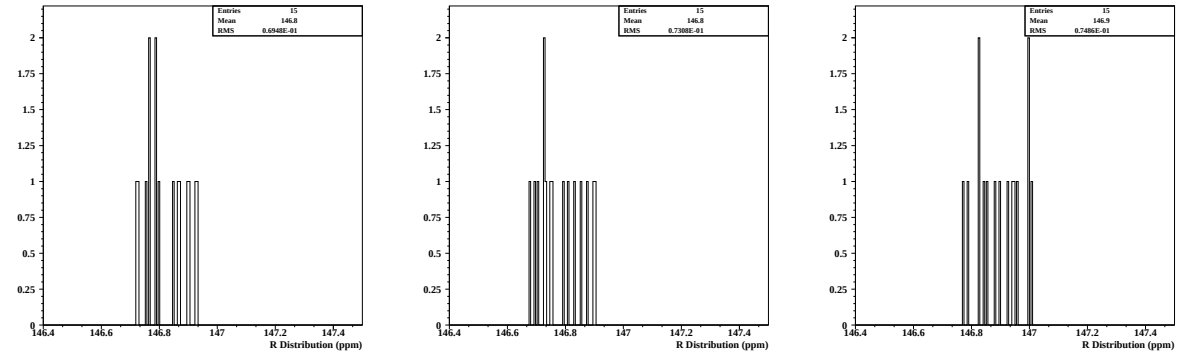

Figure 40 : The RMS distributions for three cases showed in Figure 39.

From these studies we will assign 0.07 ppm systematic due to the bin effect without depending on the functional form.

6.6 Systematic due to Pileup Subtraction Efficiency

The same pileup subtraction method was used in this analysis as 1999 [8]. The missing parts on the doubles due to high hardware thresholds were studied detail [9] before. These missing parts for constructed doubles were corrected on run by run basis where the changes in the hardware thresholds were taken into account.

The quality of the pileup subtraction can be observed from the comparison of the energy spectra at early and late times with and without pileup subtraction. However a qualitative check can be done by comparing the time spectrum of the detected positrons and constructed pileup for each detectors (Figure 41). This tells us the pileup subtraction quality is good in high energies. These spectra were constructed after 50 μs.

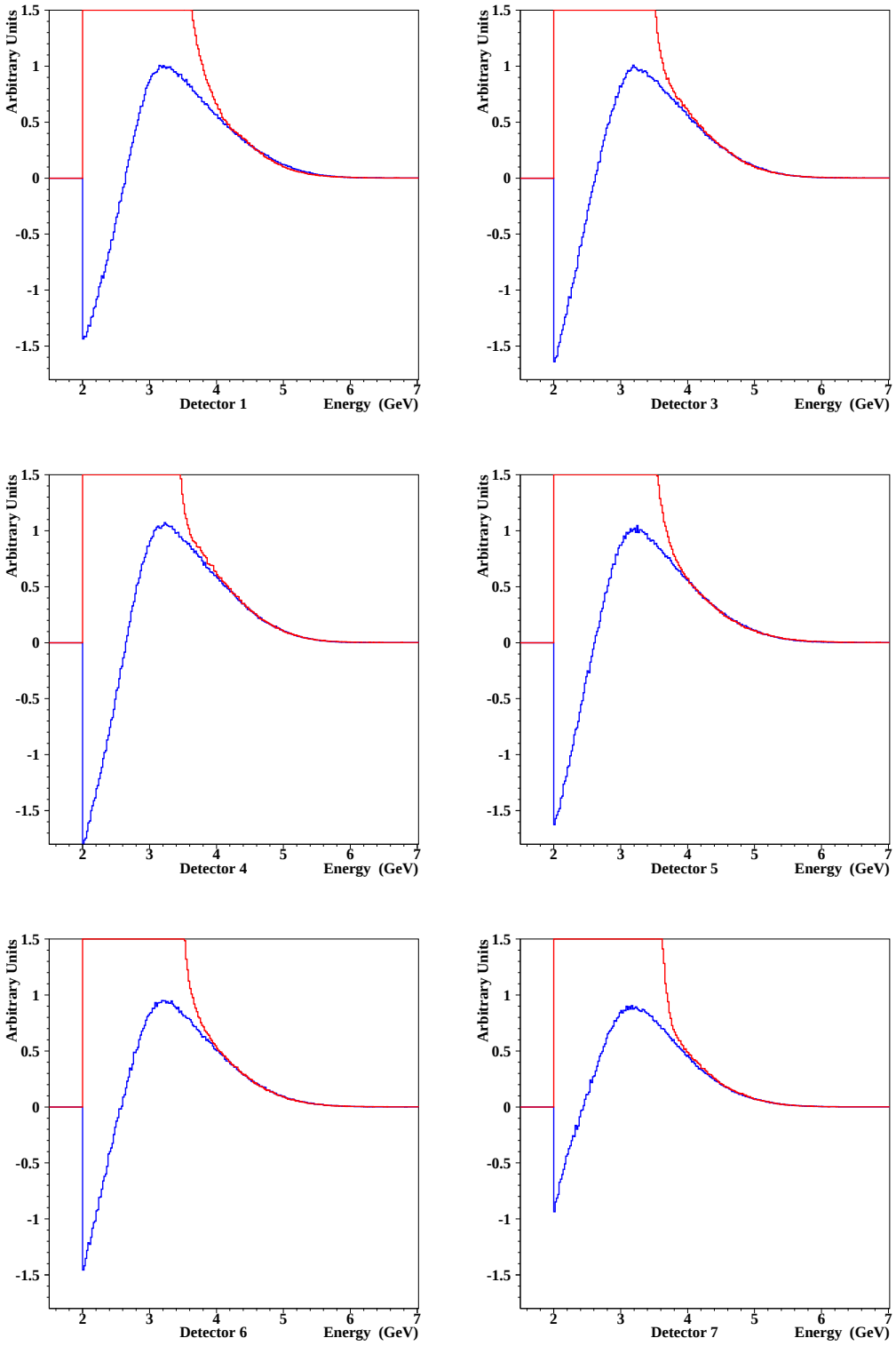

Figure 41 : The comparisons of the observed positron and the constructed pileup energy spectra.

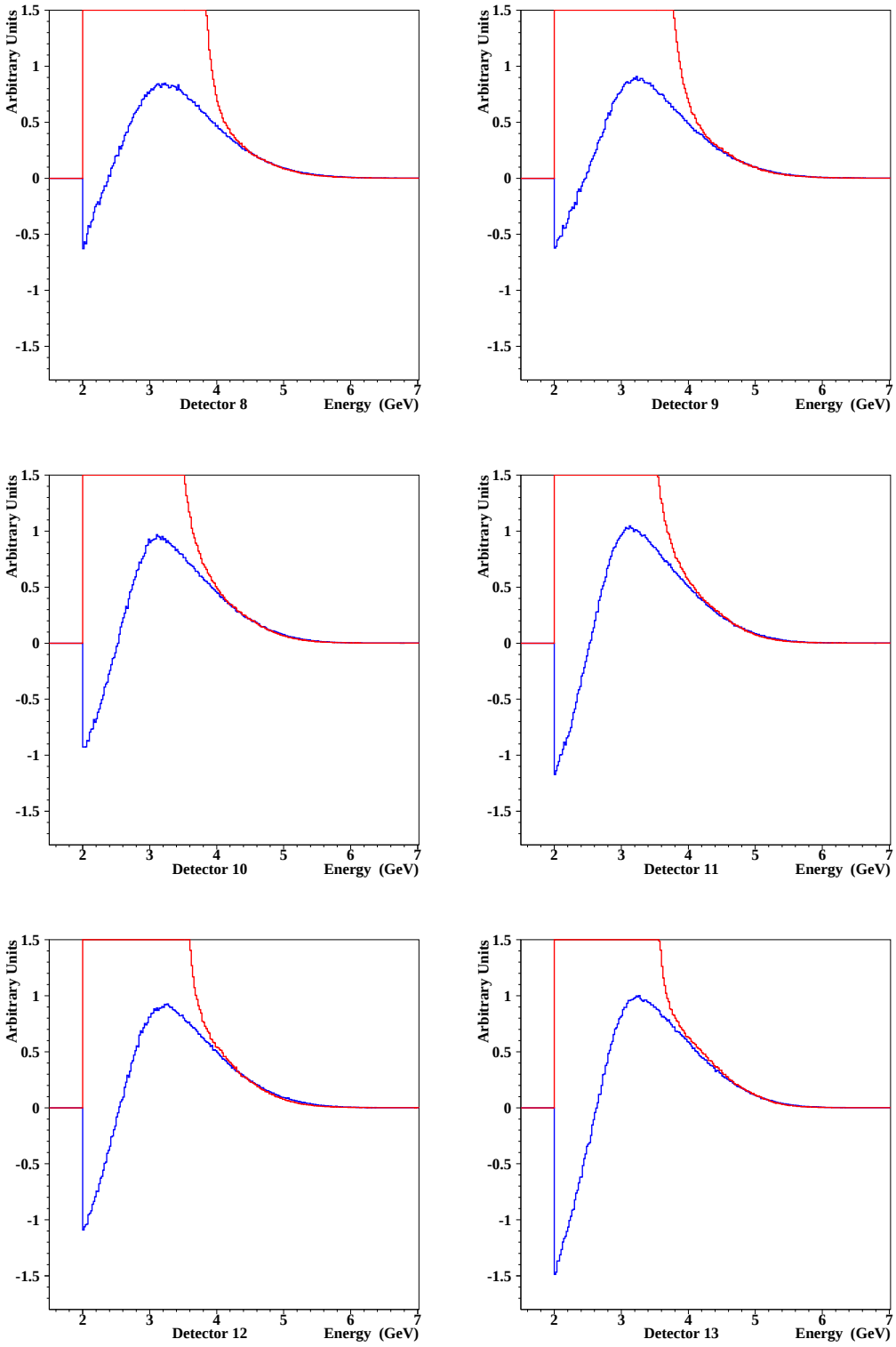

Figure 41 : continued,

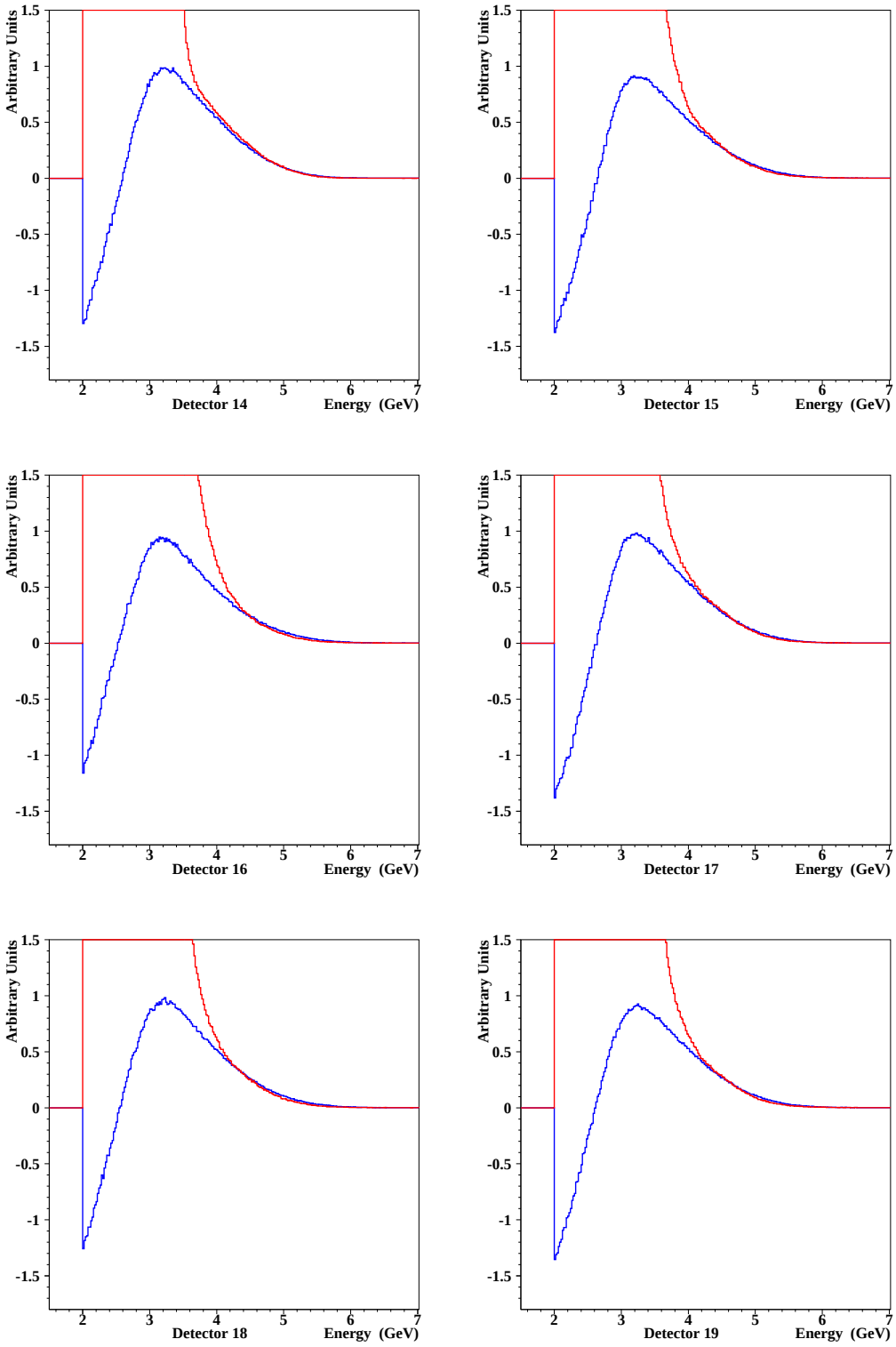

Figure 41 : continued,

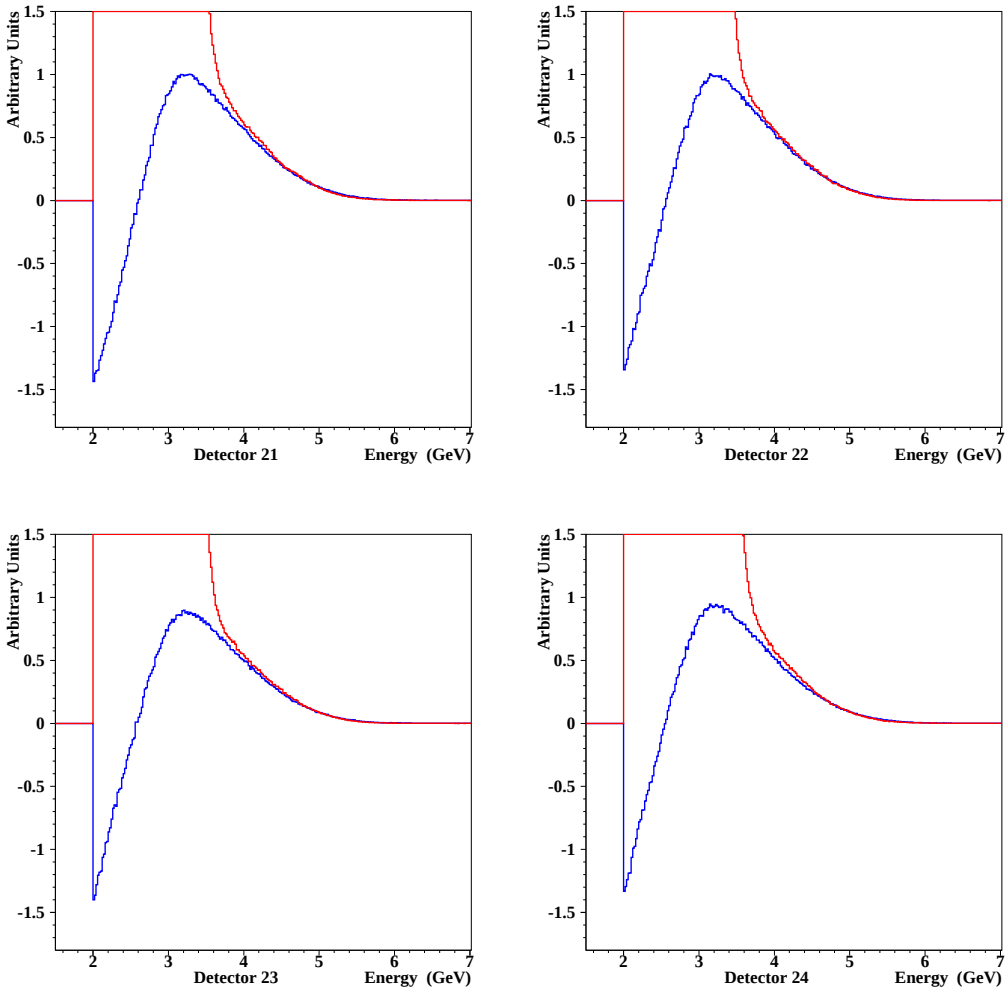

Figure 41 : continued.

The agreements between PU spectra and the positron spectra are very well. However pileup subtraction is not perfect. The difference between early to late energy spectrum with and without pileup subtraction gives the information about how well this subtraction was done.

$$P_1 = \frac{S_E^0 - S_L}{\int S_L} \qquad P_2 = \frac{S_E^- - S_L}{\int S_L} \tag{9}$$

where S_E^0 is the energy spectrum without the pileup subtraction and S_E^- is the one with the pileup subtraction. S_L is the spectrum of the singles at late times. This year we use energy dependent f-factor ($E_{doubles} = \mathbf{f}(E_{S_1} + E_{S_2})$) in the pileup subtraction which provides a better pileup subtraction. Figure 42 shows the comparisons of observed positron spectrum and the absolute value of the constructed pileup spectrum at early and late times.

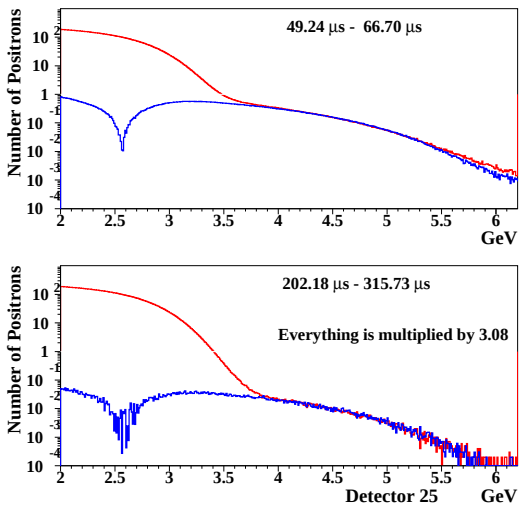

Figure 42 : Absolute PU energy spectrum (blue). Regular positron energy spectrum (red).

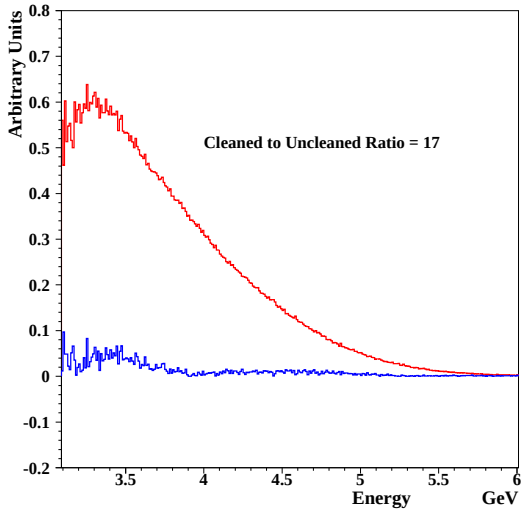

Figure 43 : P_1(red) and P_2(blue) spectra shows the pileup subtraction efficiency above 3.1 GeV.

Around 2.6 GeV (slightly different in each detector depending on the energy spectrum) the pileup spectrum crosses zero. This means the pulses lost and pulses gained are almost equal. To estimate the pileup subtraction efficiency under 3 GeV becomes difficult for noise reasons from this method. The pileup subtraction efficiency is determined above 3.1 GeV and Figure 43 shows the comparison of $P_1(t)$ and $P_2(t)$ for this energy range. For the first and the second halves this ratio is the same and ≈17.

The observed integral pileup is 0.26% after 50 μs with 0.03% RMS. This value was determined from the ratio of counts as follows :

$$100 \times \frac{\int_{50}^{500} F_{PU}(t)dt}{\int_{50}^{500} F_{All}(t)dt} \tag{10}$$

where $F_{PU}(t)$ is the pileup time spectrum and $F_{All}(t)$ is the observed positron time spectrum. This ratio and the RMS spread were determined from the individual detectors. Due to spectra difference, the kicker detectors show ≈ 10% more pileup than the others. If we clean the pileup to 6% level, there must be still 0.016% left over after 50 μs. In this case the systematic due to this small remaining can be calculated from the last year's method. We can subtract the pileup from the data and add on it to determine how much the R value changes. This method was applied to three functional forms and the results are shown in the following figures.

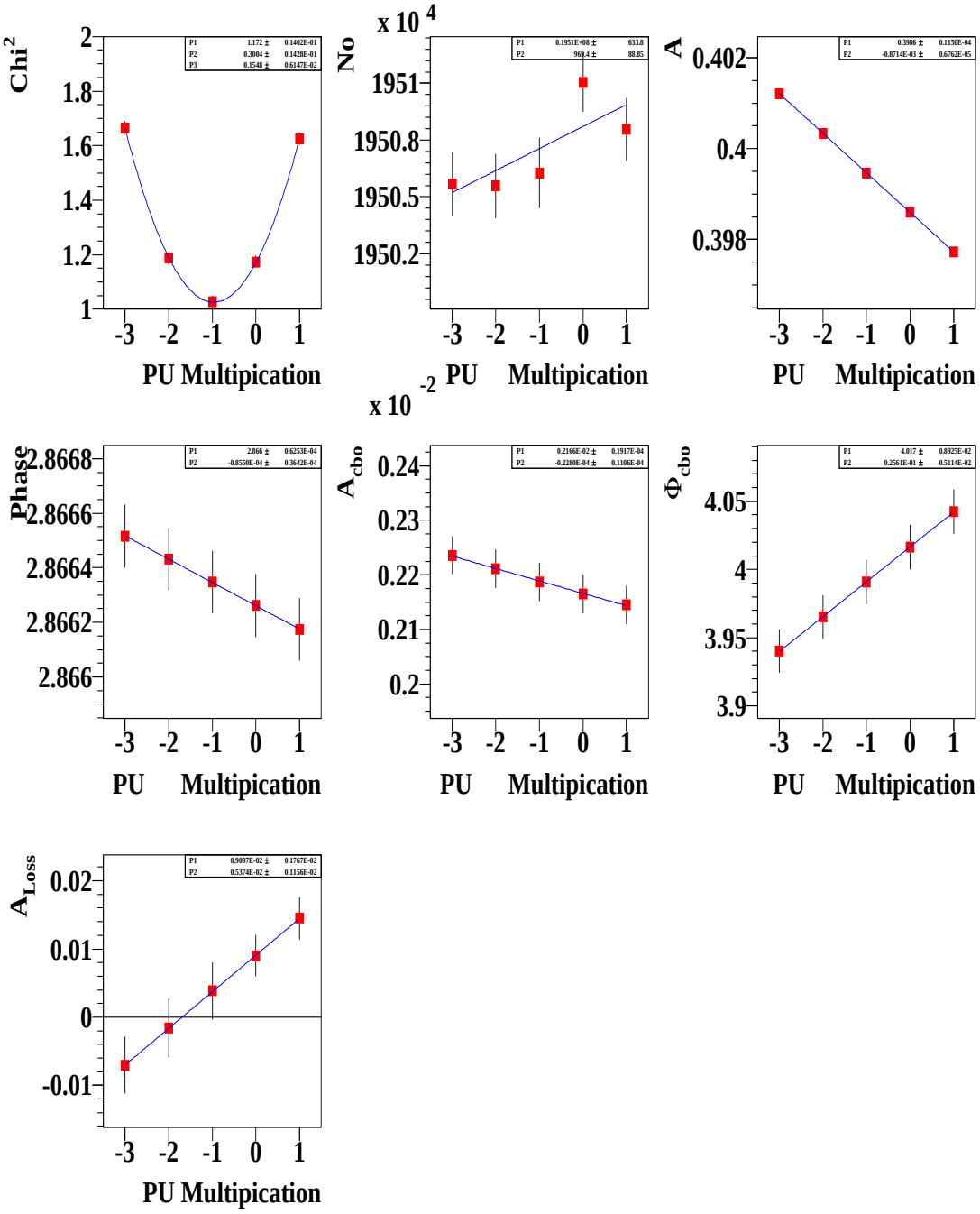

Figure 44 : Systematic shift on the parameters due to pileup for 1999 functional form.

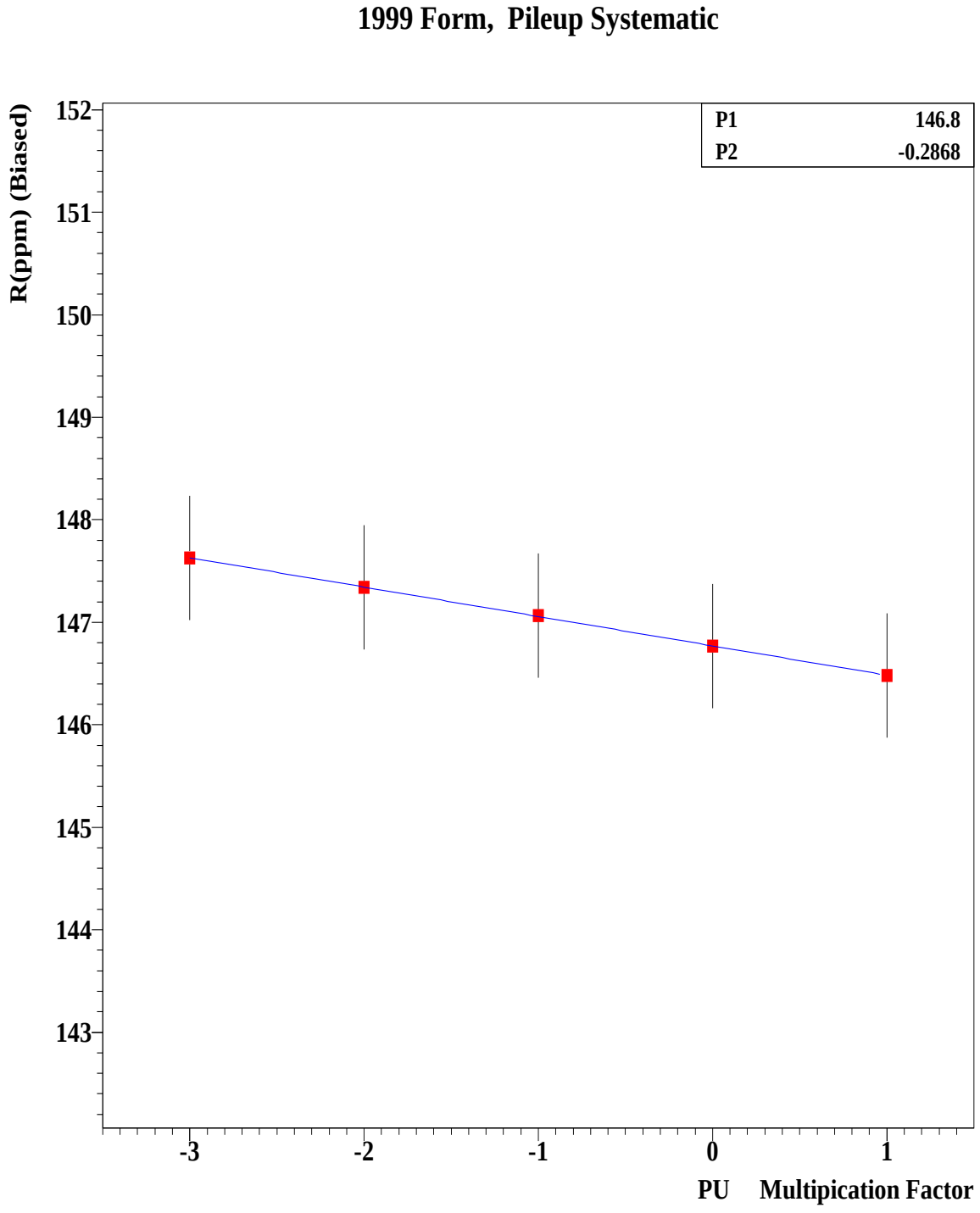

Figure 45 : Systematic shift on R due to pileup for 1999 functional form. The systematic shift on R for remaining 6% pileup is **0.02 ppm** for 1999 type functional form.

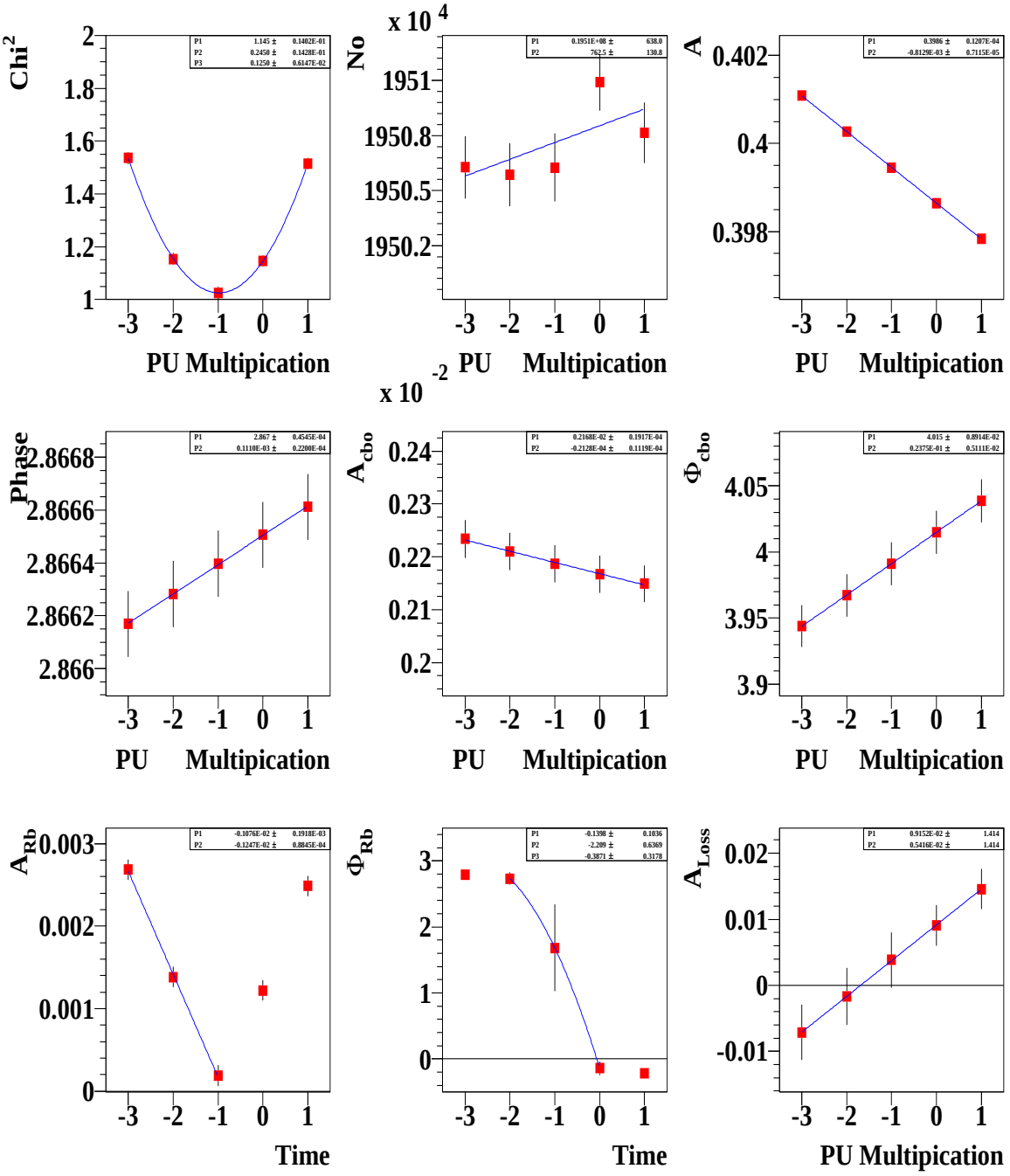

Figure 46 : Systematic shift on the parameters due to pileup for the 1999 functional form including the g-2 asymmetry modulation.

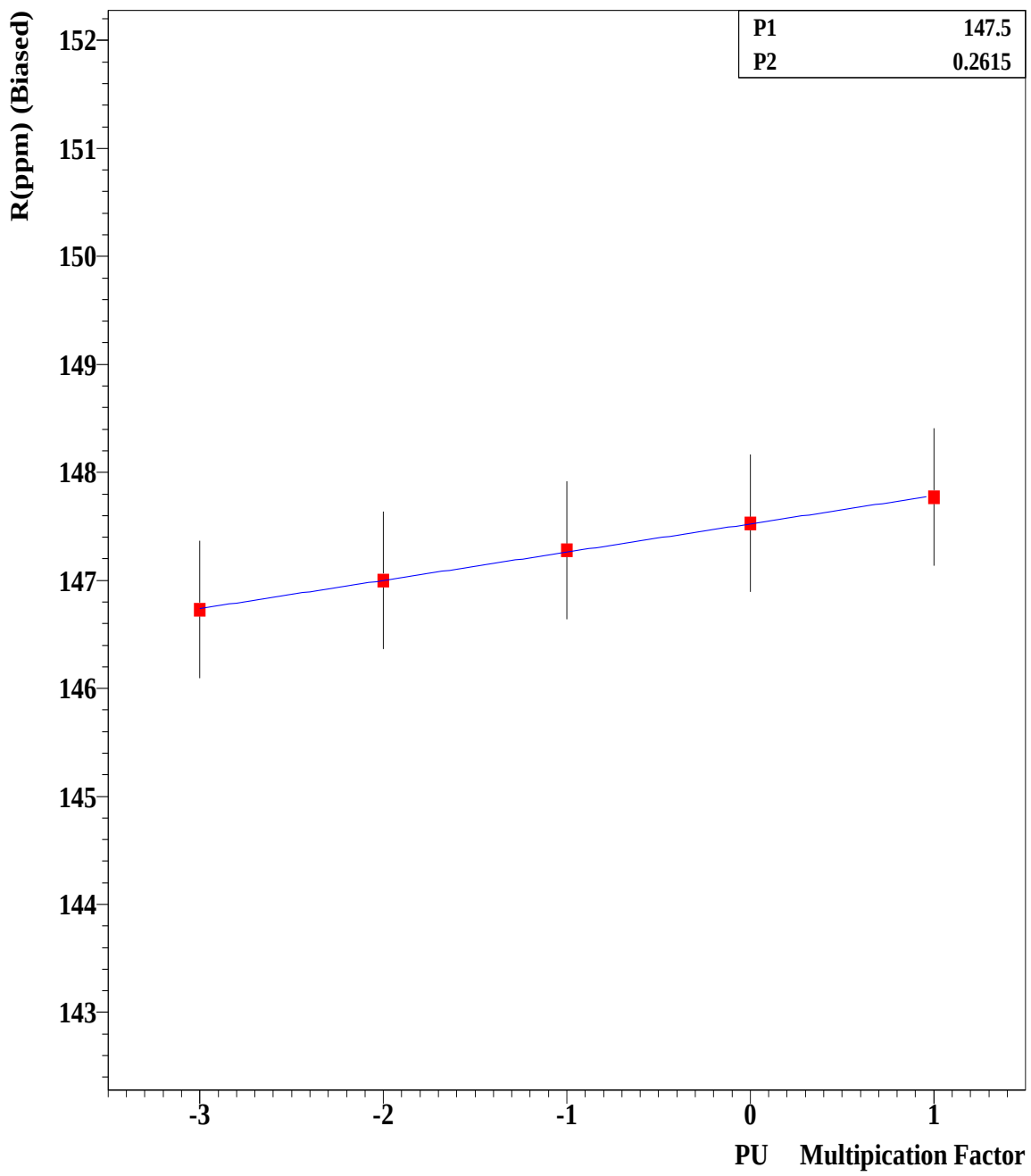

Figure 47 : Systematic shift on R due to pileup for the 1999 functional form including the g-2 asymmetry modulation. The systematic shift on R for remaining 6% pileup is **0.02 ppm** for this functional form.

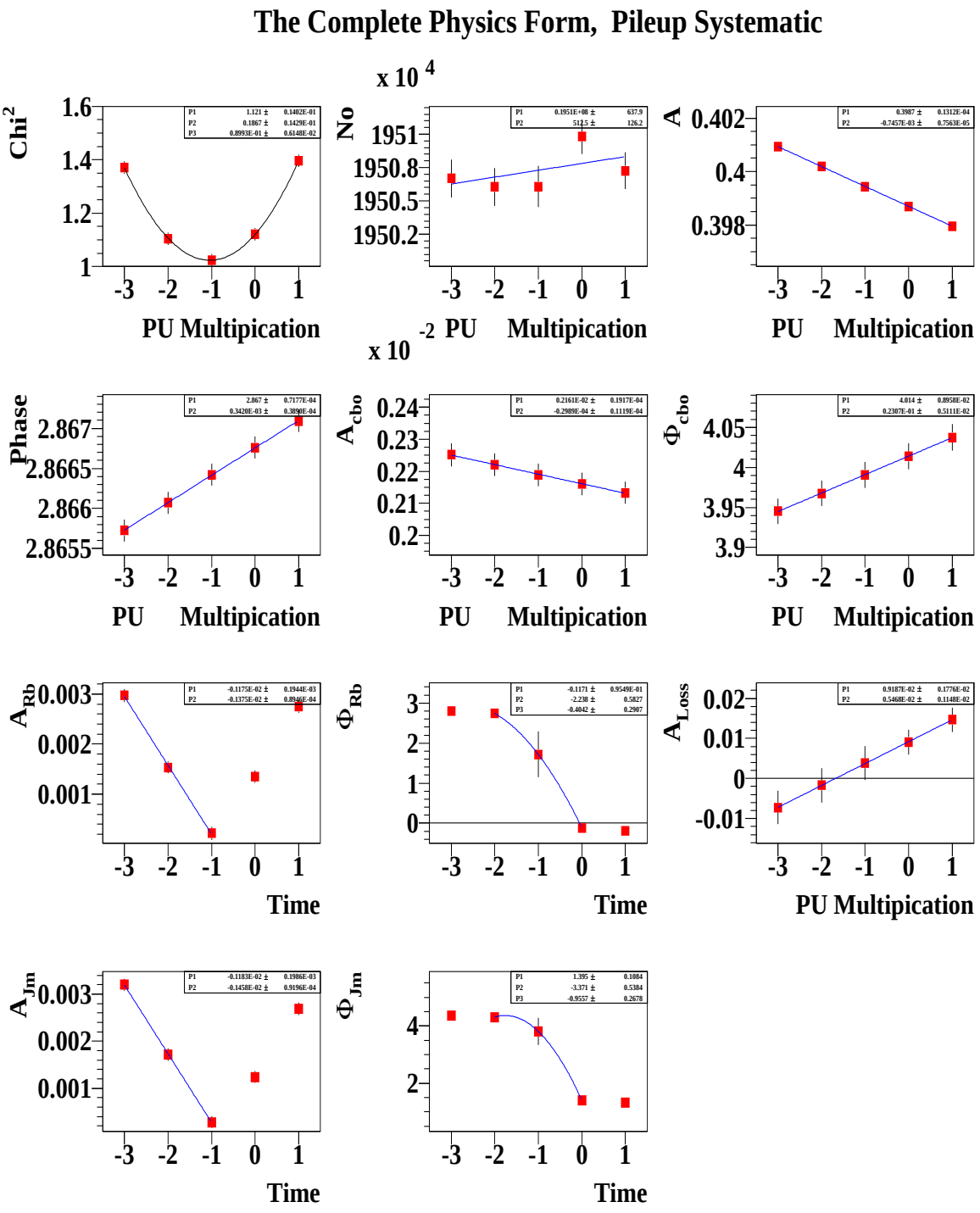

Figure 48 : Systematic shift on the parameters due to pileup on the complete physics form.

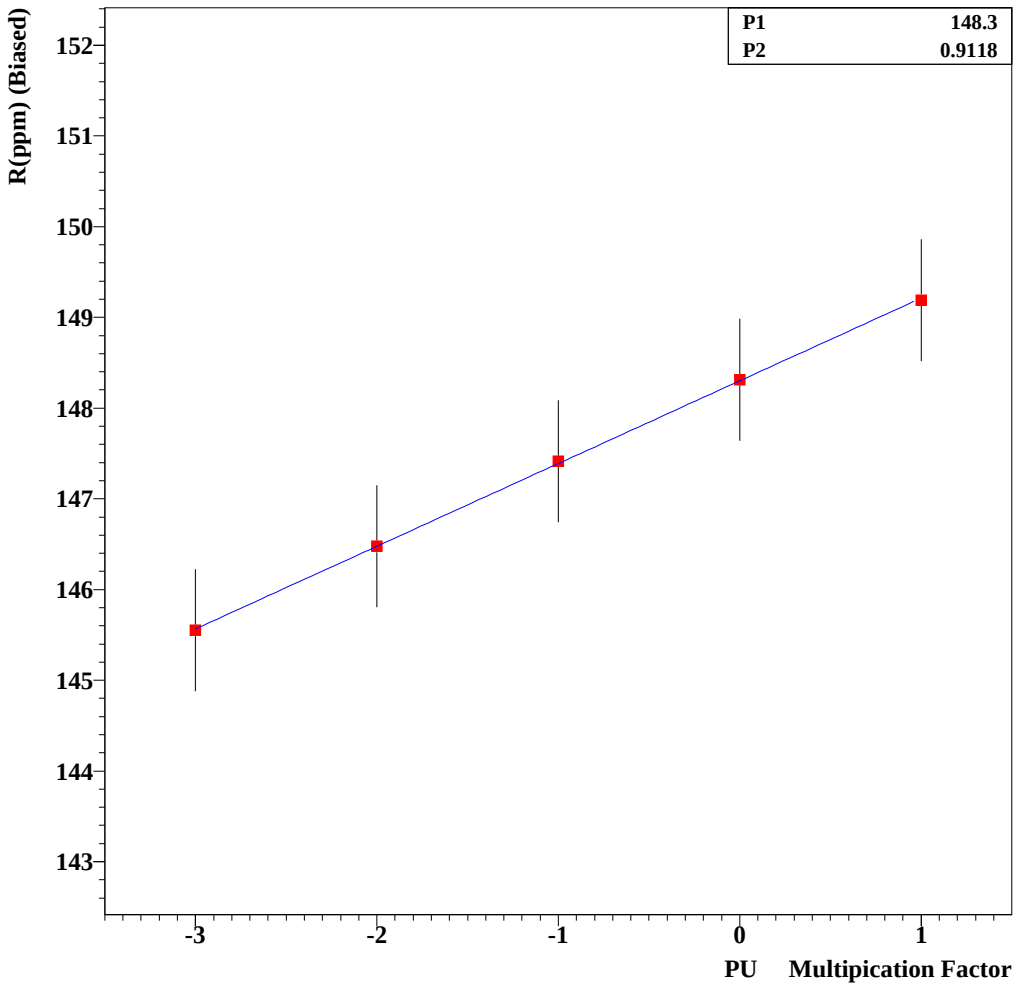

Figure 49 : Systematic shift on R due to pileup on Physics form. The systematic shift on R for remaining 6% pileup is 0.07 ppm for physics functional form.

The most important observation from this systematic study is the observation of the large changes on the amplitudes and the phase of the two effects, the amplitude and the phase modulations of g-2 due to CBO. This also proves that these parameters are really sensitive to the slow effects. Other observation is from the 1999 functional form to the 1999 functional form including g-2 asymmetry modulation, the pileup systematic changes by 0.04 ppm (taking into account also the slope is changing it's direction). From the 1999 including g-2 asymmetry modulation to the complete physics function there is another 0.05 ppm change. This also proves that 1999 functional form including g-2 asymmetry modulation gives us half of the systematics that physics function gives for slow type of effects. This result is consistent with the outcome from the gain systematic section.

Table 6 shows the comparisons of changes on the fit parameters corresponds to remaining 6% pileup.

Table 6: Influence of remaining pileup on other fit parameters.

Parameters	1999 Form	Only Asymmetry Modulation	Physics Form
ΔA	$5.22\ 10^{-5}$	$4.88\ 10^{-5}$	$4.47\ 10^{-5}$
$\Delta\phi_a$	$5.13\ 10^{-6}$	$6.66\ 10^{-6}$	$20.5\ 10^{-6}$
ΔA_{cbo}	$1.37\ 10^{-6}$	$1.27\ 10^{-6}$	$1.79\ 10^{-6}$
$\Delta\phi_{cbo}$	$1.54\ 10^{-3}$	$1.43\ 10^{-3}$	$1.38\ 10^{-3}$
ΔA_{loss}	$3.22\ 10^{-4}$	$3.25\ 10^{-4}$	$3.28\ 10^{-4}$
ΔA_{Rb}		$7.48\ 10^{-5}$	$8.25\ 10^{-5}$
$\Delta\phi_{Rb}$		≈ 0.13	≈ 0.13
ΔA_{Jm}			$8.75\ 10^{-5}$
$\Delta\phi_{Jm}$			≈ 0.13

Table 7 shows the systematic shift on R due to 6% ineficiency in the pileup subtraction for different functional forms.

Table 7: Systematics due to remaining pileup (seen).

	1999 Form	Only Asymmetry Modulation	Physics Form
ΔR	0.02 ppm	0.02 ppm	0.07 ppm

6.6.1 Pileup Phase

Constructed pileup was fitted to five parameter function to determine the PU phase. The fits were performed for 3 different energy bands of E(2.0,∞), E(2.0,2.6) and E(2.6,∞) GeV. The constructed pileup is negative in the energy range of 2.0 GeV to 2.6 GeV since the number of lost singles are larger than the gained doubles. For that reason the time spectrum is multiplied with -1 and fitted. In the fits, the precession frequency was fixed to the value obtained from the regular fits to get better error for pileup phase. Figure 50 shows the fit to the pileup data above 2 GeV. Table 8 shows the determined pileup phase for these energy bands.

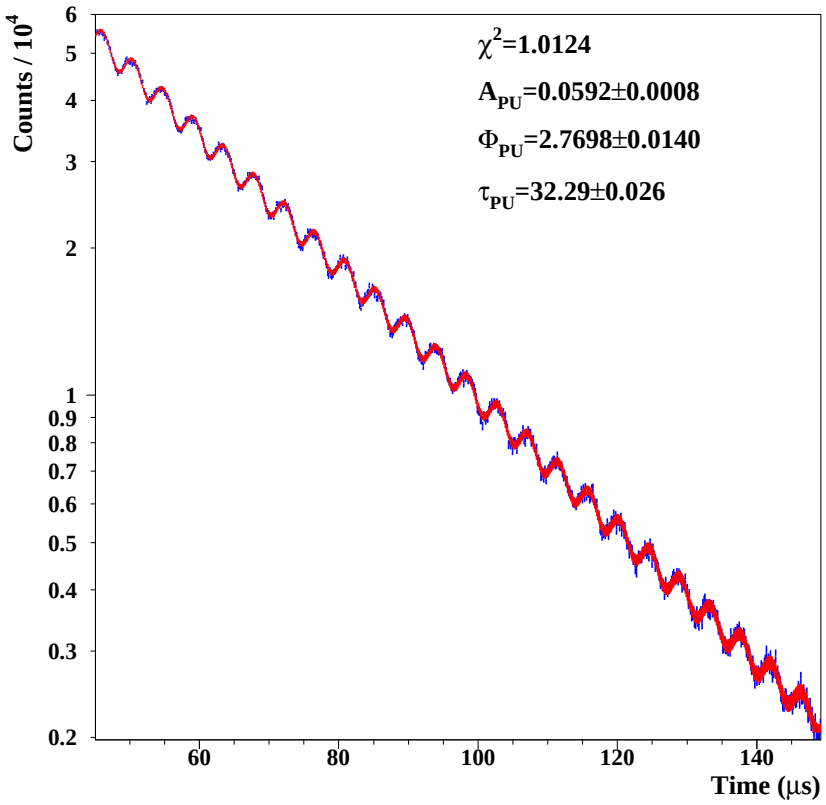

Figure 50 : Fit to constructed pileup for E>2 GeV.

Table 8: Comparison of the pileup and ω_a parameters for various energy bands. *This is actually negative, the whole pileup for this region was multiplied by -1 for the fit purposes. However, the total PU vector is the difference of the PU for $E > 2.6GeV$ minus the PU for $2 < E < 2.6$ GeV.

	2.0< E <2.6 GeV	E>2.6 GeV	E>2.0 GeV
N_0^{pu}	84286±1213	309041±425	218175±439
A_{pu}	1.10*±0.002	0.3509±0.0005	0.059±0.001
τ_{pu} (μs)	32.28±0.19	32.30±0.018	32.29±0.03
ϕ_{pu} (rad)	**2.8811±0.0030**	**2.8678±0.0016**	**2.770±0.014**
N_0^a	14922772±713	4457466±389	19505963±815
A_0^a	0.34900±0.00003	0.57330±0.00004	0.39946±0.00002
ϕ_a (rad)	**2.8658±0.0002**	**2.8676±0.0002**	**2.8663±0.0001**

The quality of the pileup subtraction is more important on the high energies than the low energies. Because most of the pileup is above 2.6 GeV. If one compares the ratio of

the pileup positrons to the observed positrons, it turns out to be the pileup fraction is 0.56% and 6.9% below and above 2.6 GeV respectively. The numbers on the table were obtained at 49.9 μs.

The vector sum of the pileup phases from the energy bands gives 2.789±0.003 rad which is in good agreement with the of 2.770±0.014 rad obtained from the fit of constructed pileup above 2.0 GeV. The vector sum was calculated from the proper addition of the phases below and above 2.6 GeV as follows :

$$\phi^{pu}(E > 2GeV) = \tan^{-1}\left[\frac{\sum_{i=1}^{2} N_i A_i \sin\phi_i}{\sum_{i=1}^{2} N_i A_i \cos\phi_i}\right] \tag{11}$$

where index i represents the two energy bins (E<2.6 GeV and E>2.6 GeV), A is the asymmetry (A_{pu}) and N is the number of pileup events in these energy bands (N_0^{pu}).

6.6.2 Systematic Due to Unseen Pileup

The systematic due to unseen pileup is determined from Bill Morse's writeup [13]. This study was based on assigning a systematic limit by looking at the asymmetry instability. To be conservative the maximum asymmetry change between 50 μs and 150 μs were taken into account for our calculations. These changes were determined to be 7.91 10^{-5} for 1999, 7.93 10^{-5} for 1999 including g-2 asymmetry modulation and 5.55 10^{-5} for the complete physics form. The statistical errors on the g-2 phase are 1.1 10^{-4}, 1.2 10^{-4} and 1.3 10^{-4} for 1999, 1999 including g-2 asymmetry modulation and the complete physics forms consecutively. From these values one can put a limit according to reference above as **0.08 ppm** for 1999 and 1999 including asymmetry modulation functional forms and **0.05 ppm** for the complete physics form.

7 The FITS

Data is fitted to 3 different functional forms. These functional forms are 1999 type, the 1999 function including the g-2 asymmetry modulation due to CBO and the complete physics function. The muon losses determined from three fold coincidence [4] for before and after the radial field was changed and they were properly statistically added and used in all the fitting functions. We will use a new name for the function covers the possible gain effects combined with the muon losses and call this function as residual slow term $\epsilon(t)$. This term includes a Gaussian term with $\approx$100 μs lifetime including the muon losses function :

$$\epsilon(t) \;=\; (\; A_l \; L(t) \;+\; A_r \; e^{-\frac{1}{2}(\frac{t}{\tau_r})^2}) \tag{12}$$

where L(t) is the muon losses time spectrum (given) and A_l, A_r and τ_r are the parameters going to be determined from the fits. Since these parameters are strongly correlated with each other the whole product with the proper evaluated error is going to be shown in most of the plots. However when we discuss the substructure of ϵ, these parameters are going to be referred individually. The R value is a measure of the precession frequency (f_a) and described as :

$$R\;(ppm) = \;bias \;+\; \frac{10^6\;(229.1\;kHz - f_a)}{229.1\;kHz} \tag{13}$$

7.1 The Fits with Energy Bins

It was preferred to study two different energy bins from the early stage of this analysis. The reason was many effects have different behavior and strength in different energy regions. For instance pileup has zero crossing around 2.6 GeV and for energies below 2.6 GeV, $D - S_1 - S_2$ is negative. The energy dependence of CBO gets much stronger above 2.6 GeV. The sensitivity to the gain effects is also larger in the higher energies. For those reasons the data was splitted into two major energy bins (E>2.6 GeV and E<2.6 GeV) and studied. Here we don't study the details of the systematics in these energy bins instead we will just try to see how the fitting functions can handle the situations like half ring effect and the residual slow terms in these different energy bands. The studies are done with only one random number seed and the run selection was used here was my original run selection which contains little more runs then Ernst's selection so the statistical error is slightly better. Three functional forms were used to study the size of the half ring effect in those energy bands mentioned. These functional forms are again 1999 type functional form, the 1999 functional form including the g-2 asymmetry modulation due to CBO (Rob effect) and the complete physics form including also g-2 phase modulation due to CBO (Jim effect) in addition to the g-2 asymmetry modulation. Let's start with 1999 type functional form.

7.1.1 1999 Functional Form on Energy Bins

The 1999 functional form including the residual slow effect ($\epsilon(t)$) is as follows :

$$F(t) = N_0\, e^{-t/\tau}\{1+Acos(2\pi f_a t+\phi_a)\}\,\{1+A_{cbo}E_{cbo}(t)cos(2\pi f_{cbo}t+\phi_{cbo})\}\,\{1+\epsilon(t)\} \quad (14)$$

where N_0 is normalization factor, τ the muon lifetime (fixed to 64.407 μs), A the g-2 asymmetry, f_a the g-2 precession frequency, ϕ_a the g-2 phase, A_{cbo} the CBO amplitude, $E_{cbo}(t)$ the determined CBO envelope, f_{cbo} is the CBO frequency and ϕ_{cbo} is the CBO phase. The studies showed that the CBO envelope has no observable energy dependence. For that reason the CBO envelope used for the fits in the different energy bins were the same.

Figure 51 shows the fit parameters of the individual detectors at 47.2 μs for $E < 2.6$ GeV and Figure 52 shows the one for $E > 2.6$. First observation from the bins is A_{cbo}(E>2.6 GeV) = $\approx$ 3.4 A_{cbo}(E<2.6 GeV). Since only one random seed was used we are not going to discuss about the goodness of the χ^2. Even though the average amplitude of the residual slow effect (ϵ) is similar in those energy bins, fluctuations are statistically much higher in the E>2.6 GeV case which may be the signature of the enhancement of the gain effects. The most deviated ones from the average are the ones that have the largest gain problems! If one looks at the ϵ for the E<2.6 GeV he can track the quad structure (Det 1->6 increases, 9->12 increases, 14->17 increases, 21->24 increases). The half ring effect is two times larger in the high energy (Figures 53-54).

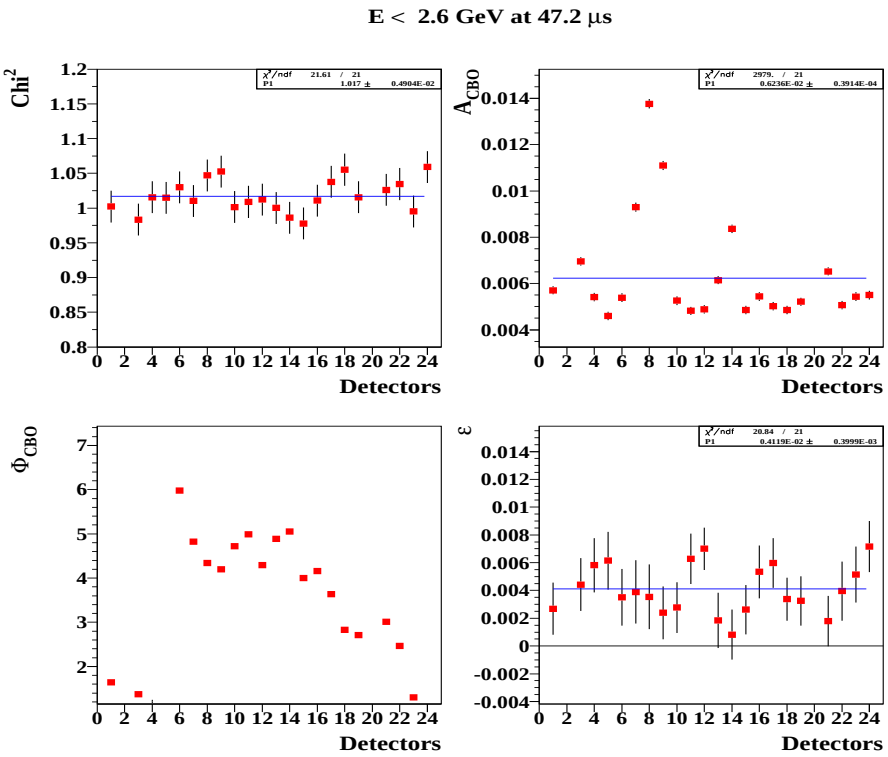

Figure 51 : Fit to 1999 functional form ($E < 2.6$) at 47.2 μs.

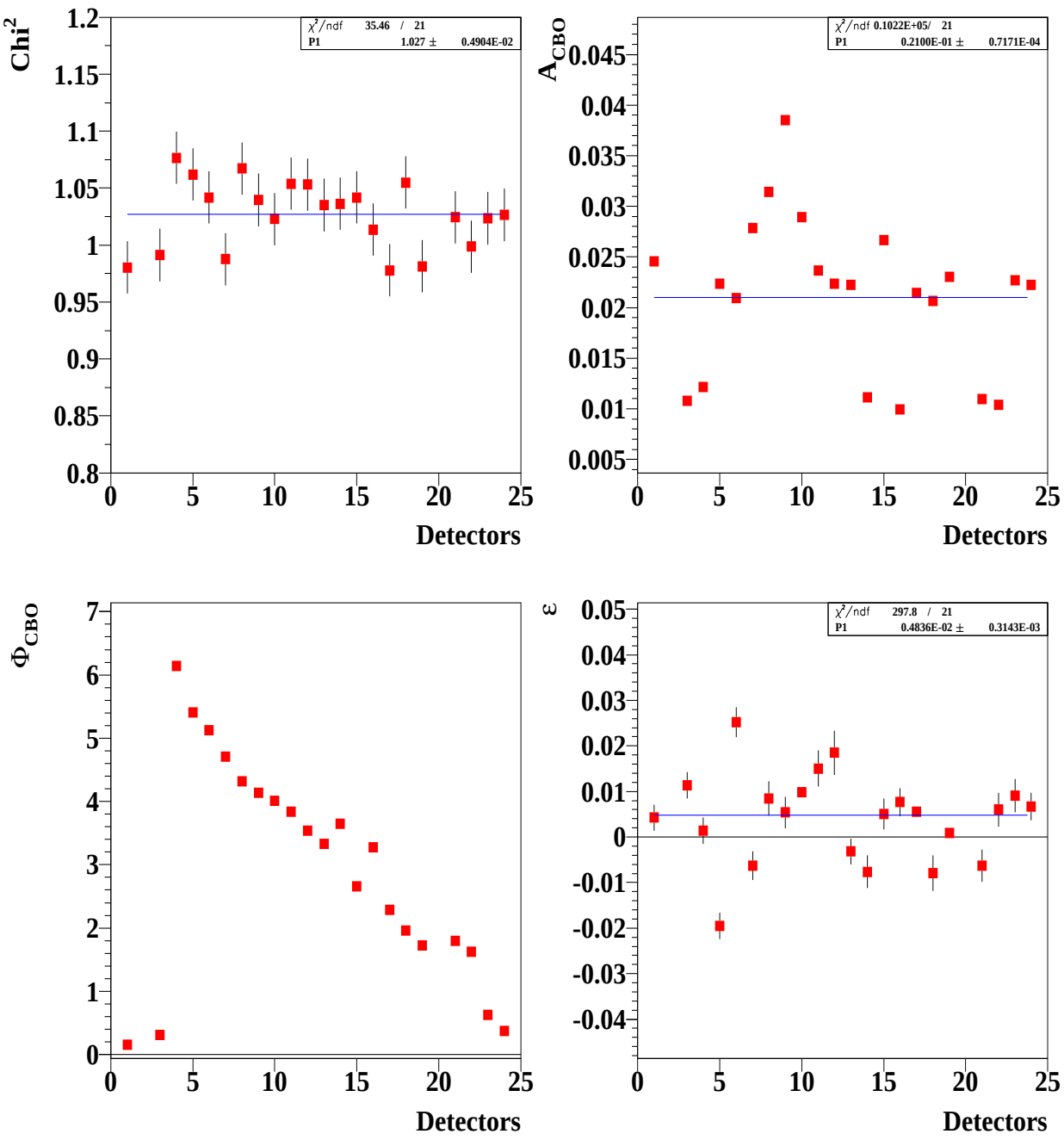

Figure 52 : Fit to 1999 functional form ($E > 2.6$) at 47.2 μs.

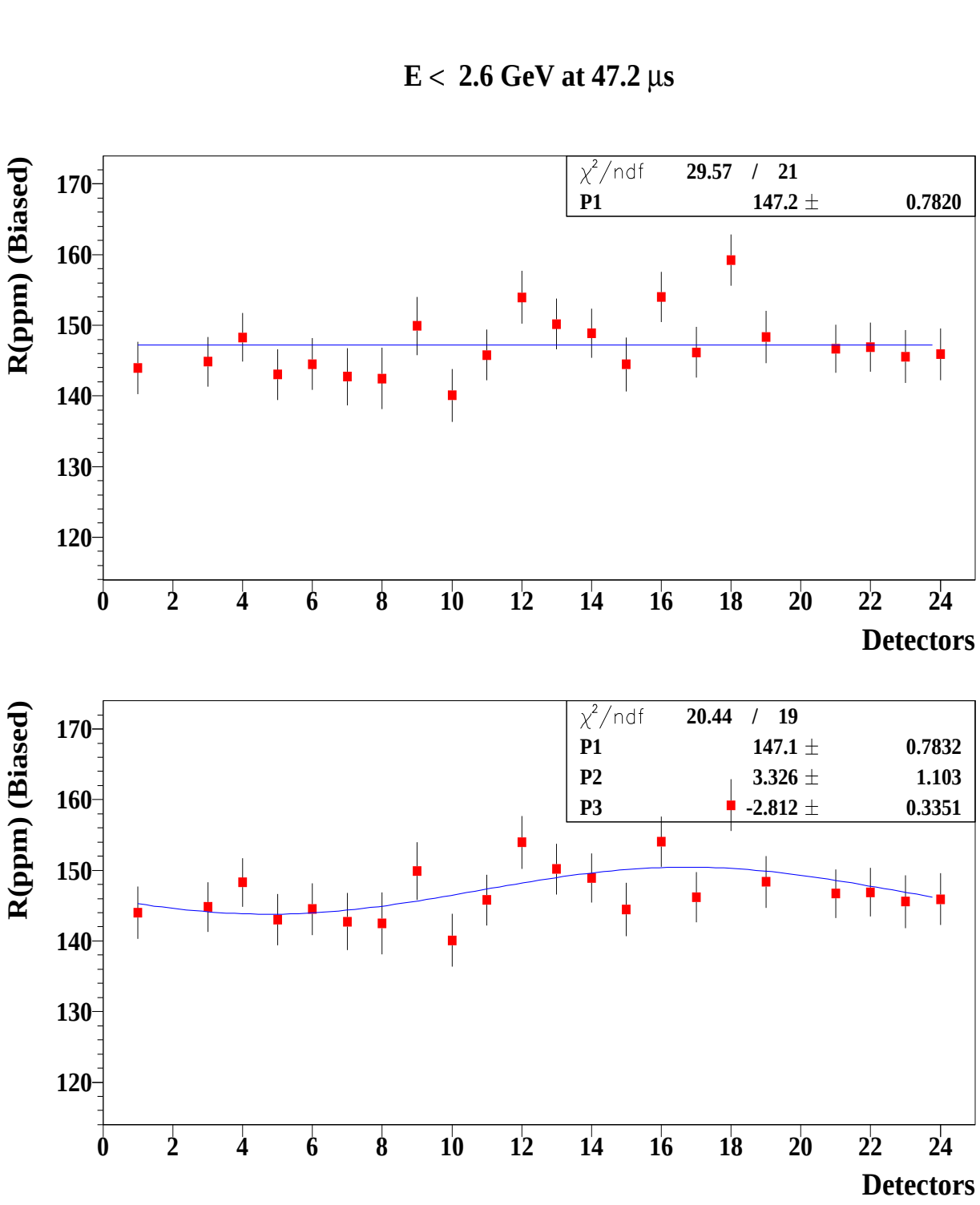

Figure 53 : Fit to 1999 functional form ($E < 2.6$) at 47.2 μs.

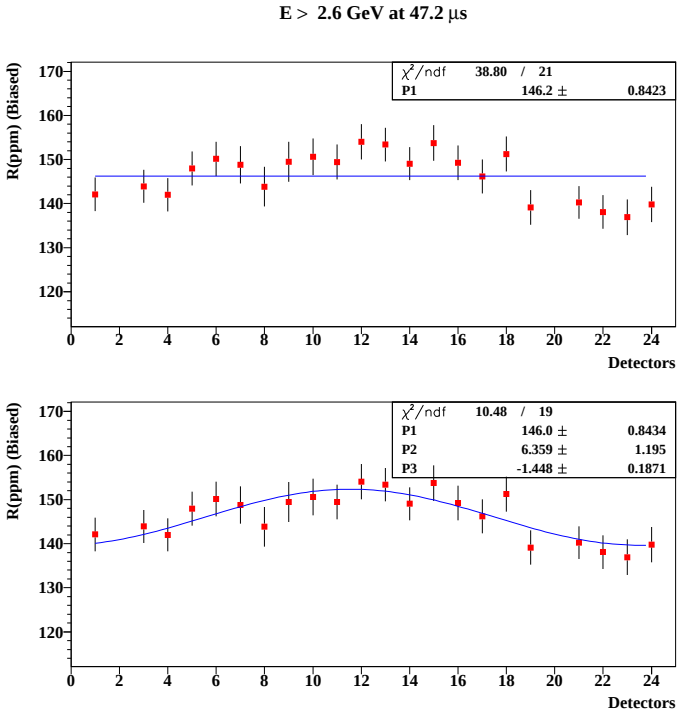

Figure 54 : Fit to 1999 functional form ($E > 2.6$) at 47.2 μs.

7.1.2 1999 Form with the g-2 Asymmetry Modulation Due to CBO on Energy Bins

We know that g-2 energy (asymmetry) is modulated by the CBO. This could be taken into account by introducing the CBO into the asymmetry parameter with an amplitude and a phase as follows :

$$F(t) = N_0 e^{-t/\tau}\{1+A_m cos(2\pi f_a t+\phi_a)\}\ \{1+A_{cbo}E_{cbo}(t)cos(2\pi f_{cbo}t+\phi_{cbo})\}\ \{1+\epsilon(t)\} \quad (15)$$

where $A_m = A\ (1 + A_{Rb}\ E_{cbo}(t)\ cos(2\pi f_{cbo}t + \phi_{Rb})$ known as g-2 asymmetry modulation due to CBO. Here A_{Rb} is the amplitude and ϕ_{Rb} is the phase of this modulation assuming these oscillations have the same time dependence $(E_{cbo}(t))$ as regular CBO.

Figures 55-58 show the fit parameters and R values for individual detectors at 47.2 μs for two energy bins.

The conclusions from these plots are as follows. The g-2 asymmetry modulation amplitude is more consistent between the individual detectors in the high energy bin. On the other hand the phase behavior of this effect is more straightforward in the low energy band. In the low energy band, half ring effect is reduced almost three times whereas in the high energy band only 25% by switching from 99 form to this functional form.

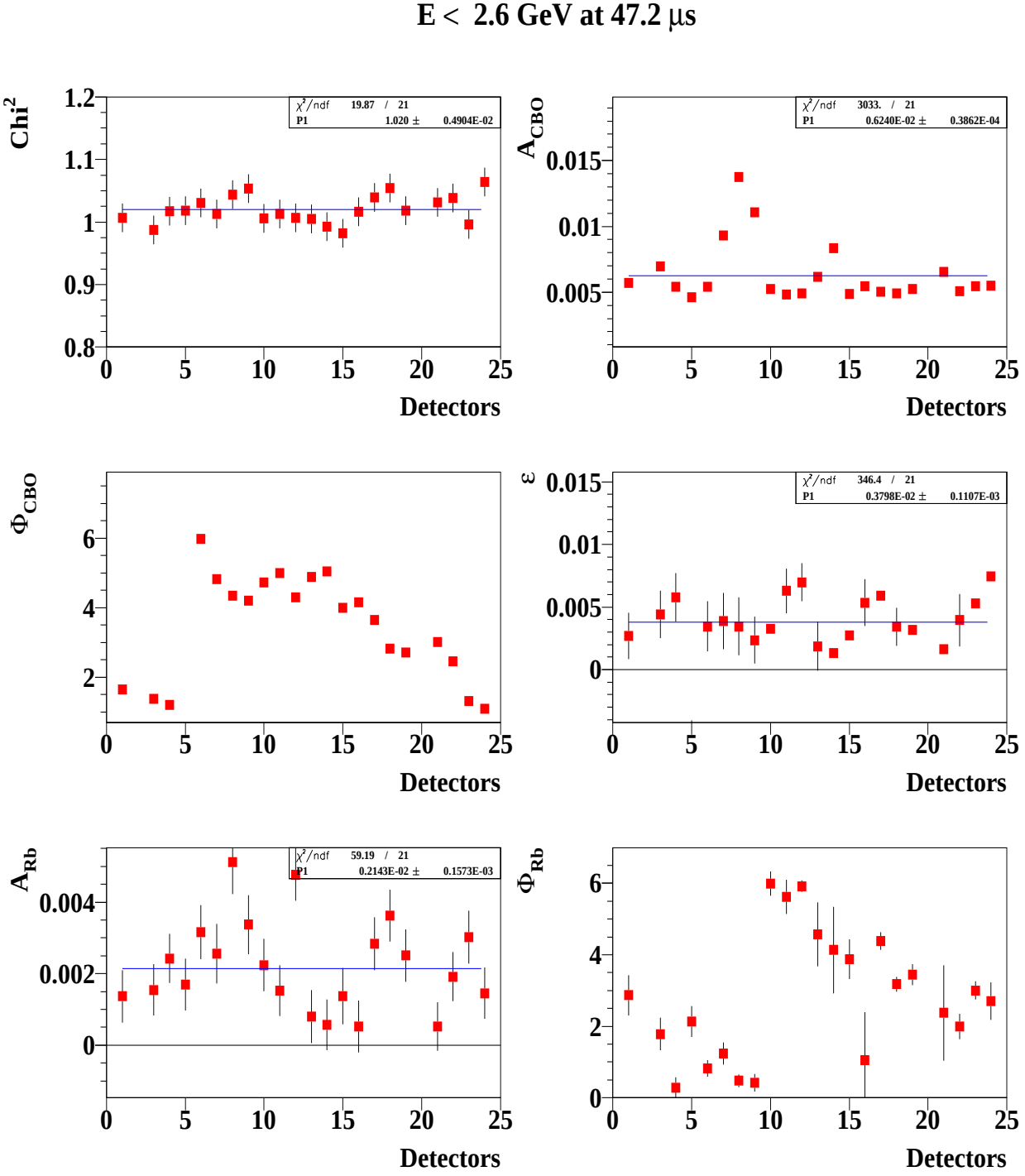

Figure 55 : Fit to 1999 functional form ($E < 2.6$) at 47.2 μs.

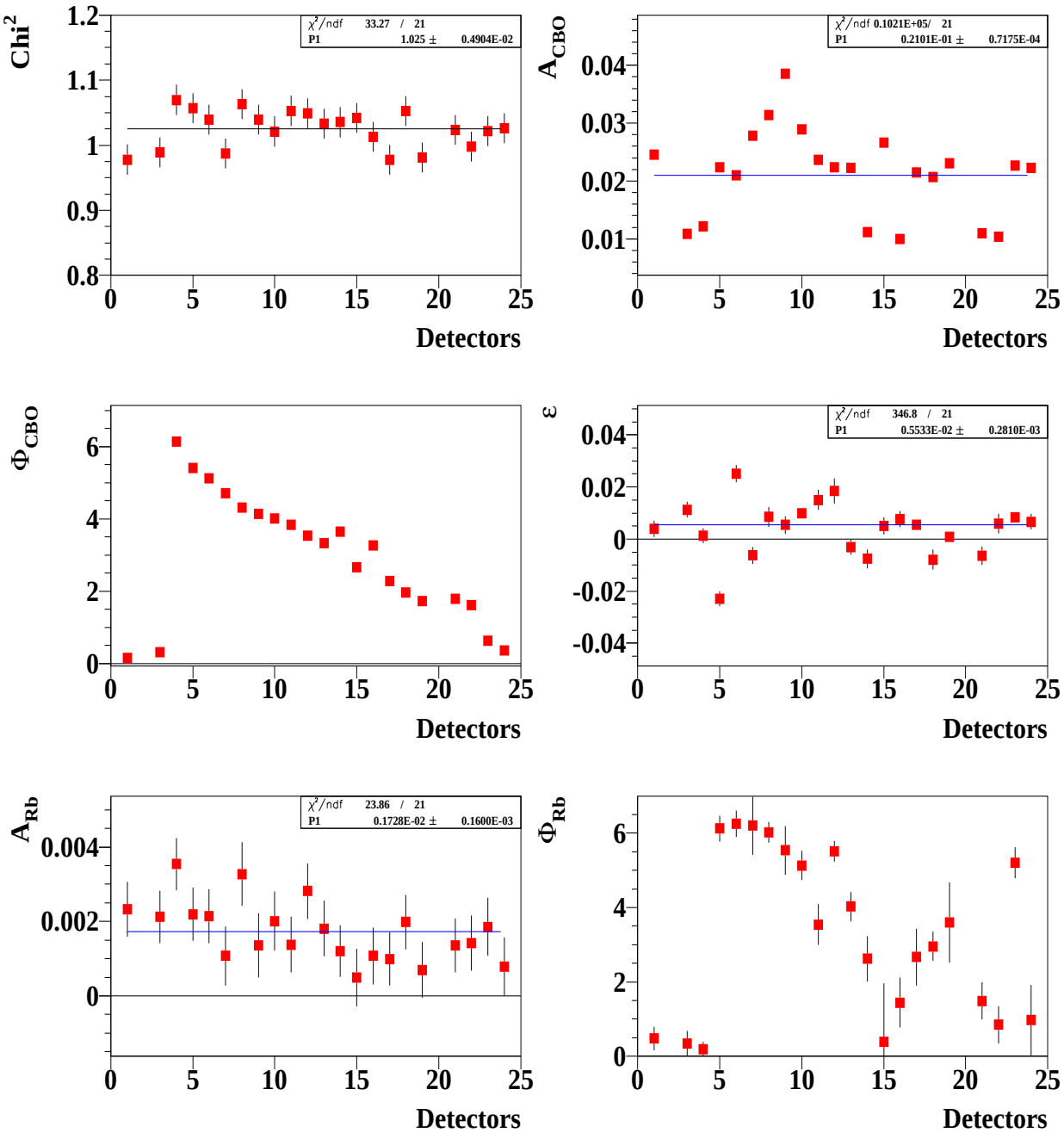

Figure 56 : Fit to the 1999 form including the g-2 asymmetry modulation (ala Rob effect) ($E > 2.6$) at 47.2 μs. There are some detectors with $A_r = 0$. The error for the ϵ product is smaller for those detectors.

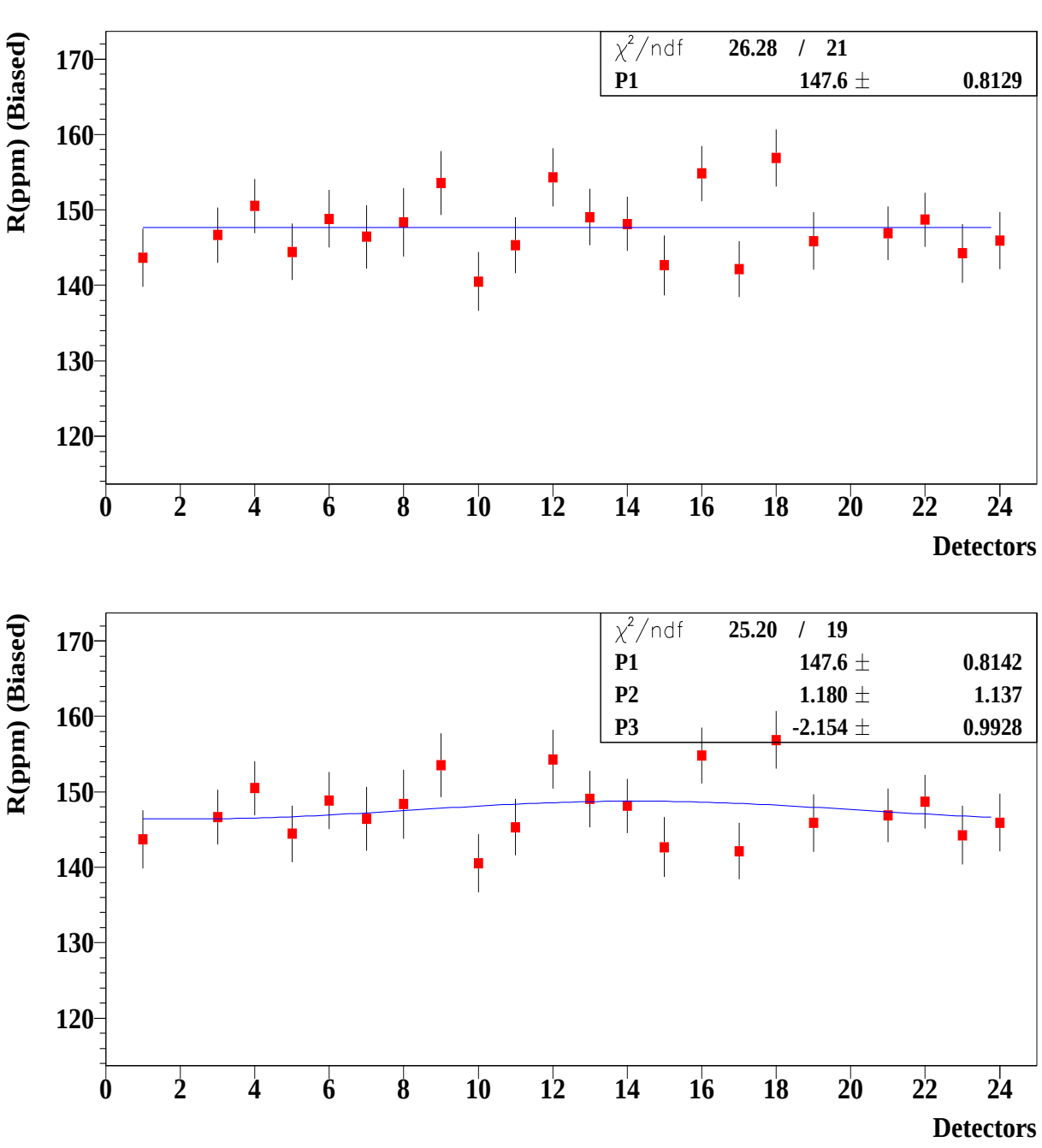

Figure 57 : Fit to the 1999 form including the g-2 asymmetry modulation (ala Rob effect) ($E < 2.6$) at 47.2 μs.

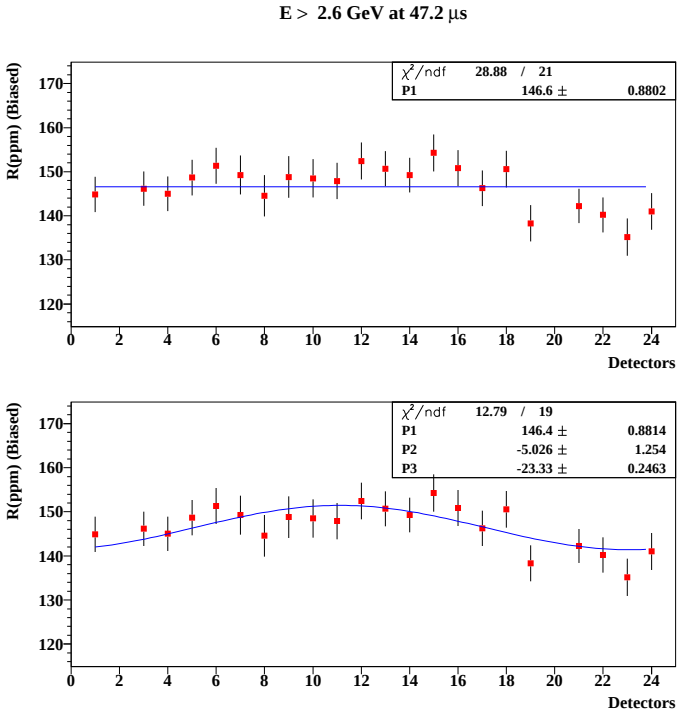

Figure 58 : Fit to the 1999 form including the g-2 asymmetry modulation ($E > 2.6$) at 47.2 μs.

7.1.3 The complete Physics Form on Energy Bins

Including the g-2 phase modulation due to CBO, the complete physics functional form becomes :

$$F(t) = N_0 e^{-t/\tau}\{1+A_m cos(2\pi f_a t+\phi_m)\}\ \{1+A_{cbo}E_{cbo}(t)cos(2\pi f_{cbo}t+\phi_{cbo})\}\ \{1+\epsilon(t)\} \quad (16)$$

where $\phi_m = \phi_a + A_{Jm}E_{cbo}cos(2\pi f_{cbo}t + \phi_{Jm})$ known as g-2 phase modulation due to CBO. Here A_{Jm} is the amplitude of the phase modulation and ϕ_{Jm} is the phase of the phase modulation.

Figure 59-62 shows the fit parameters and the R values of individual detectors at 47.2 μs for two energy bins. Both A_{Rb} and A_{Jm} amplitudes fluctuate more in the first half of the ring and higher for the energies greater than 2.6 GeV. The half ring effect looks like removed completely for the energies less than 2.6 GeV and still 1.9σ effect left in the high energy band.

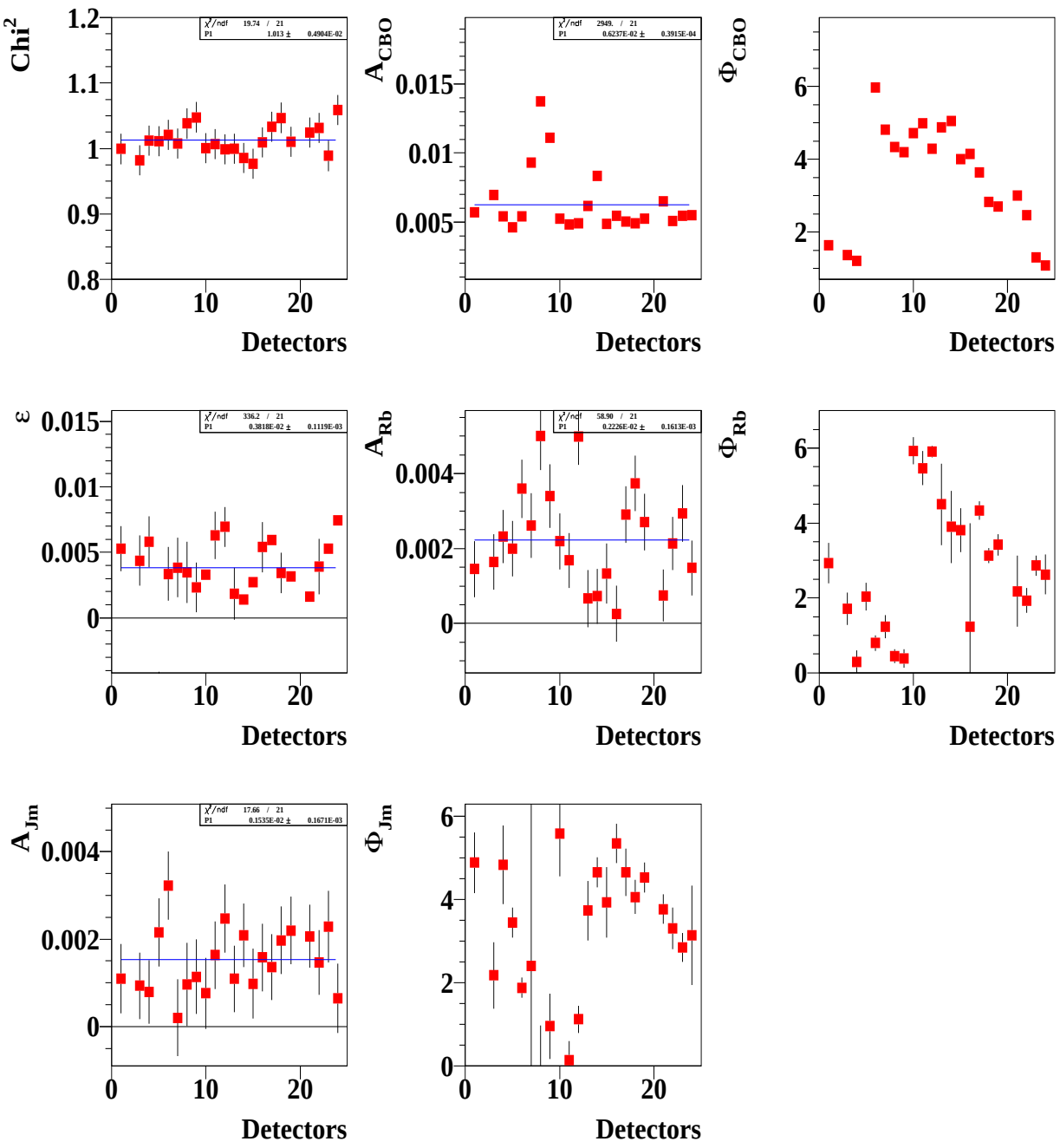

Figure 59 : Fit to the complete physics form ($E < 2.6$) at 47.2 μs.

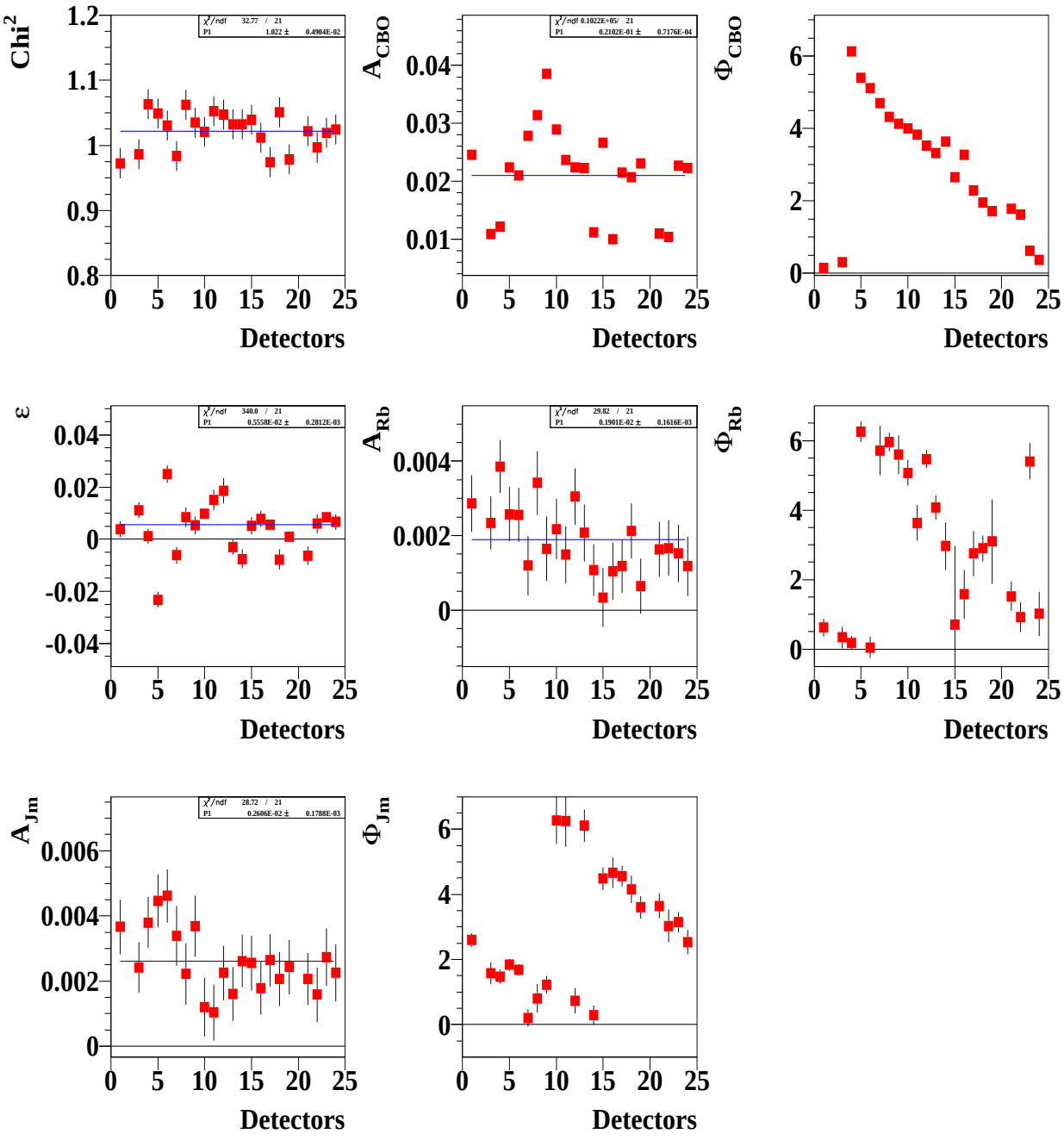

Figure 60 : Fit to the complete physics form ($E > 2.6$) at 47.2 μs.

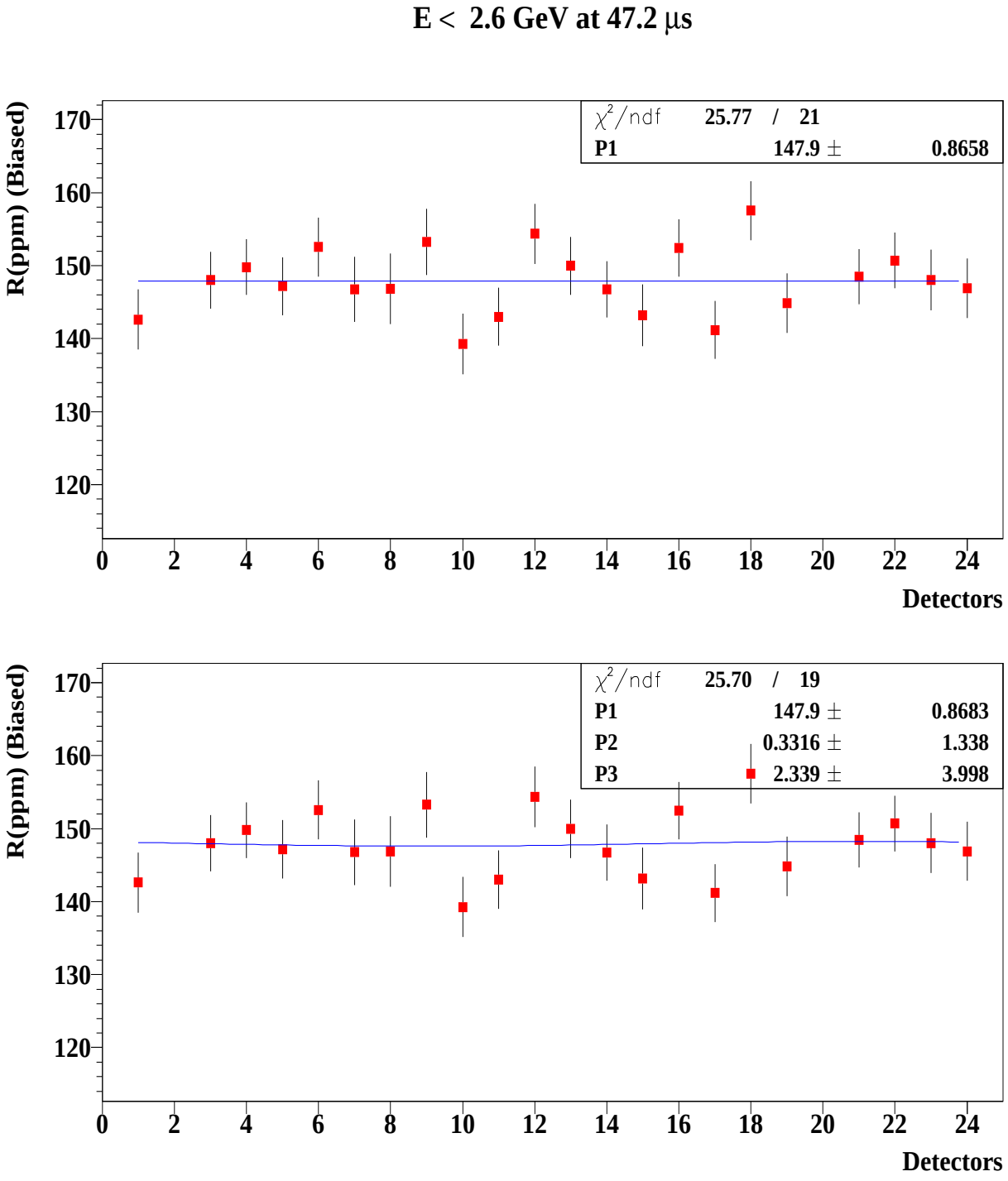

Figure 61 : Fit to the complete physics form ($E < 2.6$) at 47.2 μs.

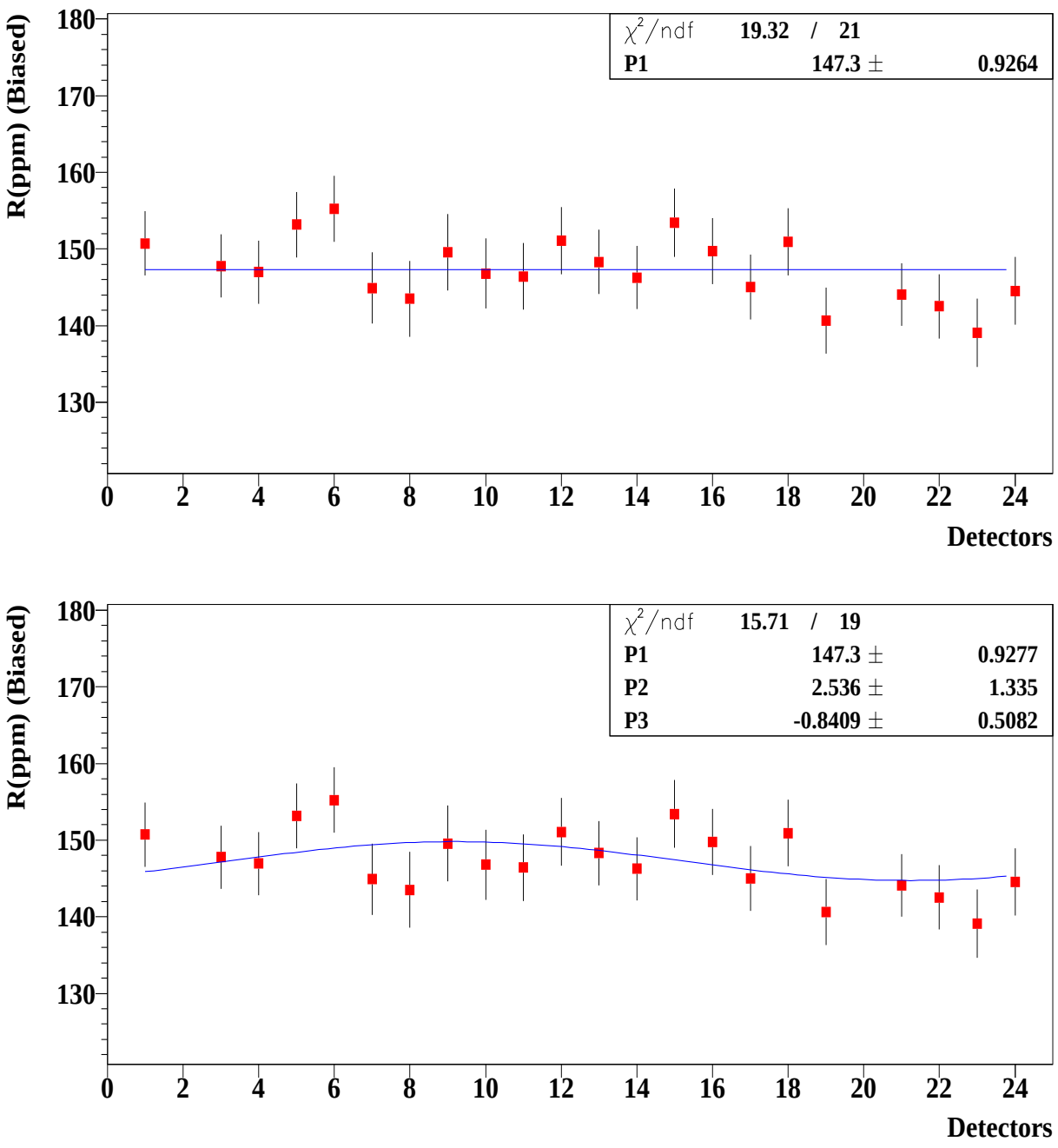

Figure 62 : Fit to the complete physics form ($E > 2.6$) at 47.2 μs.

Table 9 shows the comparison of some parameters for different functional forms and energy bands. CBO amplitude is rock solid and does not change from one functional form to the other. Asymmetry modulation amplitude is 24% higher in the low energy band (E<2.6

GeV) than the high energy band (E>2.6 GeV) . On the other hand the phase modulation amplitude is 45% higher in the high energy band. In 1999 functional form, the average of the residual slow term ϵ statistically consistent in two energy bands and it is not when the asymmetry modulation was introduced in to the functional form. This also shows the cross correlations between residual slow term and A_{Rb} and/or A_{Jm}. In all the functional forms the agreement on R values for the low and the high energy bands are excellent. However the value changes by 0.71 ppm from 1999 functional to the complete physics form for E<2.6 GeV and 1.11 ppm for E>2.6 GeV. For 1999 functional form, the half ring effect at high energy band almost two times larger than the half ring effect at low energy band. Including asymmetry modulation to the functional form one can remove the half ring effect to the level of one sigma in the low energy band. However it only makes only a small improvement (20%) in the high energy band. Including the g-2 phase modulation to the functional form reduces the half ring effect to two sigma level in the high energy band. The differences between the R values obtained from the linear and sinusoidal fits are strongly depend on the size of the half ring effect. For instance, 0.08 ppm (1999 form), 0.05 ppm (with g-2 asymmetry modulation) and 0.01 ppm (physics form) for energies less than 2.6 GeV. For energies greater than 2.6 GeV they are 0.22 ppm (1999 form), 0.17 ppm (with g-2 asymmetry modulation), and 0.06 ppm (the complete physics form).

Table 9: Comparison table of the different functions and energy bins

Parameters	1999 Form		Only Asymmetry Mod.		Complete Physics	
	E <2.6GeV	E >2.6GeV	E <2.6GeV	E >2.6GeV	E <2.6GeV	E >2.6GeV
χ^2	1.017	1.027	1.020	1.025	1.013	1.022
$A_{cbo} \times 10^3$	6.24±0.04	21.0±0.07	6.24±0.04	21.0±0.07	6.24±0.04	21.0±0.07
$A_{rob} \times 10^3$	-	-	2.14±0.16	1.73±0.16	2.23±0.16	1.90±0.16
$A_{Jm} \times 10^3$	-	-	-	-	1.54±0.17	2.60±0.18
$\epsilon \times 10^3$	4.12±0.40	4.84±0.30	3.80±0.10	5.53±0.30	3.82±0.11	5.56±0.30
R^{linear}(ppm)	147.20±0.78	146.22±0.84	147.64±0.81	146.60±0.88	147.91 ± 0.87	147.33 ± 0.93
R^{sine}(ppm)	147.12±0.78	146.00±0.84	147.59±0.81	146.43±0.88	147.92 ± 0.87	147.27 ± 0.93
Half Ring(ppm)	3.33±1.10	6.36±1.20	1.18±1.14	5.03±1.25	0.33±1.34	2.54 ± 1.34

7.2 Conventional Fits

Time spectra were constructed with 149.2105 ns bin width. This is not exactly the fast rotation period. Fast rotation period is 149.198 ns for the average beam center of 7.1146 m. Time of the positrons were randomized around the fast rotation period in order to cancel the fast rotation signal. This process were done for each fill and for each detector using 10 random seeds obtained from CERNLIB function "runlux" with luxury level four. The seeds were initialized from the date-time information of the operating system to make sure they are different.

The fits were performed with three functional forms for each detector and for each random number sets. In order to observe the size of the half ring effect, the first half (1-12) and the second half (13-24) detectors were combined together and fitted separately. Also all

the detectors were combined together and fitted. The time sweep of the fits started from 49.9 μs and ended around 150 μs. Upto 60 μs small fit steps were used ($\approx$0.5μs) in order to see if there is any g-2 phase pulling at early times and after that the fits were continued with coarser steps of $\approx$1.5μs. To give a number total 31860 fits performed for each functional form. After the fits were obtained for each random seeds they were statistically averaged. The plots show the average values for the parameters for 10 random seeds.

CBO frequency determined from the minimization of the χ^2 in the fits as 465.70 kHz and fixed all the time. The Gaussian component of the ϵ was also determined at the first point of the fits and fixed all the time. On the other hand the amplitude of the muon losses was left always float. The stability of this amplitude (A_L) is the signature of how well gain related residual slow terms were handled.

Muon lifetime was also fixed all the time to the value of 64.407 μs which was determined from the average of the radial distribution of the fast rotation Fourier analysis.

7.2.1 Conventional Fits with 1999 Functional Form

1999 functional form is the simplest functional form among those we are dealing with. This functional form as one remember contains five parameters ideal case and multiplicative CBO functional form including the residual slow term (ϵ).

Total number of free parameters comes out to be seven in this functional form. Muon lifetime τ, CBO envelope, CBO frequency (f_{cbo}), muon losses time spectrum $L(t)$ and Gaussian component of ϵ (2 parameters) were fixed in the fits.

The 1999 type functional form is ;

$$F(t) = N_0 e^{-t/\tau_\mu}\{1+Acos(2\pi(f_0-f_a)t+\phi_a)\}\{1+A_{cbo}E_{cbo}(t)cos(2\pi f_{cbo}t+\phi_{cbo})\}\ \{1+\epsilon(t)\}$$

where $\epsilon(t) = A_l\mathbf{L(t)} + \mathbf{A_r}e^{-\frac{1}{2}(\frac{t}{\tau_\mathbf{r}})^2}$ and $f_0 = 220.1$ kHz

First lets look at the first, the second half of the ring and all detectors together with the 1999 functional form (Figures 63-65).

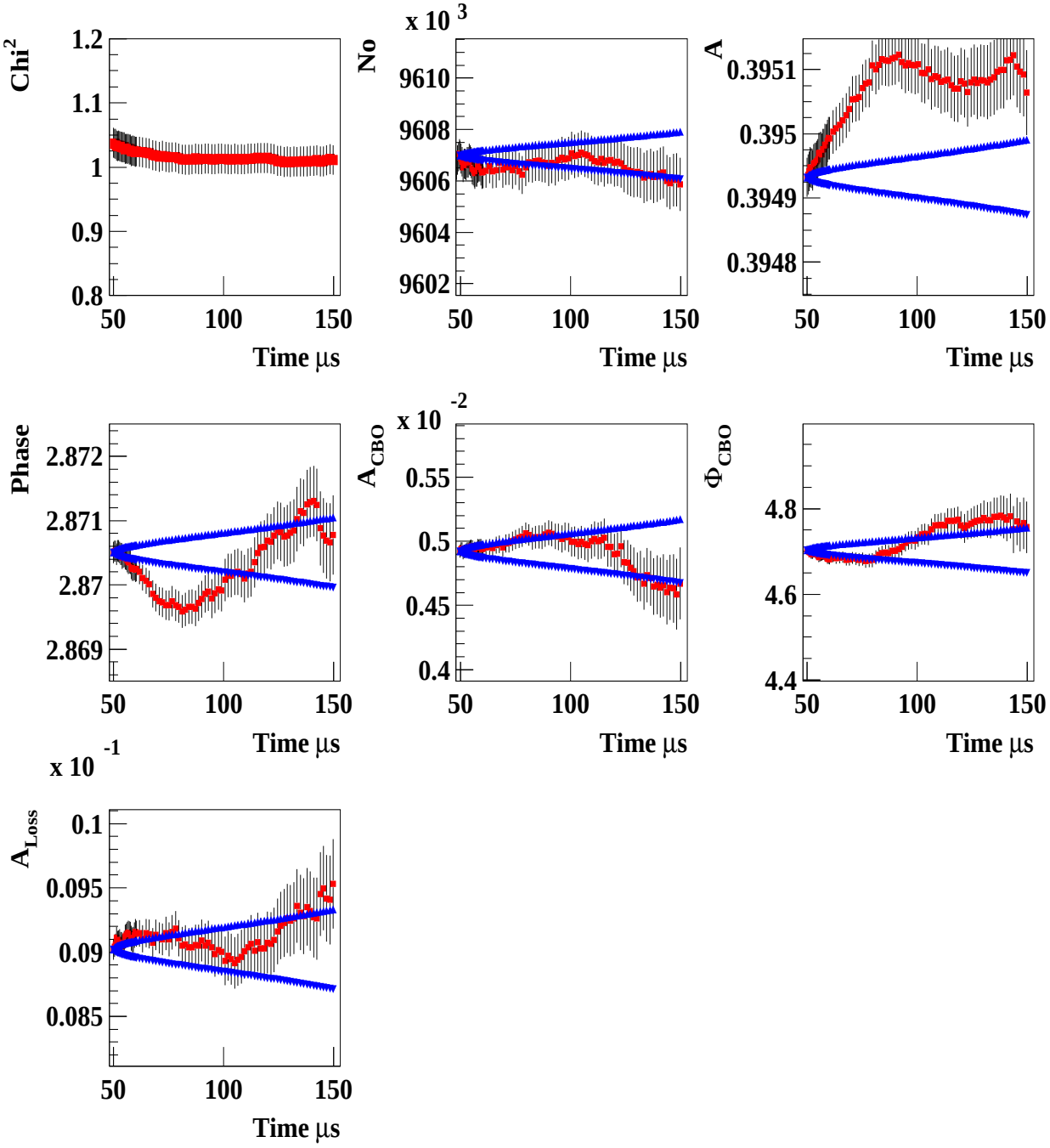

Figure 63 : Fit parameters with 1999 functional form on the first half.

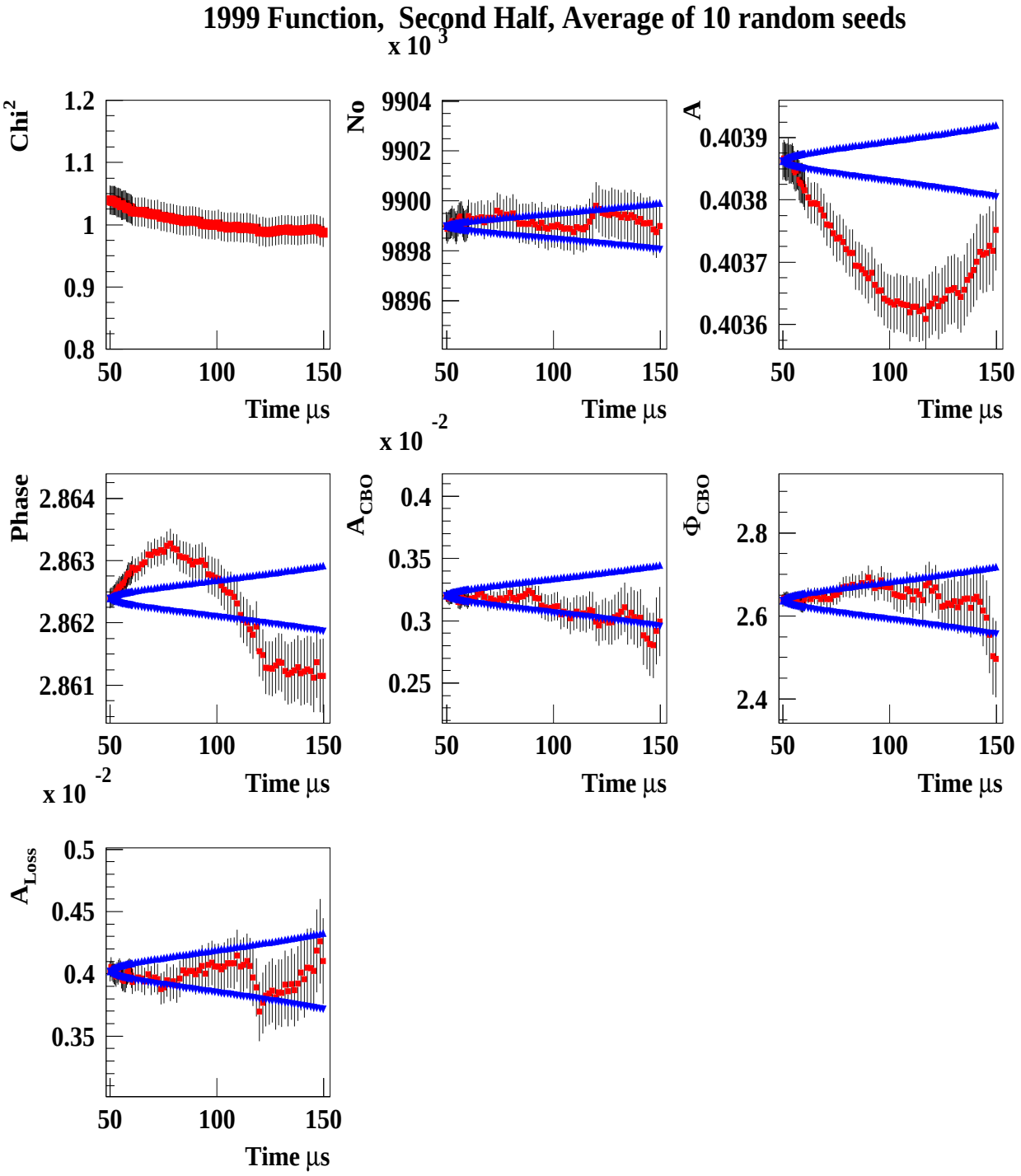

Figure 64 : Fit parameters with 1999 functional form on the second half.

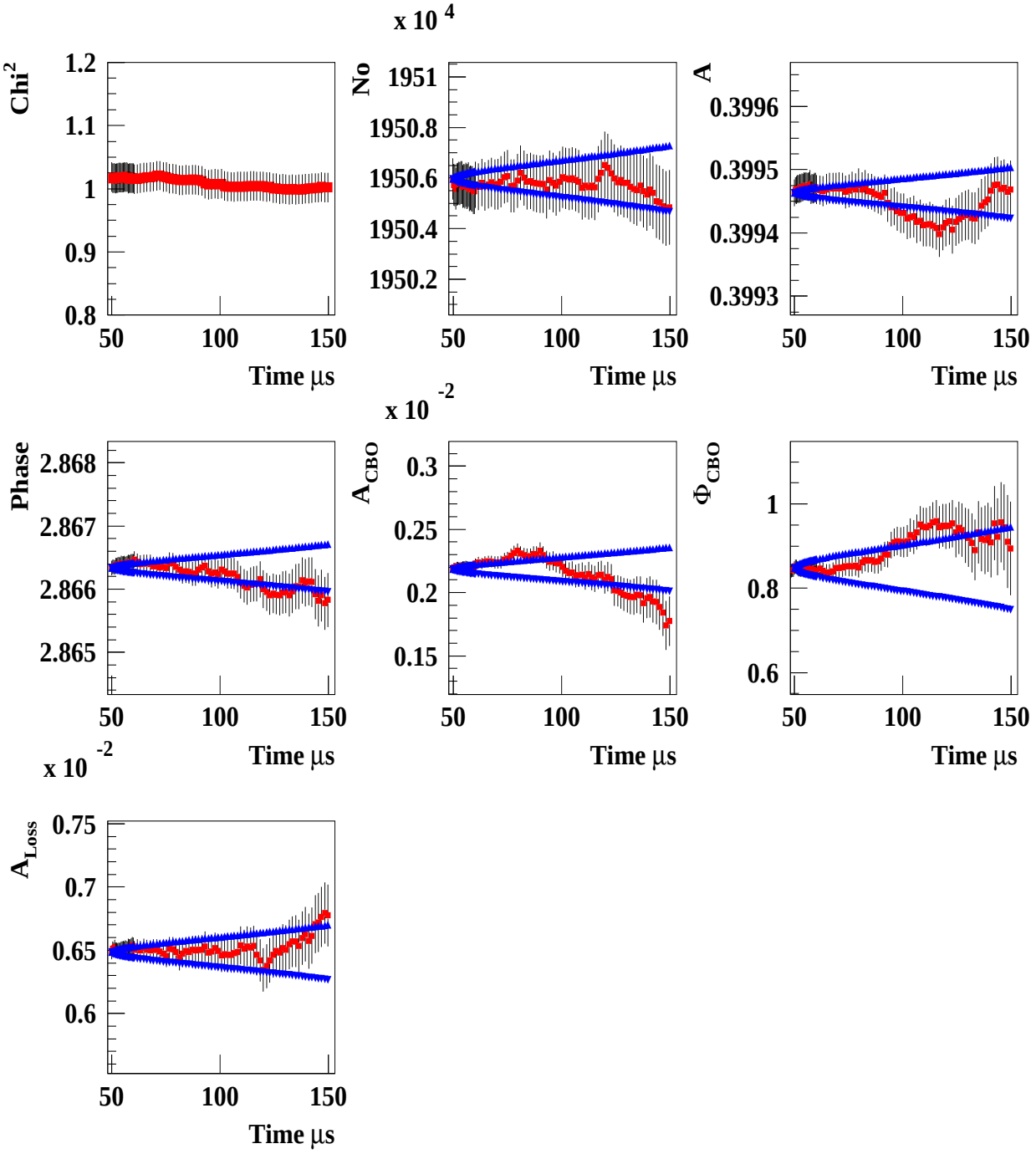

Figure 65 : Fit parameters with 1999 functional form all detectors together.

The asymmetries from both halves go completely out Kawall bands. When we look at the asymmetry of both halves (Figures 63 and 64) they are not exactly symmetric. We know that the gain, unseen pileup and the CBO related effects (g-2 asymmetry modulation and the phase modulation due to CBO) change the asymmetry. We also know that the gain effect in the first half has different shape than the second half. On the other hand in the first order CBO related effects should be the same in both halves since we believe g-2 phase and asymmetry have small dependence on kicker detectors. For that reason the shape difference between the asymmetries in the first and in the second halves are mostly the gain related and when the detectors were combined the stability does not become perfect (Figure 65). Stability on A_{cbo} is very similar with the MC simulation fit results for the combination of different n values.

In addition to the asymmetries, g-2 phase have oscillating behavior which is mostly related with the half ring effect. Hence when the detectors were combined, the half ring effect cancels to high degree and the phase becomes much more stable. The correlation between the g-2 phase and precession frequency is almost 100%. For that reason the picture one sees in the phase is the same as R. Figures 66-68 show the stability of R in the first half, second half and all detectors together for the 1999 functional form.

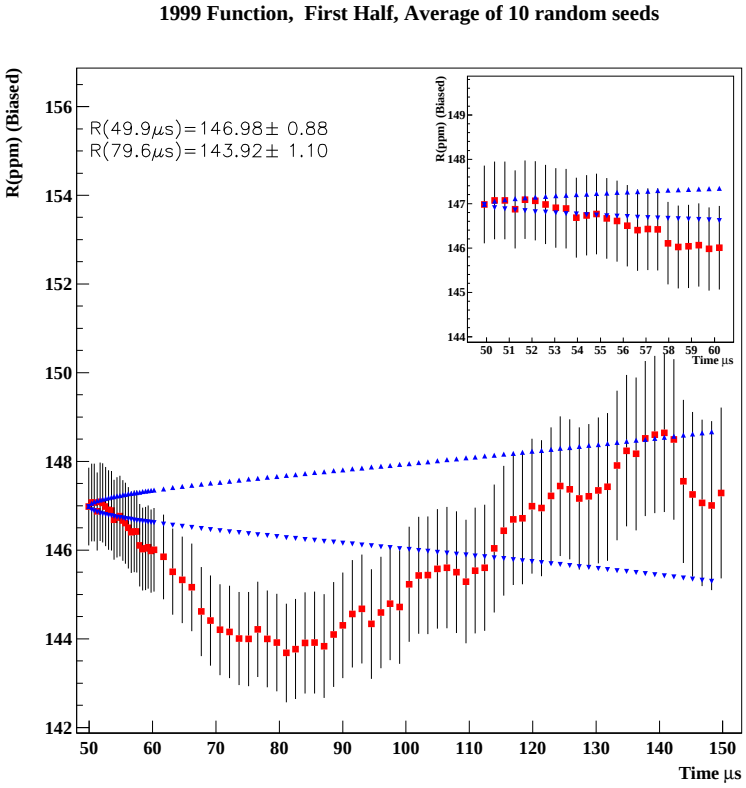

Figure 66 : The stability of R with 1999 functional form for the first half.

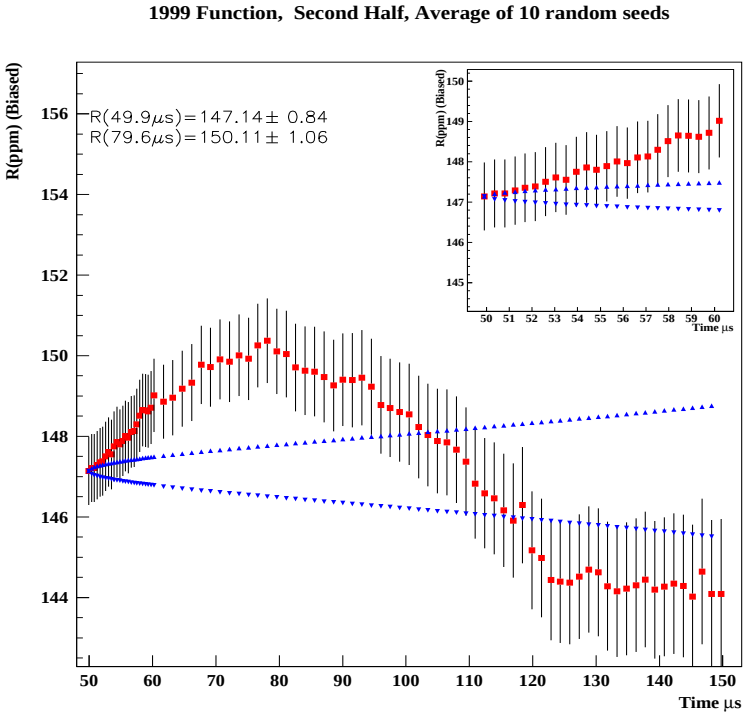

Figure 67 : The stability of R with 1999 functional form for the second half.

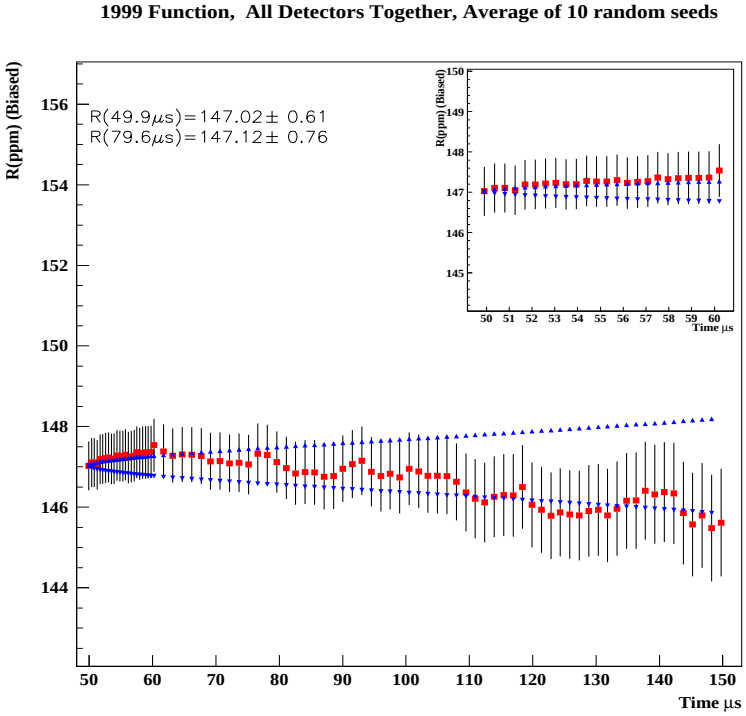

Figure 68 : The stability of R with 1999 functional form for all detectors together.

Table 10: χ^2 and R values for 10 random seeds for 1999 functional form obtained at 49.9 μs.

Random Seed	χ^2	R(ppm)
1	1.027	147.07
2	1.000	146.99
3	1.004	146.92
4	1.012	147.14
5	1.011	146.99
6	1.031	146.93
7	0.973	147.04
8	1.042	147.13
9	1.043	147.02
10	1.040	146.99
Average	**1.018**	**147.02**
RMS	**0.021**	**0.072**

One can see from the table that if one is lucky he can get excellent χ^2 depending on the seed. This is not new, we know that from previous experiences. However for the realistic comparison between the analyzers, average over many random seeds is necessary. For 1999 form we will assign $0.072/\sqrt{(10)} = 0.023$ ppm systematic error due to randomization since we used the average of 10 random seeds.

The real muon losses amplitude inside the ϵ term was determined two different ways. For quiet side of the ring (detectors 14-24) A_L's were averaged from 10 detectors. This number is turned out to be 0.0044 with the RMS of 0.0017. If we look at the detectors where the Gaussian part of the residual slow term amplitude A_r is zero (detectors 1,10 and 24), this number is 0.0042$\pm$0.0014 in the average. Since the muon losses term consist from $A_L \times L(t)$, the real losses let's say at 45 μs is going to be 0.0044$\times$L(t=45)=0.54%. L(t) can be slightly different between the analyzers depending on the relative normalization of the losses spectrum. However the $A_L \times L(t)$ should be the same at given time. The spread on the detectors for the A_L is much larger when the detectors have large gain effects. For that reason, the first half is not useful. The Gaussian lifetime of the other slow component (not muon losses) is 114$\pm$60 μs. This number is considerably different in the detectors like 4 and 7 which have relatively funny gain shapes.

Individual detectors were fitted with 1999 functional form for ten different seeds with the start time sweep between 49.9 and 150 μs. The following plots show the parameters at 49.9 (Figure 69) and 82.6 (Figure 70) μs. We also show the R vs detectors for those times in figures 71 and 72.

Table 11 shows the comparison of some fit parameters between the first and the second halves at 49.9 μs.

Table 11: The comparison of some parameters with the 1999 functional form @ 50 μs.

Parameters	First Half		Second Half		All Detectors	
A	0.39493	±3.0473E-05	0.40386	±2.9912E-05	0.39946	±2.1347E-05
Φ_a (rad)	2.8705	±1.6584E-04	2.8624	±1.5961E-04	2.8663	±1.1499E-04
A_{cbo}	4.9378E-03	±4.9943E-05	3.2039E-03	±4.9508E-05	2.1865E-03	±3.5011E-05
Φ_{cbo}(rad)	4.7030	±1.0163E-02	2.6345	±1.5330E-02	3.9909	±1.6123E-02
$\epsilon(A_L)$	8.4690E-03	±3.9179E-04	4.1347E-03	±3.8654E-04	6.2700E-03	±2.7514E-04
$\epsilon(A_r)$	-7.4633E-03	±4.2231E-04	-1.9956E-03	±4.1639E-04	-4.6890E-03	±2.9652E-04
$\epsilon(\tau_r)(\mu s)$	100.39	±1.8531	100.36	±6.9494	100.38	±2.0790

The correlation matrix gives the correct information when the functional form is 100% accurate. In our situation we still don't know how accurate our functional form is. There are still some unresolved issues like if CBO has a width effect, and/or if the asymmetry and the phase modulations have different envelopes. For that reason the correlation matrix does not give the exact information. However in order to give an idea, the correlation matrix's, the standard output of MINUIT, are going to be given for each functional forms at 49.9 μs. Table 12 shows the correlation matrix for 1999 functional form at 49.9 μs.

Table 12: Correlation matrix for 1999 functional form

	Total	N_0	A	R	Φ_a	A_{cbo}	Φ_{cbo}	$\epsilon(A_L)$	$\epsilon(A_r)$	$\epsilon(\tau_r)$
N_0	0.97930	1.000	0.008	-0.007	-0.009	-0.009	-0.007	**-0.481**	**0.321**	**0.837**
A	0.03663	0.008	1.000	-0.002	-0.003	0.006	0.012	-0.027	0.024	-0.003
R	0.87346	-0.007	-0.002	1.000	**0.873**	0.017	0.003	0.024	-0.022	0.004
Φ_a	0.87360	-0.009	-0.003	**0.873**	1.000	0.024	0.004	0.033	-0.030	0.005
A_{cbo}	0.04519	-0.009	0.006	0.017	0.024	1.000	0.004	0.030	-0.028	0.004
Φ_{cbo}	0.03444	-0.007	0.012	0.003	0.004	0.004	1.000	0.025	-0.023	0.003
$\epsilon(A_L)$	0.99691	**-0.481**	-0.027	0.024	0.033	0.030	0.025	1.000	**-0.975**	**-0.288**
$\epsilon(A_r)$	0.99623	**0.321**	0.024	-0.022	-0.030	-0.028	-0.023	**-0.975**	1.000	**0.208**
$\epsilon(\tau_r)$	0.94792	**0.837**	-0.003	0.004	0.005	0.004	0.003	**-0.288**	**0.208**	1.000

Table 13 shows the value of R in the case of linear and sinusoidal fit applied in addition to the half ring effect. As one predicts the size of the half ring effect stays the same but statistical significance of it gets smaller at late times.

Table 13: Comparison of the R values at 49.9 and 82.6 μ s.

Time	49.9 μs		82.6 μs	
	R (ppm)	χ^2/DOF	R (ppm)	χ^2/DOF
Linear Fit	147.18±0.61	46.2/21	146.90±0.78	38.9/21
Sine Wave Fit	147.02±0.61	23.6/19	146.88±0.78	25.0/19
Half Ring Effect(ppm)	4.06±0.86		4.15±1.12	

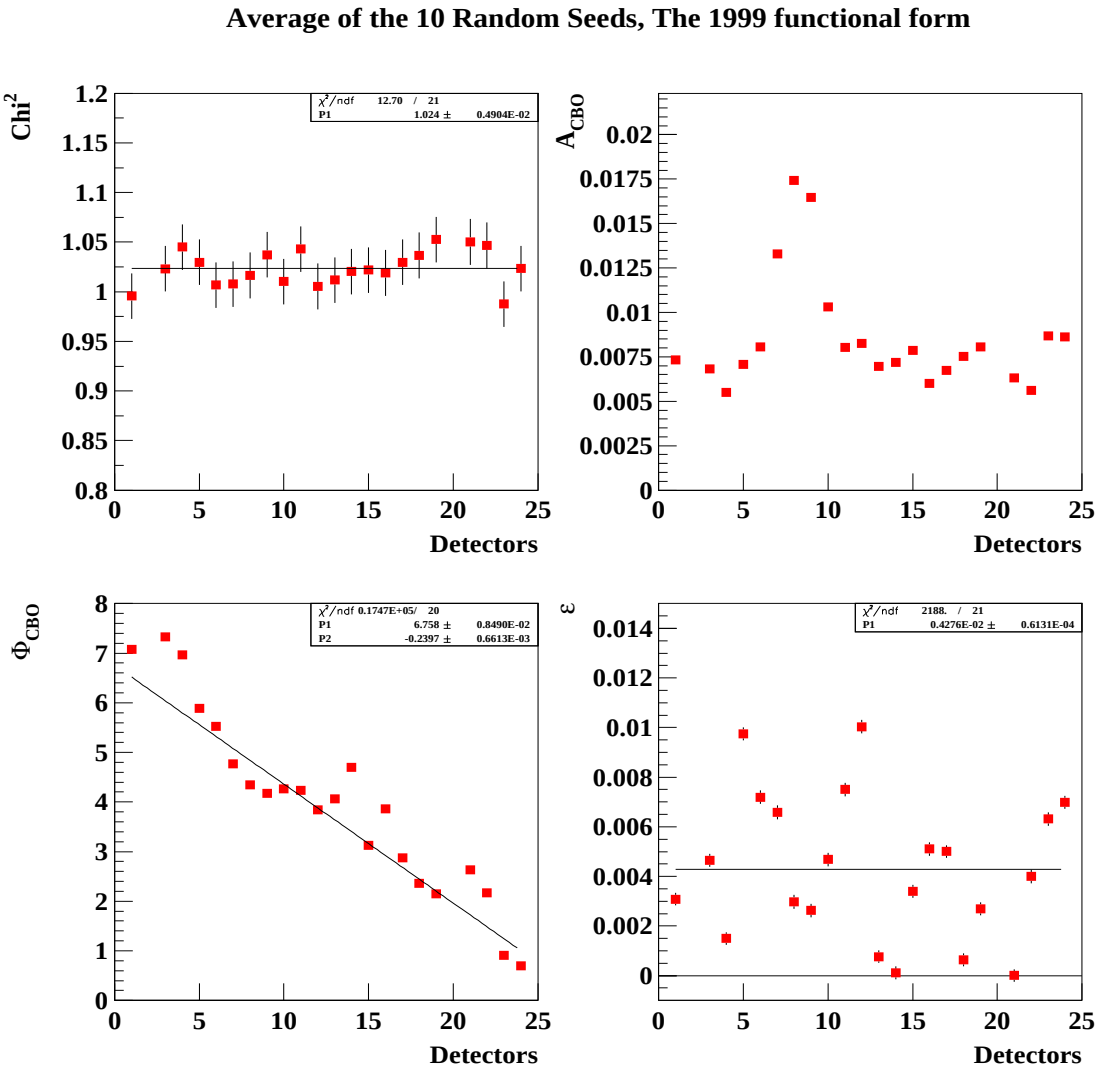

Figure 69 : Fit parameters at 49.9 μs for 1999 functional form.

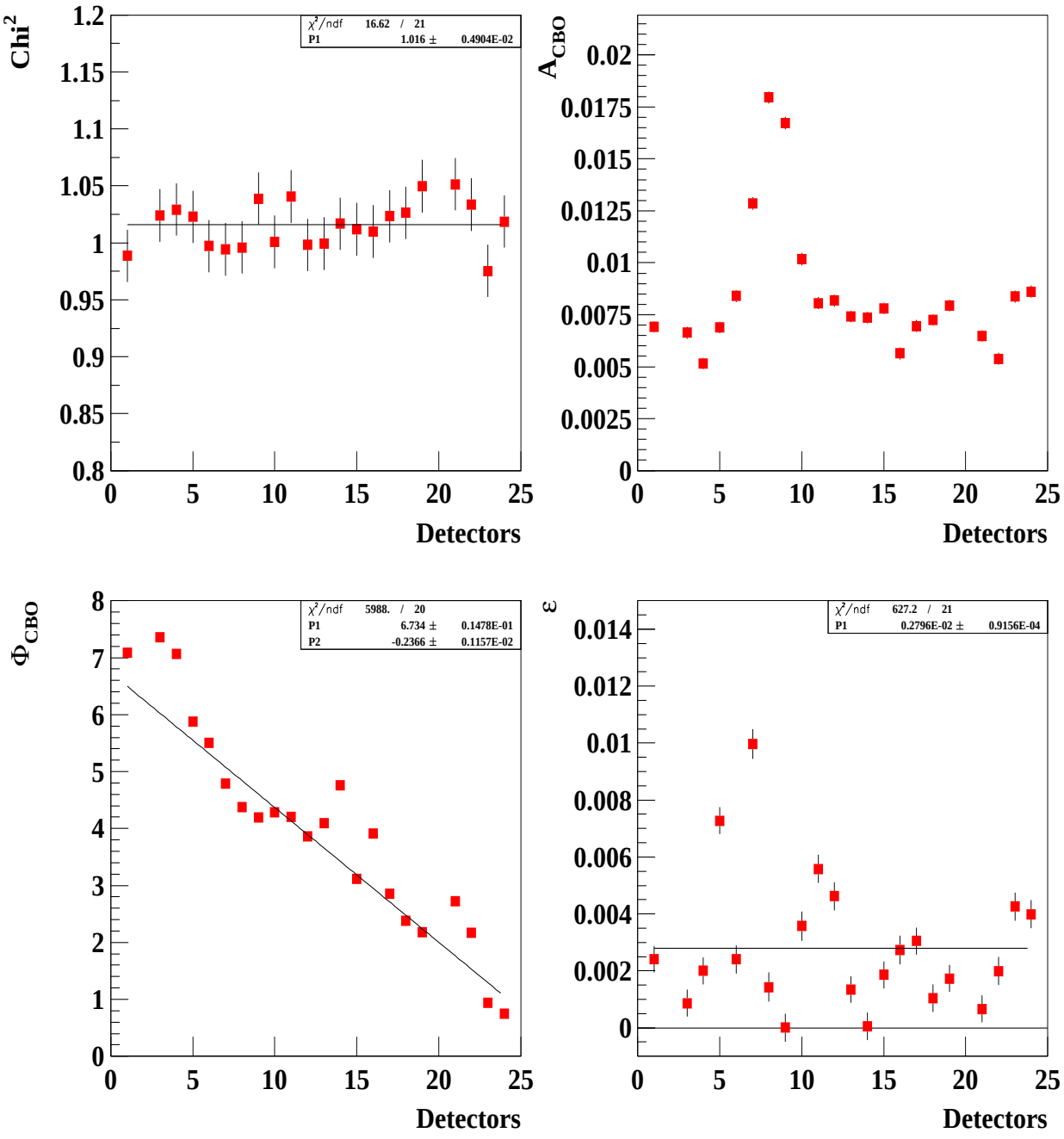

Figure 70 : Fit parameters at 82.6 μs for 1999 functional form.

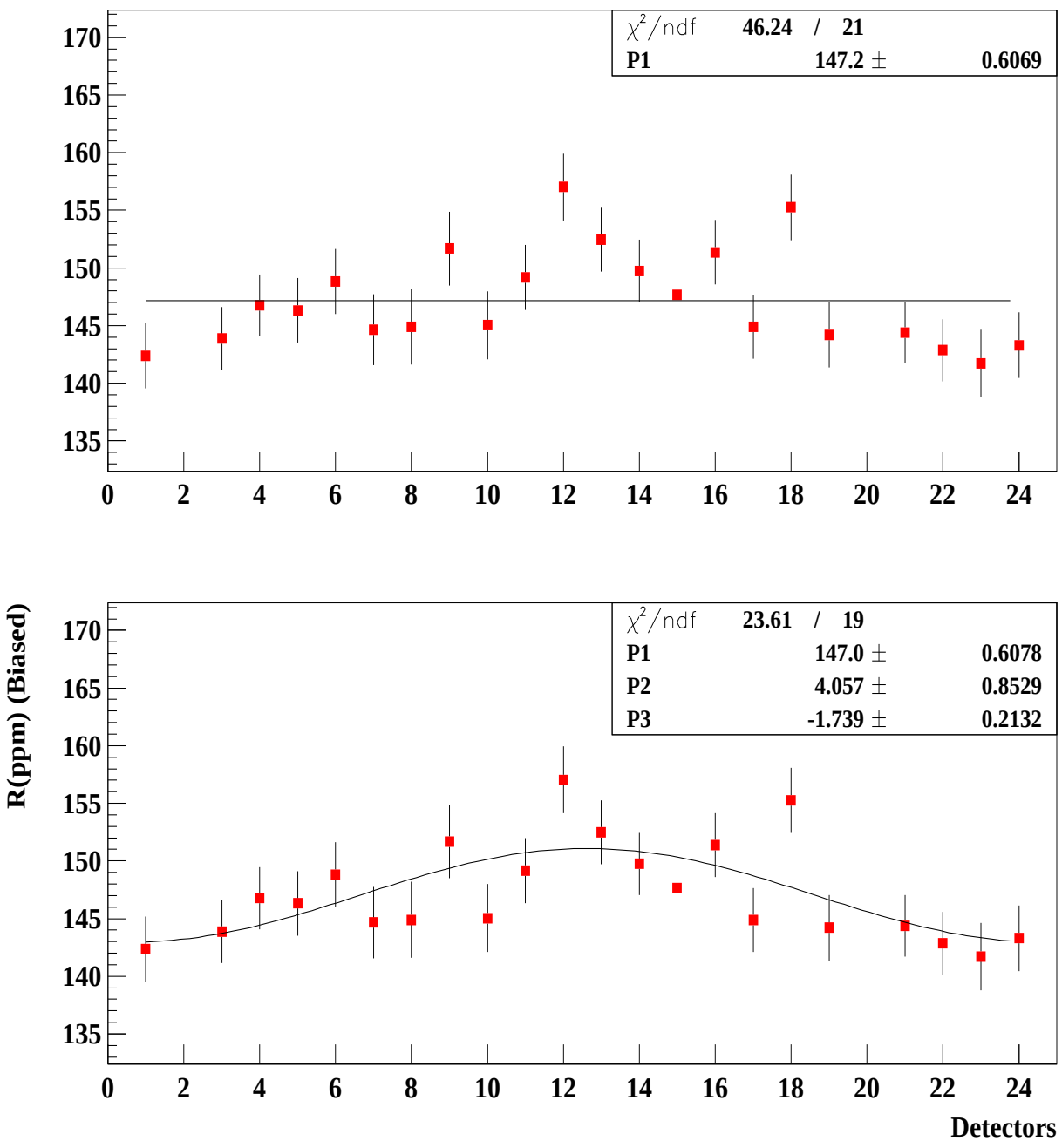

Figure 71 : R value at 49.9 μs for 1999 functional form.

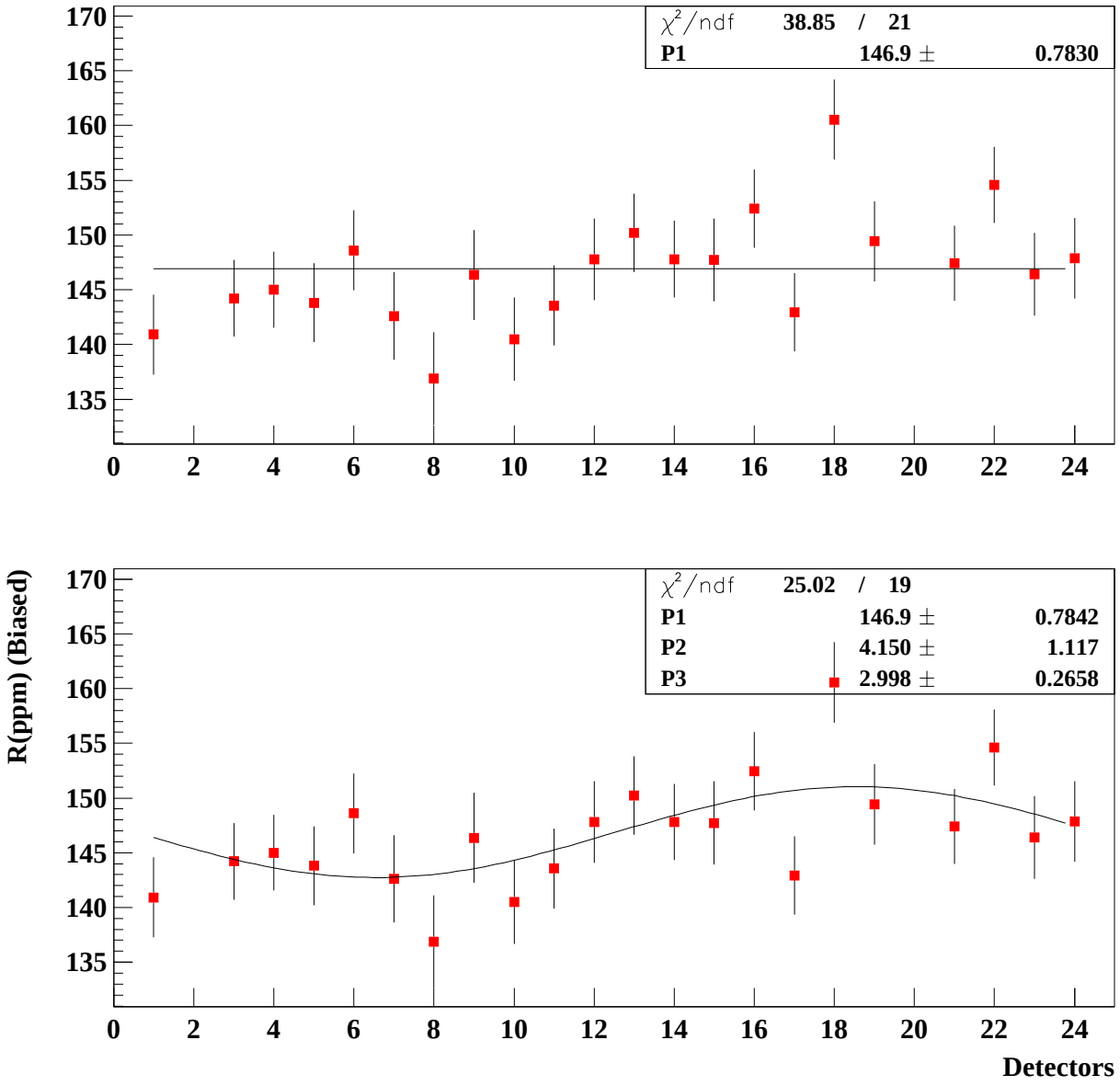

Figure 72 : R value at 82.6 μs for 1999 functional form.

The R stability for individual detectors are shown at Figure 73. By looking at the individual detectors one can justify that statistically there is no problem on R for individual detectors.

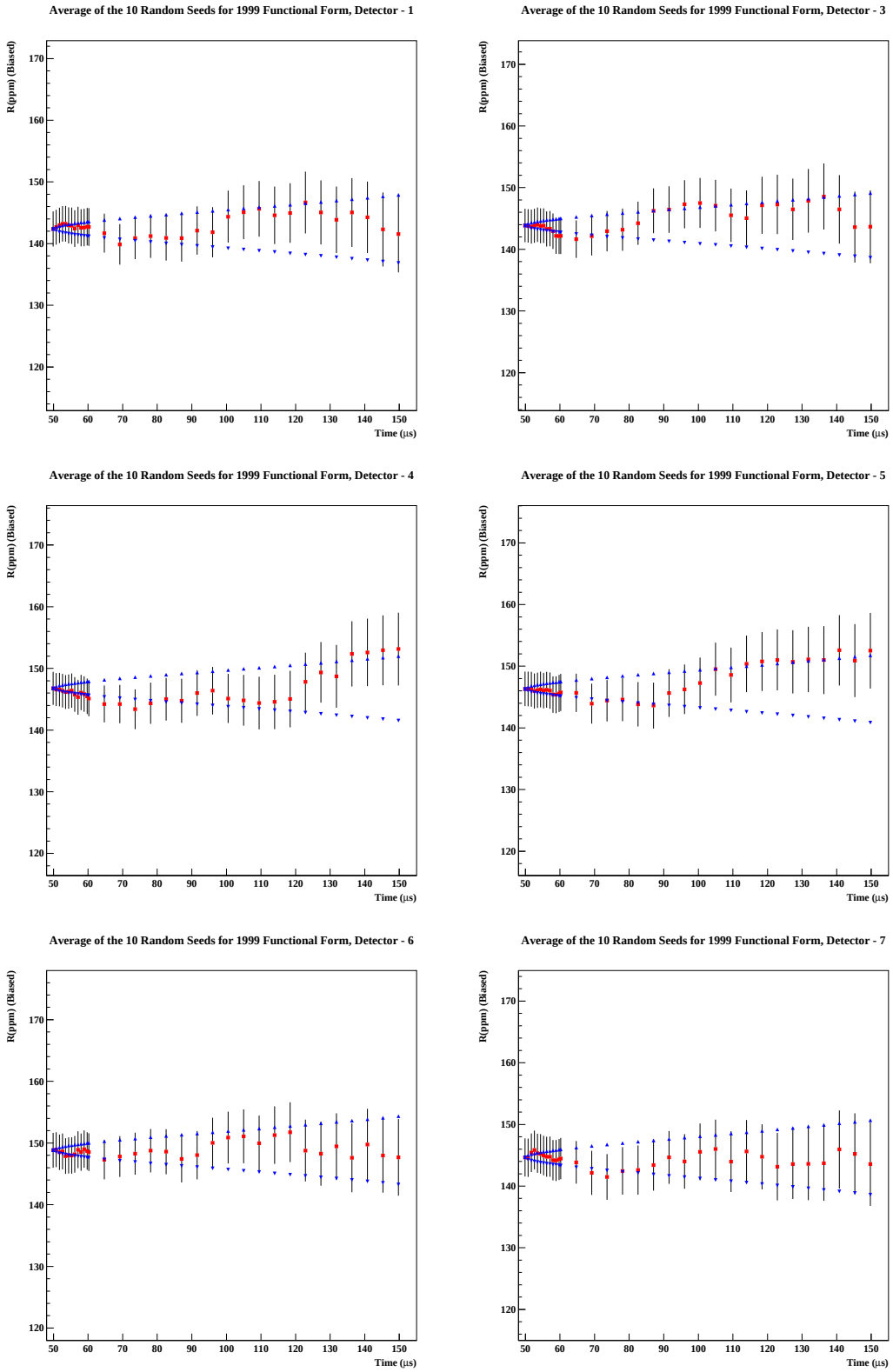

Figure 73 : The stability of R for individual detectors for 1999 type functional form.

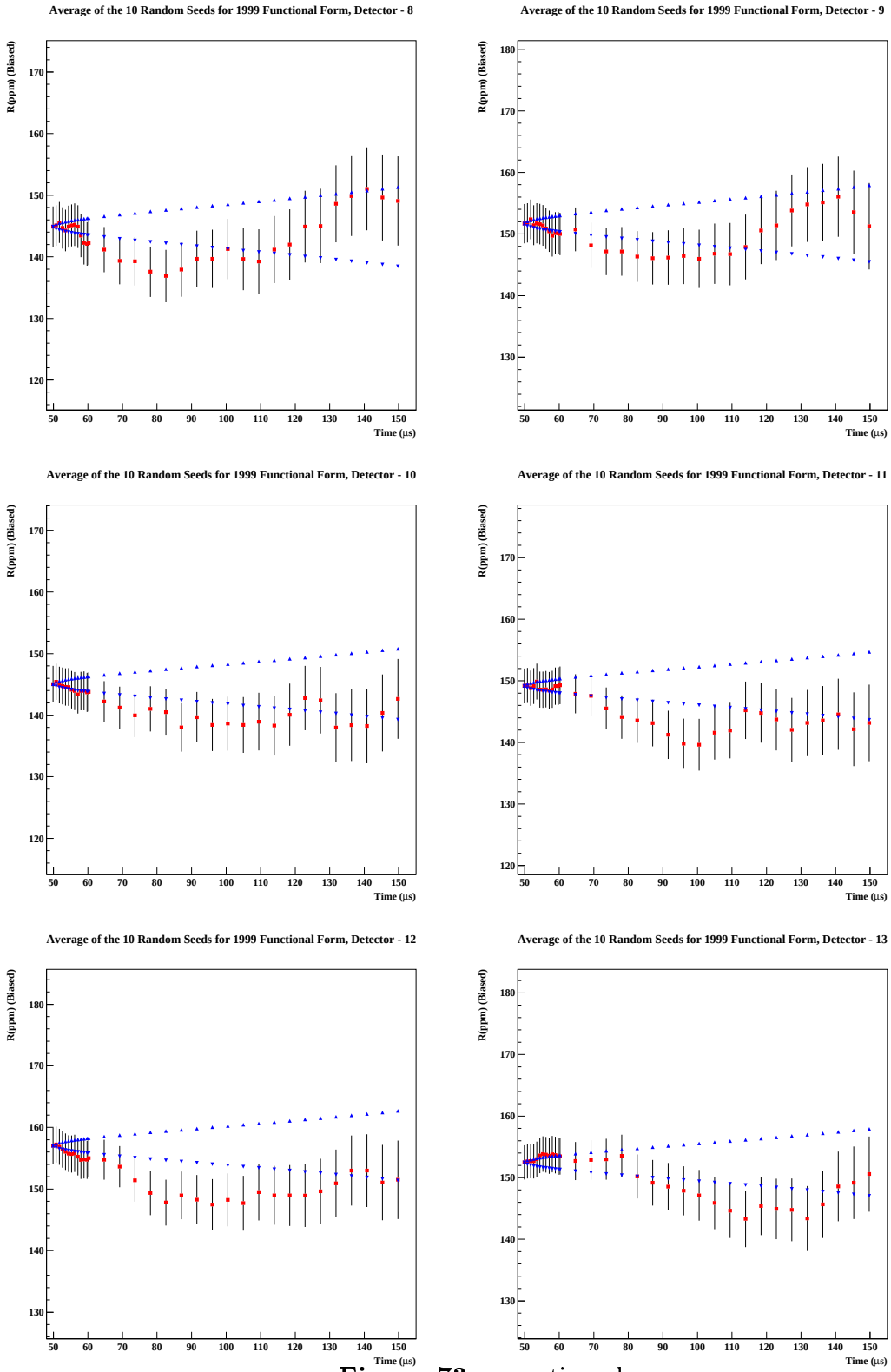

Figure 73 : continued,

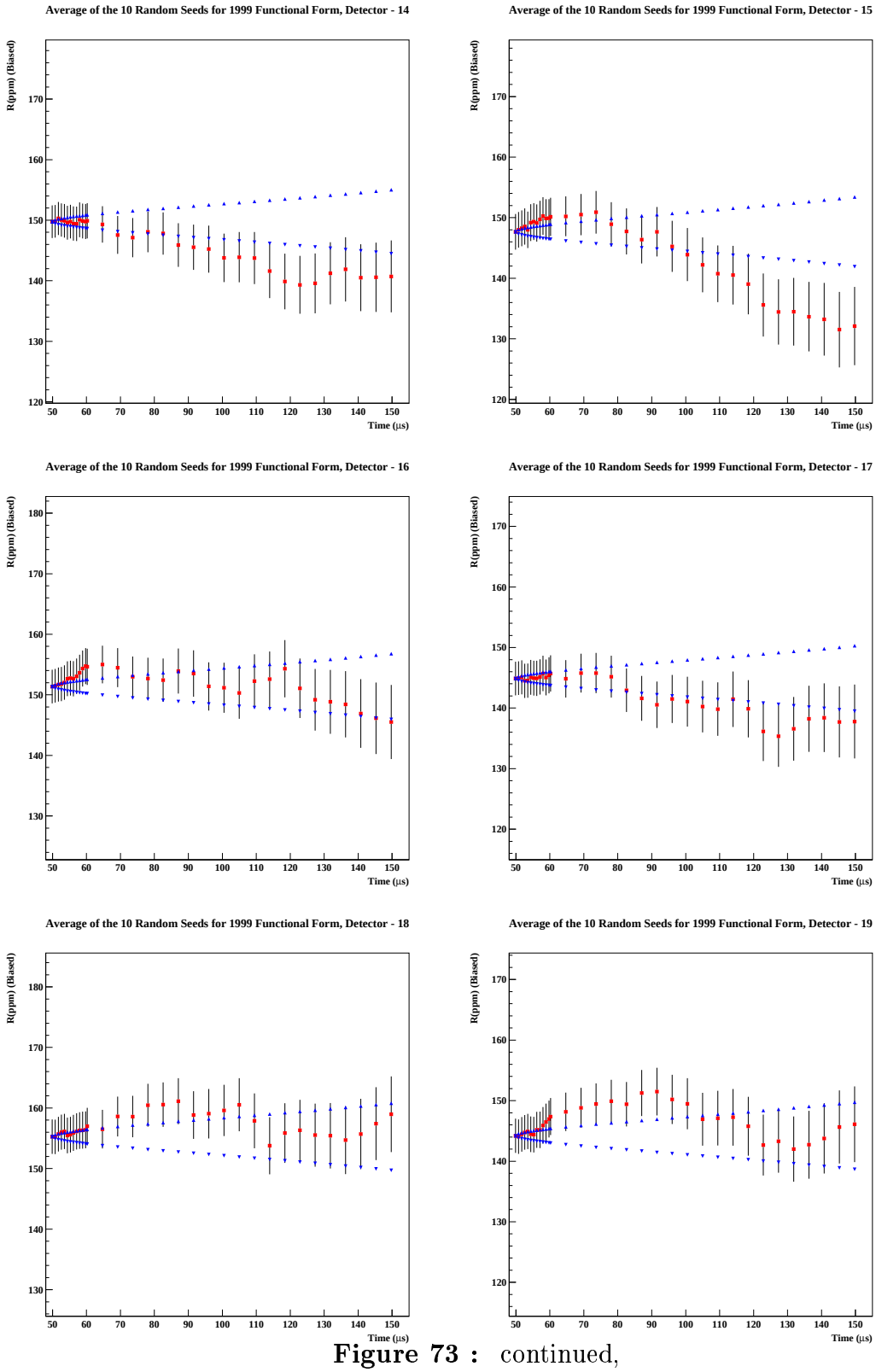

Figure 73 : continued,

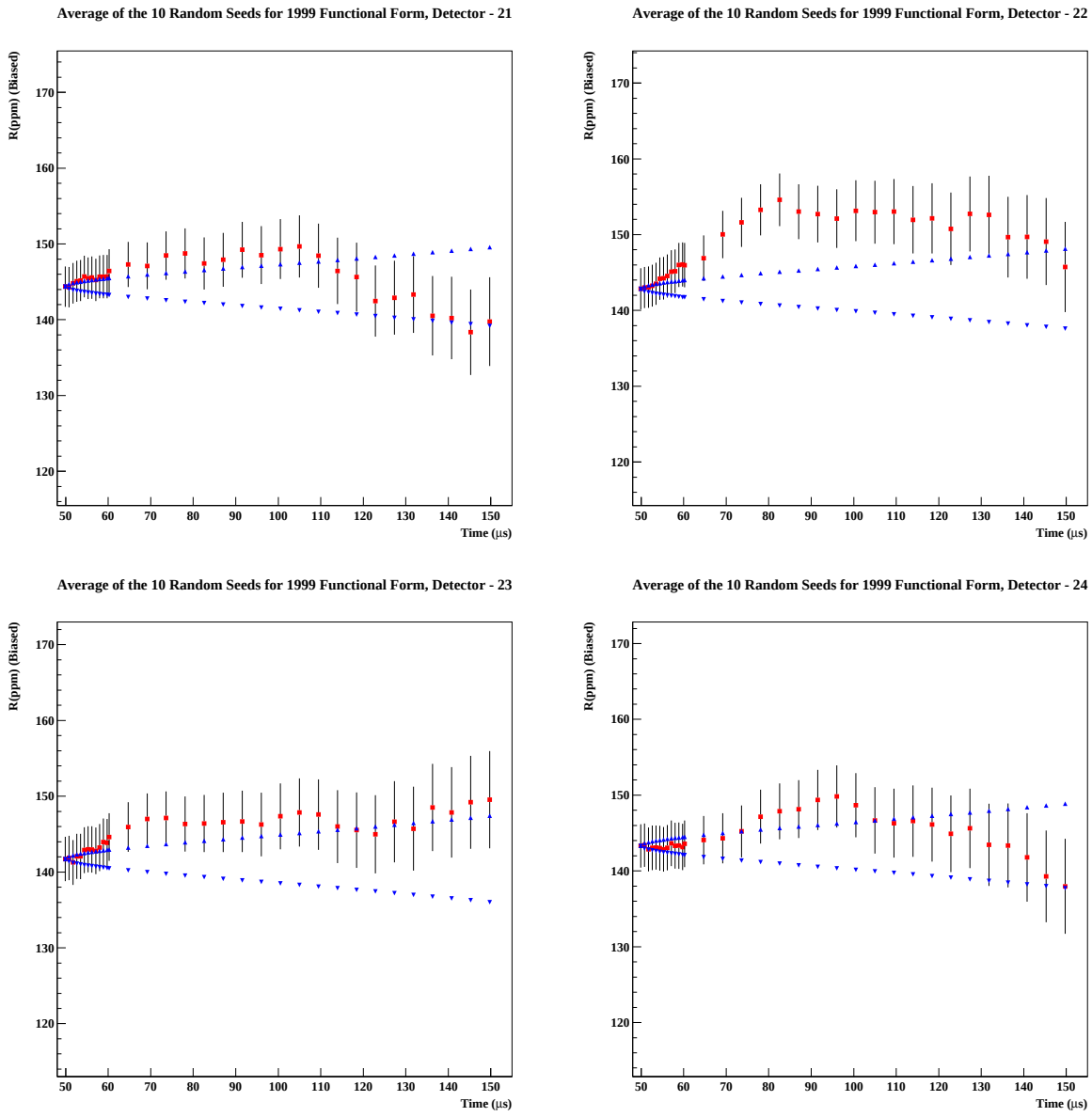

Figure 73 : continued.

The stability of other parameters are shown in the Figure 74 for each detectors. Asymmetries are most of the time out of the Kawall band for the detectors 4, 6, 9, 11, 12, 13, 14, 15, 17, 18, 19, 21 and 24. Stability of the ϵ, which has close relations with the stability of the gain, is not good for detectors 4, 6, 7, 10 and 24 for this functional form. Detectors 8, 9 ,10, 11, 12, 13, 14, 15, 22 and 23 have more g-2 phase (also R) instability compared to the others. CBO phase generally looks OK. However detectors 4, 8 and 9 are slightly worse than the others. CBO amplitude looks generally OK with only the exemptions of detectors 1 and 18.

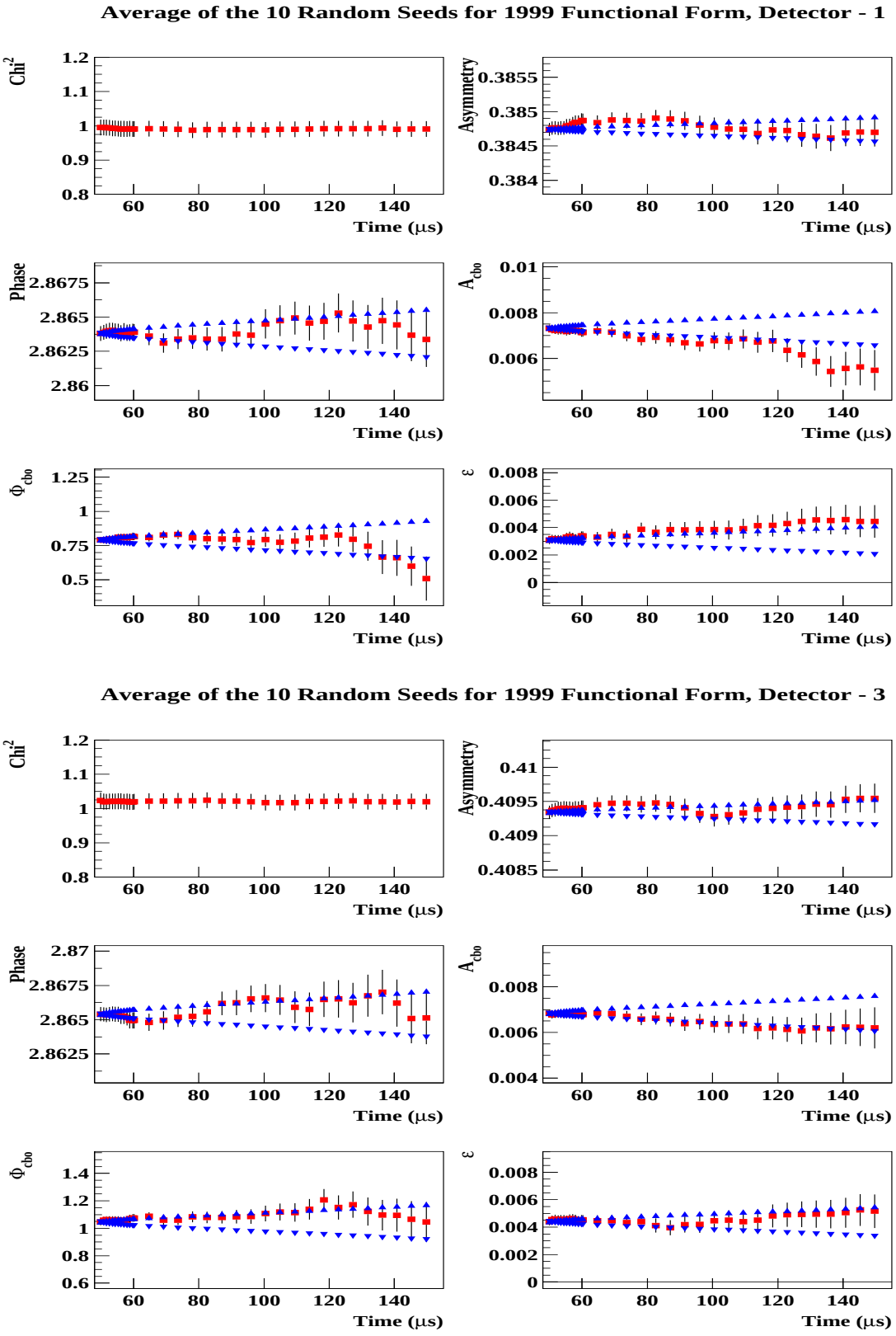

Figure 74 : The stability of R for individual detectors for 1999 type functional form.

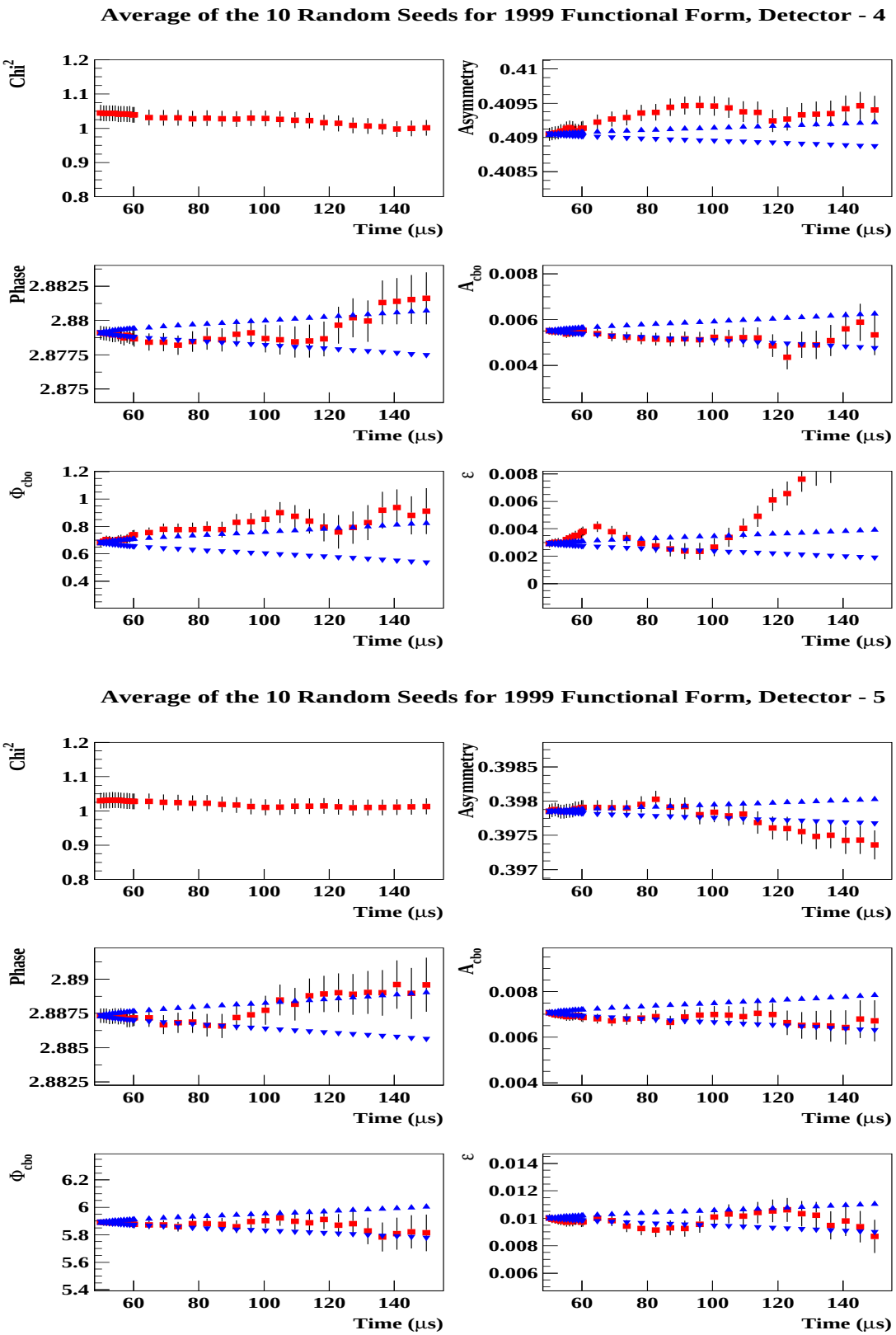

Figure 74 : continued,

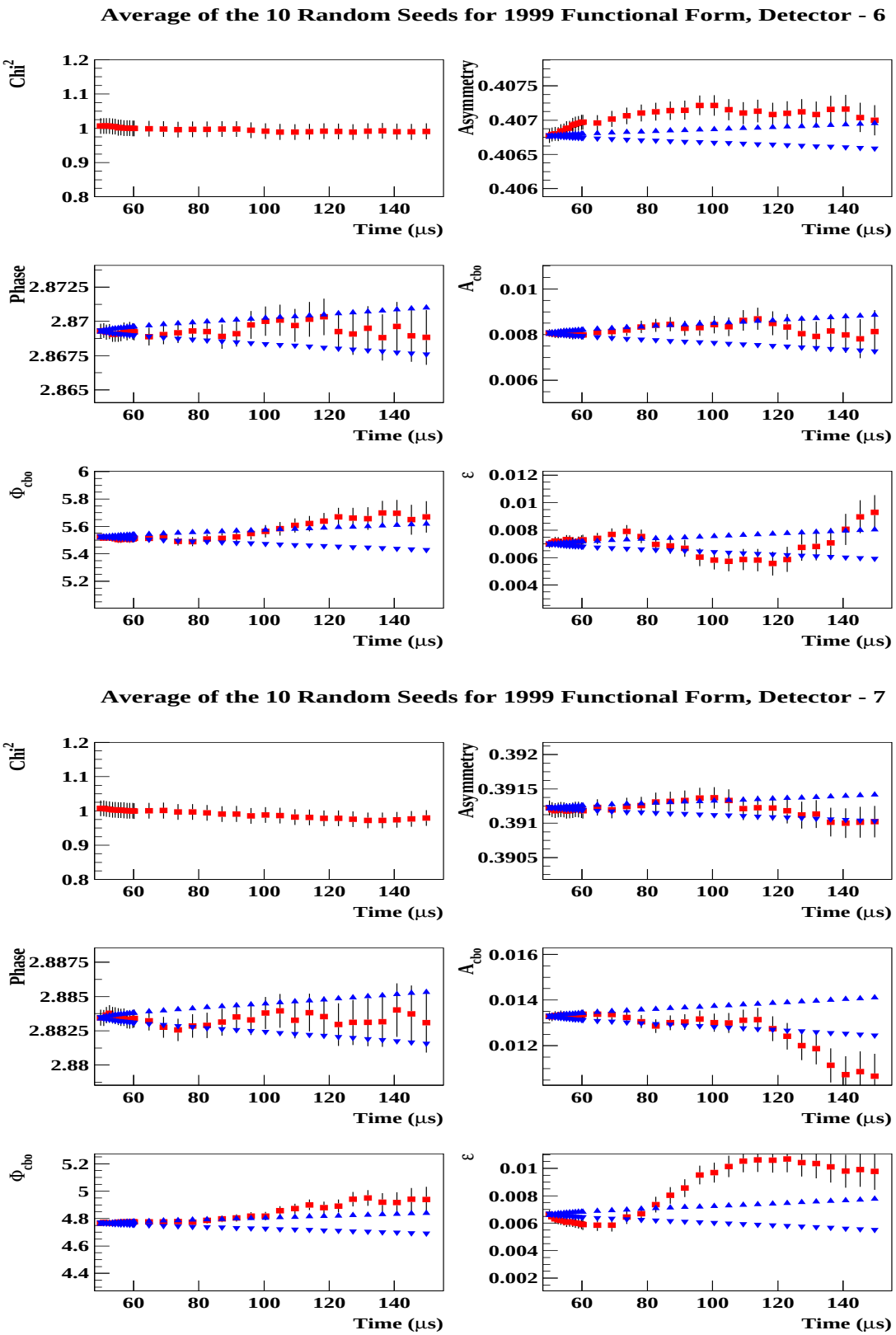

Figure 74 : continued,

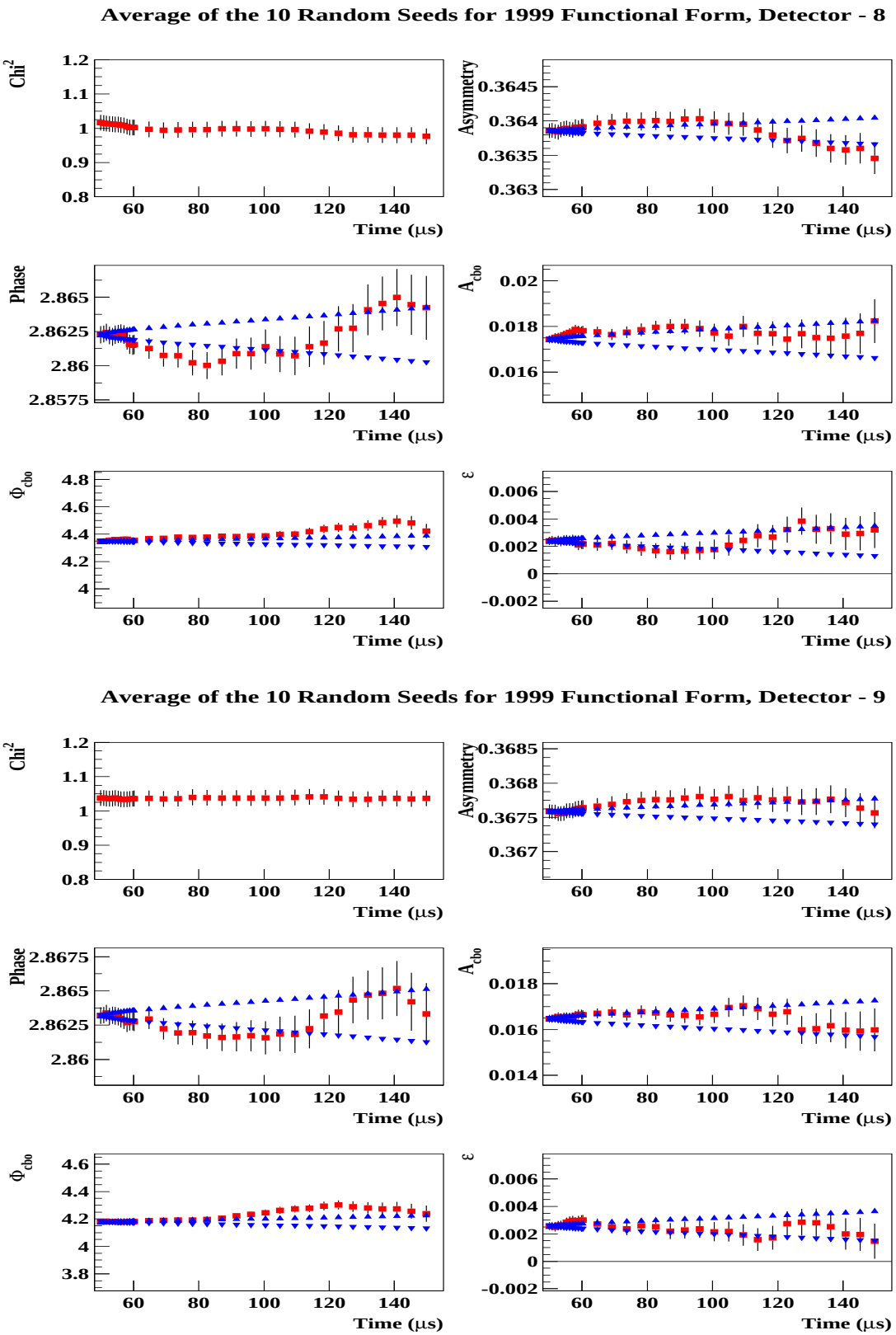

Figure 74 : continued,

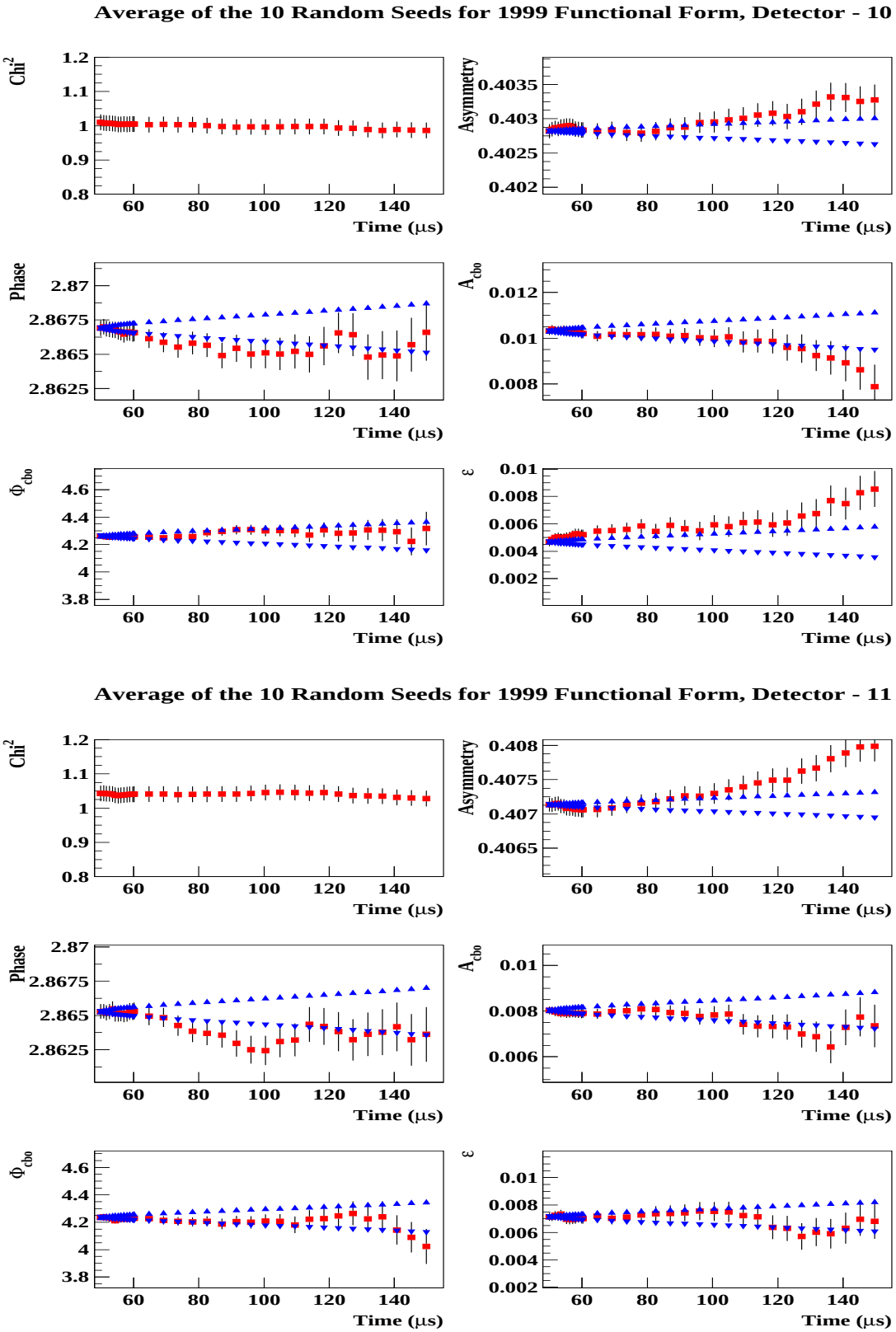

Figure 74 : continued,

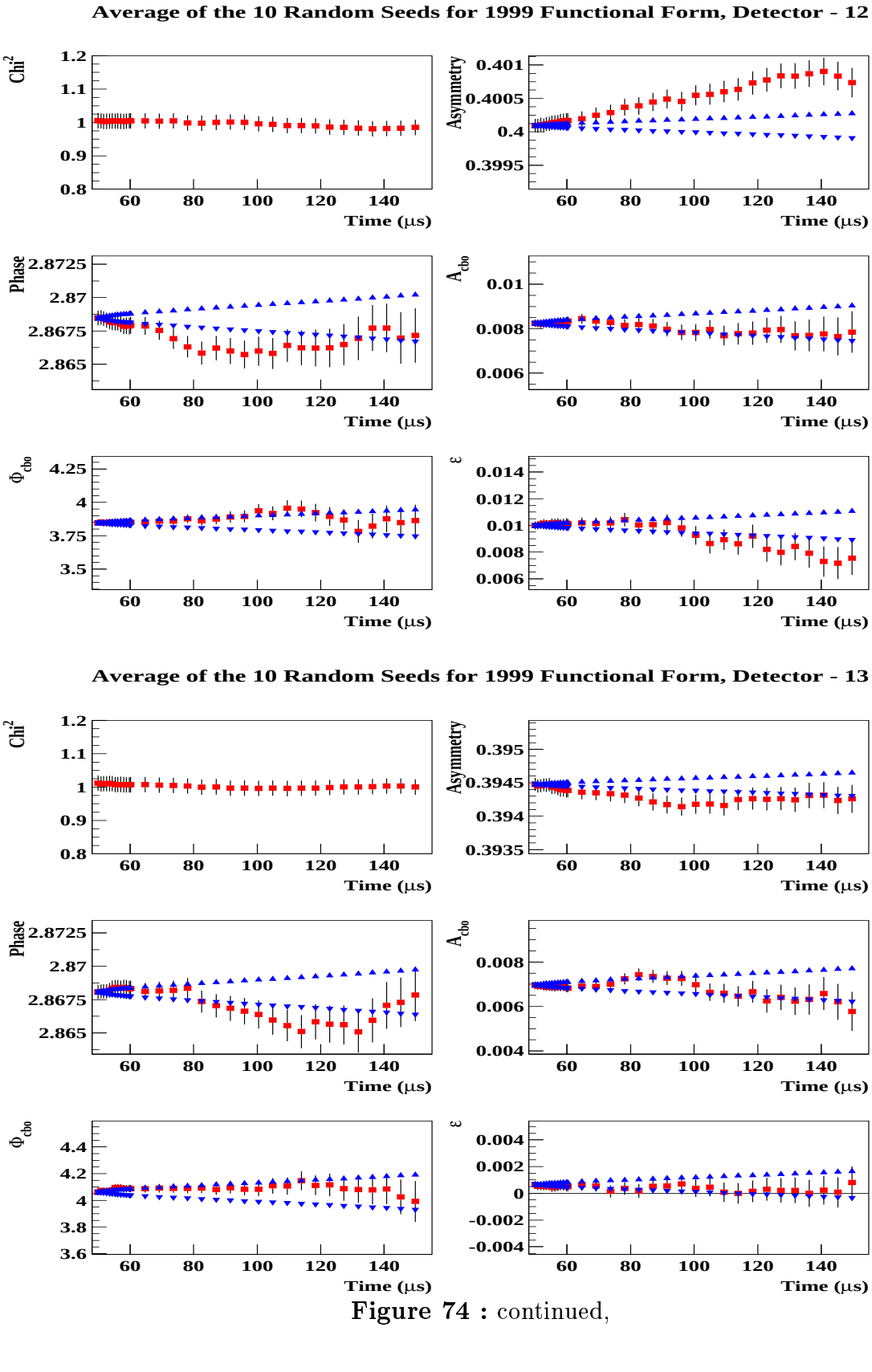

Figure 74 : continued,

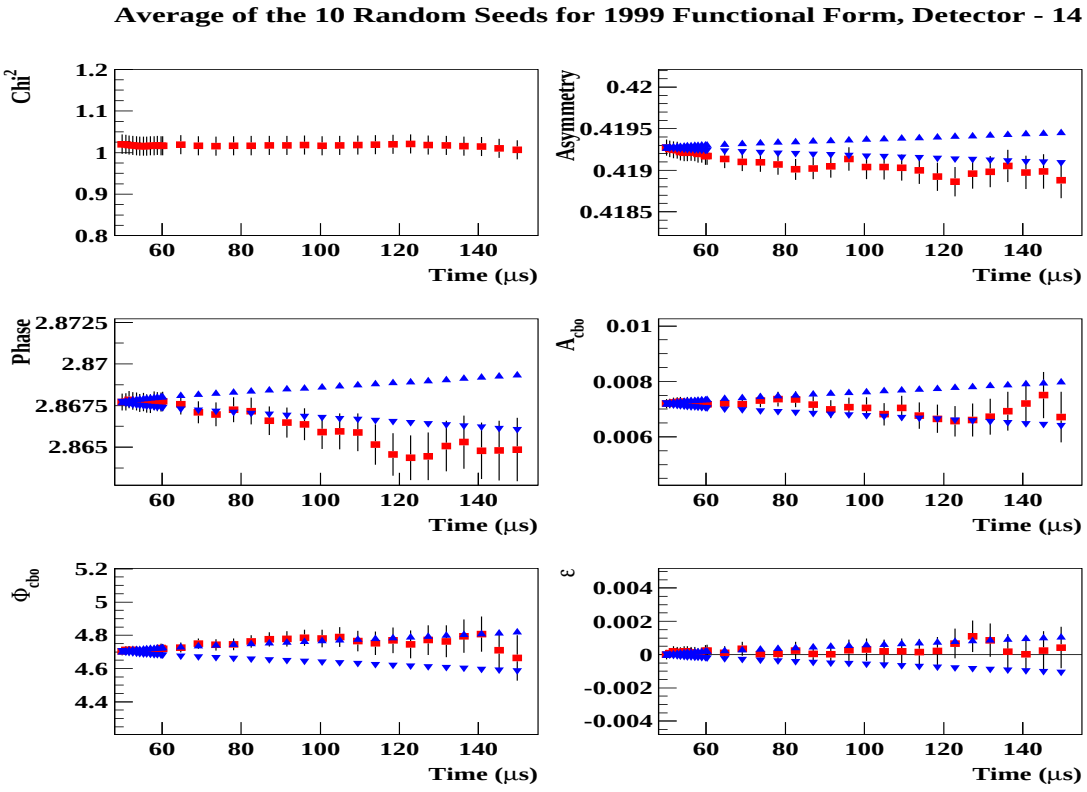

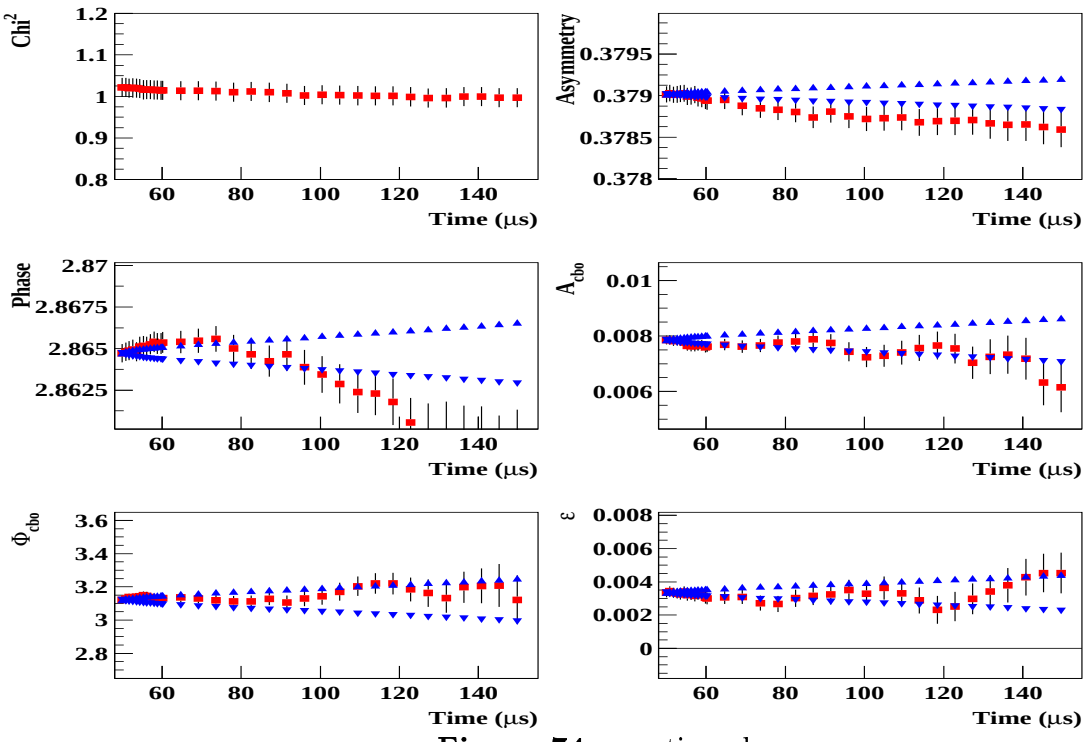

Figure 74 : continued,

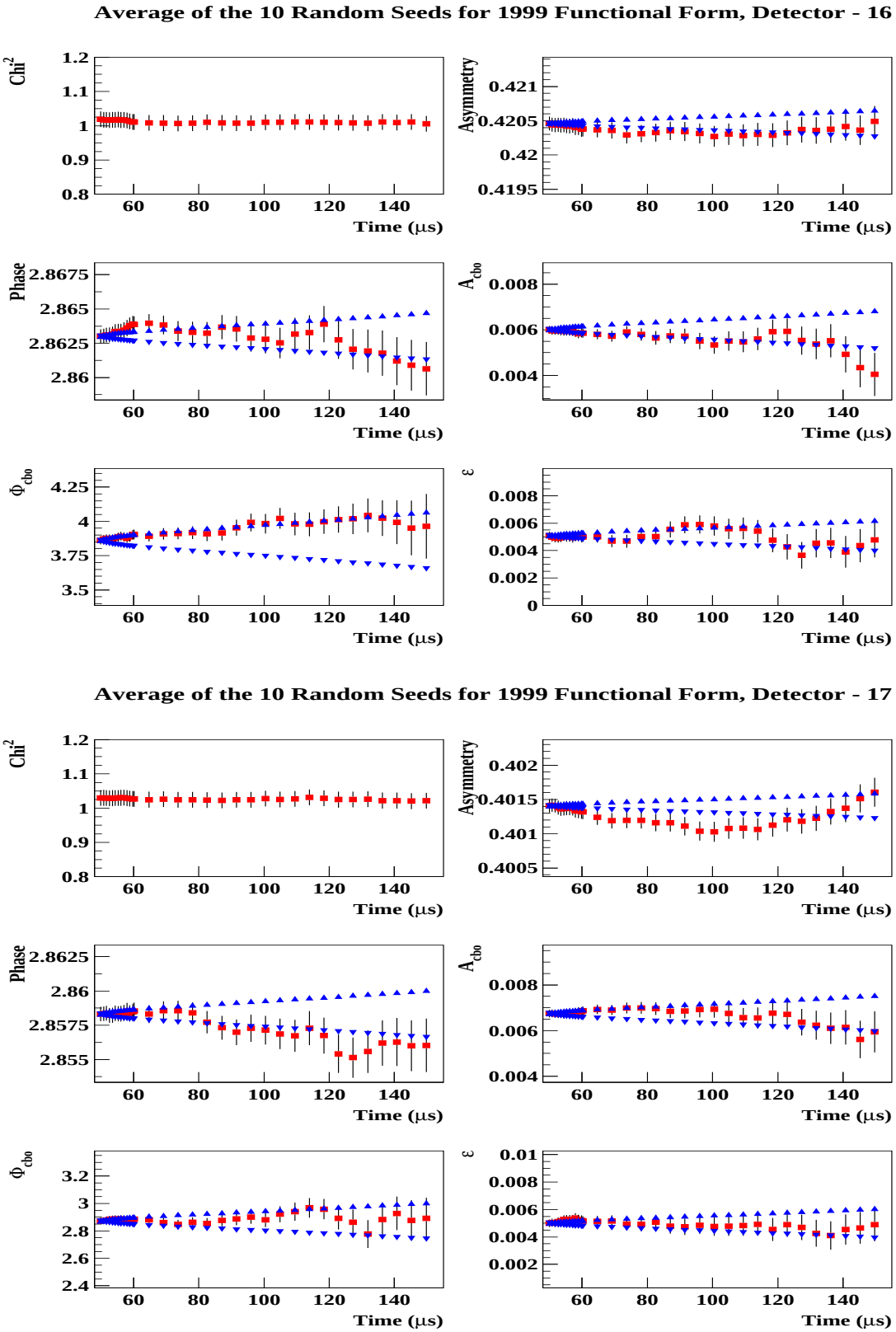

Figure 74 : continued,

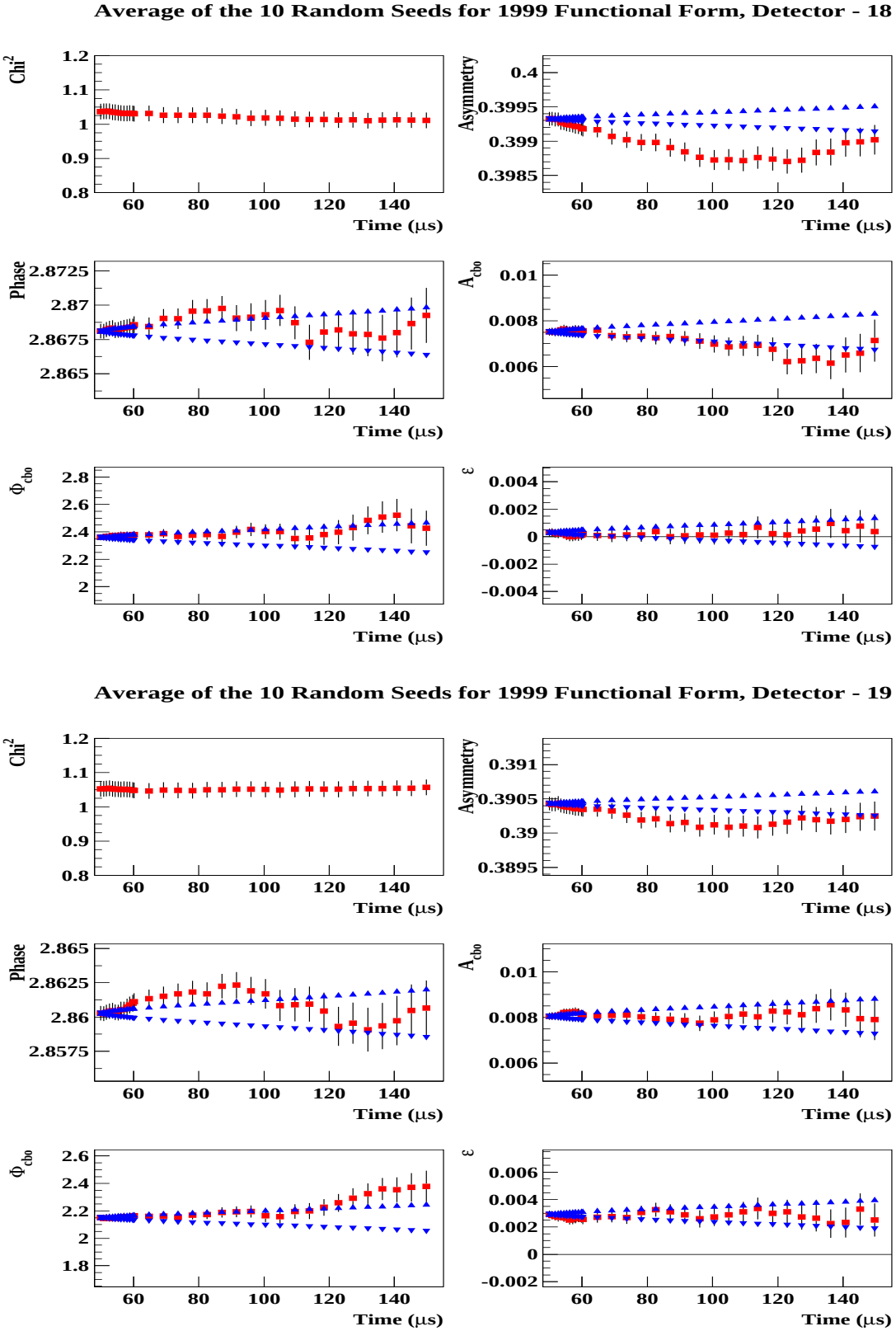

Figure 74 : continued,

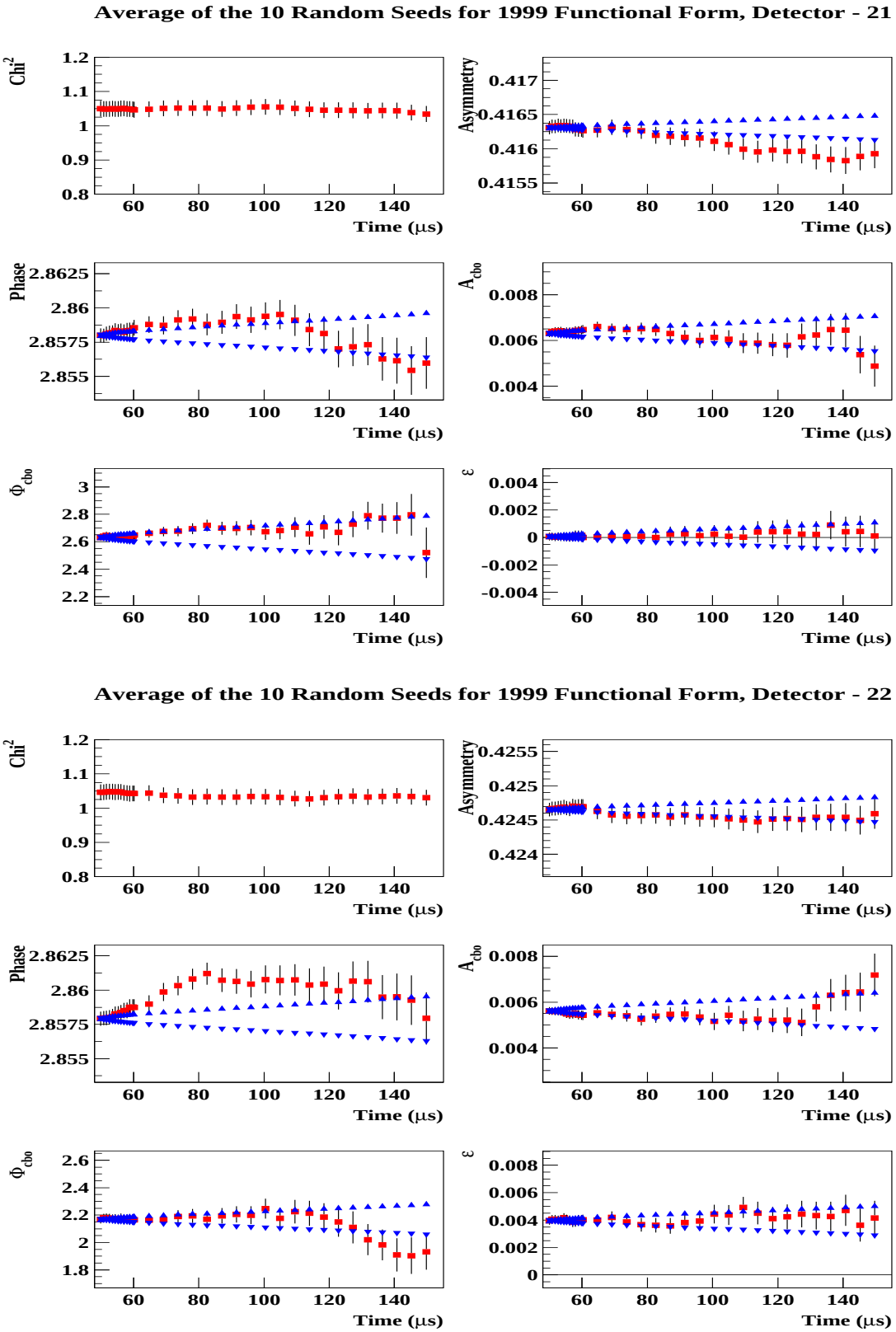

Figure 74 : continued,

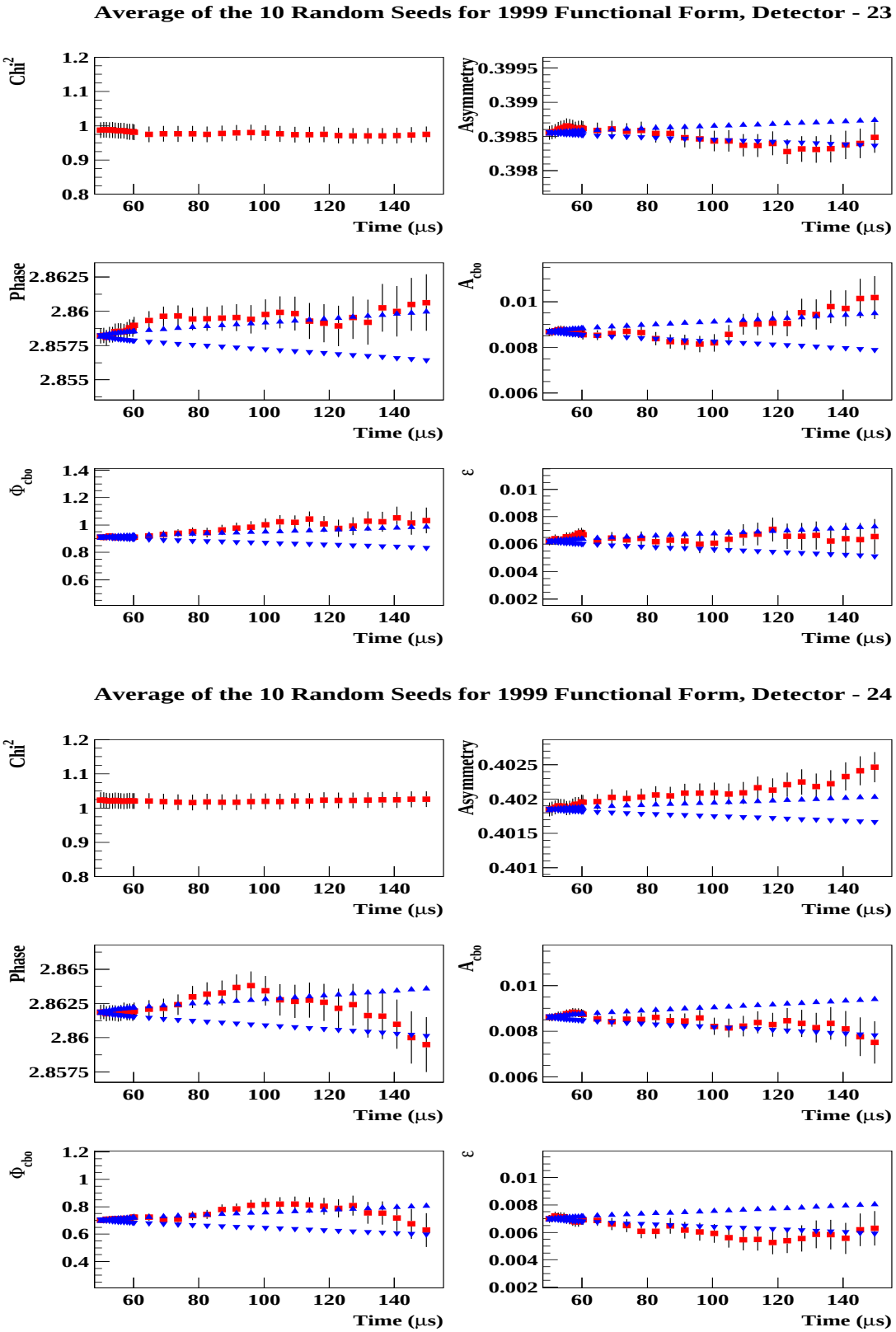

Figure 74 : continued.

7.2.2 1999 form including the g-2 asymmetry modulation due to g-2

When the asymmetry modulation was included into the 1999 function, the number of free parameters increased by two. This functional form is still simple since the envelope of the asymmetry modulation is expected to be the same as the main CBO. However sensitivity to the gain effects increases with this functional form. Please refer to the artificial gain study section. It was showed by Yannis that the correlations between gain and amplitude and the phase of g-2 modulations due to CBO occurs through the asymmetry. The asymmetry and R value have strong correlations.

Let's remind the functional form once more :

$$F(t) = N_0 e^{-t/\tau_\mu}\{1+A' cos(2\pi(f_0-f_a)t+\phi_a)\}\{1+A_{cbo}\mathbf{E_{cbo}(t)}cos(2\pi f_{cbo}t+\phi_{cbo})\}\ \{1+\epsilon(t)\}$$

where $A' = A\ \{1 + A_{Rb}\ \mathbf{E_{cbo}(t)}\ cos(2\pi f_{cbo}t + \phi_{Rb})\}$ called as g-2 asymmetry modulation due to CBO and A_{Rb} is the amplitude and ϕ_{Rb} is the phase of these modulations.

Just like we did in 1999 form, we will look at the first and second halves and detectors together. Figures 75-77 show the parameter stability for the first, second half and when all the detectors were combined. Figures 78-80 show the stability of R for this functional form.

The parameter stability are generally better compared to 99 form. χ^2 is slightly better, asymmetries from both halves are much closer to their Kawall bands compared to 1999 functional form. In both halves, the asymmetry modulation amplitudes are nicely stable and their amplitudes are very similar. This already shows that the g-2 asymmetry modulation amplitude (A_{Rb}) does not have strong acceptance dependence. For example it is not higher in the kicker region. For this functional form we will assign $0.076/\sqrt{(10)} = 0.024$ ppm systematic error due to randomization since we used 10 random seeds here.

Table 14: χ^2 and R values for 10 random seeds for the functional form with only g-2 asymmetry modulation included into 1999 form. These values were obtained at 49.9 μs.

Random Seed	χ^2	R(ppm)
1	1.026	147.29
2	0.999	147.23
3	1.003	147.16
4	1.011	147.42
5	1.010	147.24
6	1.031	147.21
7	0.972	147.28
8	1.041	147.39
9	1.042	147.32
10	1.039	147.26
Average	**1.018**	**147.25**
RMS	**0.021**	**0.076**

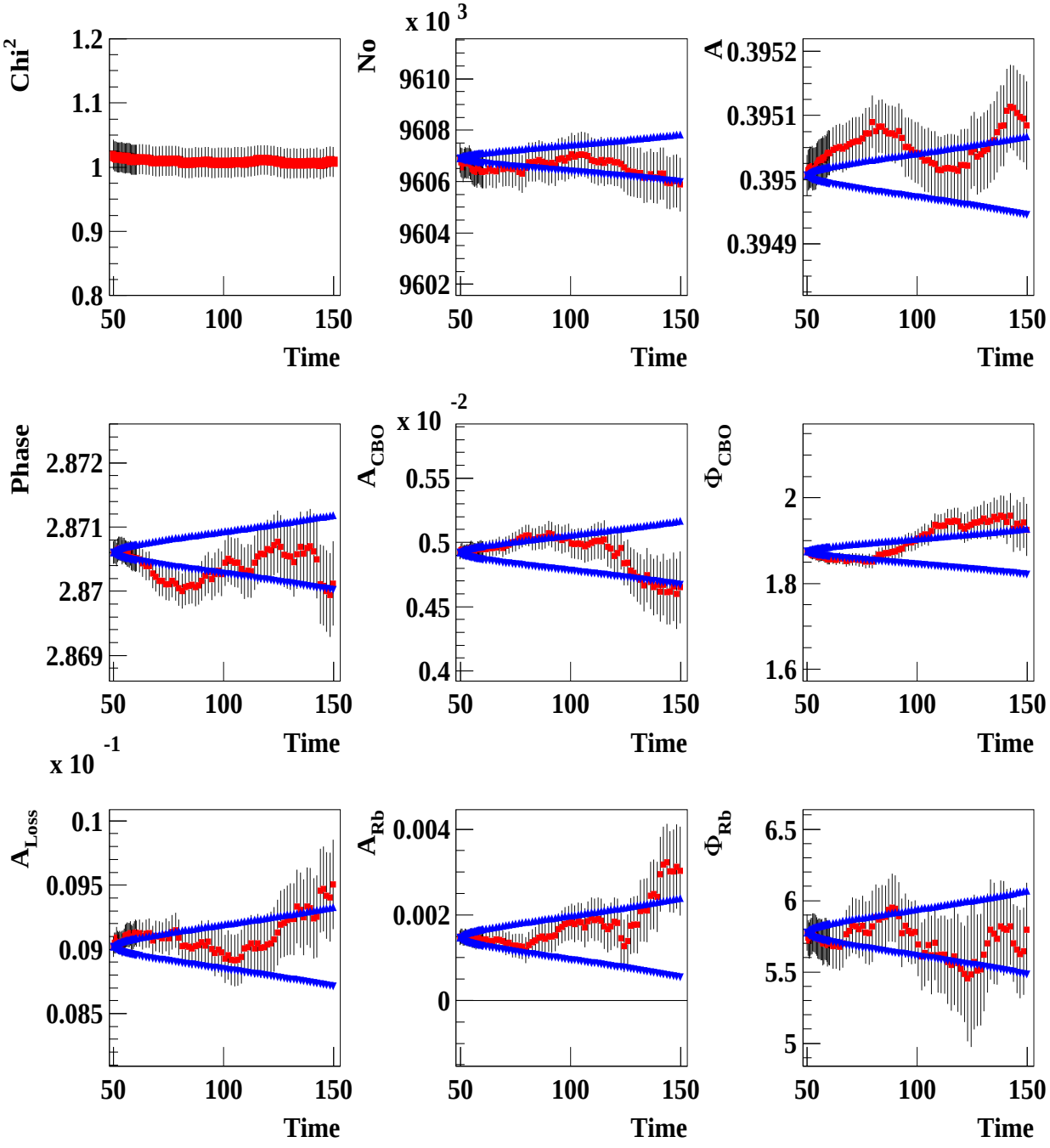

Figure 75: Fit parameters with the asymmetry modulation on the first half.

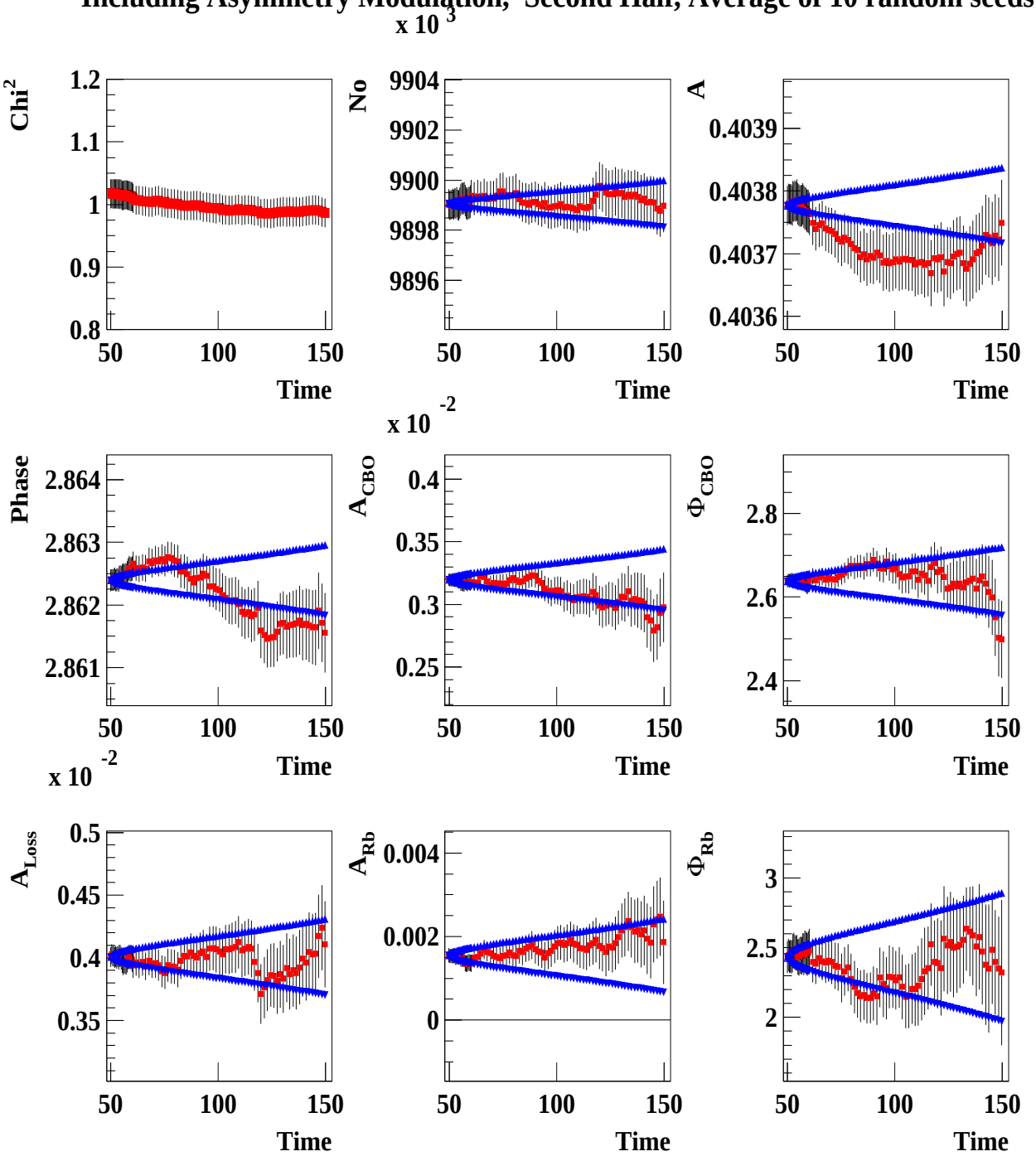

Figure 76: Fit parameters with the asymmetry modulation on the second half.

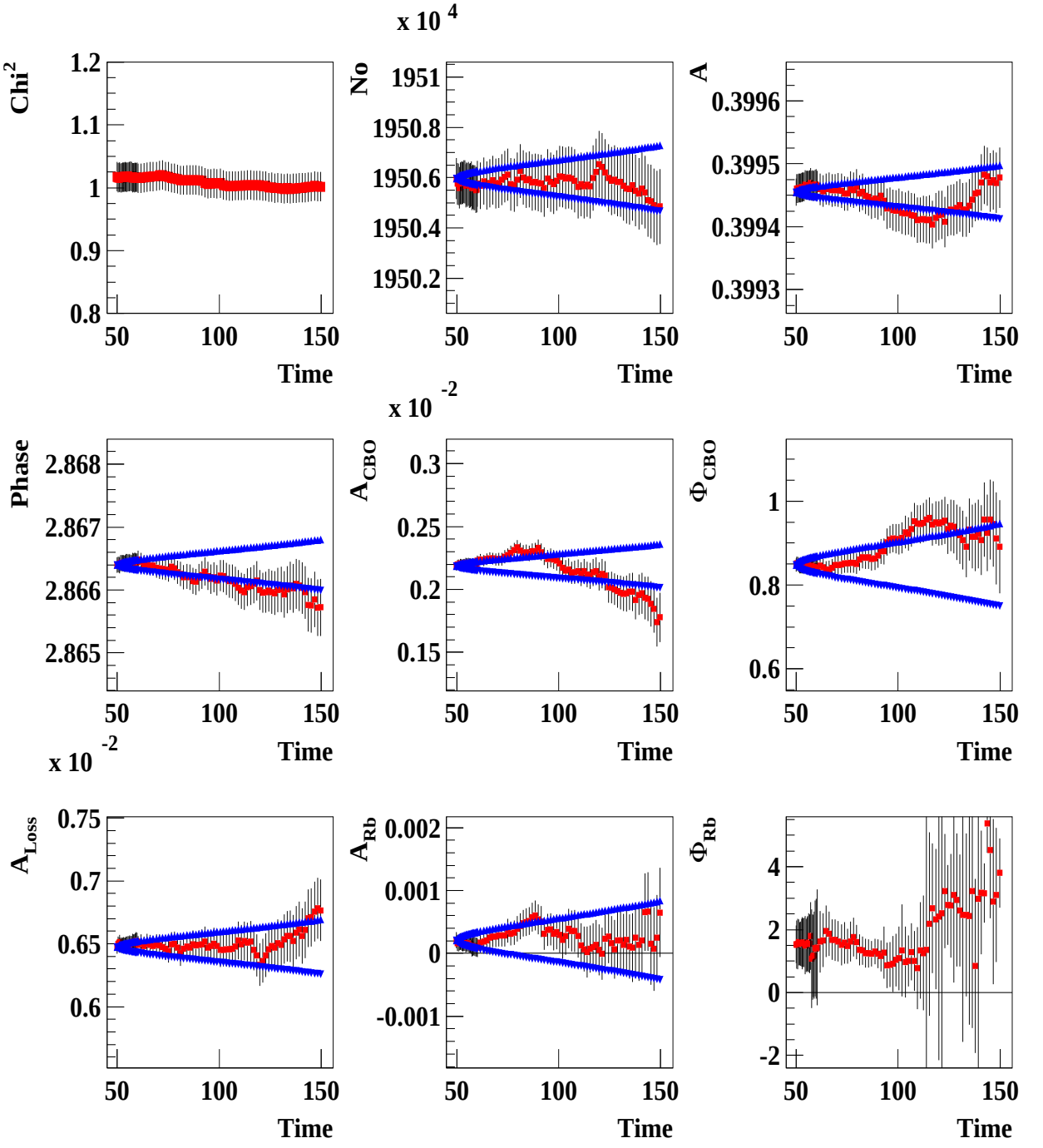

Figure 77: Fit parameters with the asymmetry modulation for all detectors together.

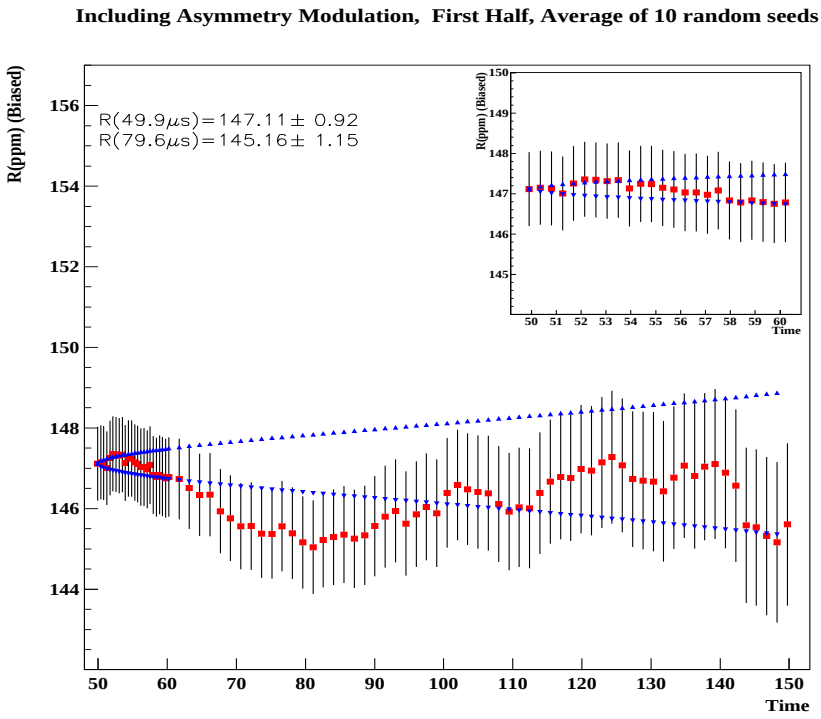

Figure 78: The stability of R with 1999 functional form including the g-2 asymmetry modulation on the first half.

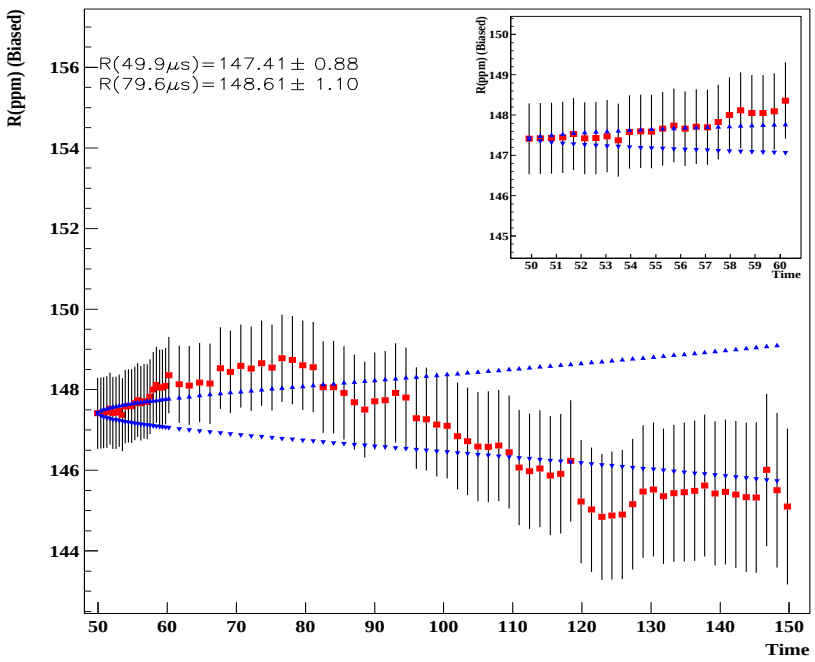

Figure 79: The stability of R with 1999 functional form including the g-2 asymmetry modulation on the second half.

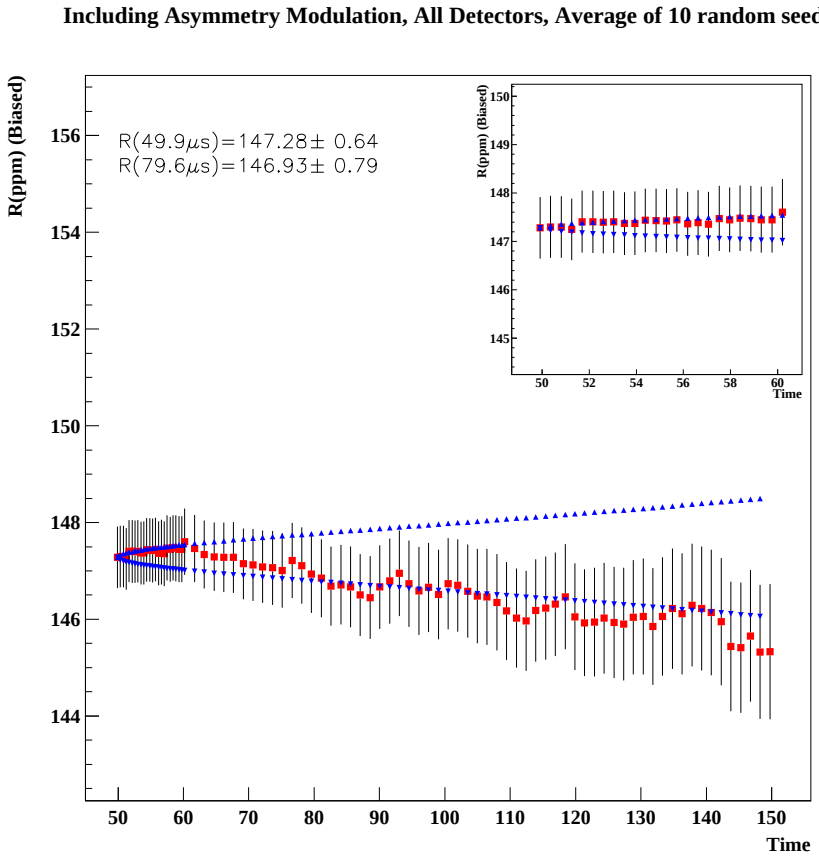

Figure 80: The stability of R with 1999 functional form including the g-2 asymmetry modulation all detectors together.

Table 15 gives the comparison of some parameters for the first, second halves and all the detectors together for this functional form. These values are given at 49.9 μs.

Table 15: Comparison table of the fit parameters for the 1999 functional form including the g-2 asymmetry modulation due to CBO.

Parameters	First Half		Second Half		All Detectors	
A	0.39501	±3.1965E-05	0.40378	±3.1412E-05	0.39946	±2.2401E-05
Φ_a	2.8706	±1.7967E-04	2.8624	±1.7530E-04	2.8664	±1.2478E-04
A_{cbo}	4.9342E-03	±4.9955E-05	3.1983E-03	±4.9512E-05	2.1875E-03	±3.5019E-05
Φ_{cbo}	4.7023	±1.0173E-02	2.6355	±1.5361E-02	3.9912	±1.6118E-02
A_{Rb}	1.4717E-03	±1.7711E-04	1.5758E-03	±1.7029E-04	1.8937E-04	±1.2617E-04
Φ_{Rb}	5.7607	±0.12564	2.4588	±0.11279	1.6836	± 0.65853
$\epsilon(A_L)$	8.5727E-03	±3.9260E-04	4.0404E-03	±3.8717E-04	6.2655E-03	±2.7540E-04
$\epsilon(A_r)$	-7.5643E-03	±4.2306E-04	-1.9037E-03	±4.1712E-04	-4.6838E-03	±2.9676E-04
$\epsilon(\tau_r)$	100.46	±1.8351	100.08	±7.2125	100.40	±2.0810

The parameter correlation coefficients (all detectors together @ 49.9 μs) for this functional

form is given in Table 16.

Table 16: Correlation matrix for the functional form with g-2 asymmetry modulation due to CBO.

	Total	N_0	A	R	Φ_a	A_{cbo}	Φ_{cbo}	A_{Rb}	Φ_{Rb}	$\epsilon(A_L)$	$\epsilon(A_r)$	$\epsilon(\tau_r)$
N_0	0.97929	1.000	0.006	-0.009	-0.013	-0.009	-0.007	-0.003	0.013	**-0.481**	**0.321**	**0.837**
A	0.30323	0.006	1.000	-0.030	-0.027	0.009	0.008	**-0.251**	**-0.152**	-0.020	0.019	-0.002
R	0.88532	-0.009	-0.030	1.000	**0.883**	0.010	0.005	**0.233**	**-0.196**	0.034	-0.031	0.005
Φ_a	0.89409	-0.013	-0.027	**0.883**	1.000	0.013	0.006	**0.278**	**-0.290**	0.045	-0.041	0.007
A_{cbo}	0.05015	-0.009	0.009	0.010	0.013	1.000	0.004	-0.018	0.013	0.030	-0.027	0.004
Φ_{cbo}	0.03714	-0.007	0.008	0.005	0.006	0.004	1.000	0.012	0.006	0.025	-0.022	0.003
A_{Rb}	0.37185	-0.003	**-0.251**	**0.233**	**0.278**	-0.018	0.012	1.000	-0.054	0.009	-0.008	0.001
Φ_{Rb}	0.35731	0.013	**-0.152**	**-0.196**	**-0.290**	0.013	0.006	-0.054	1.000	-0.045	0.041	-0.007
$\epsilon(A_L)$	0.99692	**-0.481**	-0.020	0.034	0.045	0.030	0.025	0.009	-0.045	1.000	**-0.975**	**-0.287**
$\epsilon(A_r)$	0.99624	**0.321**	0.019	-0.031	-0.041	-0.027	-0.022	-0.008	0.041	**-0.975**	1.000	**0.208**
$\epsilon(\tau_r)$	0.94789	**0.837**	-0.002	0.005	0.007	0.004	0.003	0.001	-0.007	**-0.287**	**0.208**	1.000

Table 17 shows the value of R and the size of the half ring effect in the case of linear and sinusoidal fit applied to R vs detectors. This table is determined from figures 83 and 84.

Table 17: Comparison of the R values at 49.9 and 82.6 μ s.

Time	49.9 μs		82.6 μs	
	R (ppm)	χ^2/DOF	R (ppm)	χ^2/DOF
Linear Fit	147.27±0.64	29.3/21	146.73±0.82	21.4/21
Sine Wave Fit	147.20±0.64	25.1/19	146.75±0.82	18.1/19
Half Ring Effect(ppm)	1.82±0.89		2.13±1.18	

Individual detectors were fitted with this functional form for ten random seeds between 49.9 and 150 μs. The following plots show the parameters at 49.9 (Figure 81) and 82.6 (Figure 82) μs. Figures 83-84 show the R values for individual detectors at those times.

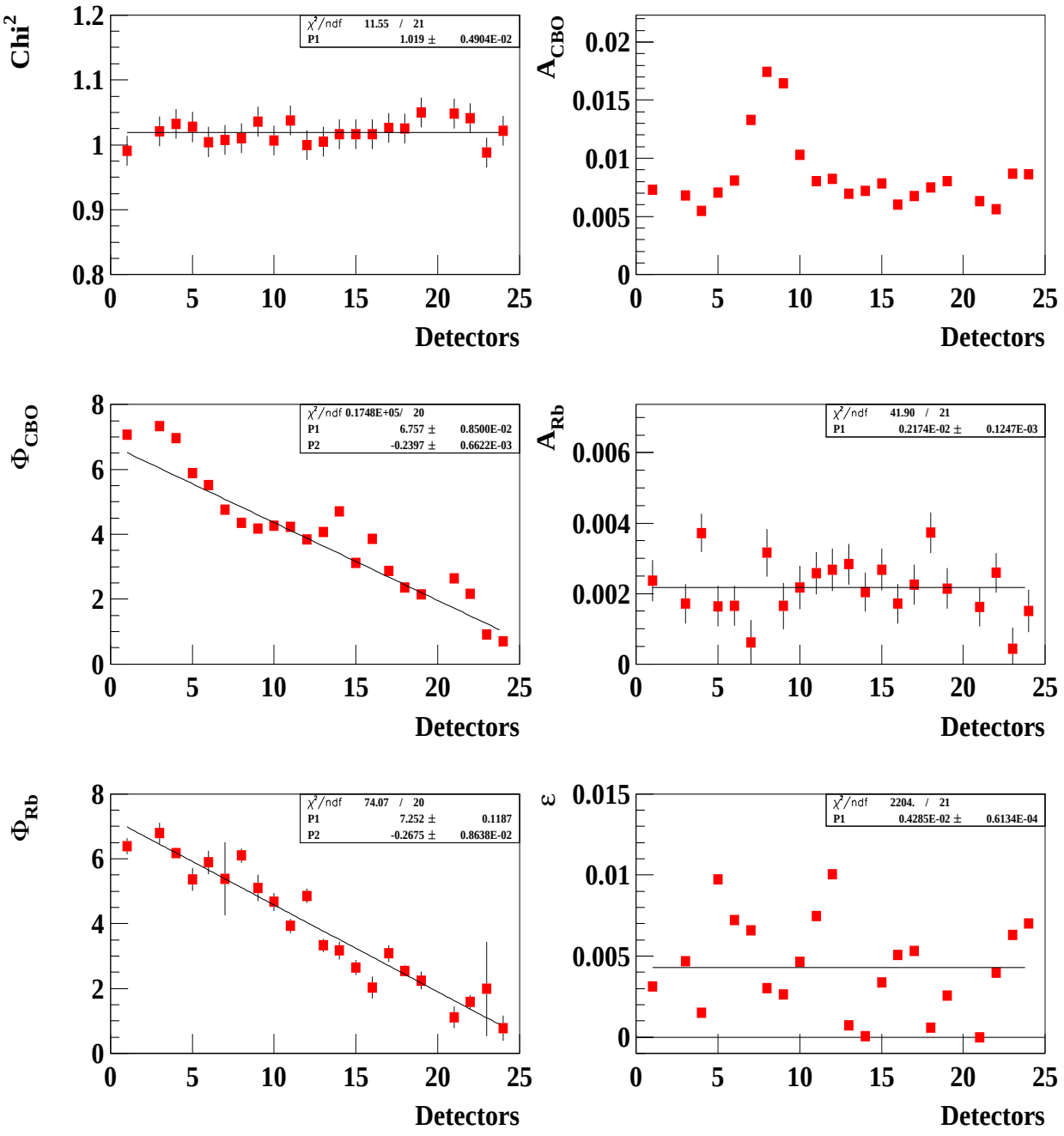

Figure 81 : Fit parameters at 49.9 μs with 1999 form including the g-2 asymmetry modulation.

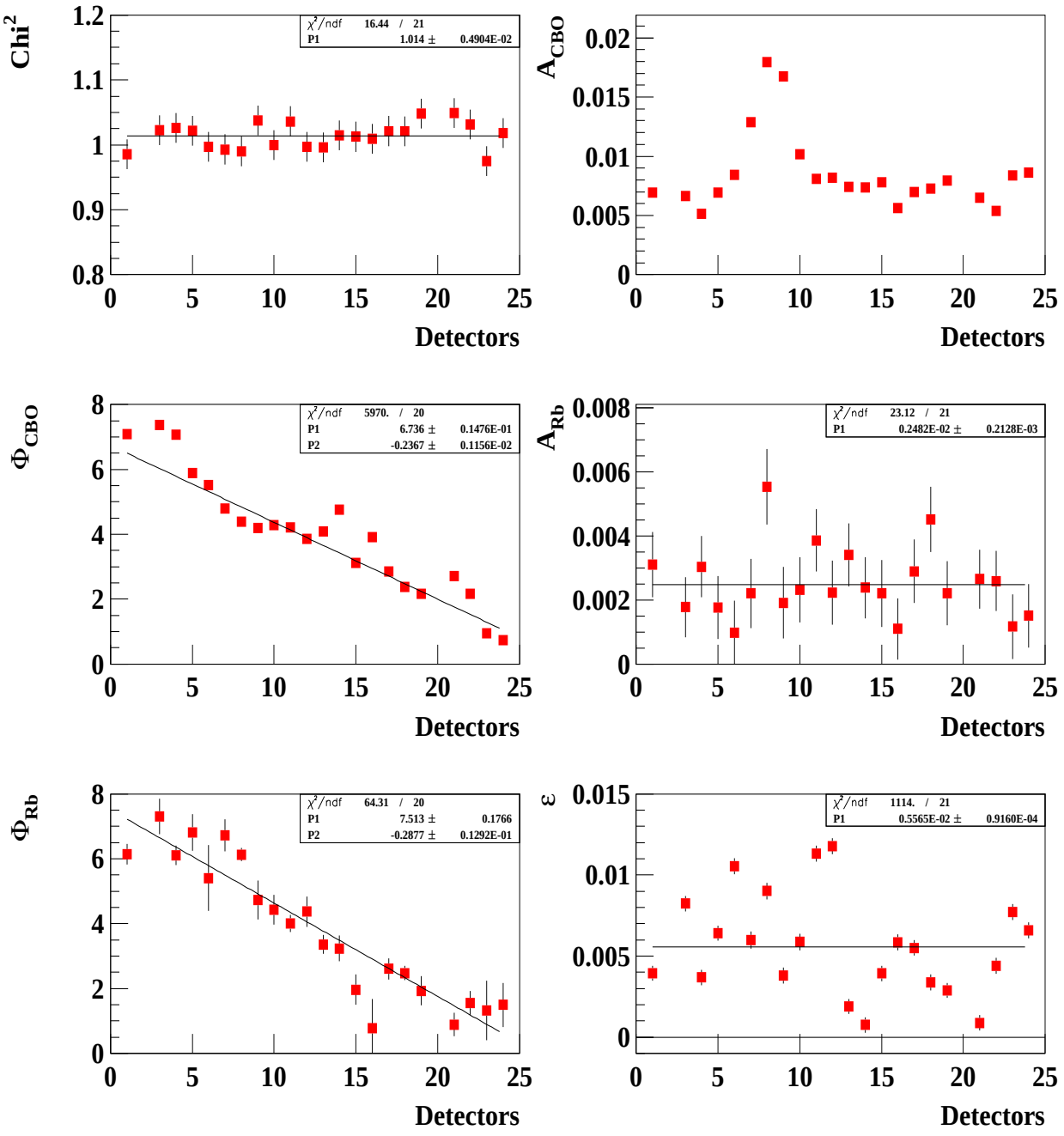

Figure 82 : Fit parameters at 82.6 μs with 1999 form including the g-2 asymmetry modulation.

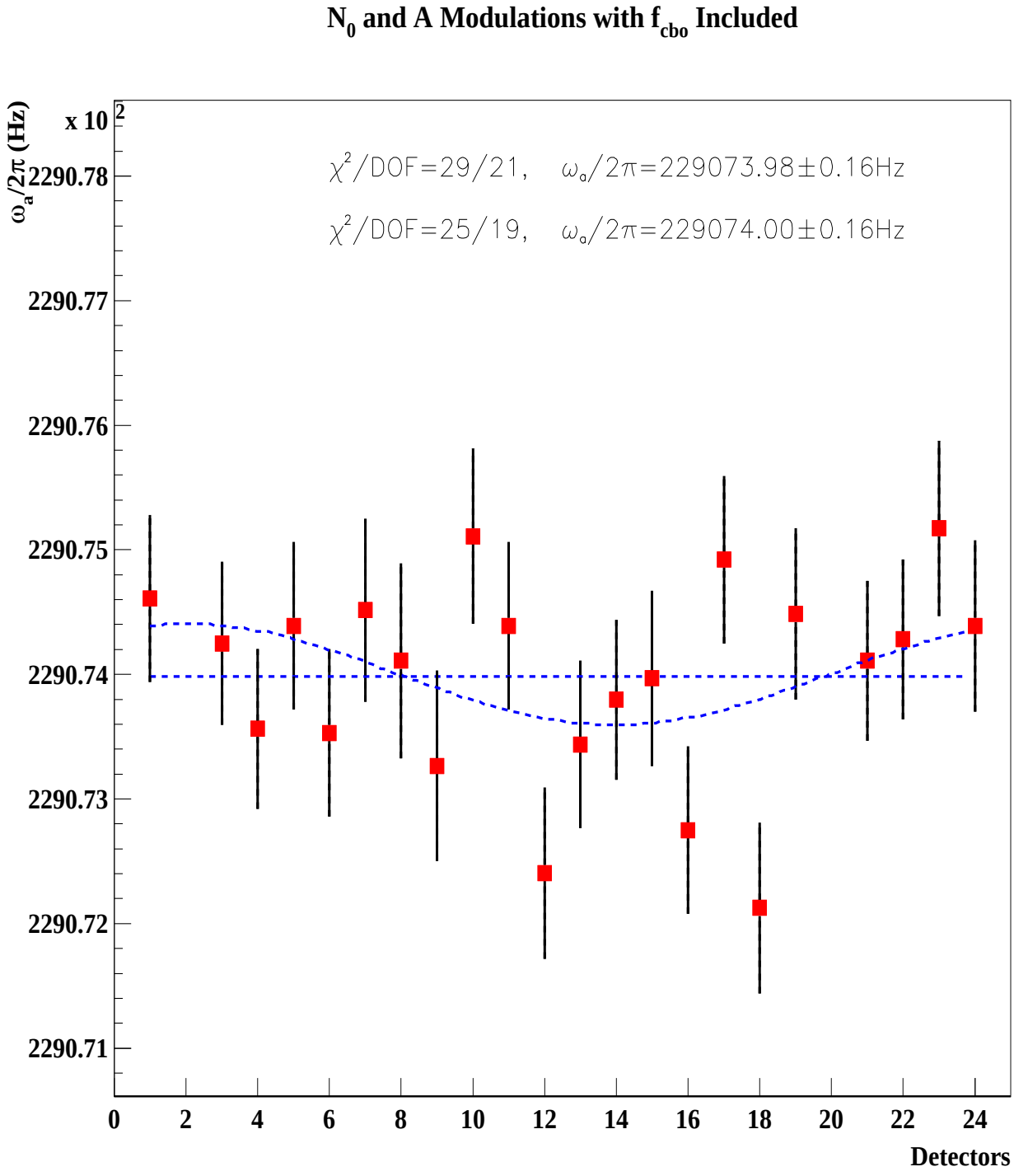

Figure 83 : R value at 49.9 μs with including the g-2 asymmetry modulation into the fit function.

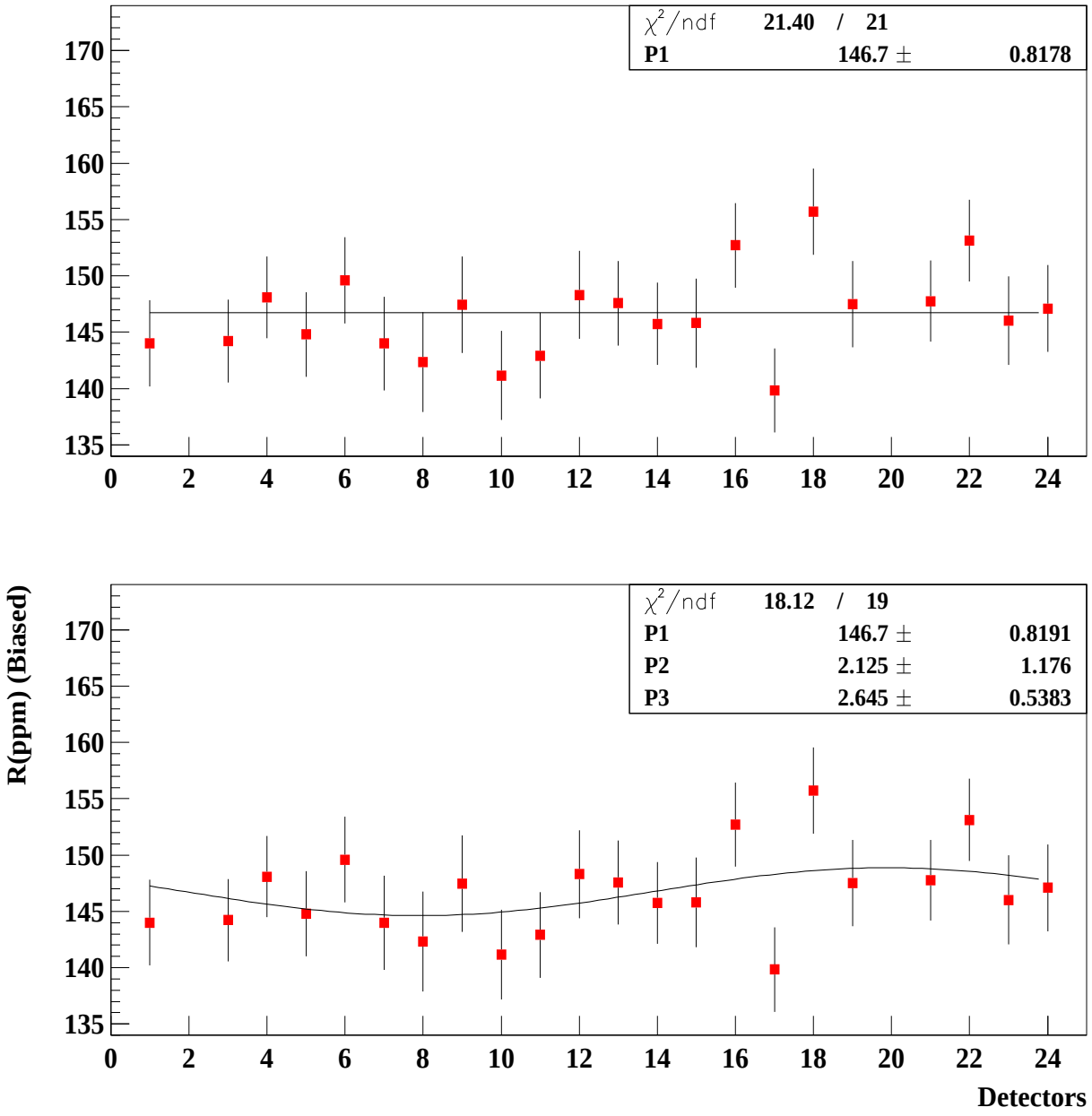

Figure 84 : R value at 82.6 μs with including the g-2 asymmetry modulation into the fit function.

The stability of R for individual detectors are shown in figure 85. The R versus time stability for each detectors is much better compared to the ones with 1999 functional form.

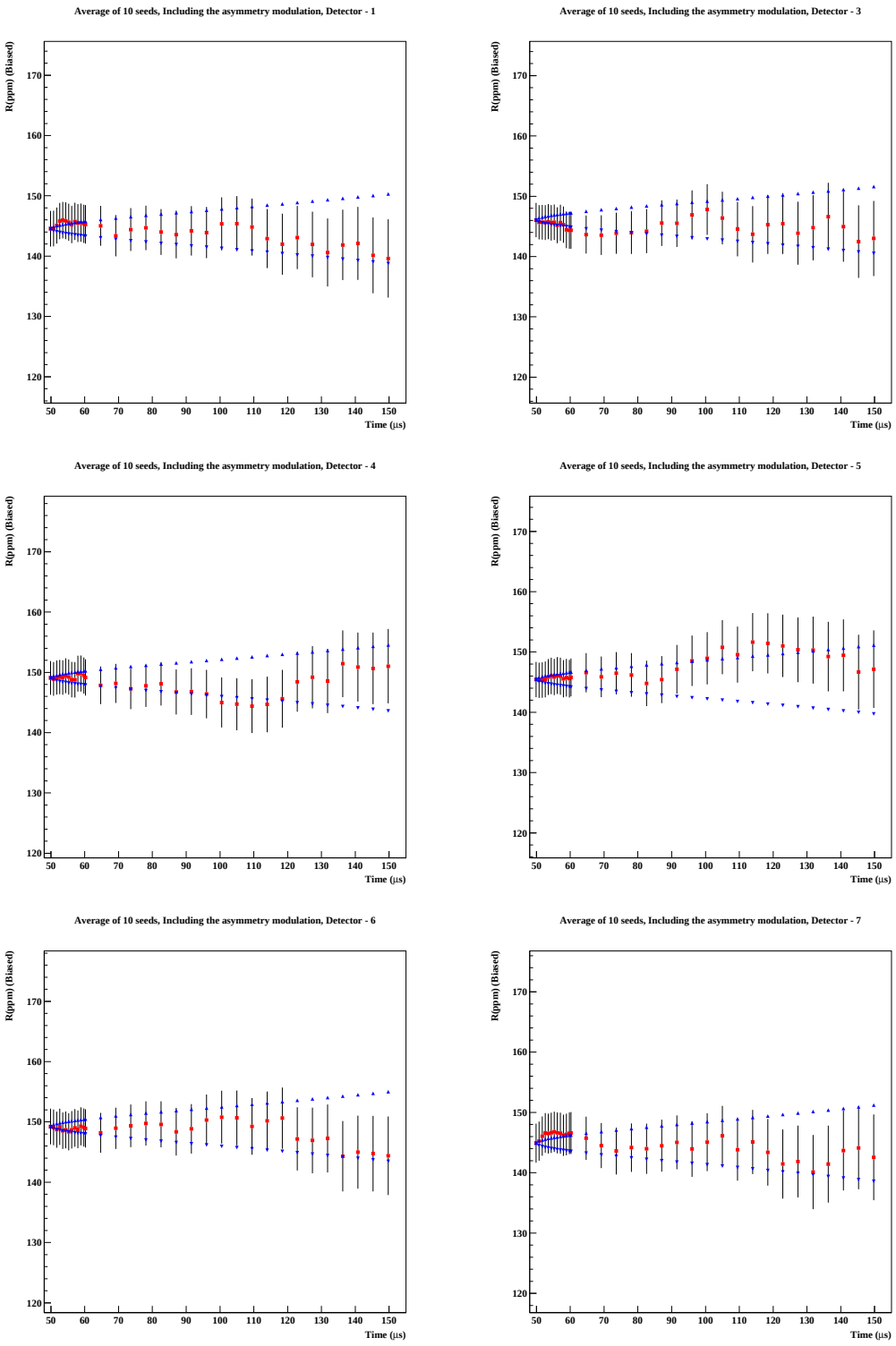

Figure 85 : The stability of R for individual detectors when the asymmetry modulation was included into the 1999 fitting function.

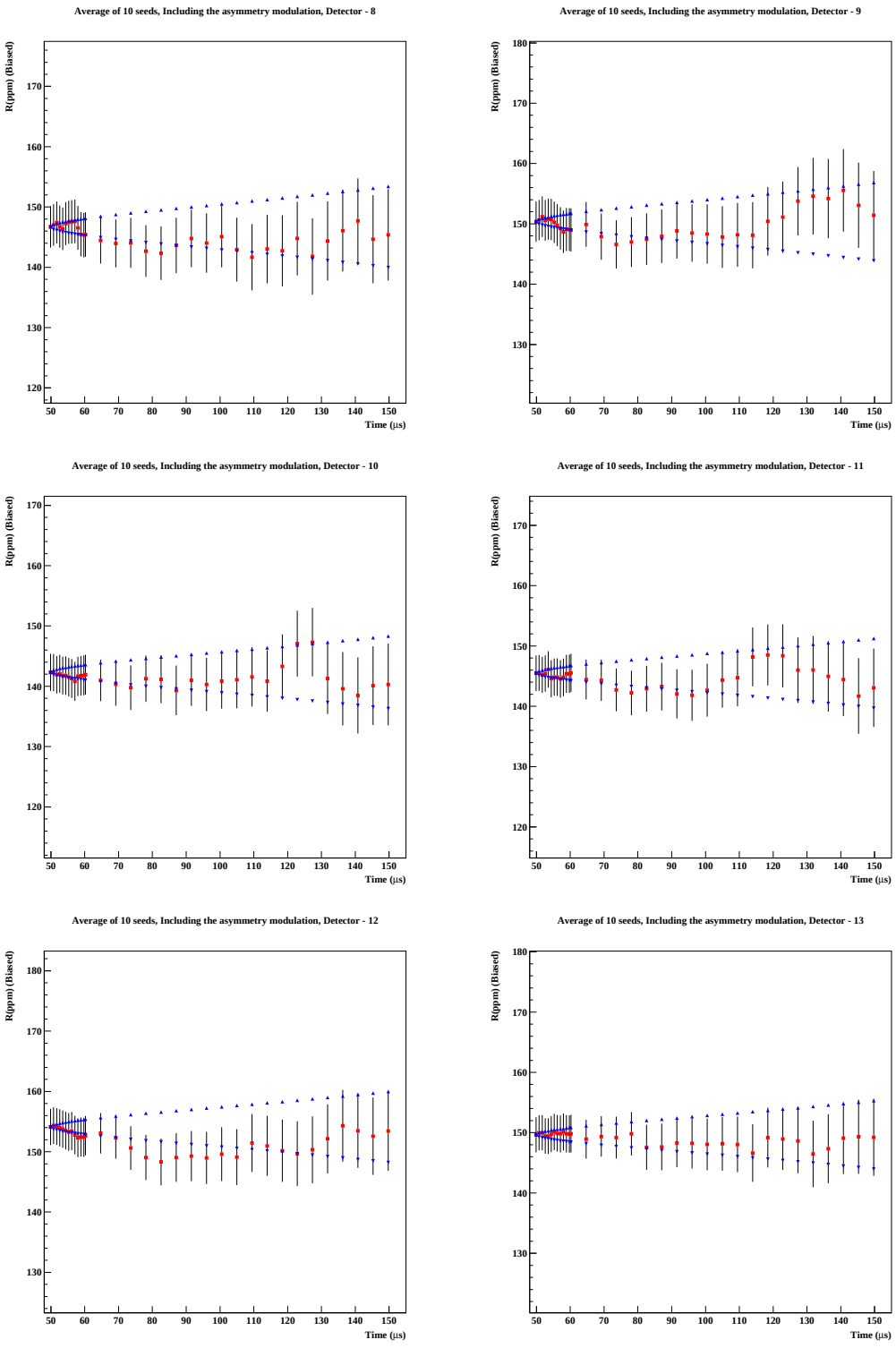

Figure 85 : continued,

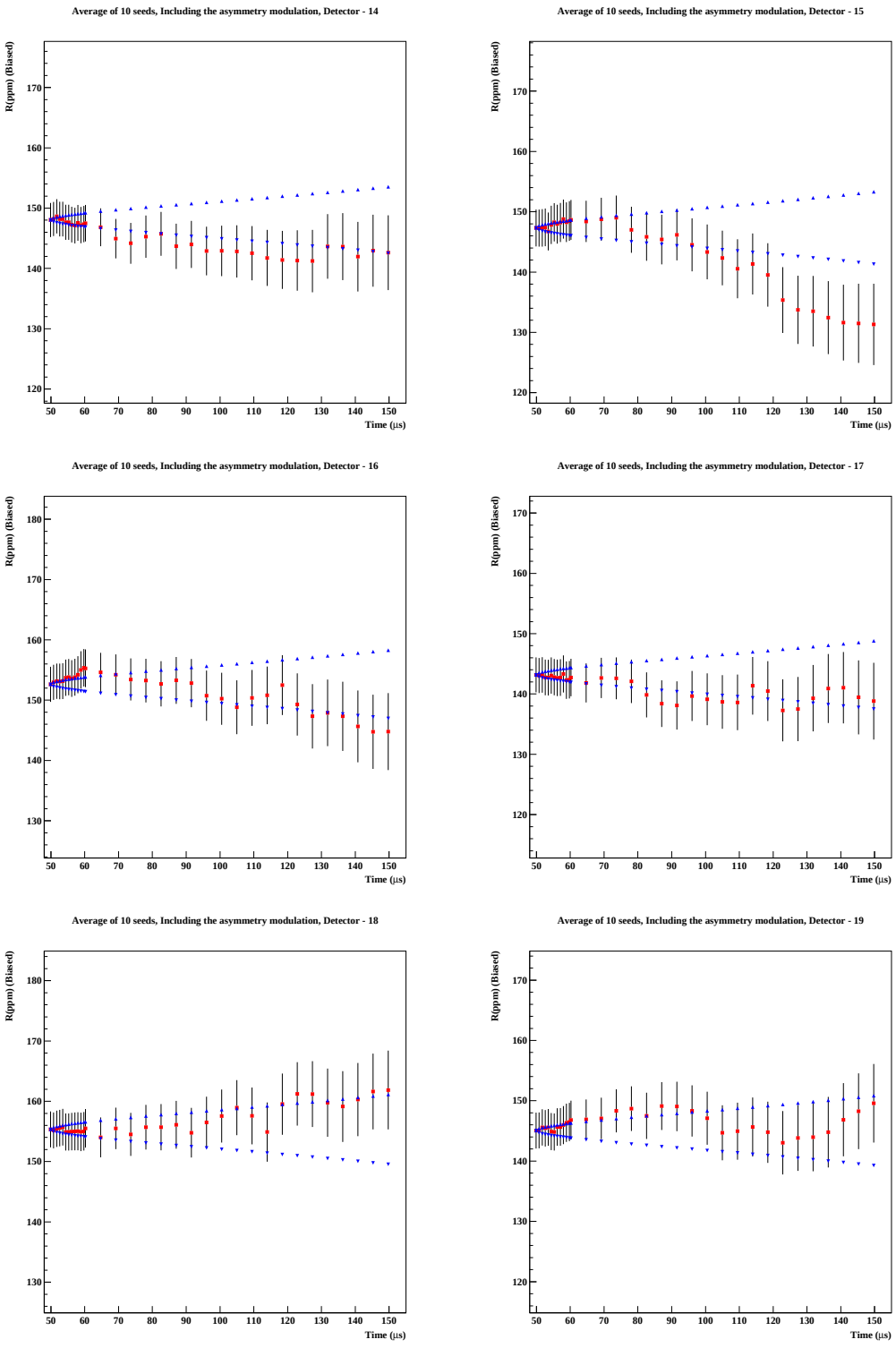

Figure 85 : continued,

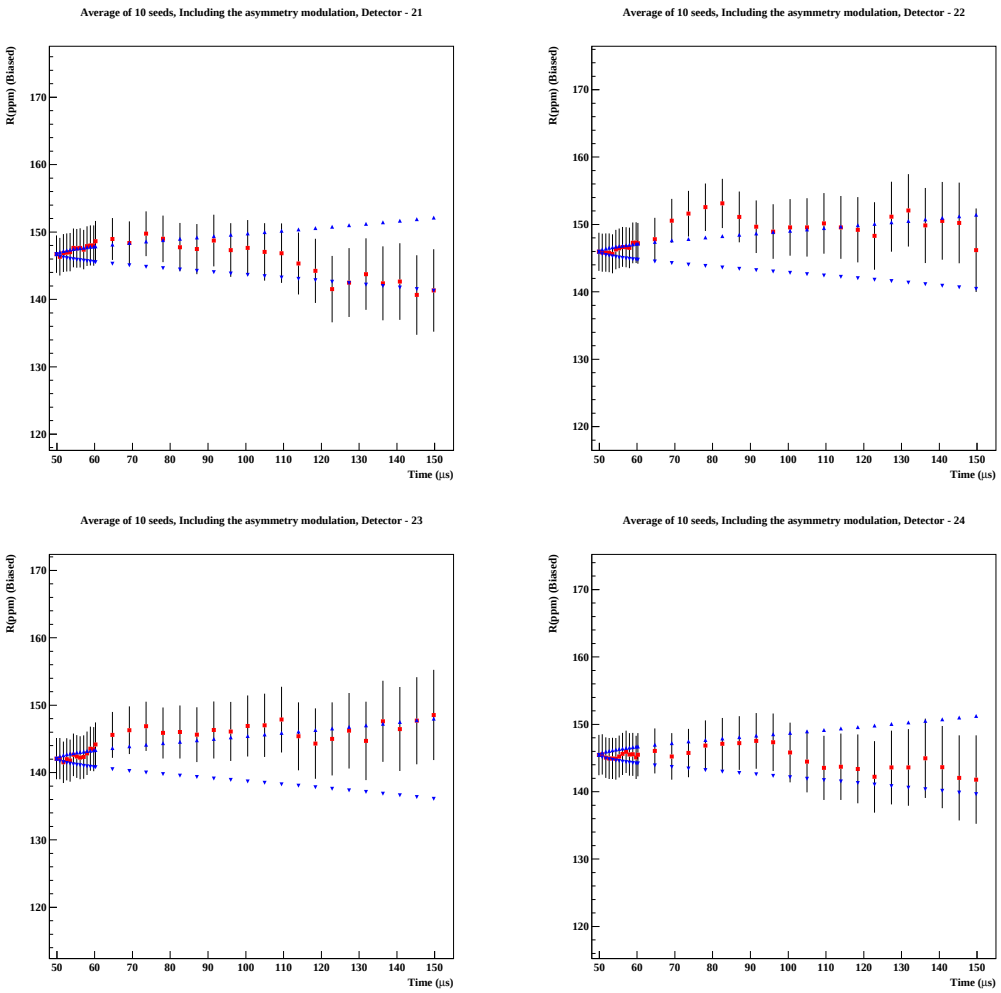

Figure 85 : continued.

The stability of other parameters are shown in the Figure 86 for each detectors for this functional form as average of ten random seeds. Asymmetry stabilities are improved dramatically compared to 1999 functional form eventhough it is still outside the Kawall band for detectors 11, 12, 18, 21 and 24. Stability of the ϵ did not changed compared to 1999 type functional form. Stability of the g-2 phase (also R) also improved drastically with this functional form for almost all the detectors. The stability of CBO phase and amplitude are stayed generally the same. The g-2 asymmetry modulation amplitude A_{Rb} stays out of the Kawall band most of the time for the kicker detectors 7 and 8. When the g-2 asymmetry modulation amplitude is very close to zero, the phase (ϕ_{Rb}) is undetermined and the fit enlarges the error. In this case it is not possible to draw the Kawall band. For that reason the Kawall bands are not shown for the g-2 asymmetry modulation phase ϕ_{Rb}. When the ϵ and the ϕ_{Rb} stabilities are compared, one can see the correlation between two of them (detectors four and seven). This is also signature of the gain and ϕ_{Rb} relations.

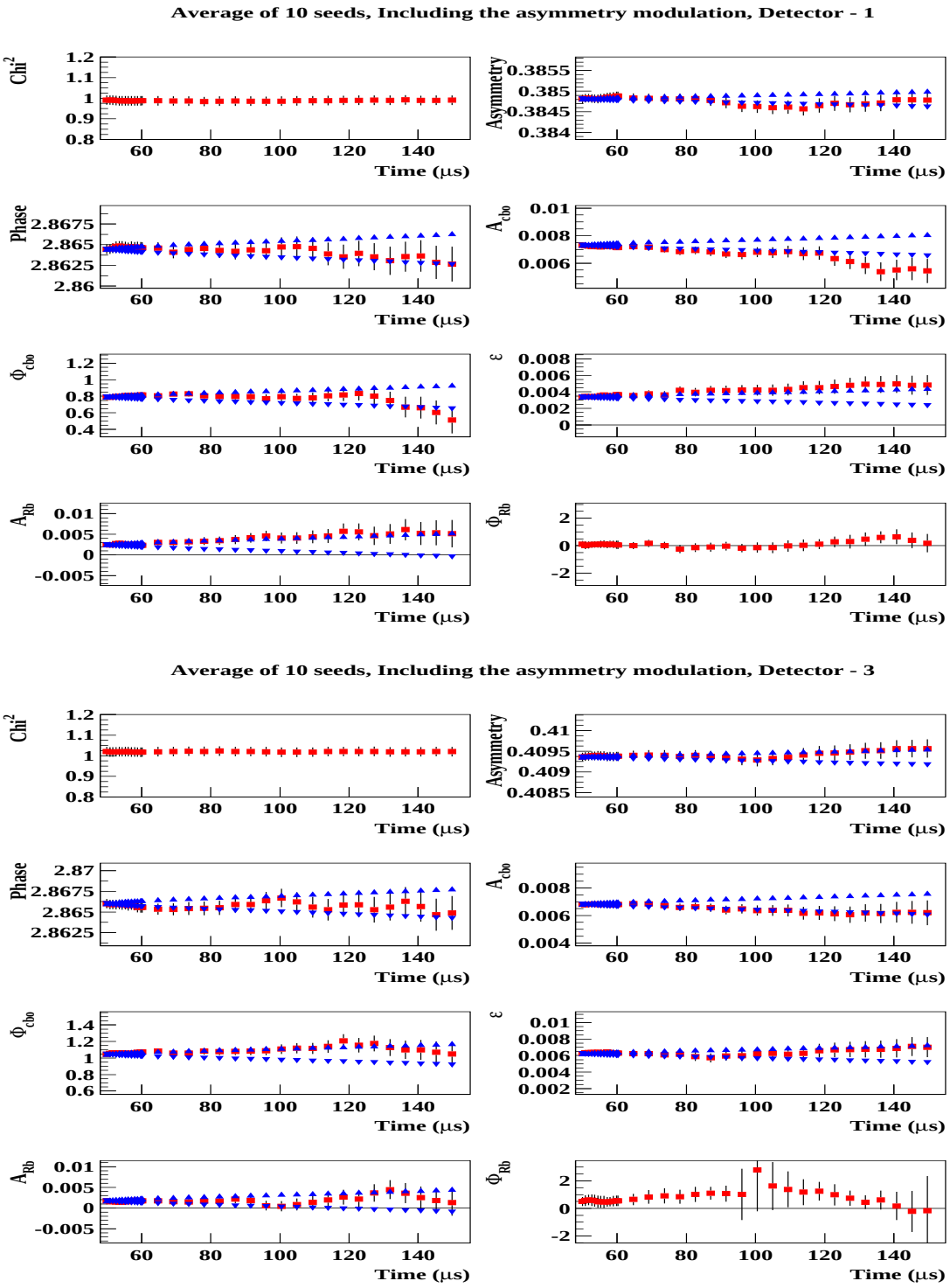

Figure 86 : The stability of R for individual detectors when the asymmetry modulation terms were included into the 1999 fitting function.

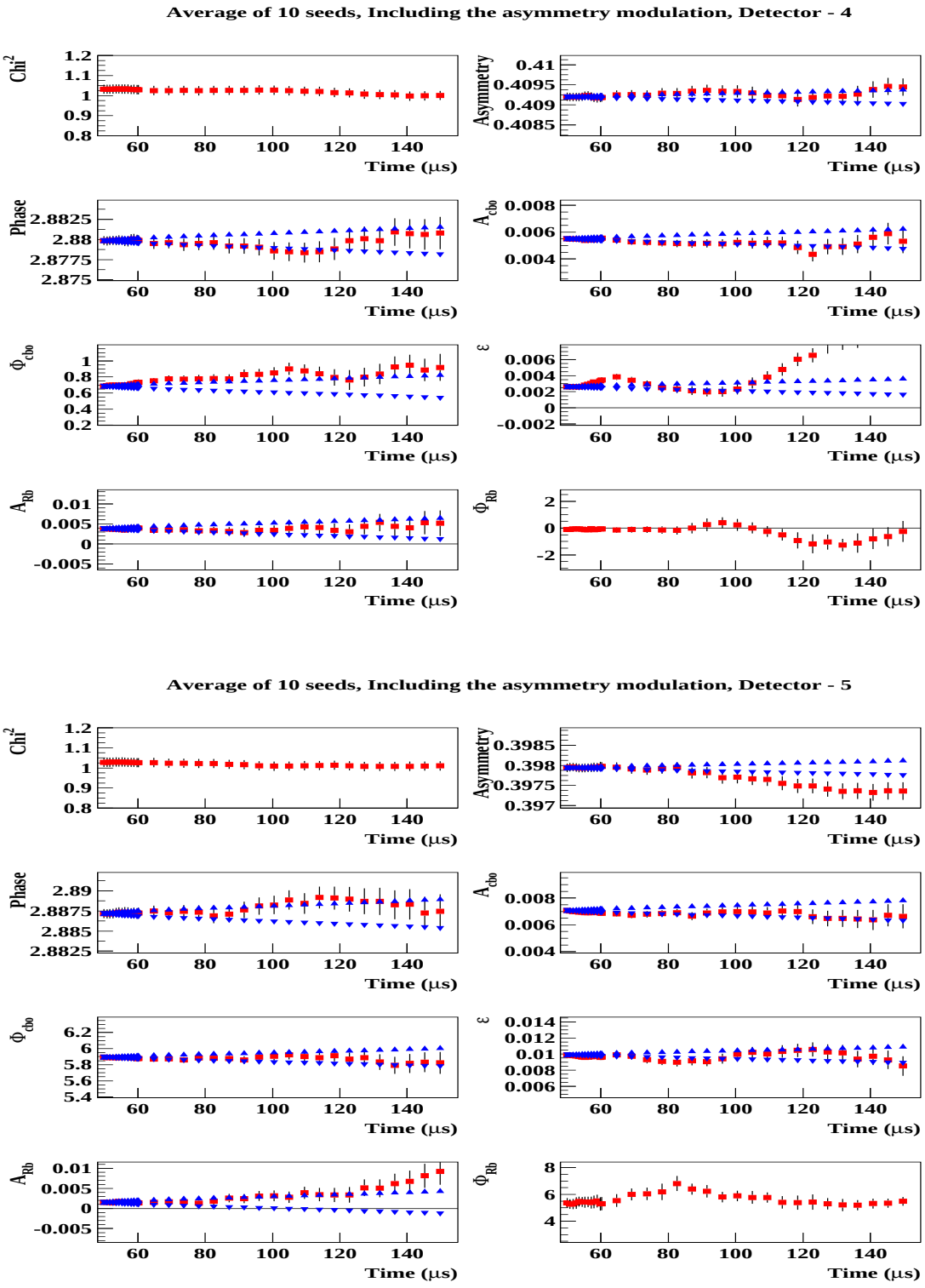

Figure 86 : continued,

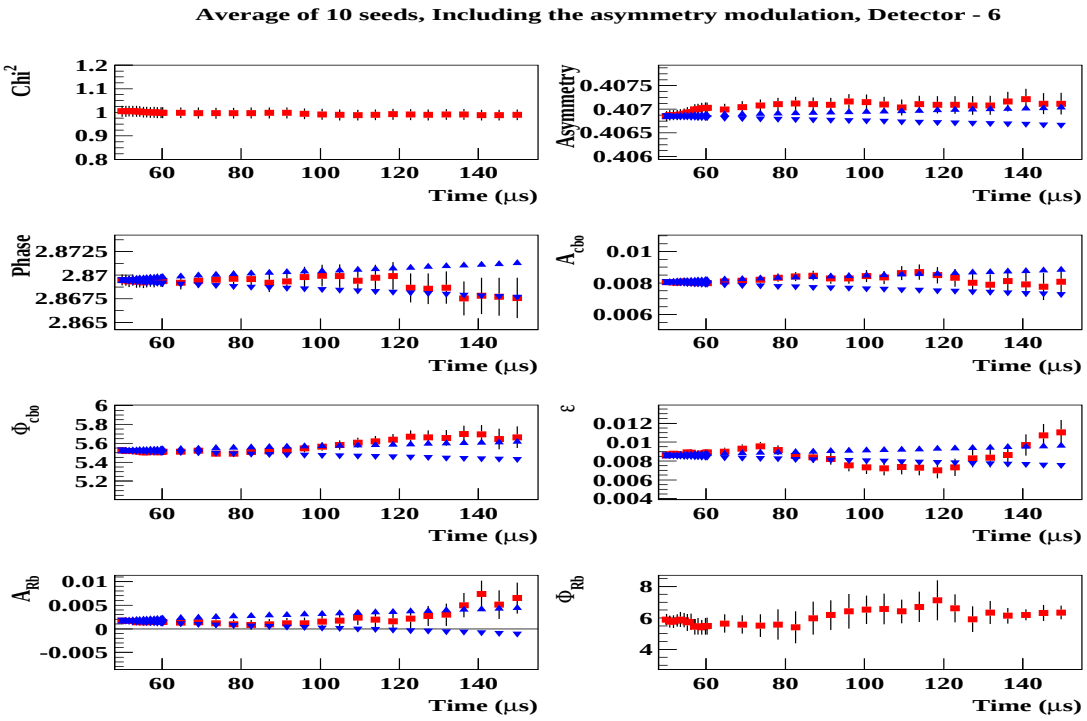

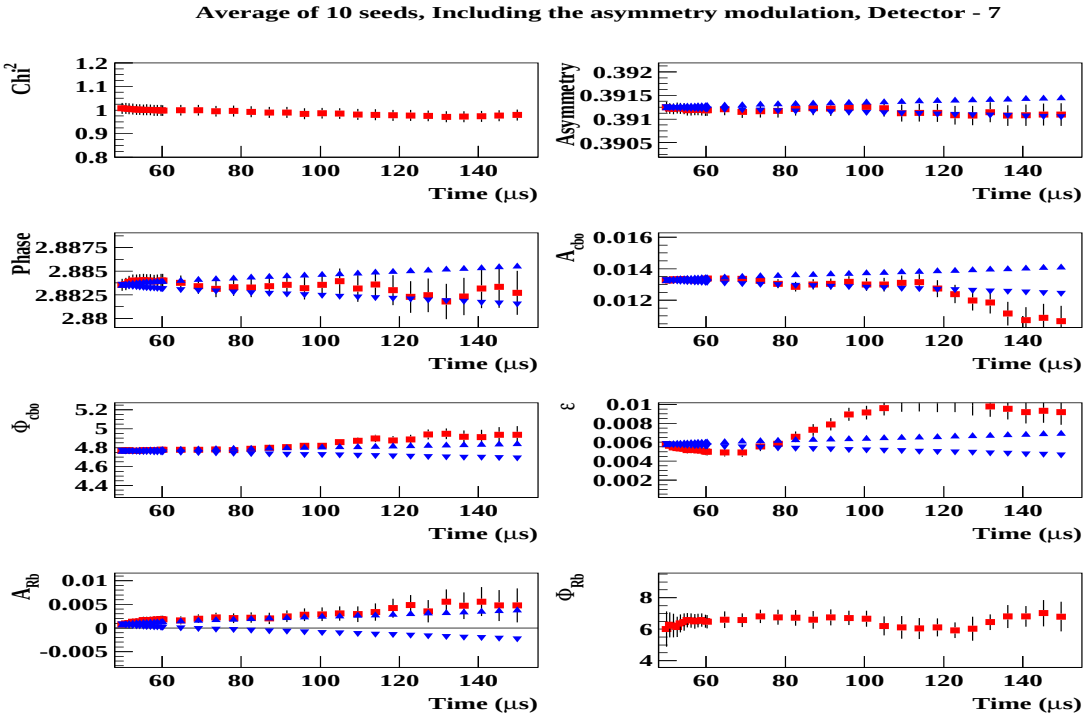

Figure 86 : continued,

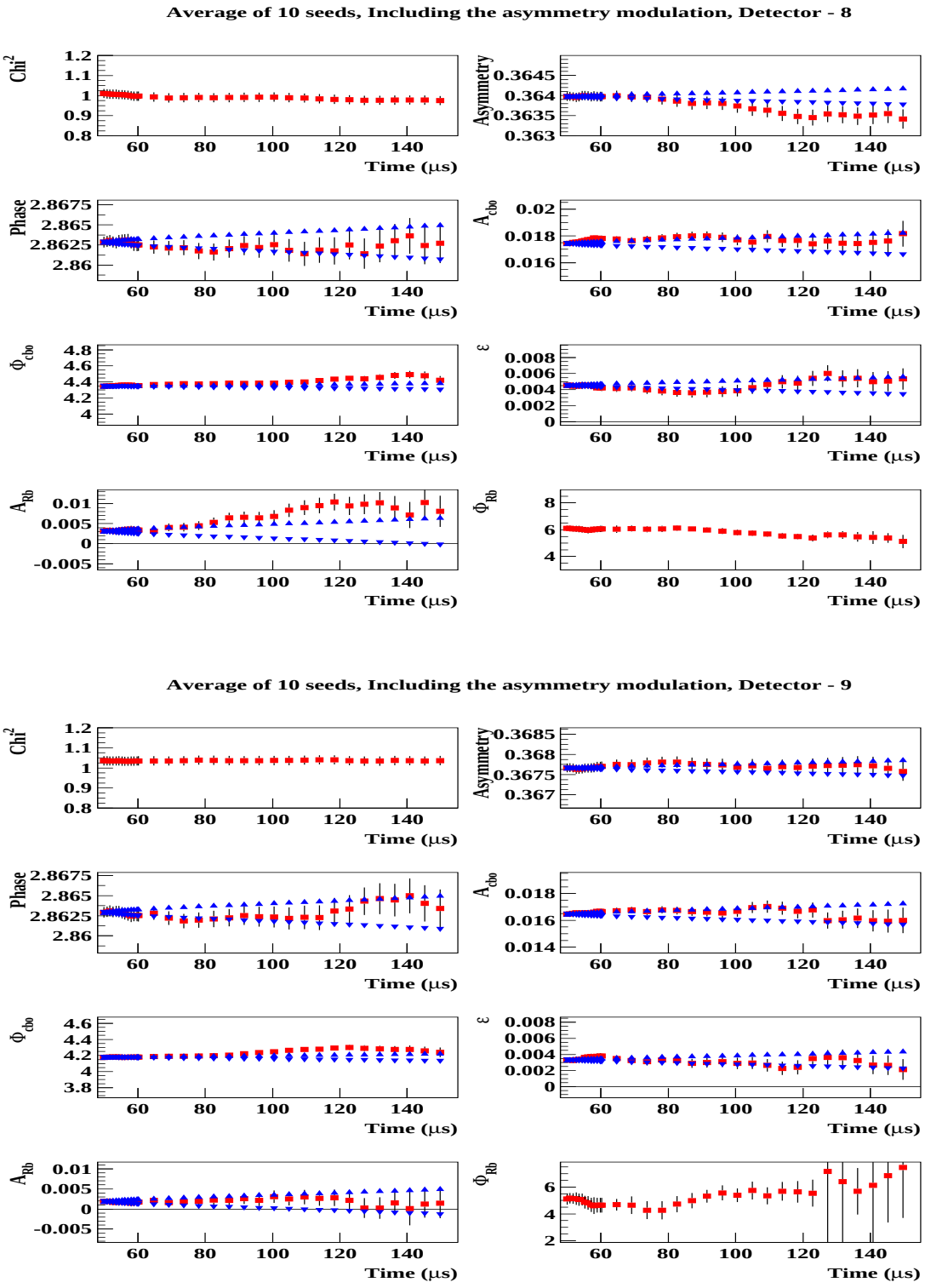

Figure 86 : continued,

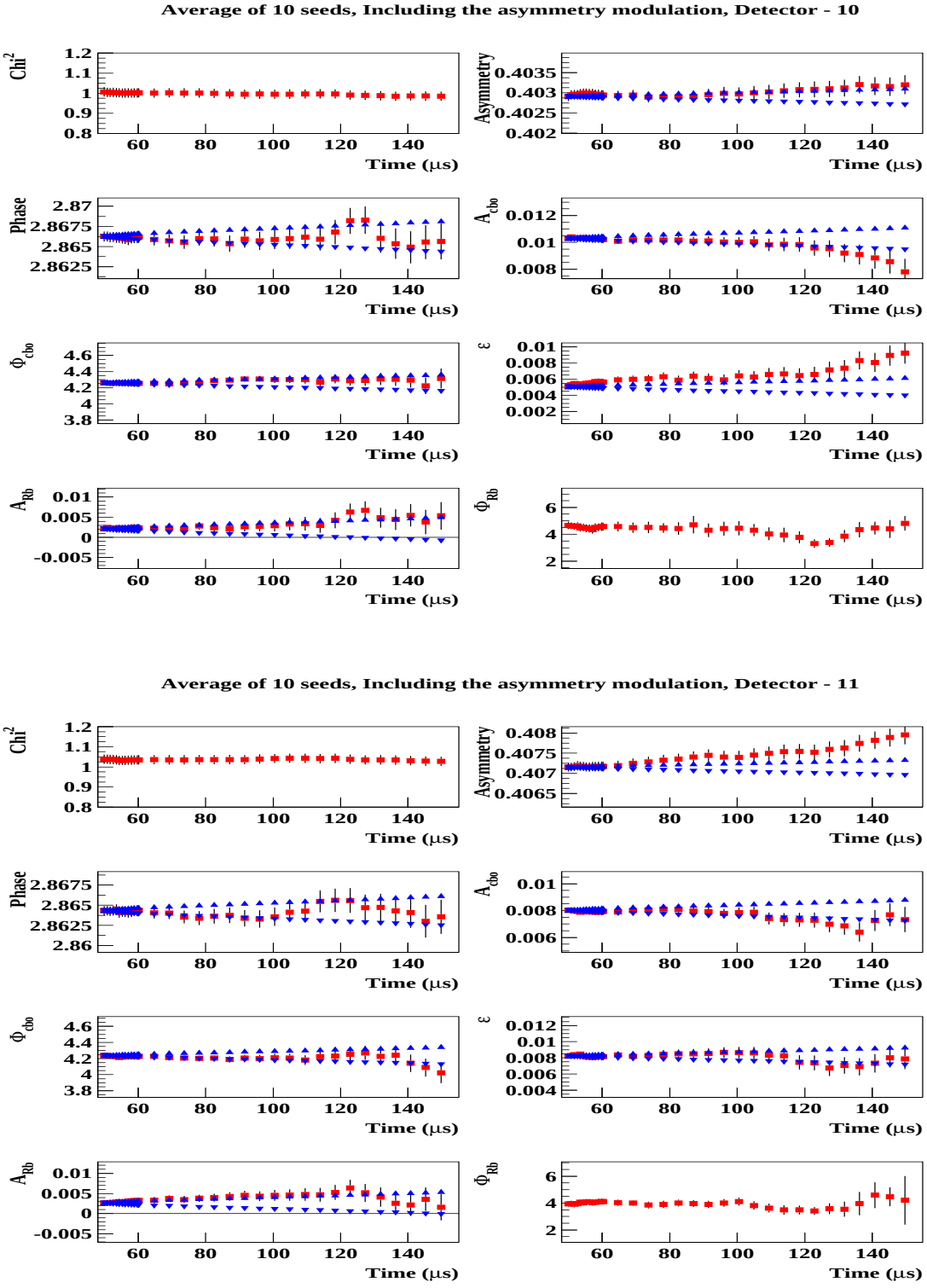

Figure 86 : continued,

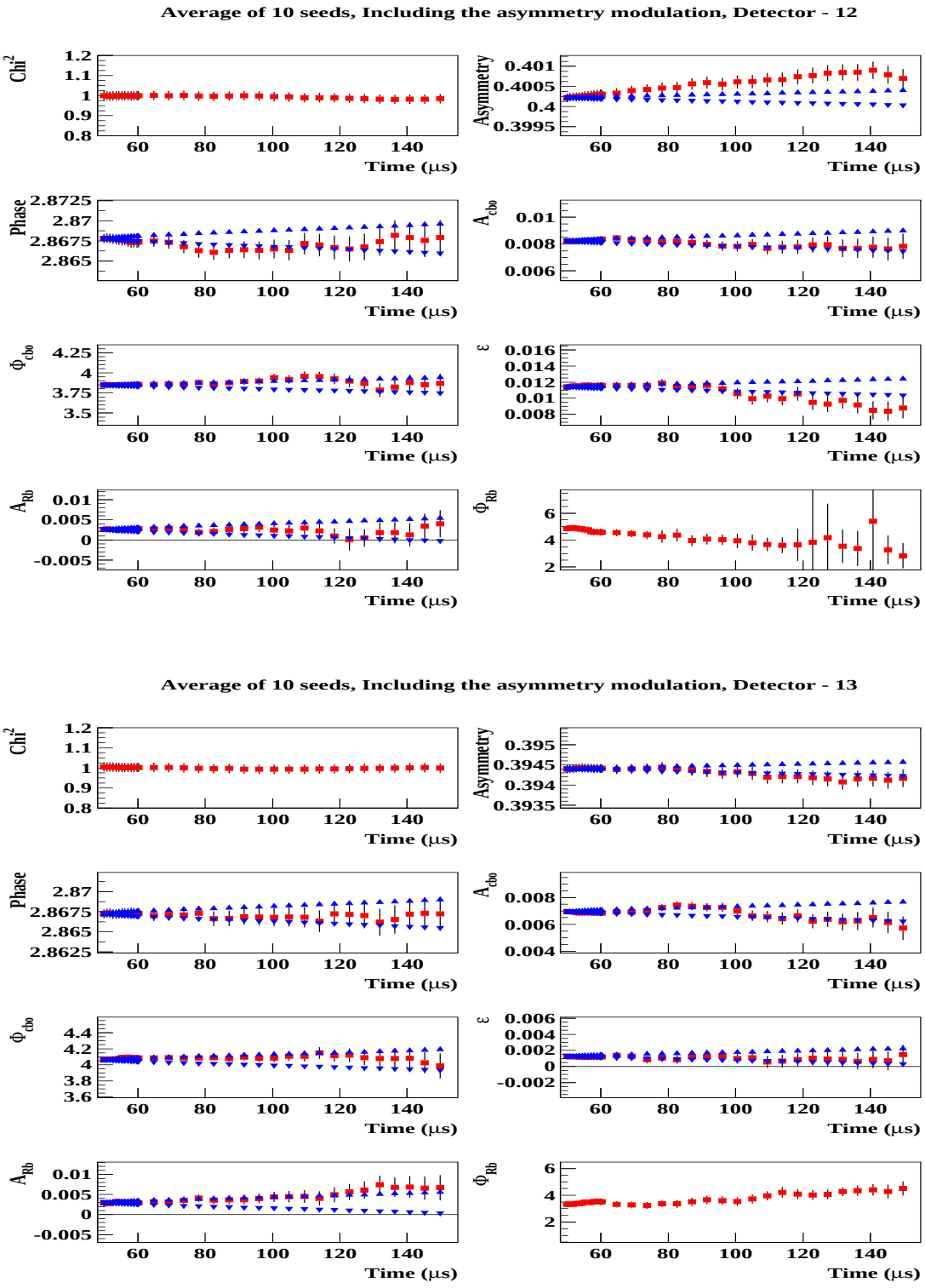

Figure 86 : continued,

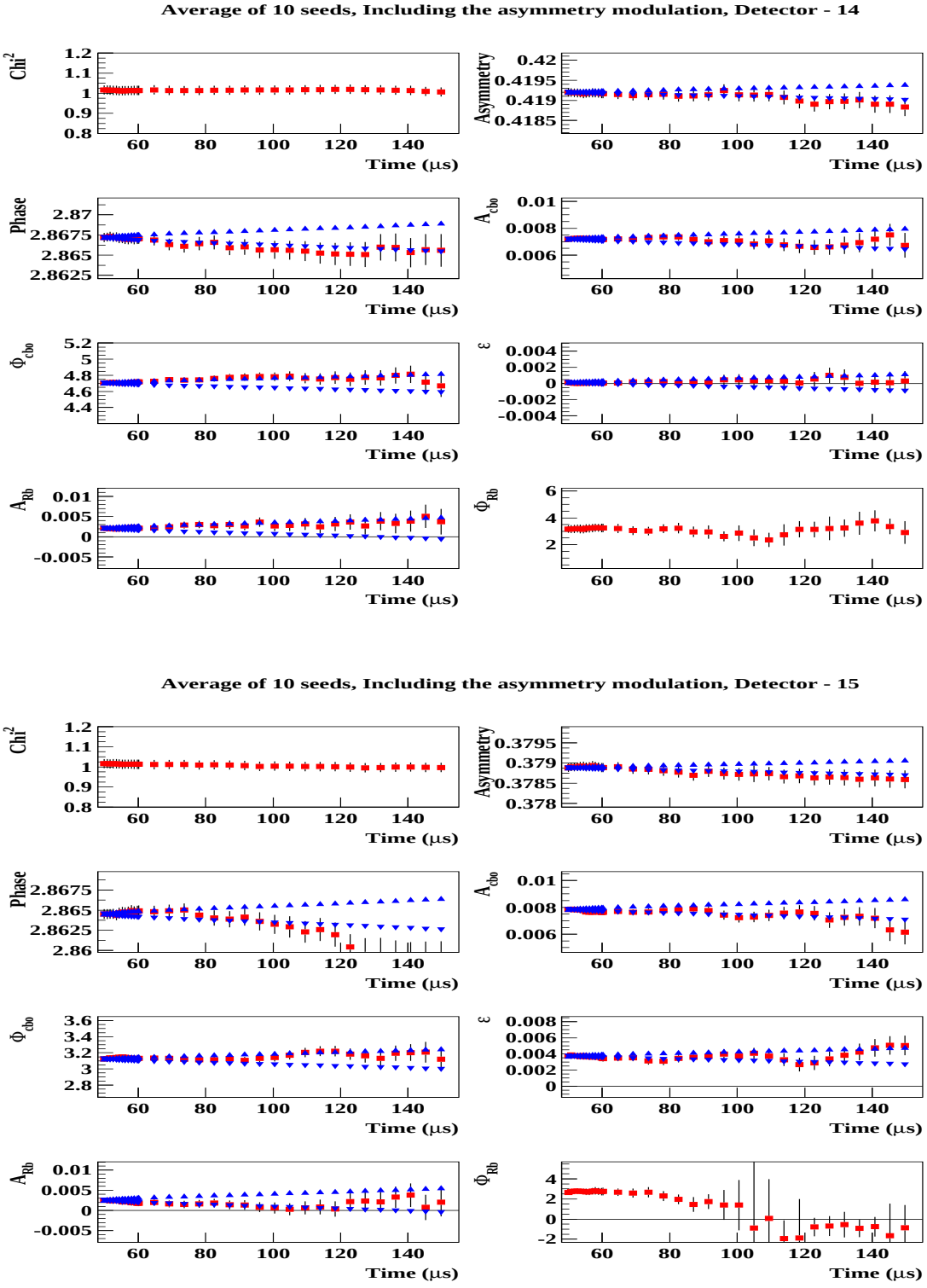

Figure 86 : continued,

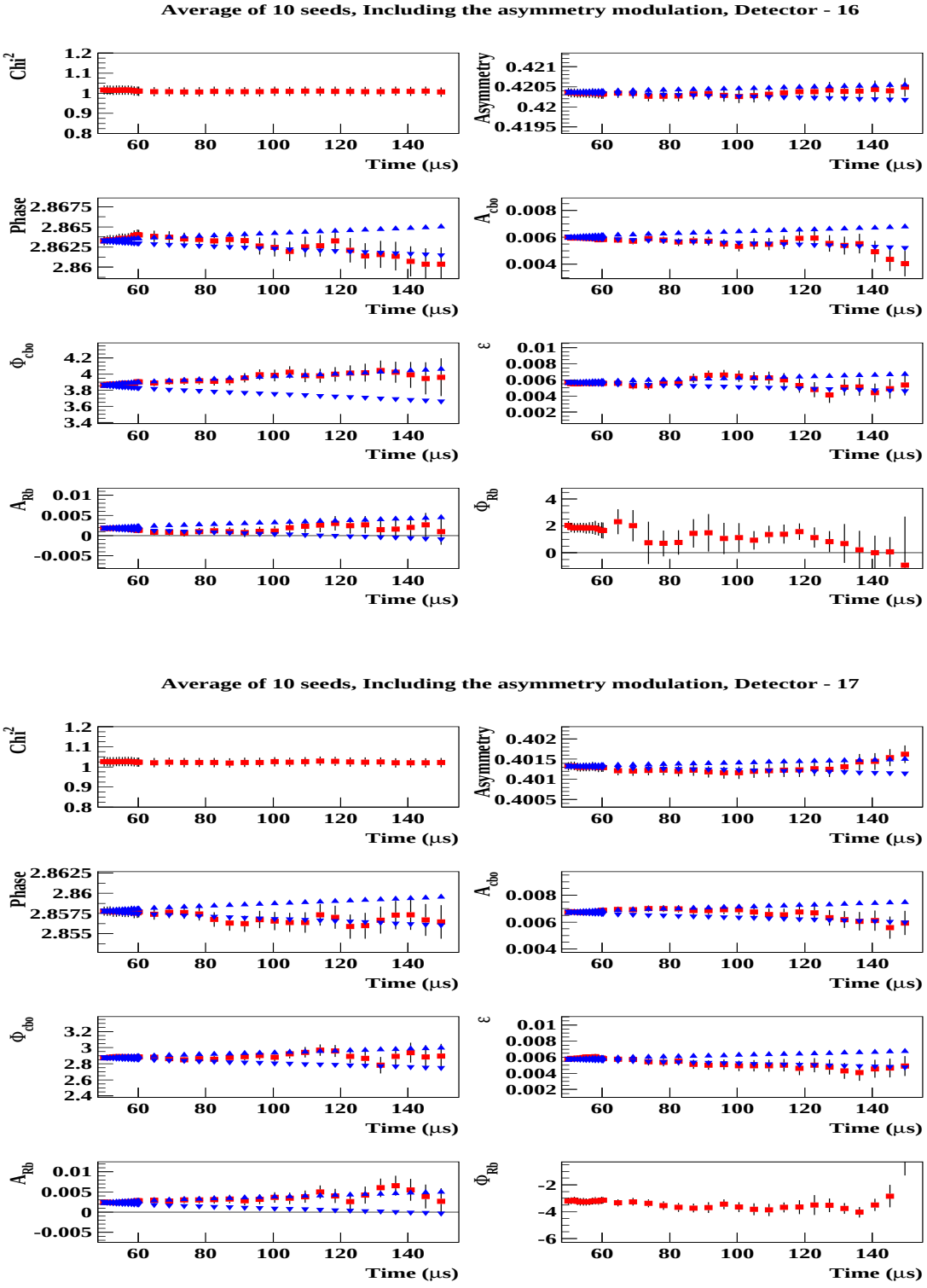

Figure 86 : continued,

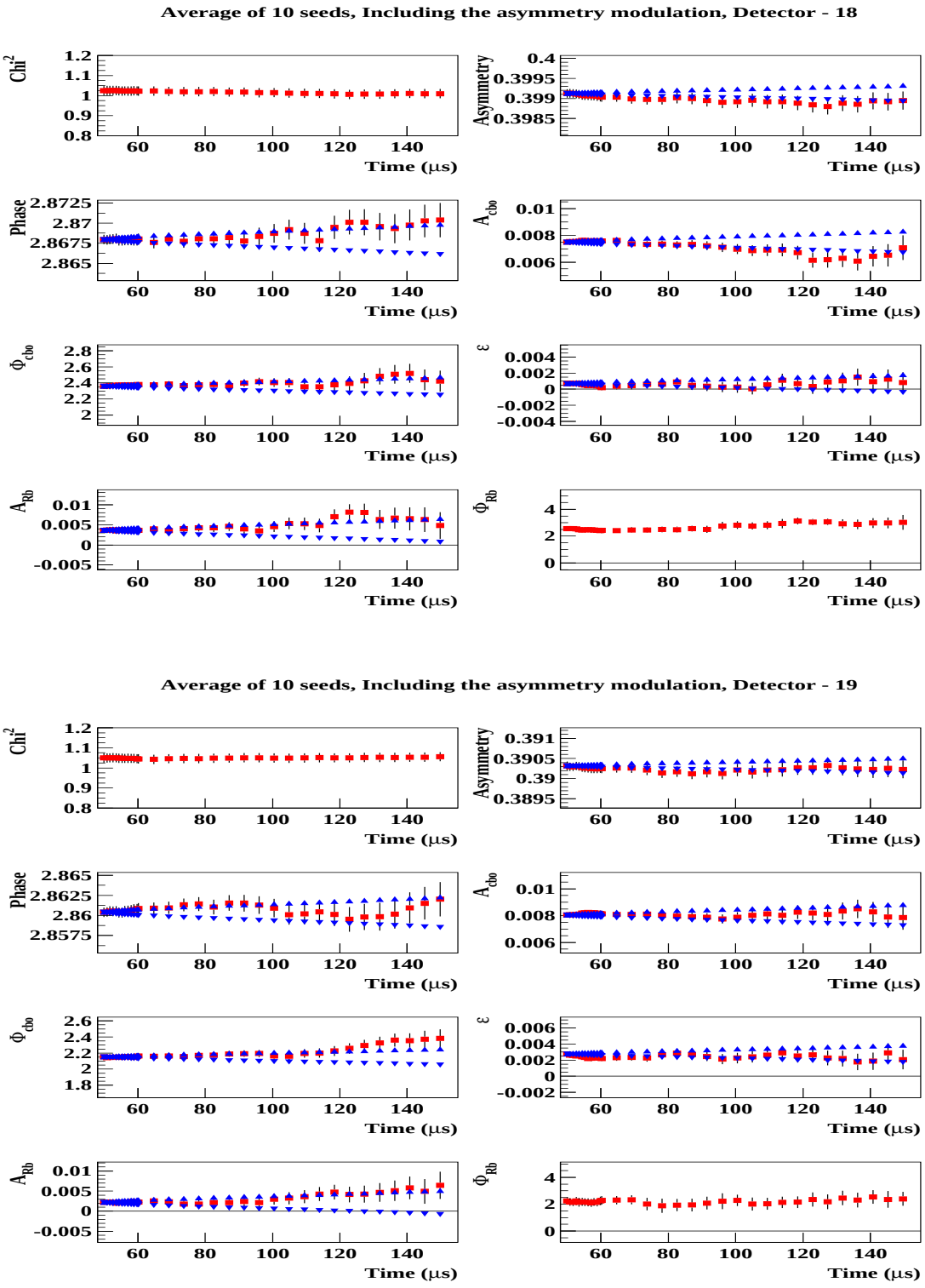

Figure 86 : continued,

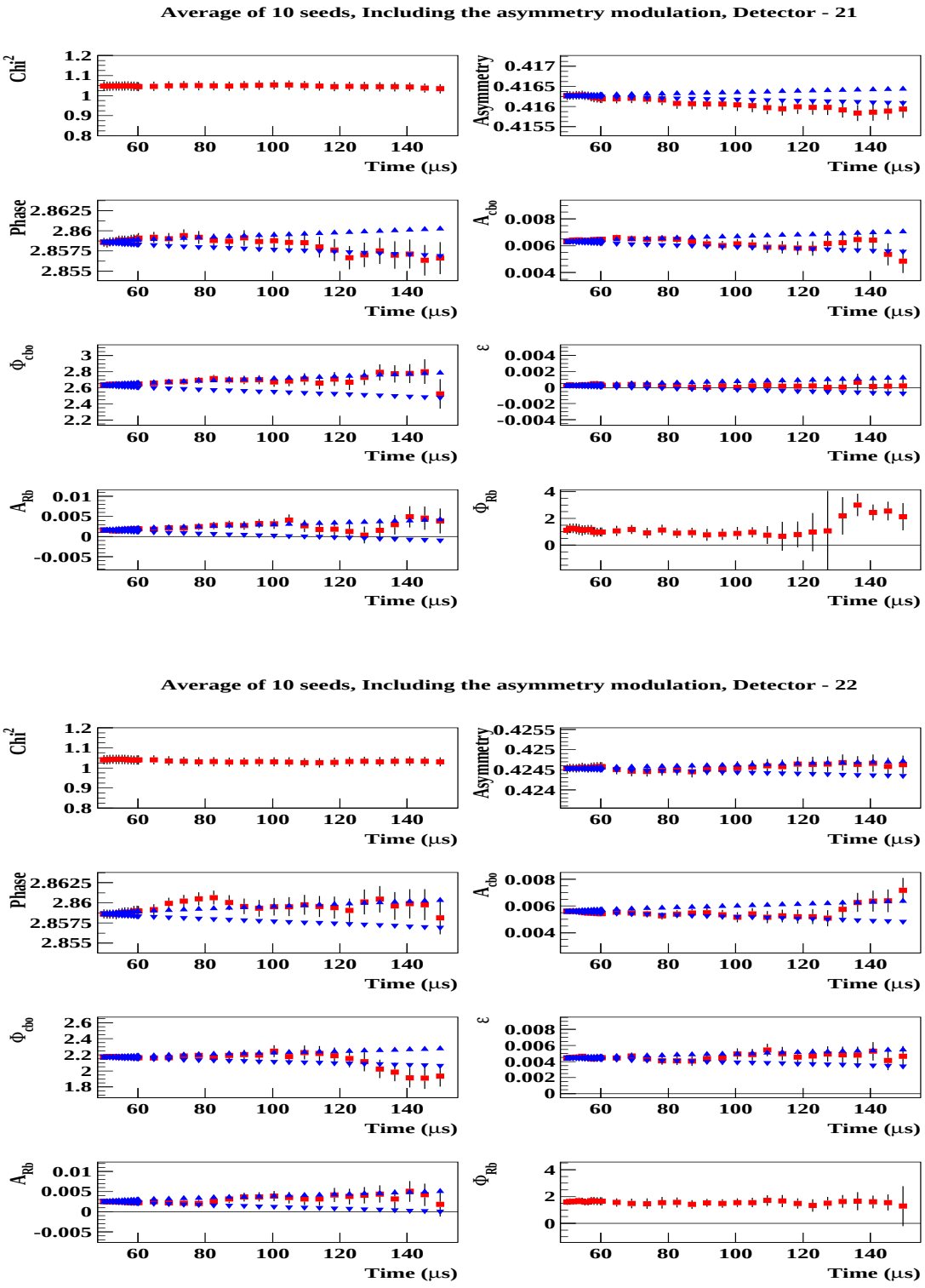

Figure 86 : continued,

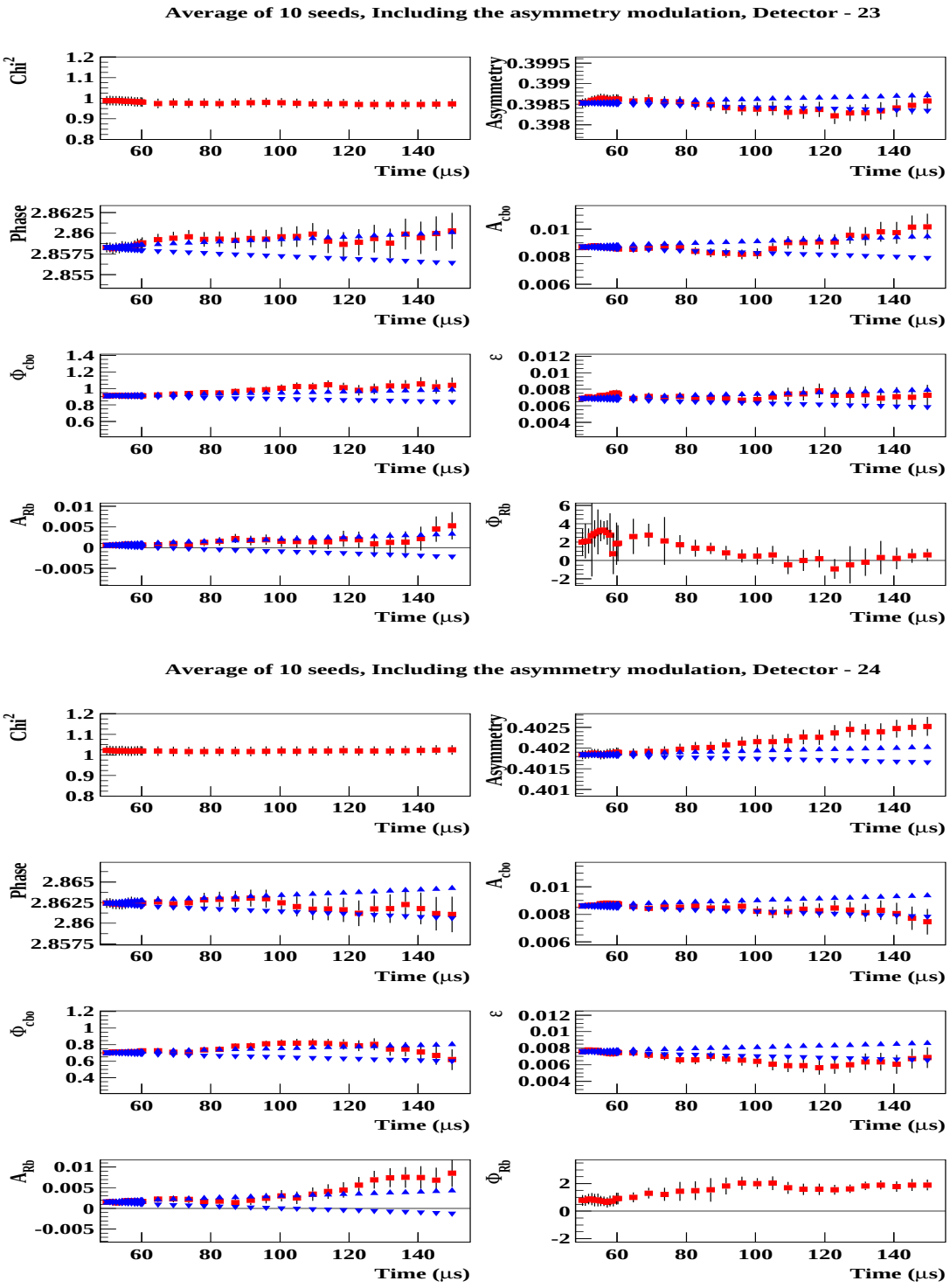

Figure 86 : continued.

7.2.3 The complete physics form

In the complete physics form as one remembers the both of the g-2 asymmetry and the phase modulations were introduced into the 1999 type functional form.

$$F(t) = N_0 e^{-t/\tau_\mu}\{1+A\prime cos(2\pi(f_0-f_a)t+\phi\prime)\}\{1+A_{cbo}\mathbf{E_{cbo}(t)}cos(2\pi f_{cbo}t+\phi_{cbo})\}\ \{1+\epsilon(t)\}$$

Here $\phi\prime = \phi + \mathbf{A_{Jm}\ E_{cbo}(t)\ cos(2\pi f_{cbo}t + \phi_{Jm})}$ and the bold part considered as g-2 phase modulation due to CBO.

This function provides the complete picture of the effects in our data and for that reason I prefer to called it physics function. This functional form is my favorite eventhough it is more sensitive to the gain changes than the other functional forms. Early studies showed that there is a discrepancy between the Monte Carlo and the fit outcome for A_{Jm}. However this issue is still under investigation by Rob and Mario. On the other hand when 2001 data with different n values were fit, the similar amplitudes for g-2 phase modulation were obtained compared to 2000 data which gives more confident about the reality of this number. So we believe this effect with this visible size (from the fit) is there. When we look at the phase of the phase modulation for detectors, we see they are aligned between 0 to 2π just like the CBO and the phase of asymmetry modulation. This also shows the CBO connection of this effect. When this effect was introduced into the fits, the half ring effect removed completely (look at the individual detectors).

In the second half this functional form works perfect but not in the first half. Most probably this is due to gain behavior differences between the first and the second halves. Asymmetry parameters gets into the Kawall band with this functional form. Only problem is the amplitude and the phase parameters for g-2 phase modulation are not stable in the first half (especially the phase). The diving behavior in the amplitude of the g-2 phase modulation (starts with an amplitude at 49 μs and goes to zero around 100μs) is the signature of the gain shape in the first half. Please refer to artificial gain study also. In order to put the A_{Jm} into Kawall band one needs a longer phase modulation envelope lifetime for the second half and shorter lifetime for the first half which can be again easily explained from the shape of the gain differences. The gain trends are opposite in the first and the second halves. The first half has decreasing trend whereas the second half has increasing trend which makes the lifetime of the phase modulation envelope shorter in the first and longer in the second half due to strong correlations between the gain and the phase modulation.

Figures 87-89 shows the stability of the fit parameters for the first, the second half and the all detectors together for the complete physics function. Figures 90-92 show the R stability versus fit start time.

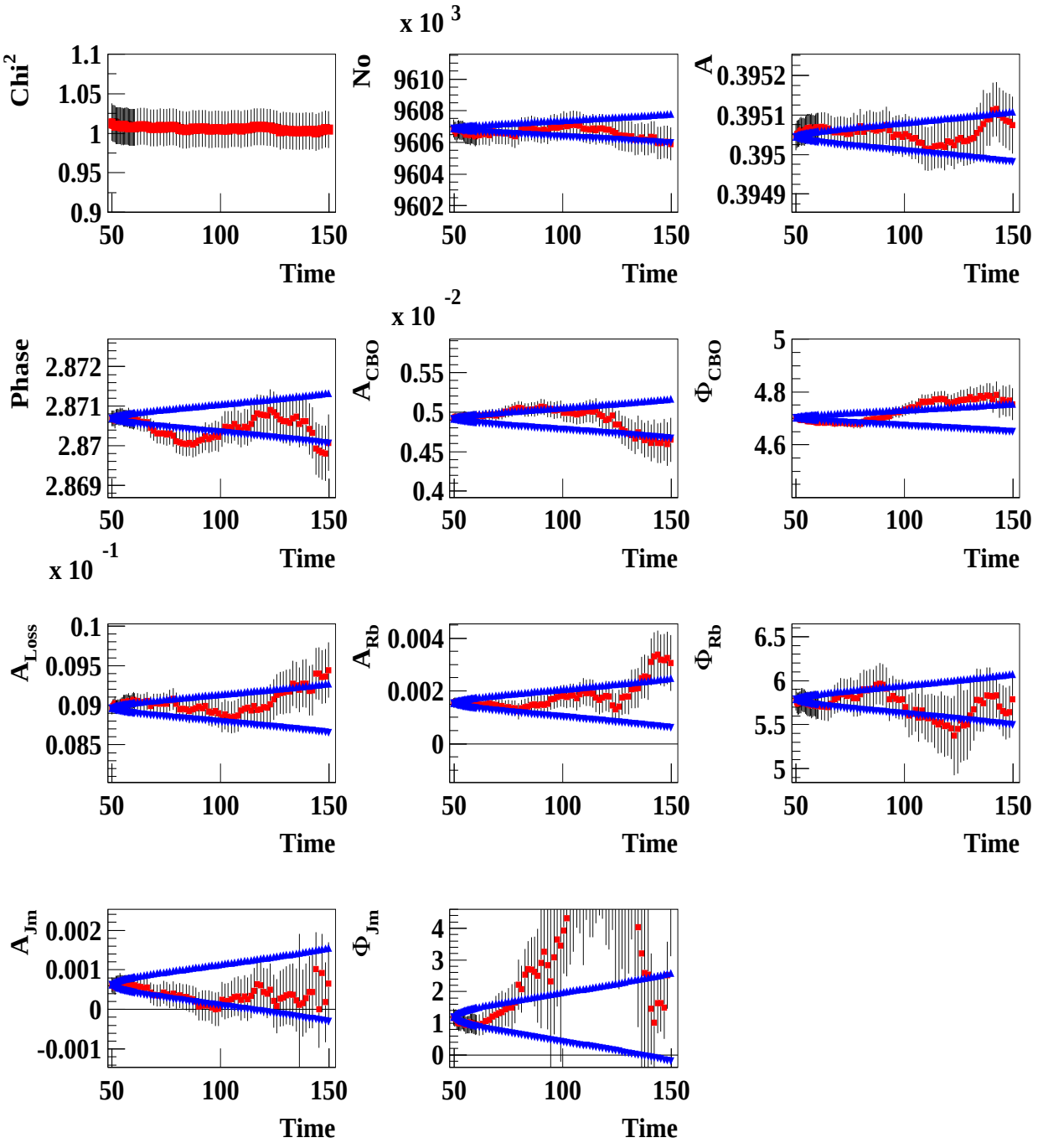

Figure 87 : Fit parameters with the complete physics function on the first half.

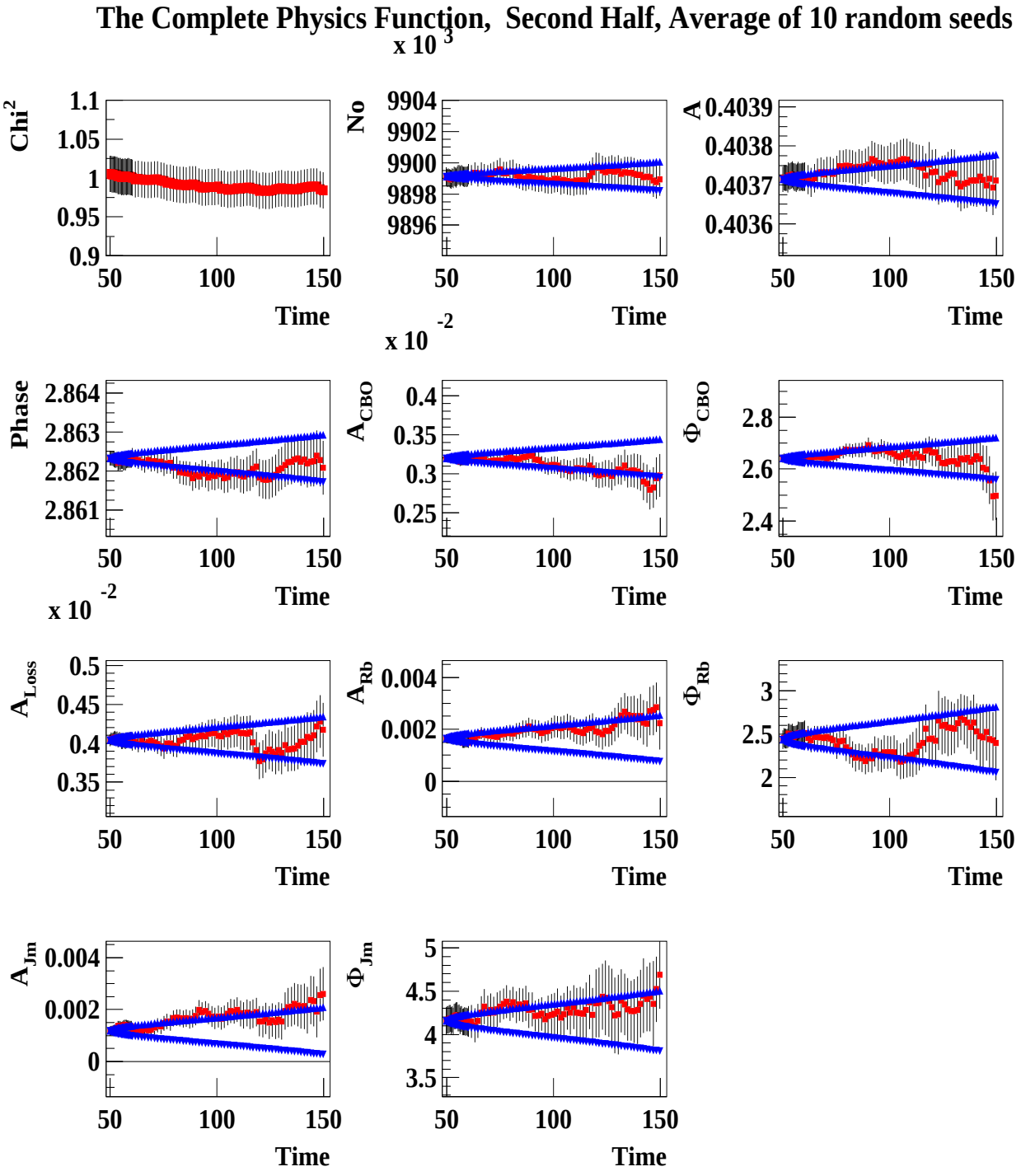

Figure 88 : Fit parameters with the complete physics function on the second half.

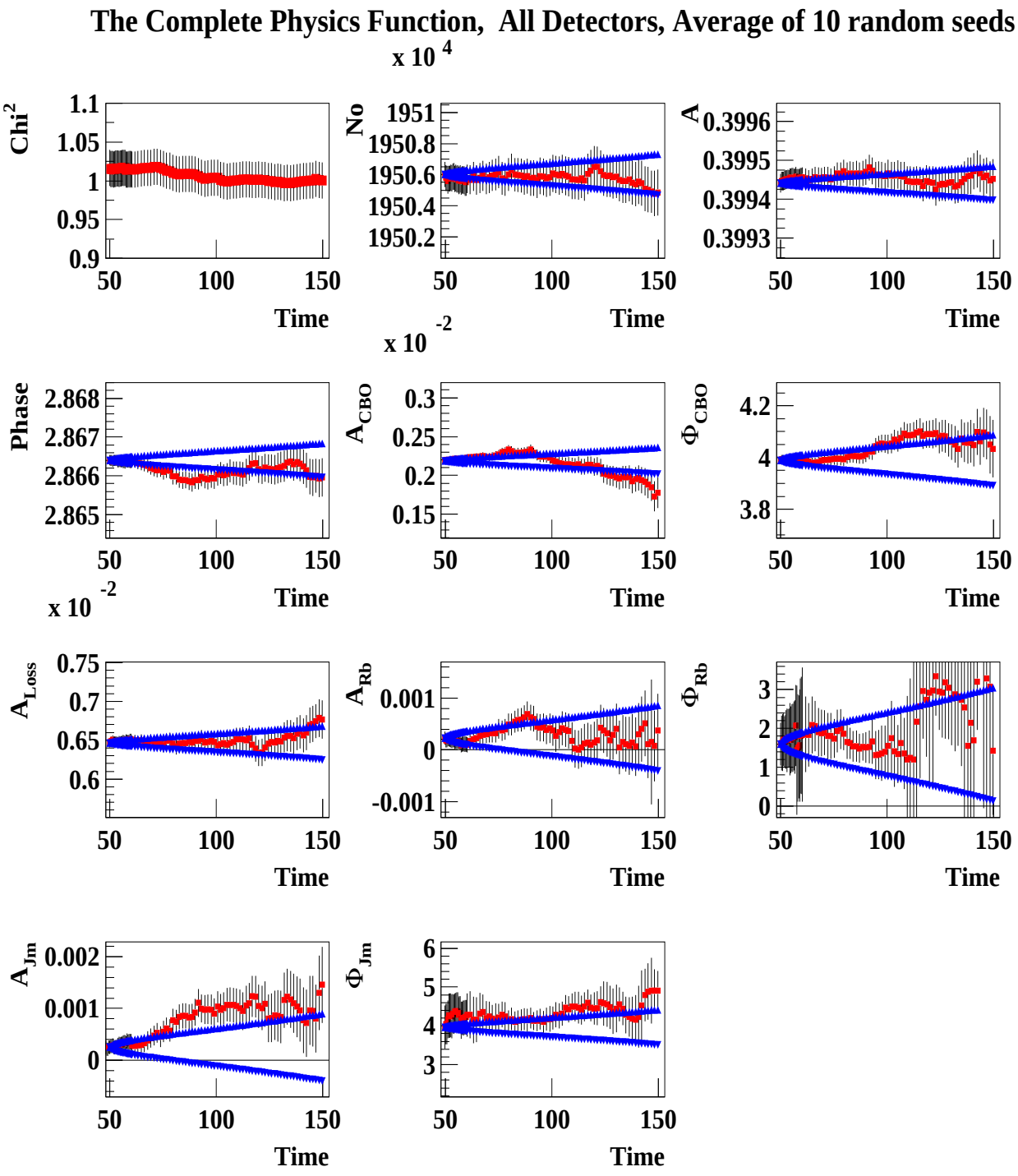

Figure 89 : Fit parameters with the complete physics function for all detectors together.

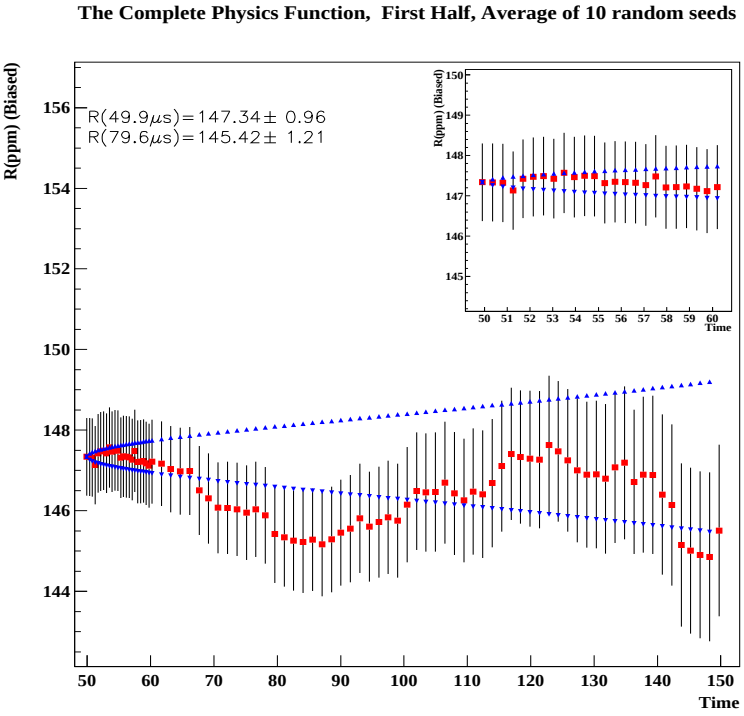

Figure 90 : The stability of R with the complete physics function on the first half.

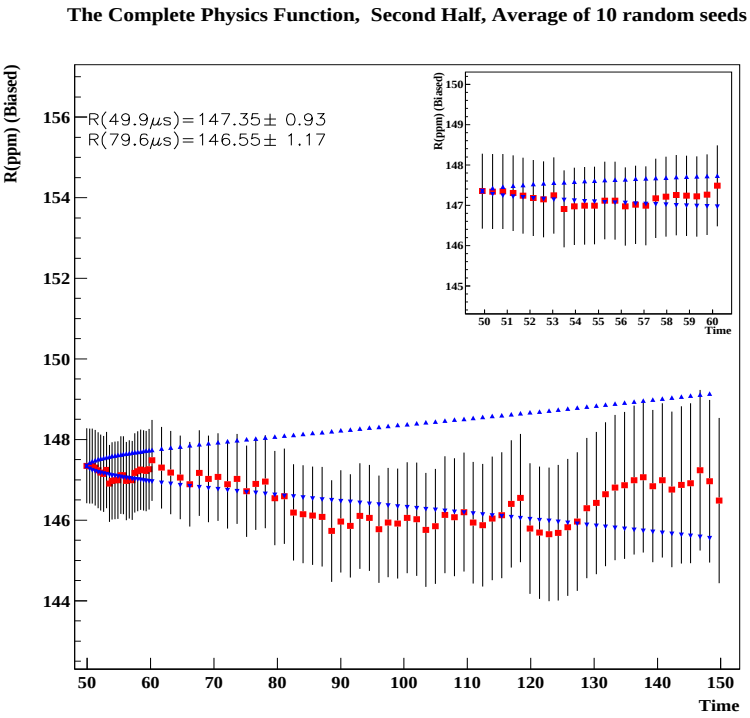

Figure 91 : The stability of R with the complete physics function on the second half.

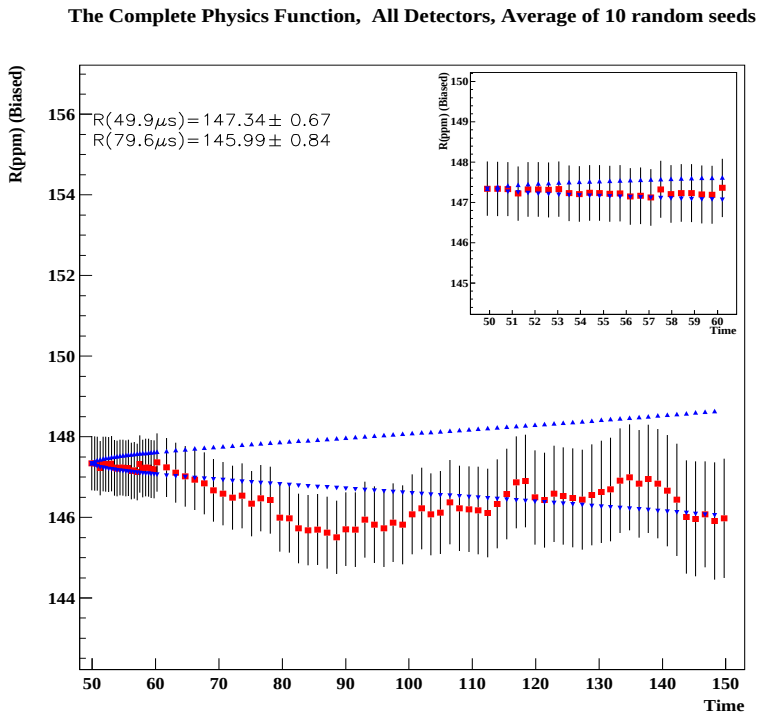

Figure 92 : The stability of R with the complete physics function for all detectors together.

Table 18: The R values and the fit χ^2 obtained from 10 random seeds at 49.9 μs. (All detectors together case)

Random Seed	χ^2	R(ppm)
1	1.025	147.43
2	0.998	147.33
3	1.002	147.24
4	1.010	147.42
5	1.009	147.29
6	1.029	147.29
7	0.972	147.36
8	1.040	147.44
9	1.041	147.31
10	1.038	147.32
Average	**1.017**	**147.34**
RMS	**0.022**	**0.065**

Table 19 shows the comparison of the parameters between the first and the second halves. These parameters were obtained from the fit values at 49.9 μs.

When we look at the correlation matrix in Table 20, we see ϕ_{Jm} has 39% percent correlation to R value whereas ϕ_{Rb} also has 31%. These two numbers are close to each other. However the effect on R from the phase of the g-2 phase modulation (ϕ_{Jm}) is much larger than the phase of the asymmetry modulation (ϕ_{Jm}).

Table 19: Comparison table of the fit parameters for the complete physics function.

Parameters	First Half		Second Half		All Detectors	
A	0.39504	±3.3671E-05	0.40371	±3.3083E-05	0.39944	±2.2326E-05
Φ_a	2.8707	±1.9695E-04	2.8624	±1.8945E-04	2.8664	±1.3594E-04
A_{cbo}	4.9306E-03	±4.9968E-05	3.2014E-03	±4.9536E-05	2.1895E-03	±3.5032E-05
Φ_{cbo}	4.7027	±1.0185E-02	2.6377	±1.5349E-02	3.9353	±1.6109E-02
A_{Rb}	1.5362E-03	±1.7791E-04	1.6836E-03	±1.7116E-04	2.1880E-04	±1.2760E-04
Φ_{Rb}	5.7761	±0.12269	2.4565	±0.10736	1.6486	±0.5746
$\epsilon(A_L)$	8.6343E-03	±3.9286E-04	3.9436E-03	±3.8743E-04	6.2452E-03	±2.7558E-04
$\epsilon(A_r)$	-7.6246E-03	±4.2322E-04	-1.8093E-03	±4.1754E-04	-4.6650E-03	±2.9693E-04
$\epsilon(\tau_r)$	100.51	±1.8239	99.777	±7.4994	100.35	±2.0870
A_{Jm}	7.7282E-04	±1.8589E-04	1.1757E-03	±1.7899E-04	2.8885E-04	±1.3001E-04
Φ_{Jm}	1.2457	±0.2700	4.1031	±0.16123	1.6836	±0.46731

Table 20: Correlation matrix for the functional form of the complete physics function

	Total	N_0	A	R	Φ_a	A_{cbo}	Φ_{cbo}	A_{Rb}	Φ_{Rb}	$\epsilon(A_L)$	$\epsilon(A_r)$	$\epsilon(\tau_r)$	A_{Jm}	Φ_{Jm}
N_0	0.97928	1.000	0.003	-0.010	-0.014	-0.009	-0.007	-0.002	0.014	**-0.481**	**0.322**	**0.836**	0.009	0.007
A	0.42037	0.003	1.000	-0.062	-0.055	0.015	0.012	**-0.269**	**-0.145**	-0.010	0.009	-0.001	**-0.309**	0.010
R	0.89725	-0.010	-0.062	1.000	**0.893**	0.009	-0.005	**0.262**	**-0.223**	0.036	-0.033	0.005	**0.120**	**-0.298**
Φ_a	0.91166	-0.014	-0.055	**0.893**	1.000	0.012	-0.007	**0.304**	**-0.313**	0.048	-0.044	0.007	**0.113**	**-0.390**
A_{cbo}	0.05576	-0.009	0.015	0.009	0.012	1.000	0.005	-0.020	0.012	0.031	-0.028	0.004	-0.022	-0.005
Φ_{cbo}	0.04722	-0.007	0.012	-0.005	-0.007	0.005	1.000	0.008	0.009	0.024	-0.022	0.003	-0.015	0.027
A_{Rb}	0.39750	-0.002	**-0.269**	**0.262**	**0.304**	-0.020	0.008	1.000	-0.065	0.008	-0.007	0.001	**0.118**	**-0.122**
Φ_{Rb}	0.37619	0.014	**-0.145**	**-0.223**	**-0.313**	0.012	0.009	-0.065	1.000	-0.049	0.044	-0.007	0.011	**0.134**
$\epsilon(A_L)$	0.99692	**-0.481**	-0.010	0.036	0.048	0.031	0.024	0.008	-0.049	1.000	**-0.975**	**-0.286**	-0.030	-0.025
$\epsilon(A_r)$	0.99624	**0.322**	0.009	-0.033	-0.044	-0.028	-0.022	-0.007	0.044	**-0.975**	1.000	**0.207**	0.027	0.023
$\epsilon(\tau_r)$	0.94785	**0.836**	-0.001	0.005	0.007	0.004	0.003	0.001	-0.007	**-0.286**	**0.207**	1.000	-0.005	-0.003
A_{Jm}	0.33005	0.009	**-0.309**	**0.120**	**0.113**	-0.022	-0.015	**0.118**	0.011	-0.030	0.027	-0.005	1.000	-0.048
Φ_{Jm}	0.40719	0.007	0.010	**-0.298**	**-0.390**	-0.005	0.027	**-0.122**	**0.134**	-0.025	0.023	-0.003	-0.048	1.000

Here (Table 21) we give the comparison of the R values at 49.9 and 82.6 μs for the complete physics form. These numbers were obtained from the average of the individual detectors.

Table 21: Comparison of the R values at 49.9 and 82.6 μ s. Half ring effect here is the amplitude of the sine wave in the fit. Error on the R value for sine-wave fit at 49.9 is not realistic due to unconverged fit (couldn't succeed).

Time	49.9 μs		82.6 μs	
	R (ppm)	χ^2/DOF	R (ppm)	χ^2/DOF
Linear Fit	147.35±0.67	24/21	145.78±0.86	24/21
Sine Wave Fit	147.35±0.63	24/19	145.79±0.86	24/19
Half Ring Effect(ppm)	0.10±1.00		0.40±1.30	

This table shows that with the complete physics function the half ring effect is removed since there is no sine wave amplitude to be fitted.

The individual detectors also fitted to the complete physics function and the parameters are shown at Figures 93-96 for two different fit start time 49.9 and 82.6 μs. These fits were done with again 10 random seeds and the average values are showed on the plots.

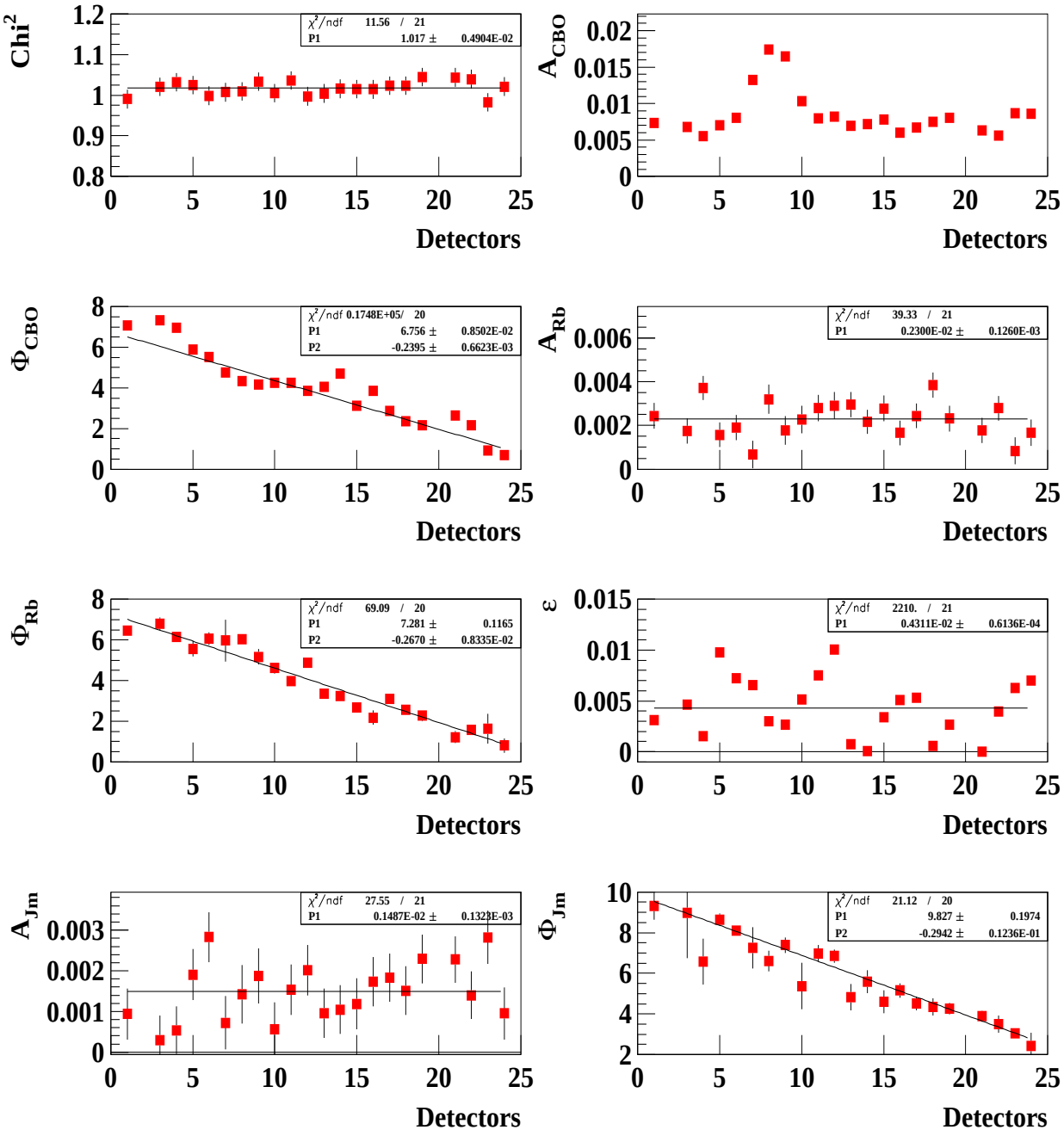

Figure 93 : Fit parameters at 49.9 μs with the complete physics function.

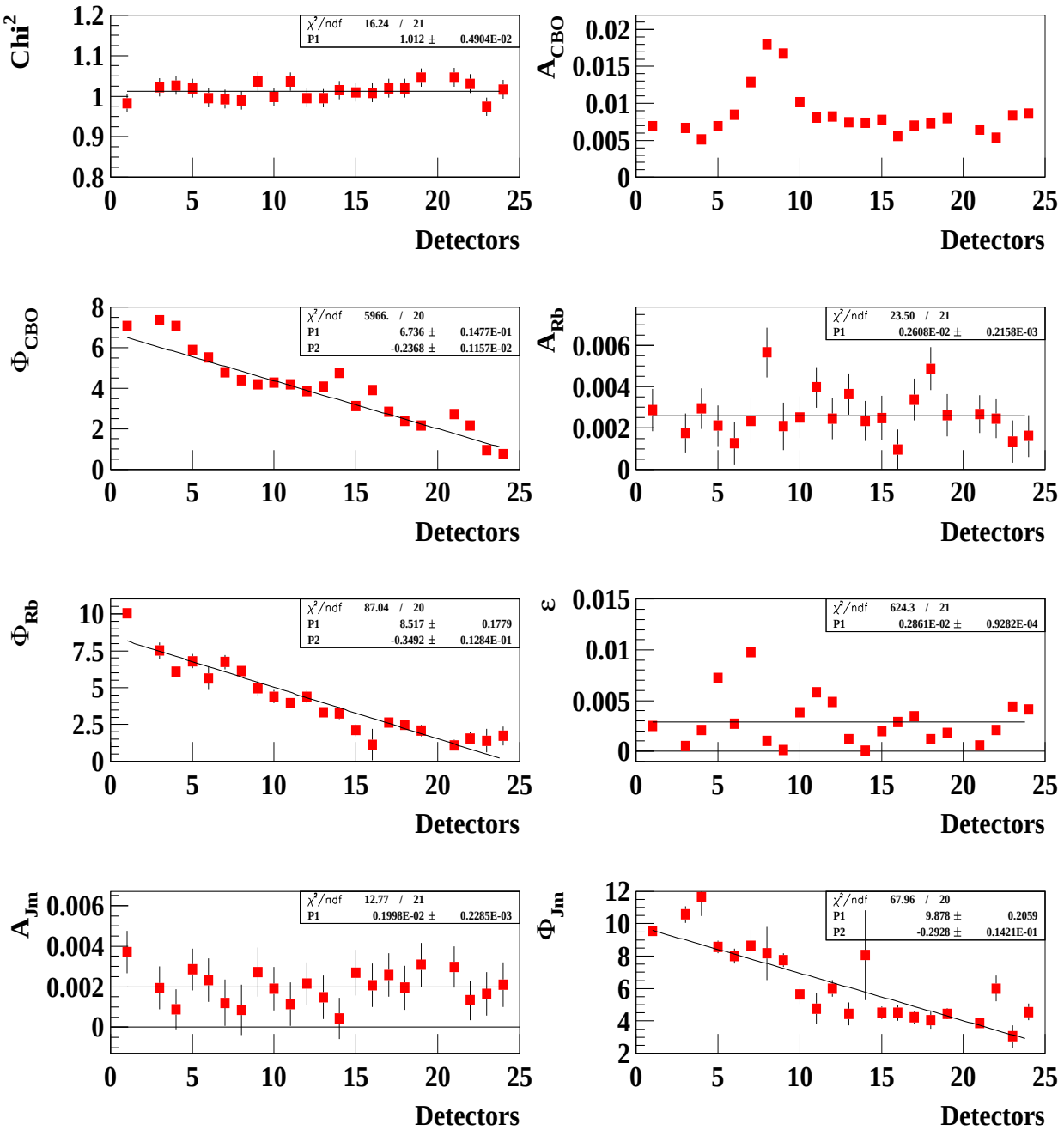

Figure 94 : Fit parameters at 82.6 μs with the complete physics function.

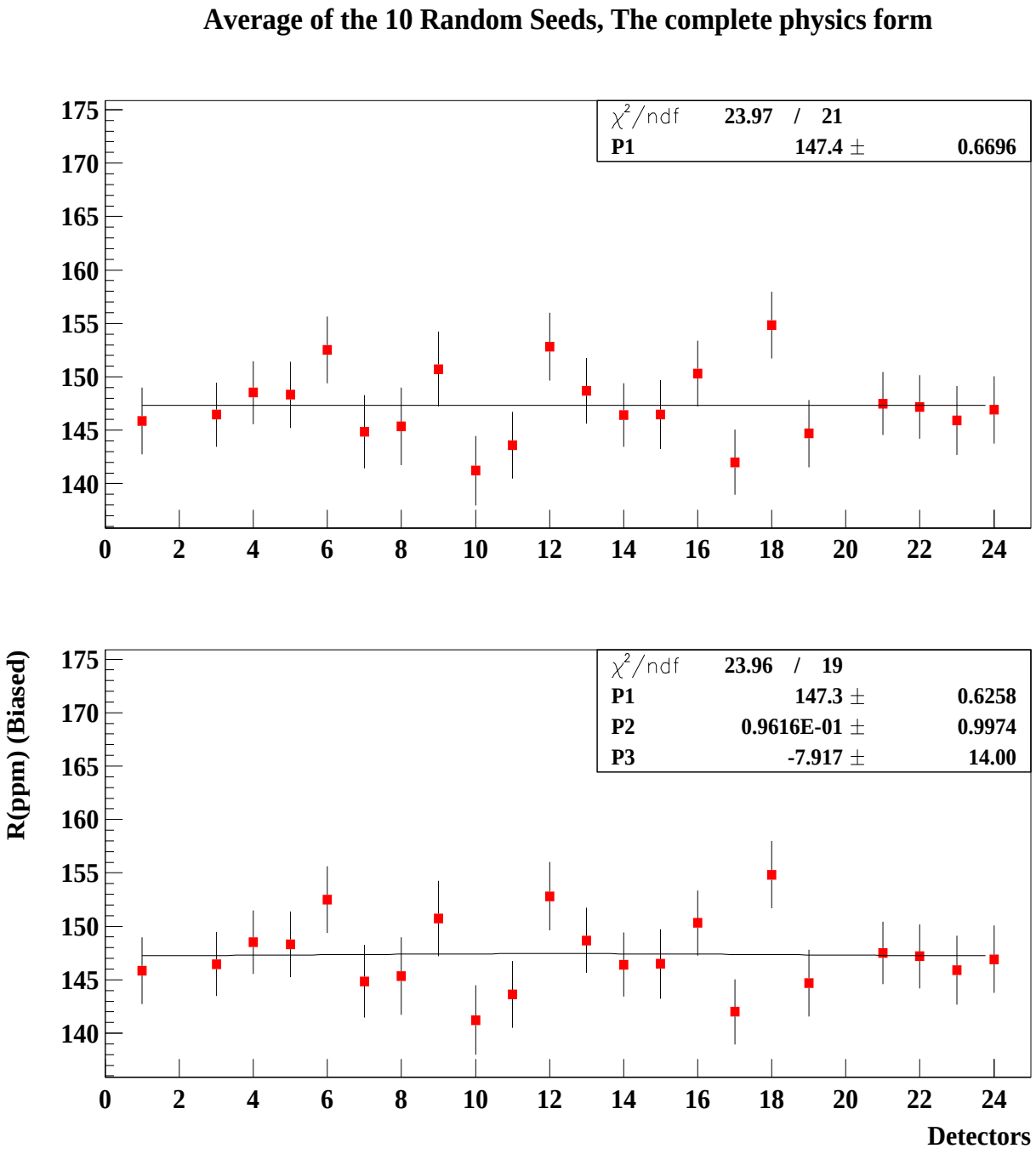

Figure 95 : R value at 49.9 μs with the complete physics function. The error on the R value for sine-wave fit is not realistic. This is due to fit can not handle the sine wave to this so flat behavior and screws the error.

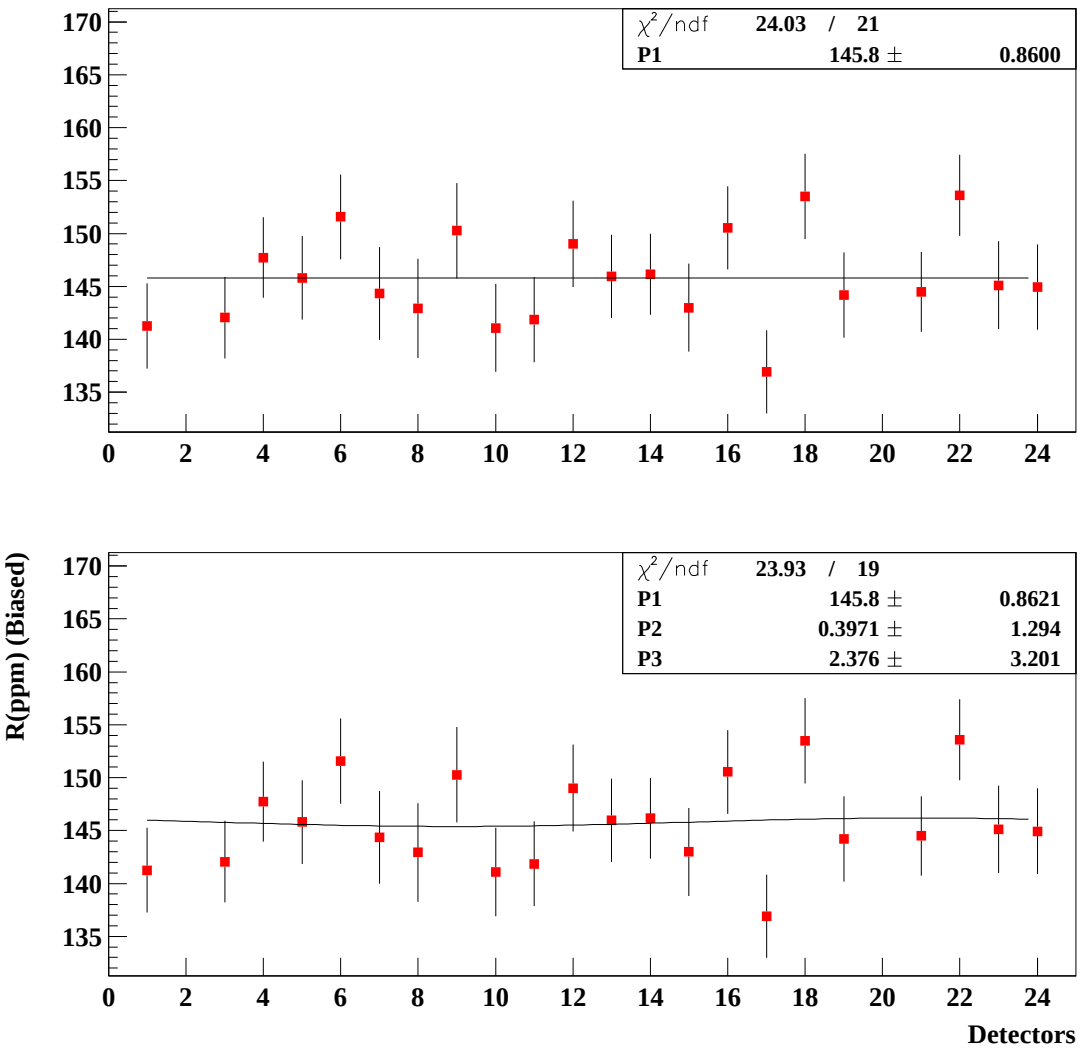

Figure 96 : R value at 82.6 μs with the complete physics function.

As one can see from R versus detector stability and the χ^2, there is no visible half ring effect exist anymore with this functional form. The fit quality (χ^2) is the same at early (49.9 μs) and late times (82.6 μs).

The stability of R for the individual detectors are shown in figure 97. The R versus time stability for each detectors are excellent.

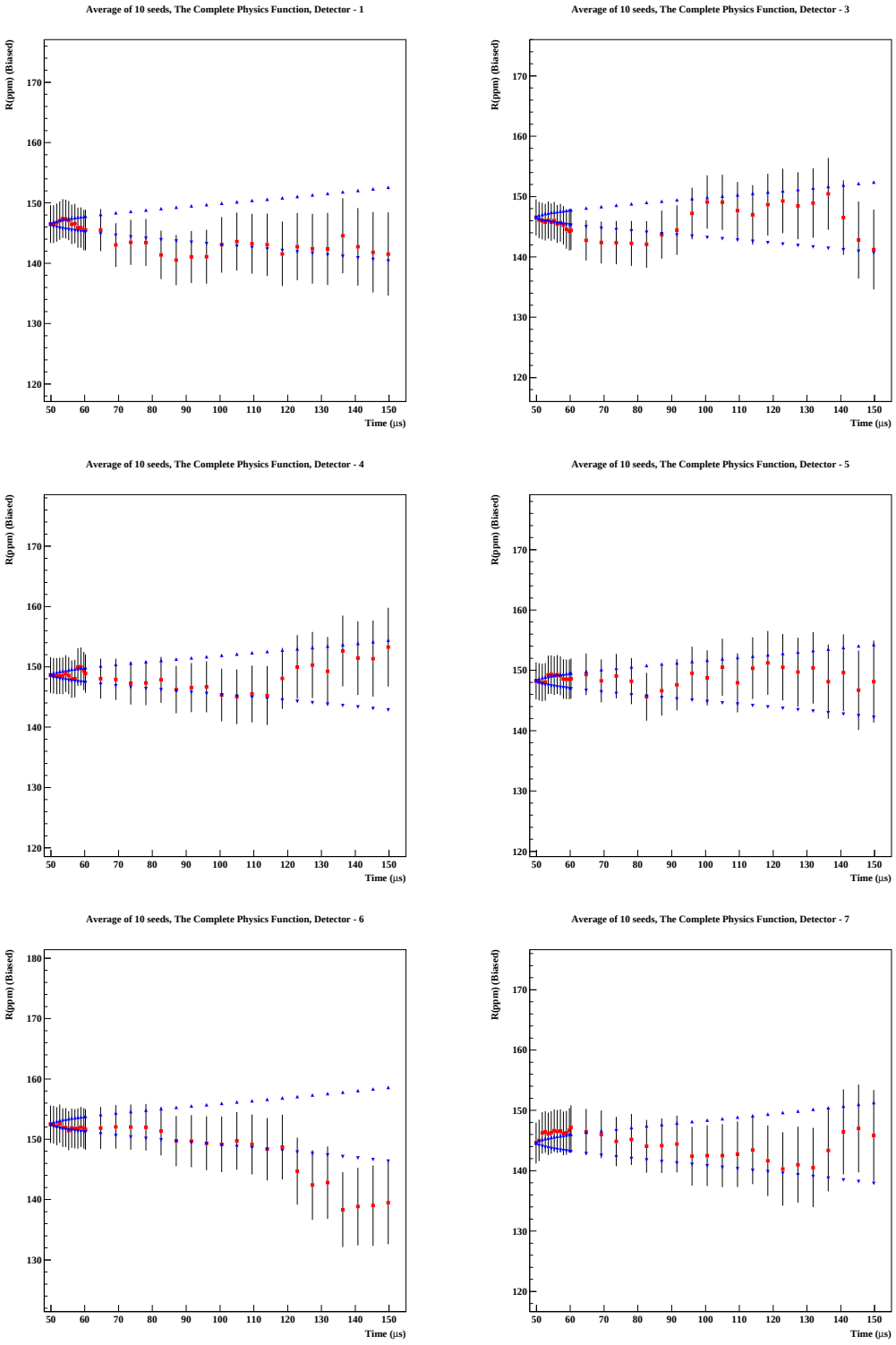

Figure 97 : The stability of R for individual detectors when the complete physics function used in the fits.

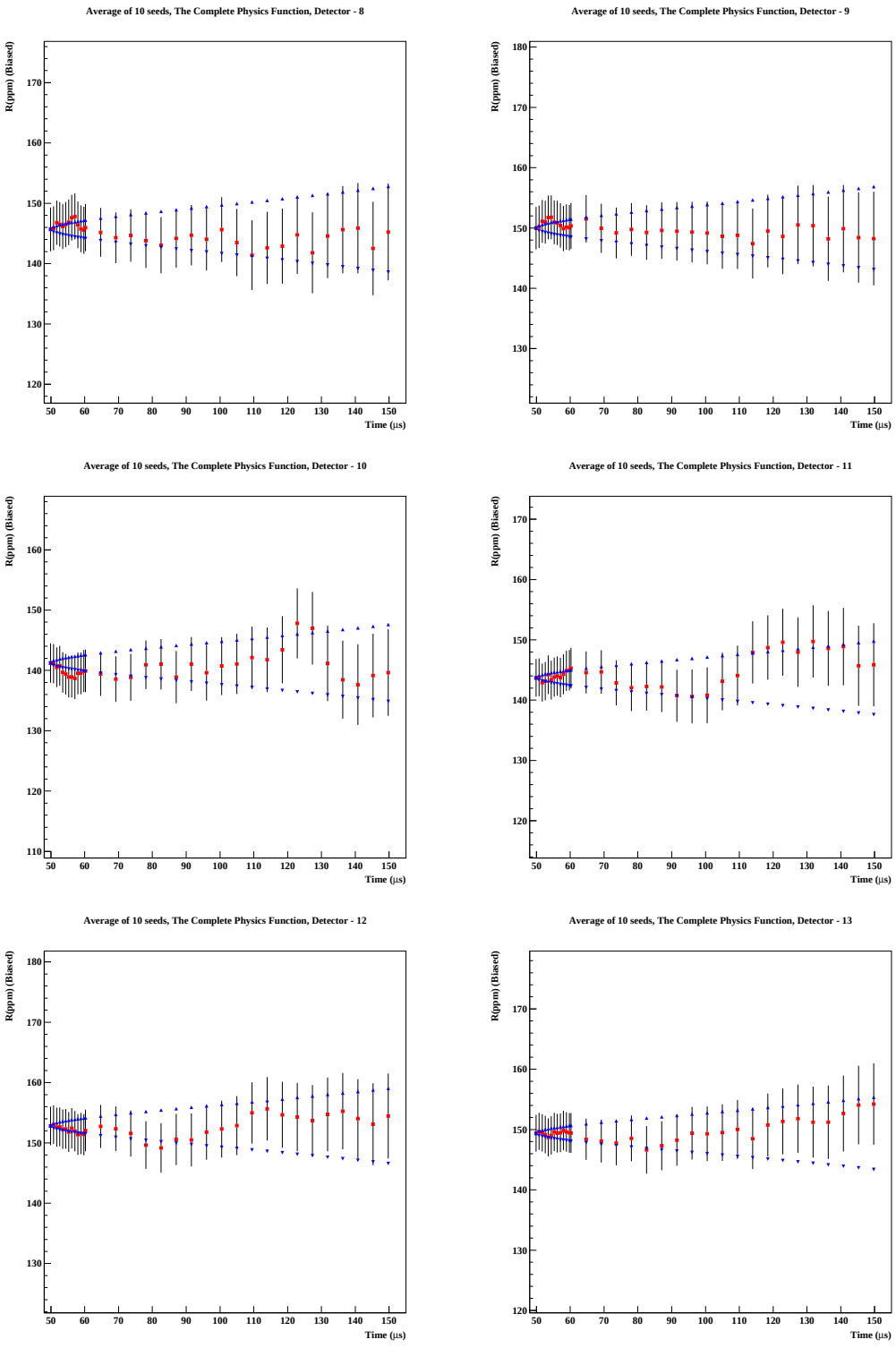

Figure 97 : continued,

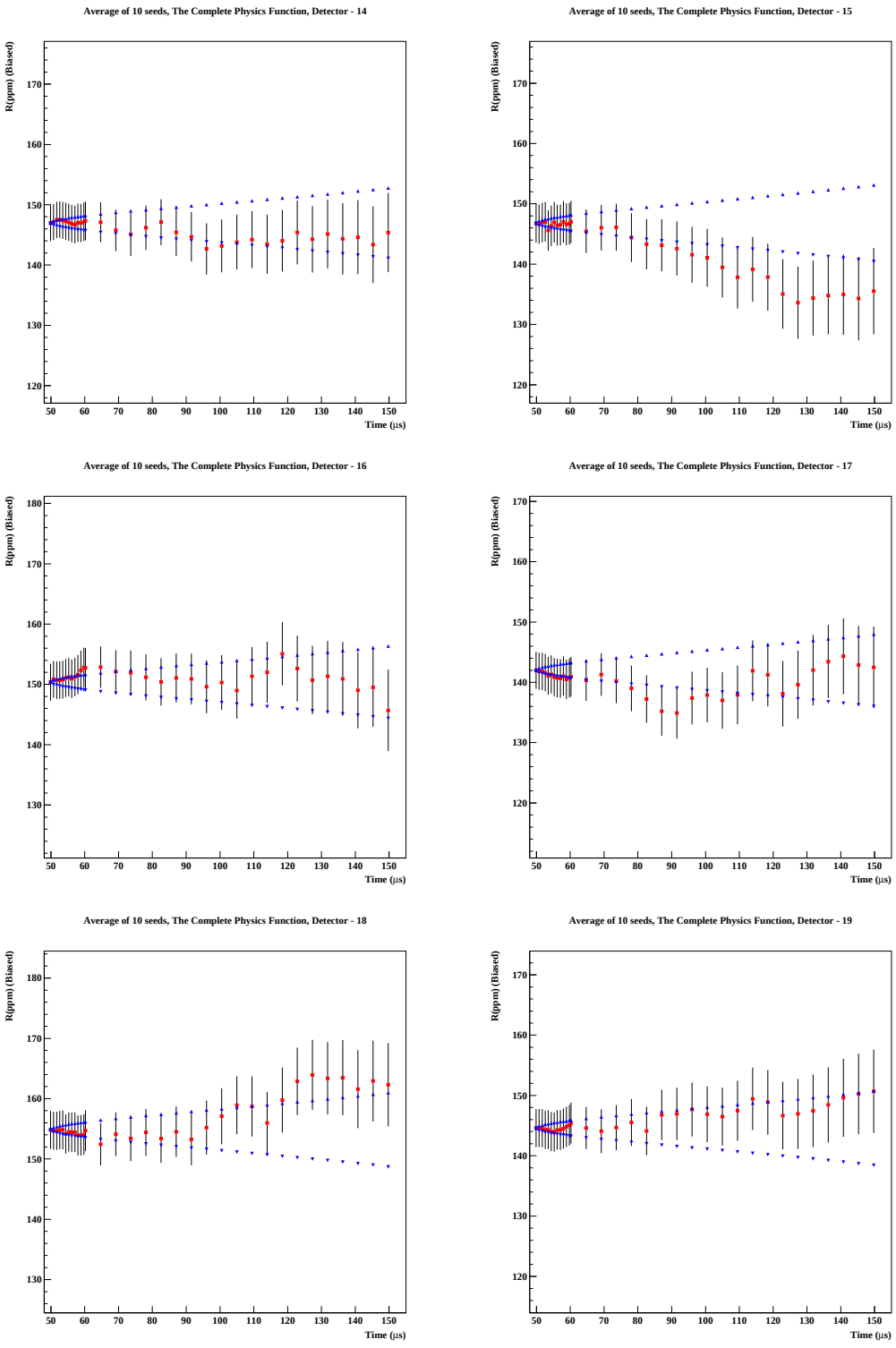

Figure 97 : continued,

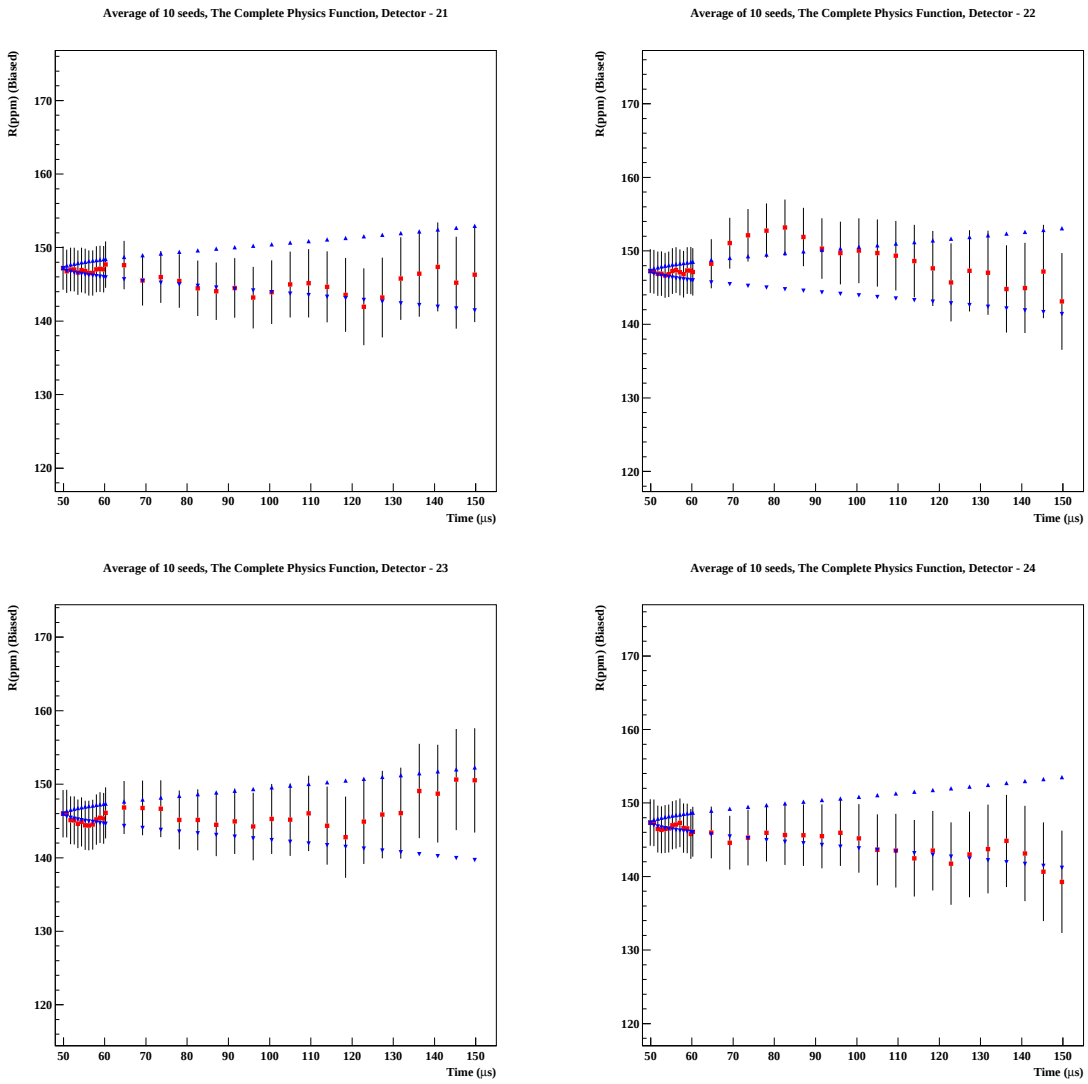

Figure 97 : continued.

The parameter stability for each detectors is shown in Figure 98. The parameter stability is generally very good. When A_{Rb} and A_{Jm} amplitudes are close to zero, the phase is undetermined and the error becomes large. For the detectors with suspected gain problems, the stability of the Φ_{Rb}, Φ_{Jm} phases are not good (mostly Φ_{Jm}). That is as we know the cross correlations between these parameters and the gain effects. Other than that we can say that the parameter stability for this functional form is acceptable.

Figure 98 shows the stability of R for individual detectors.

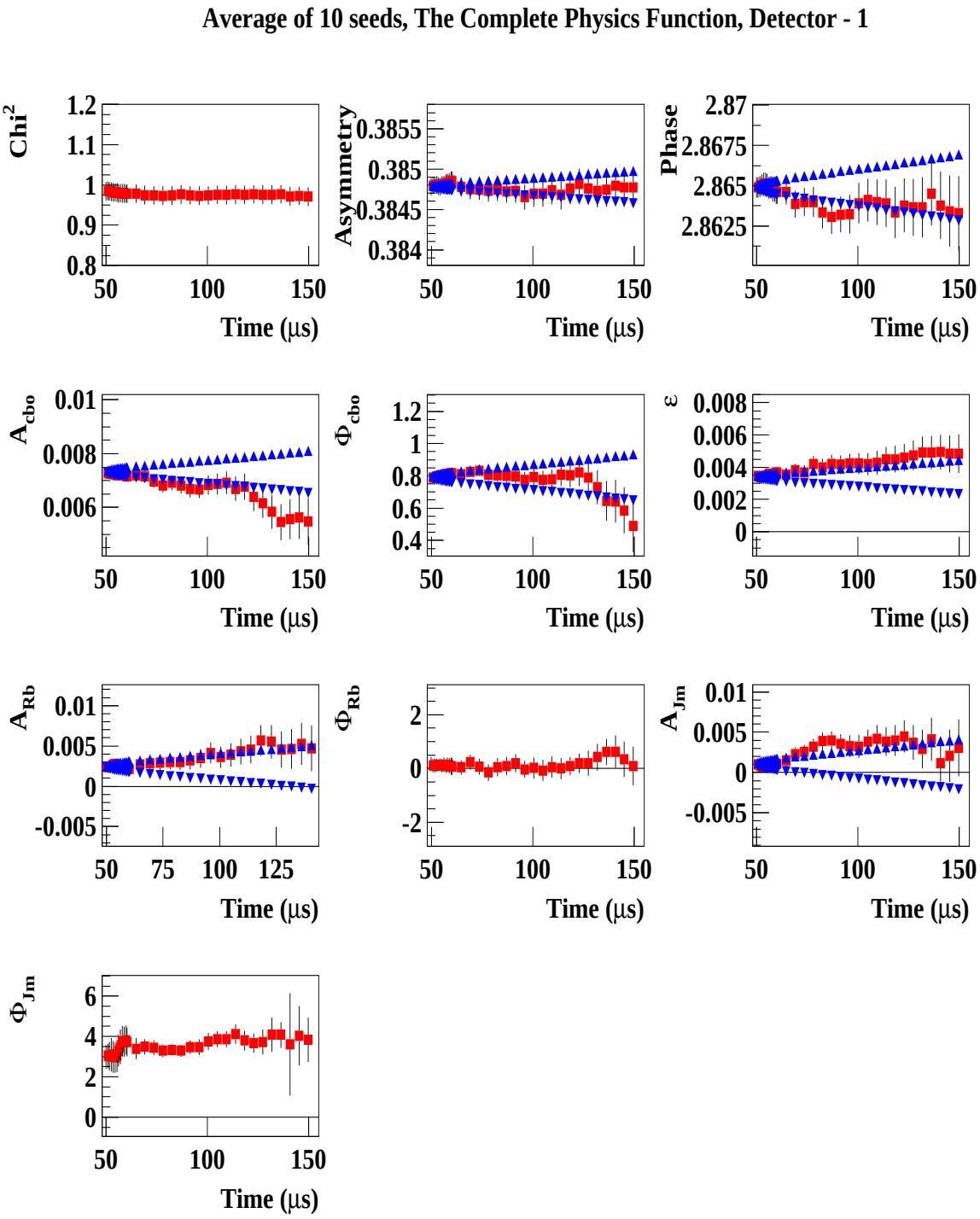

Figure 98 : The stability of R for individual detectors when the complete physics function was used for the fit.

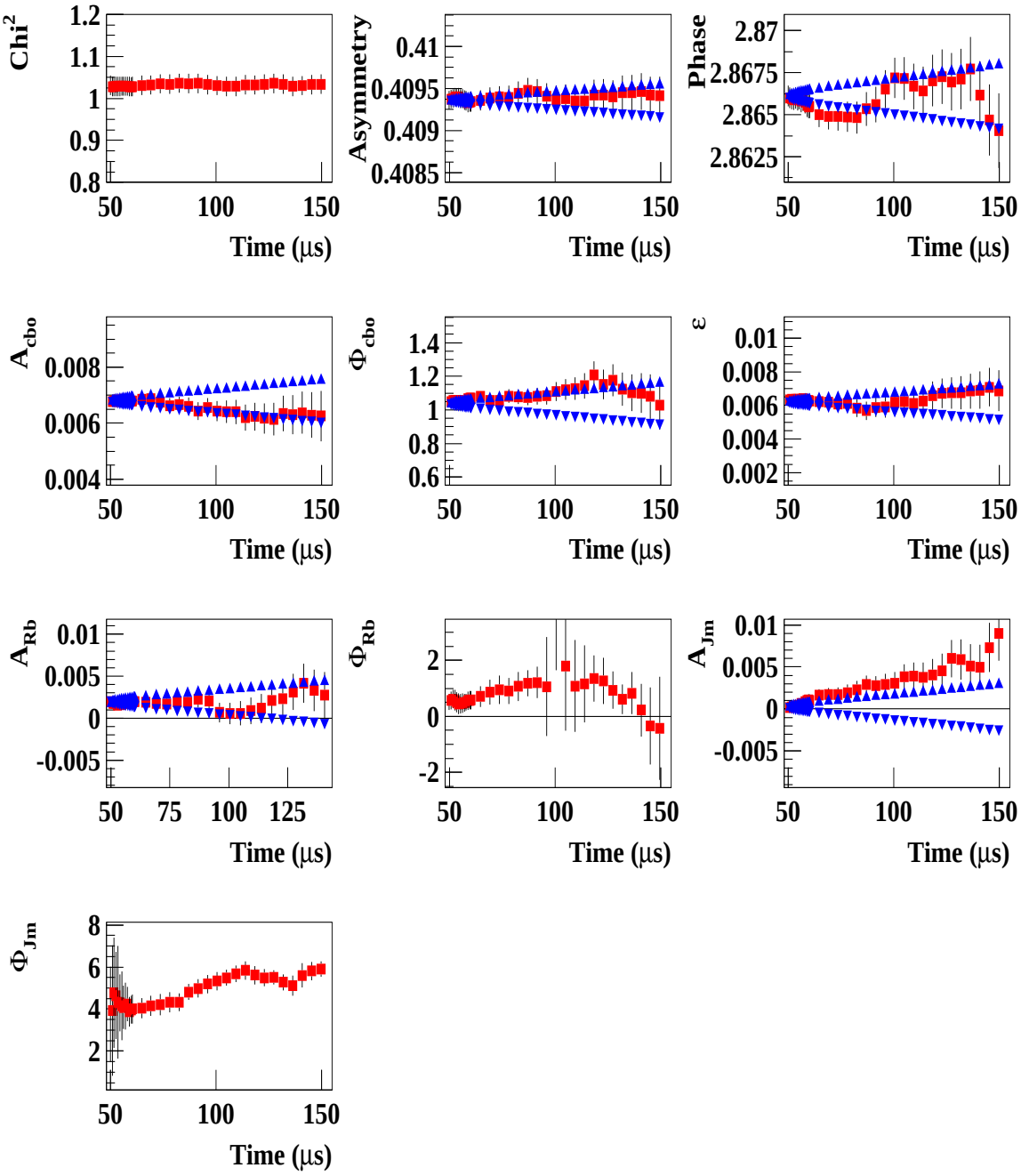

Figure 98 : continued,

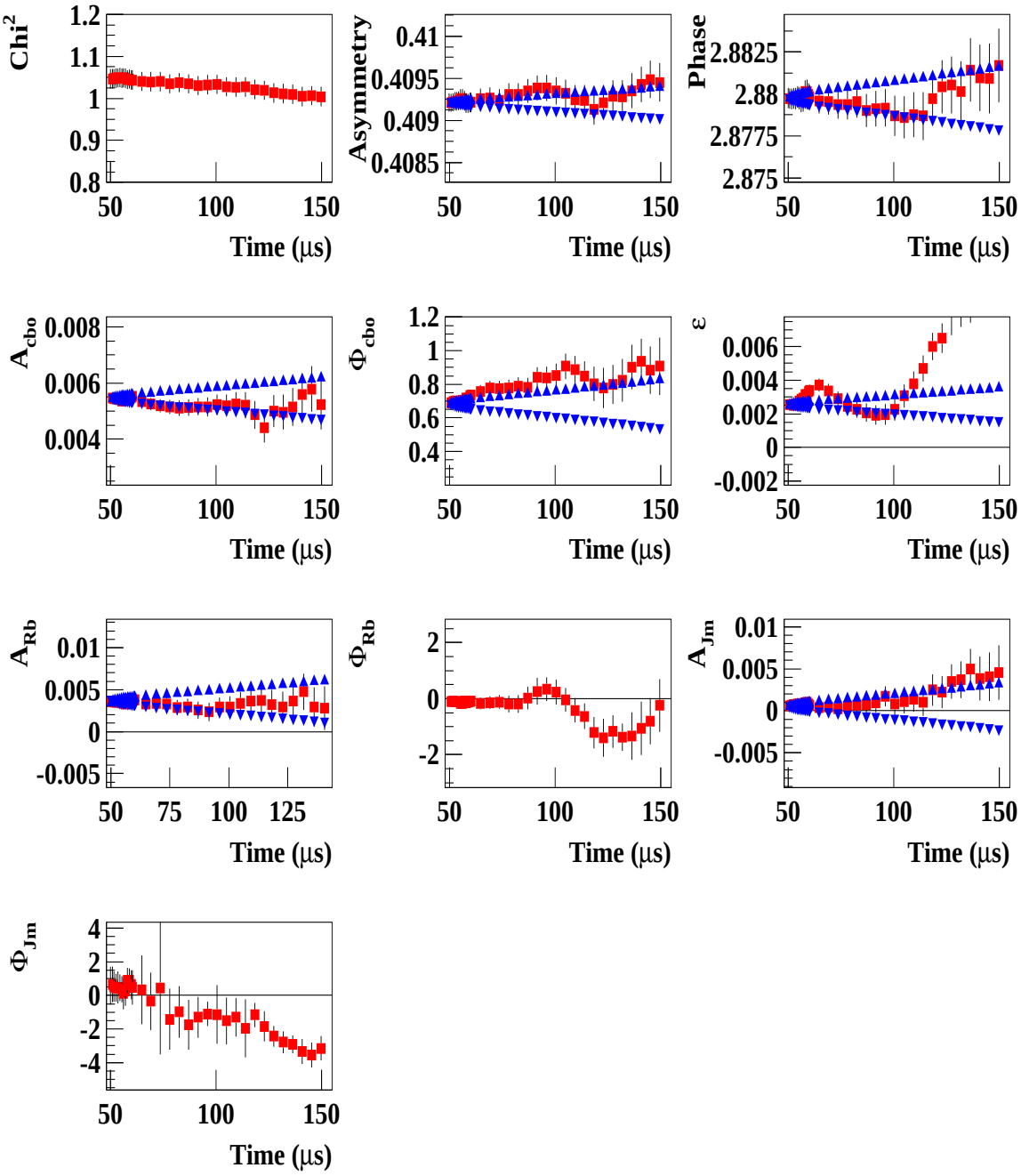

Figure 98 : continued,

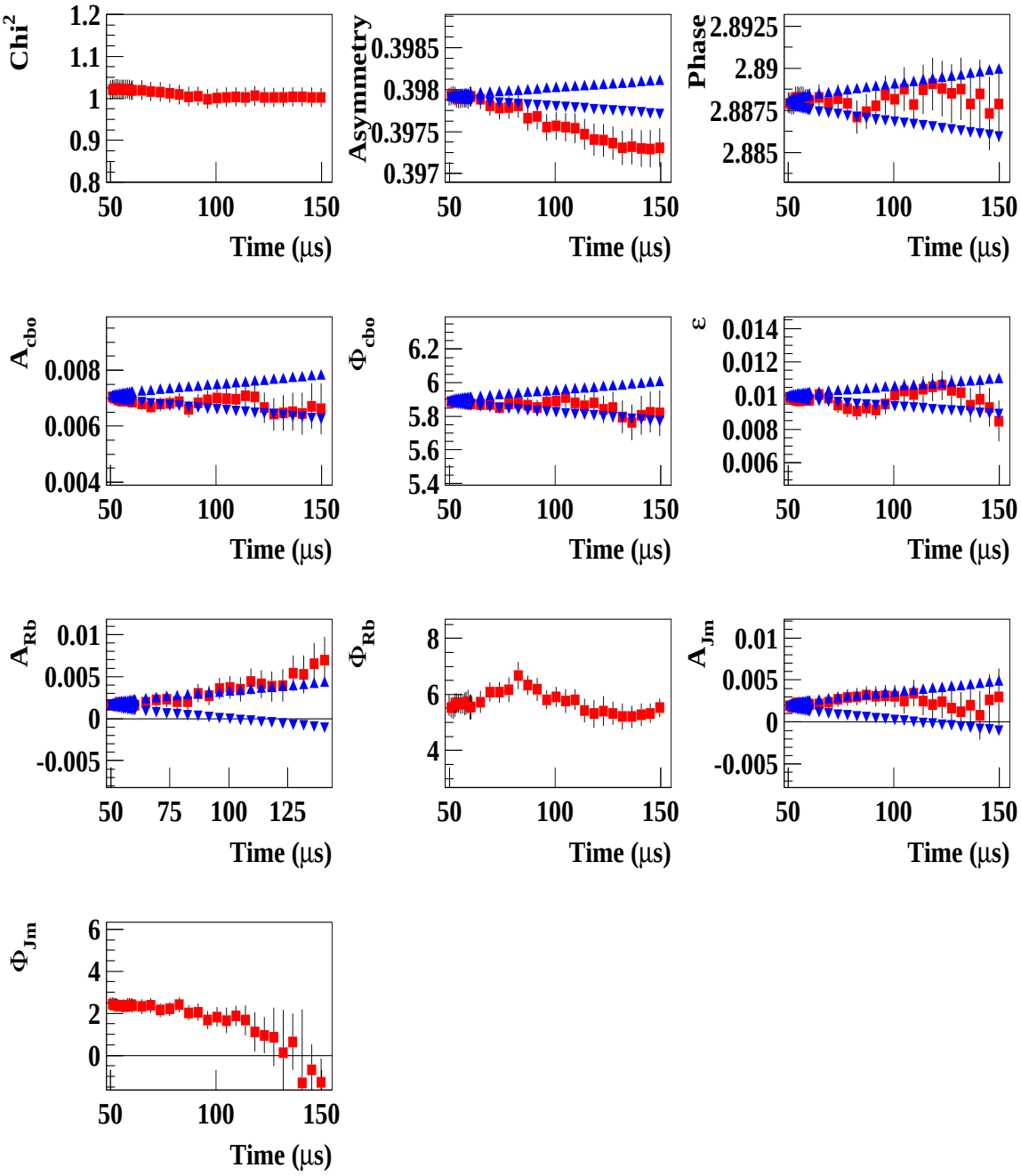

Figure 98 : continued,

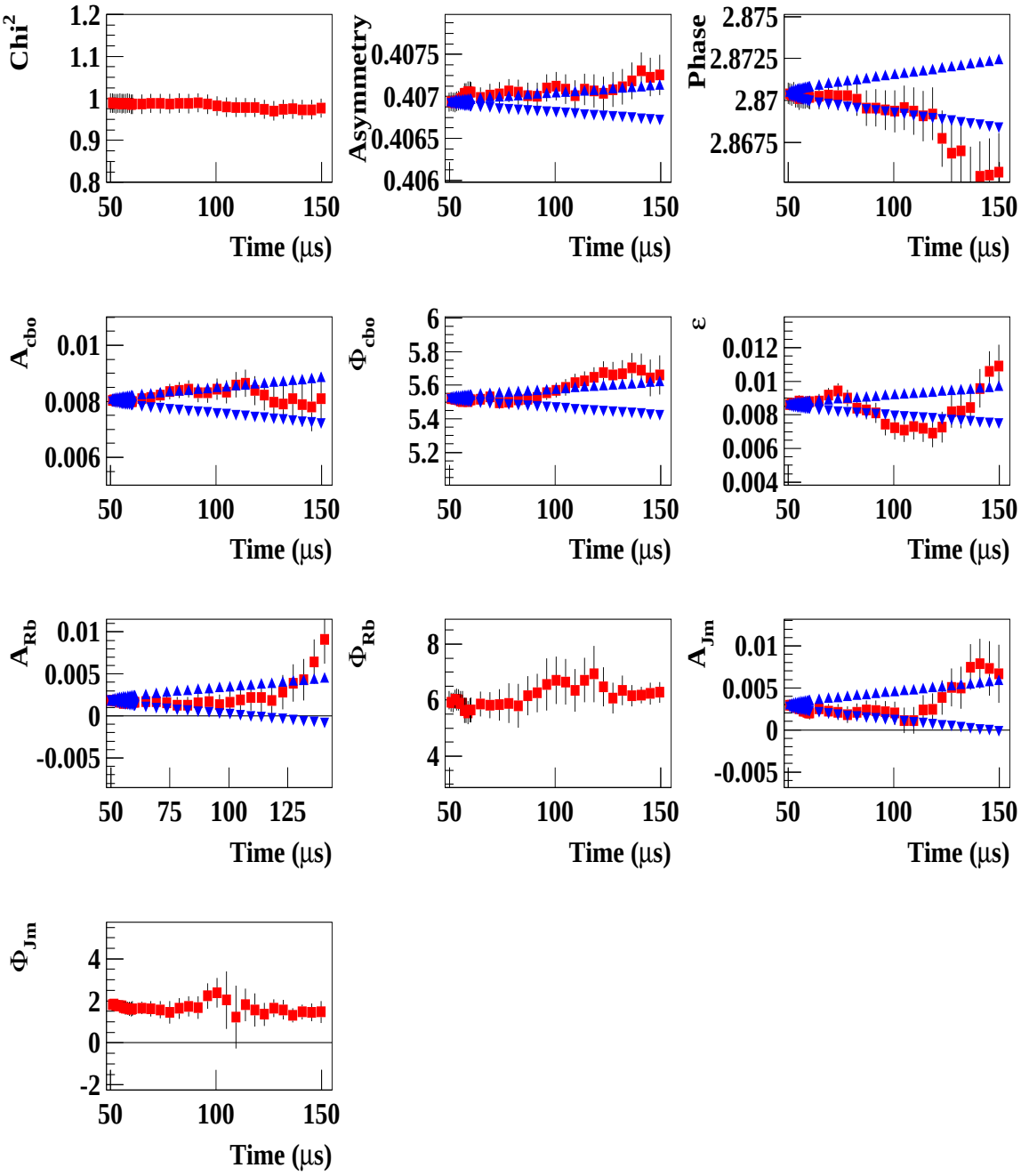

Figure 98 : continued,

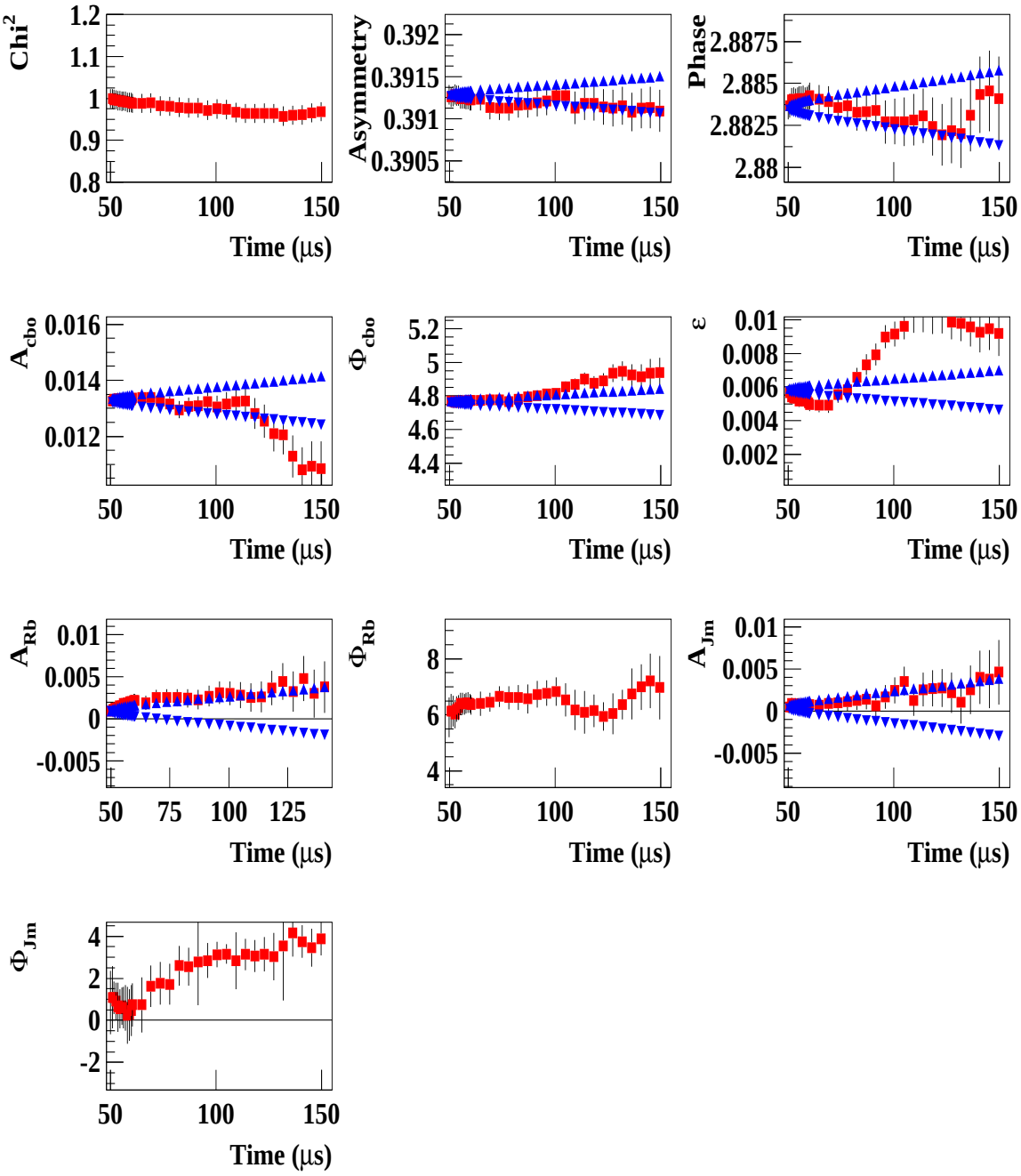

Figure 98 : continued,

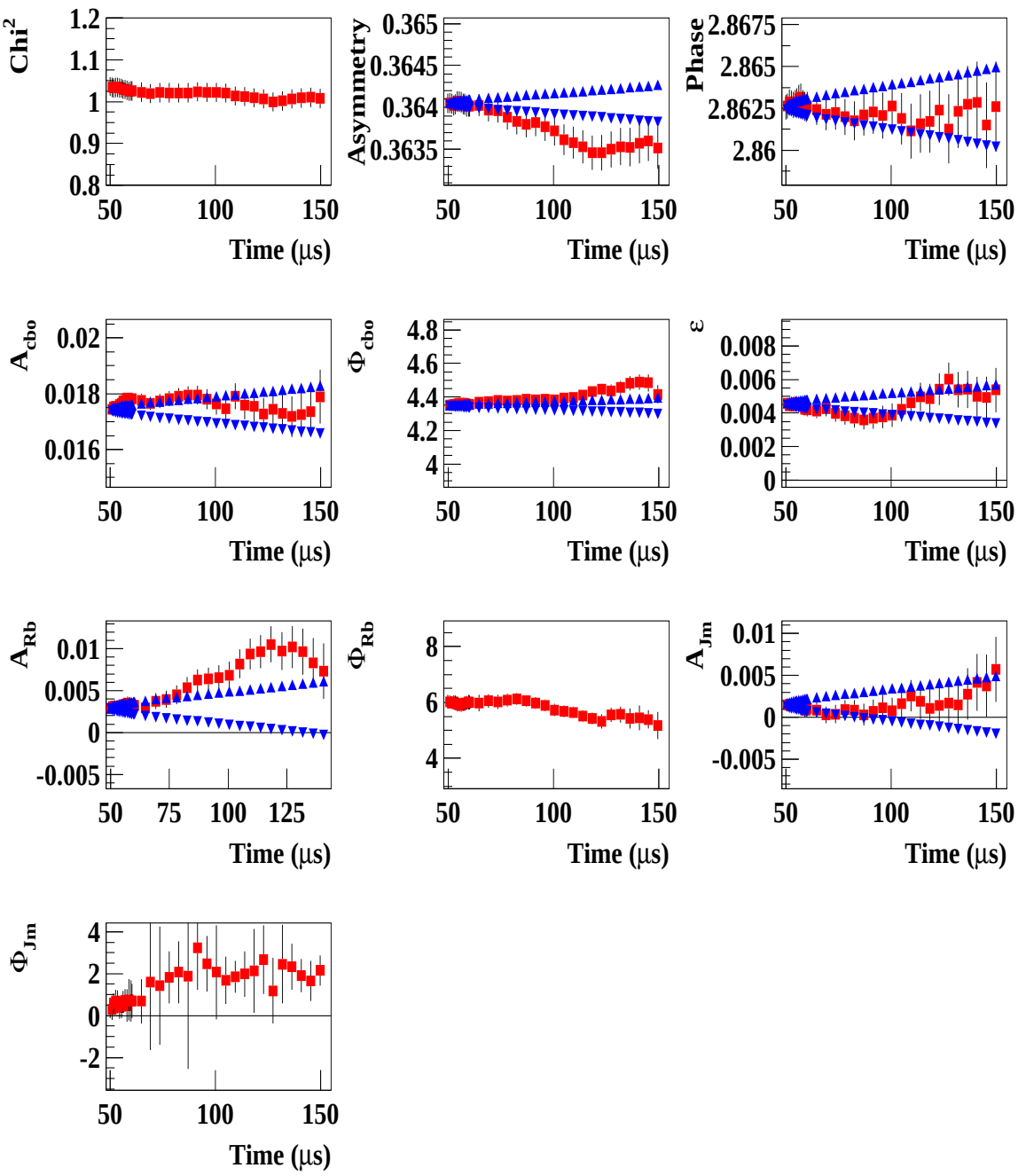

Figure 98 : continued,

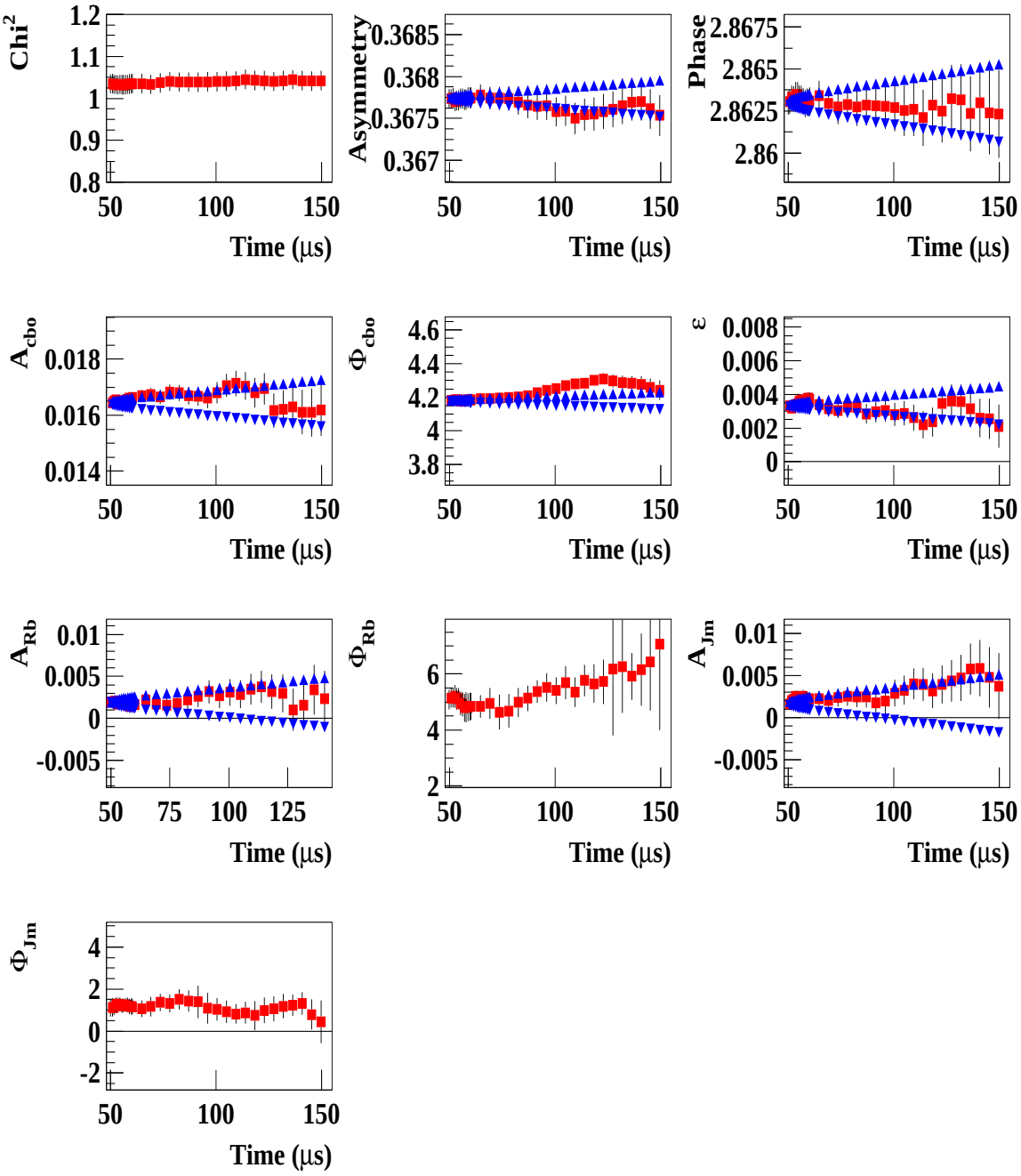

Figure 98 : continued,

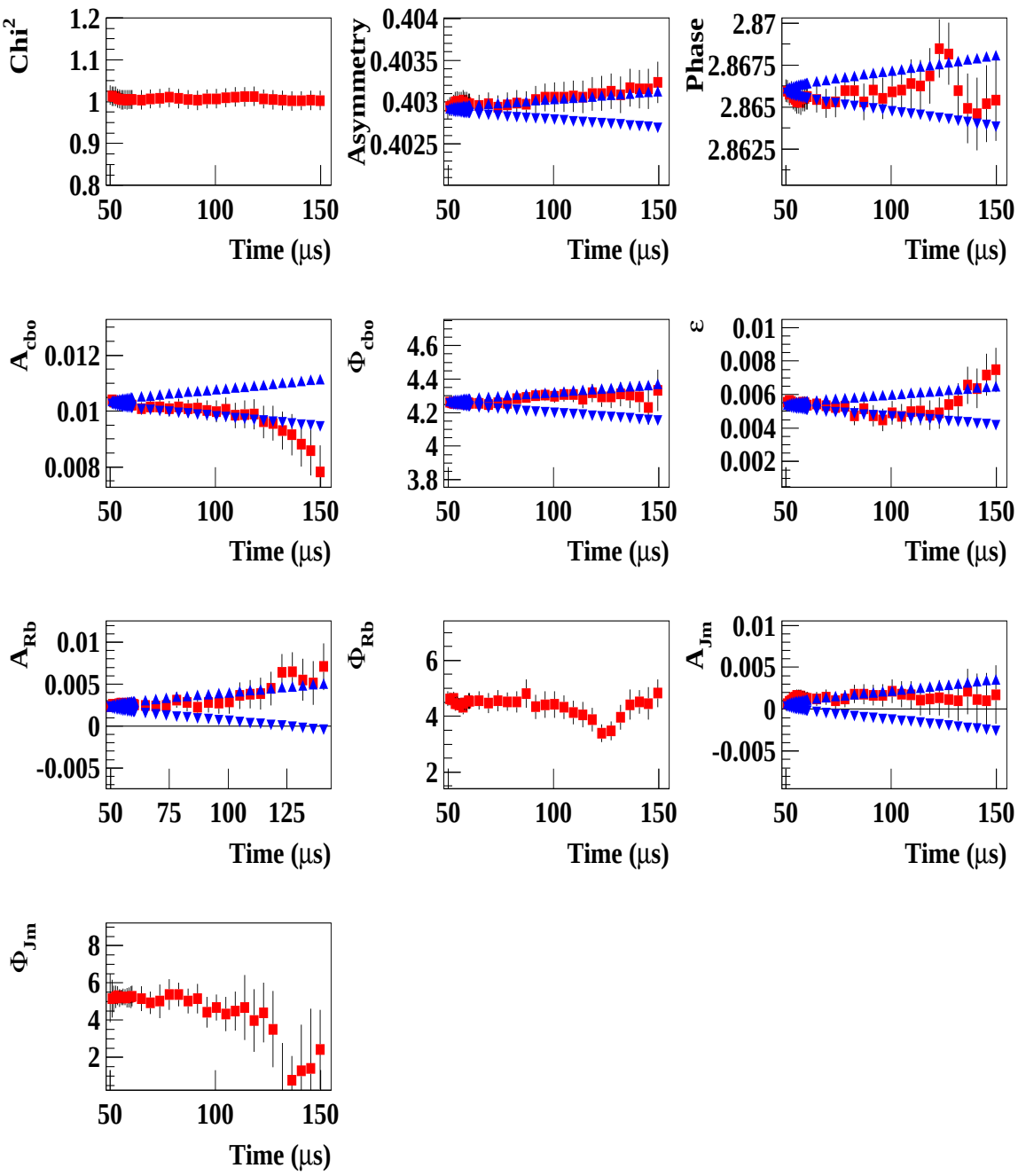

Figure 98 : continued,

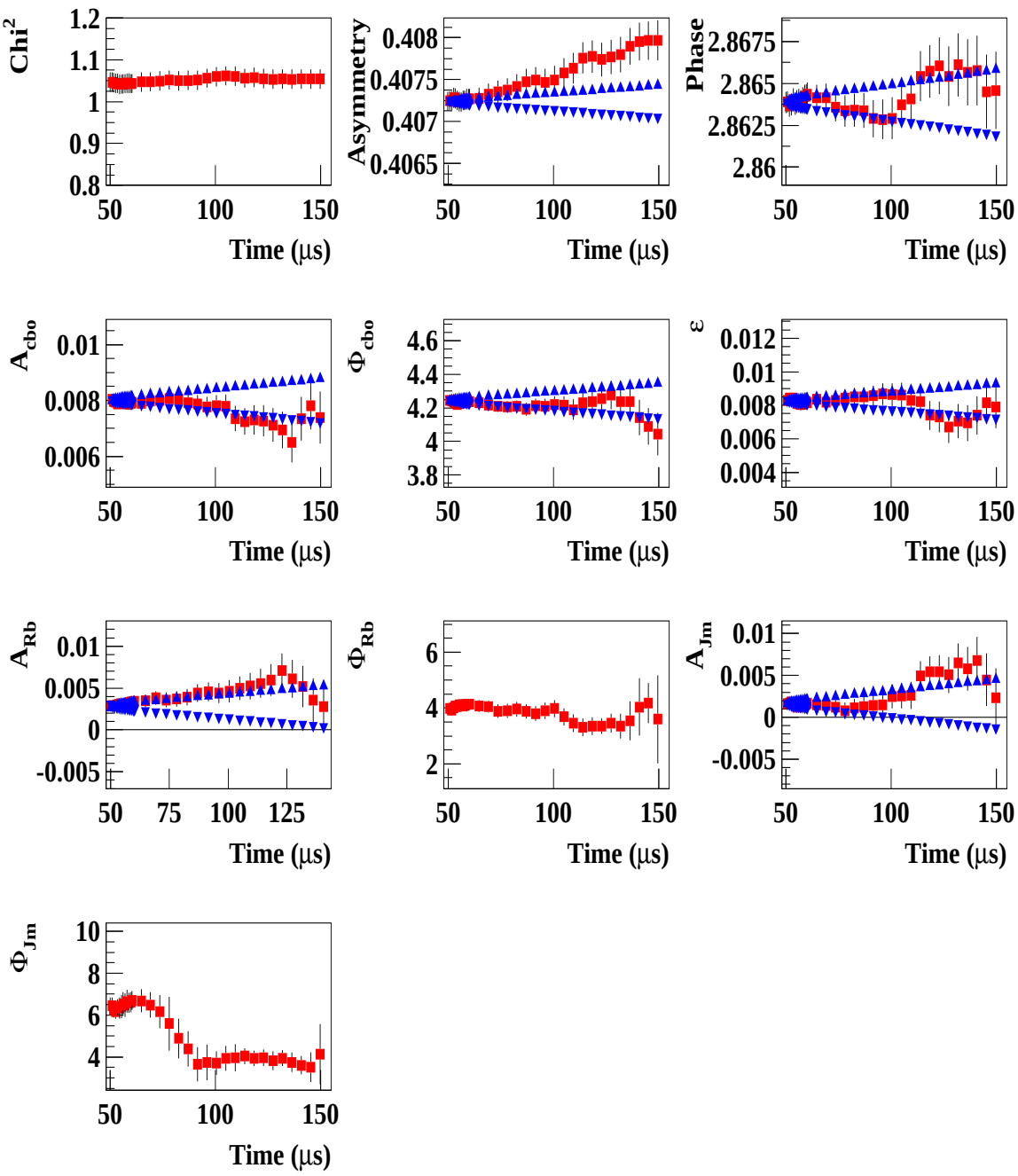

Figure 98 : continued,

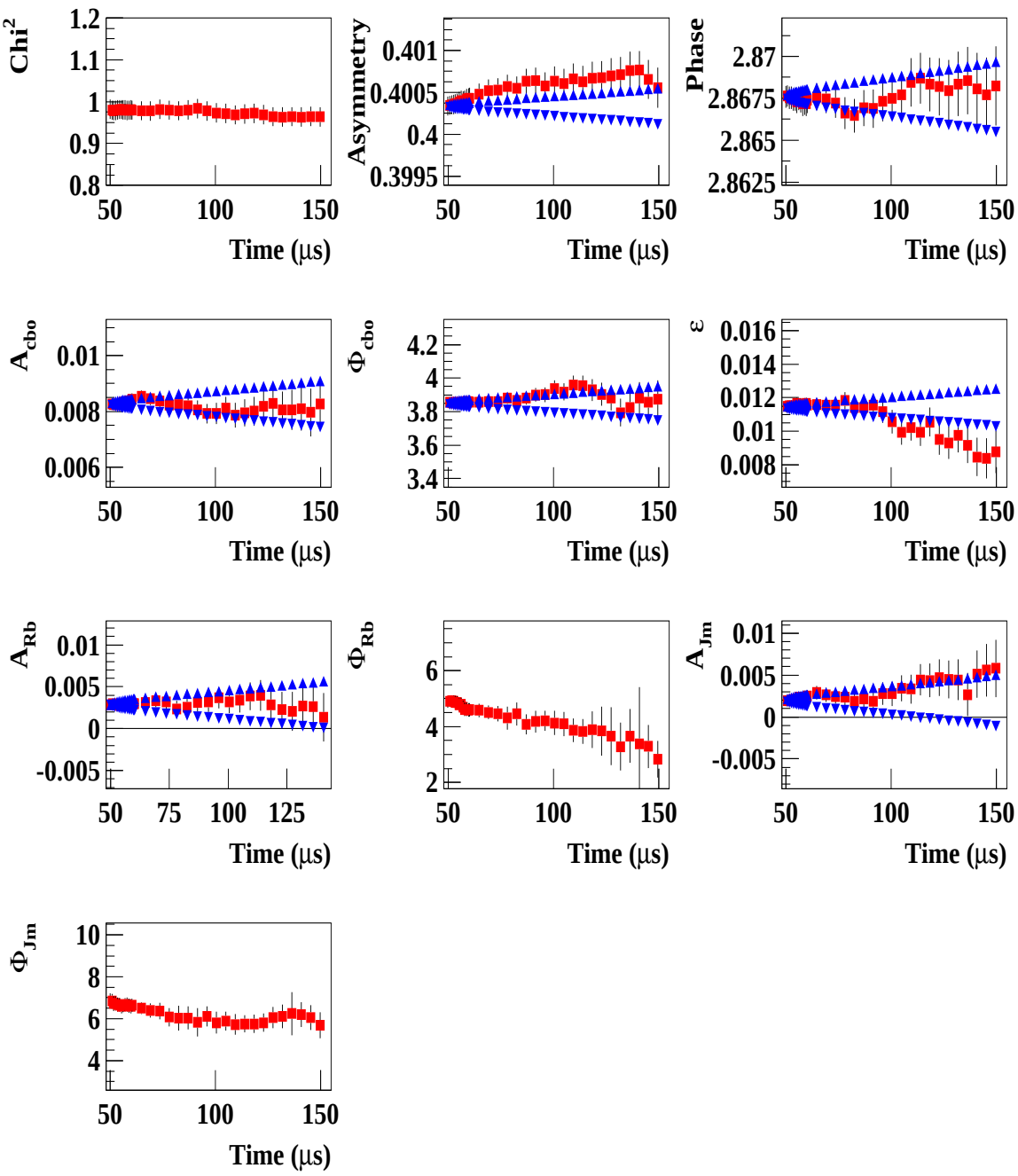

Figure 98 : continued,

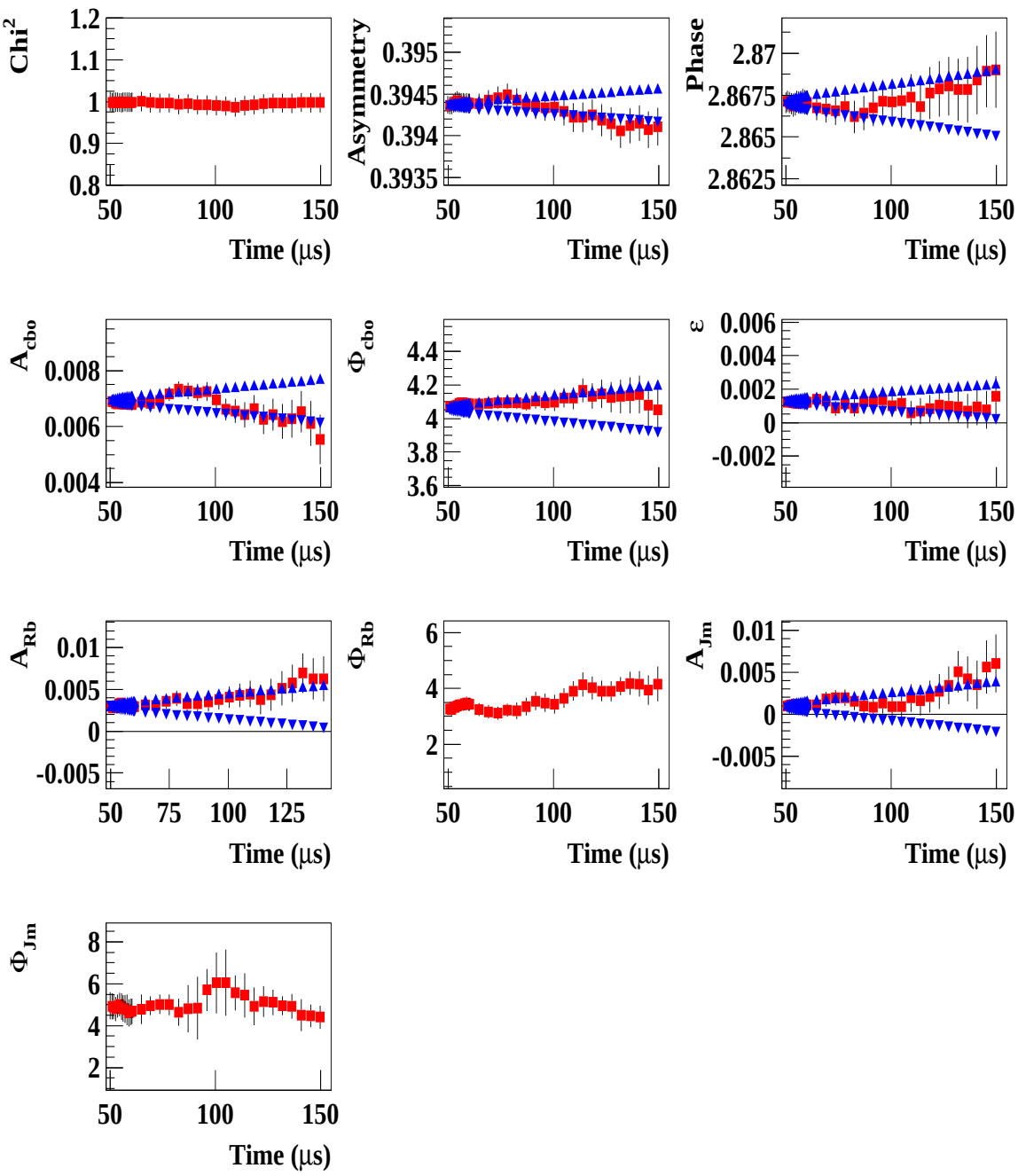

Figure 98 : continued,

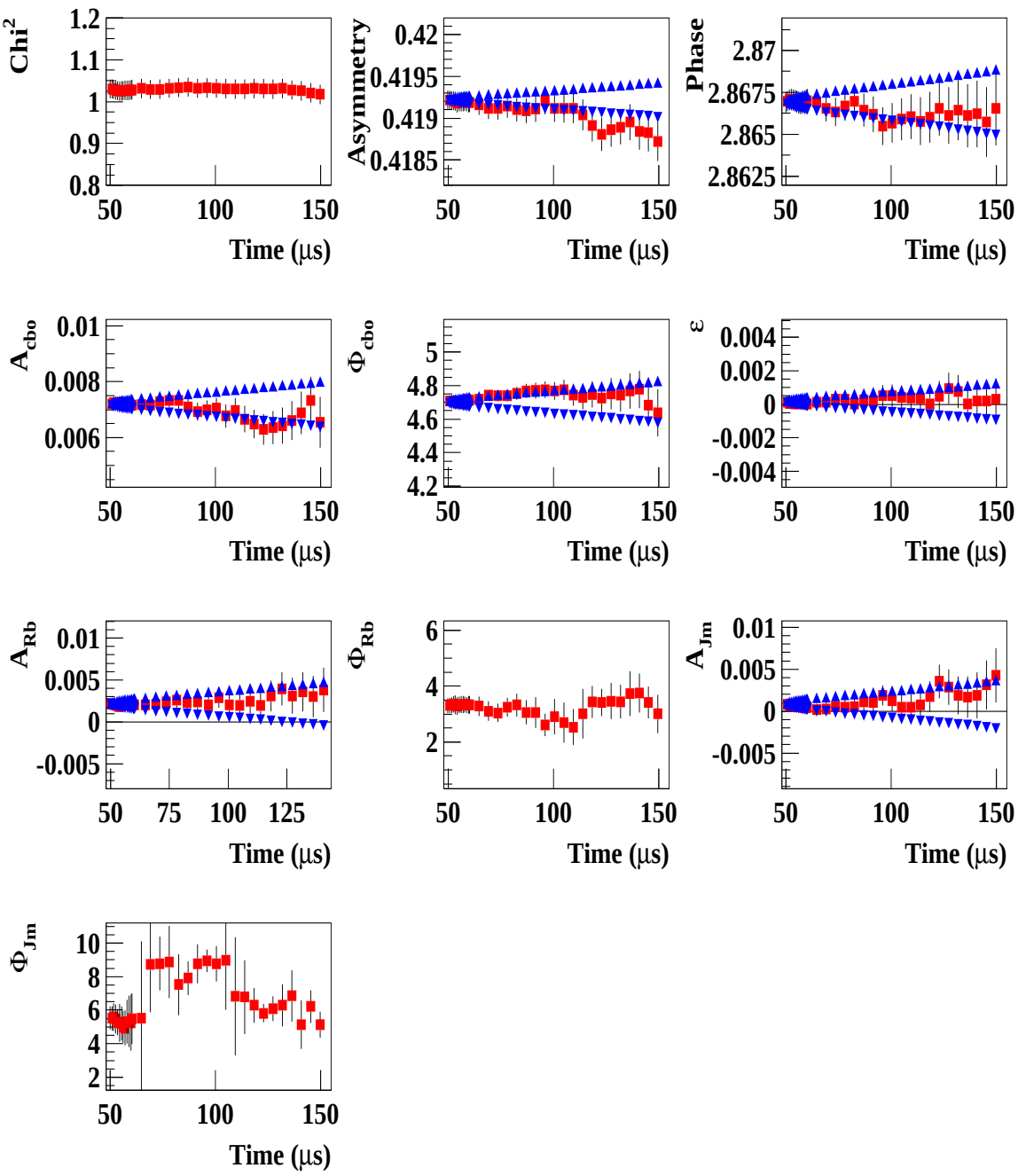

Figure 98 : continued,

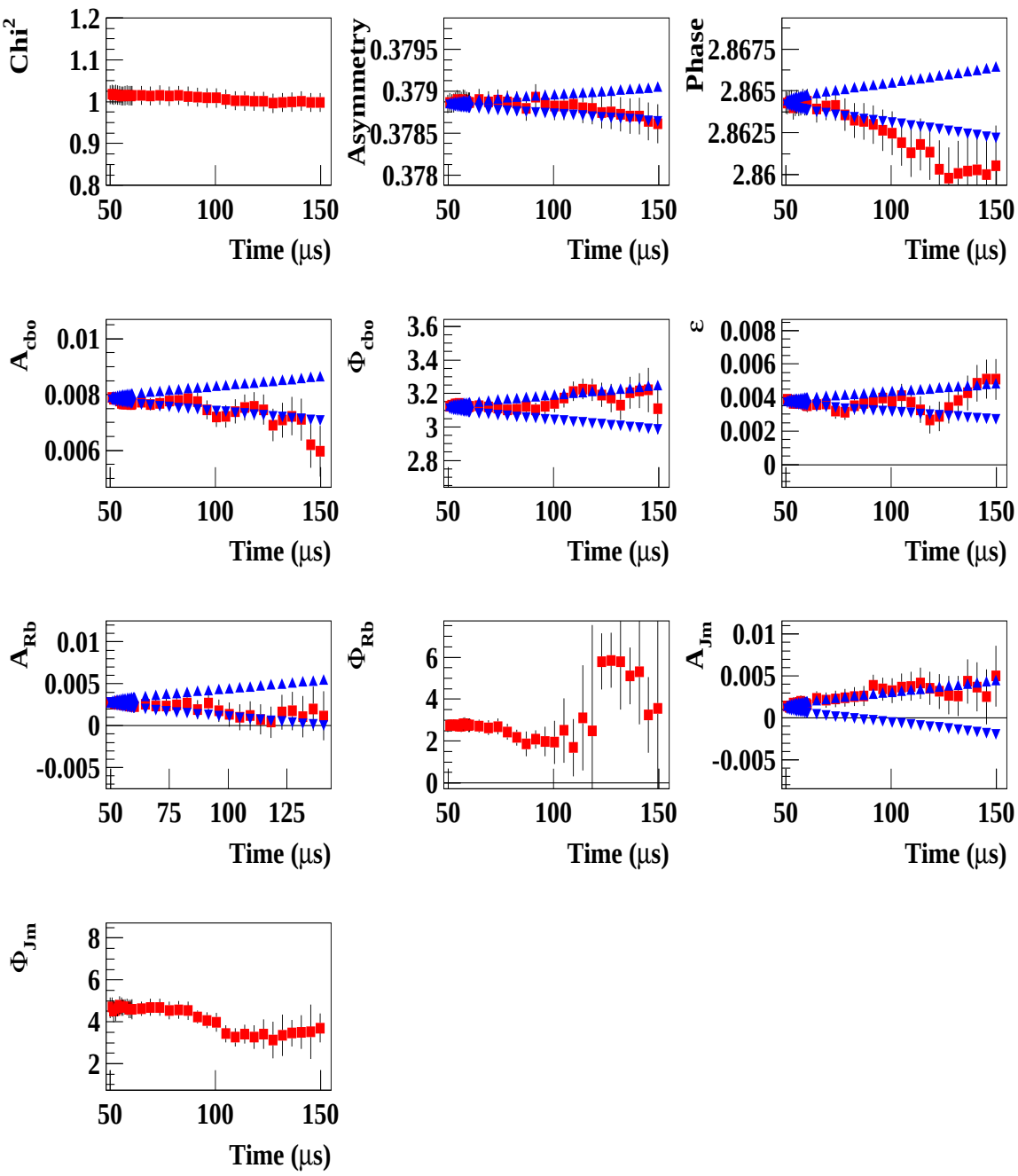

Figure 98 : continued,

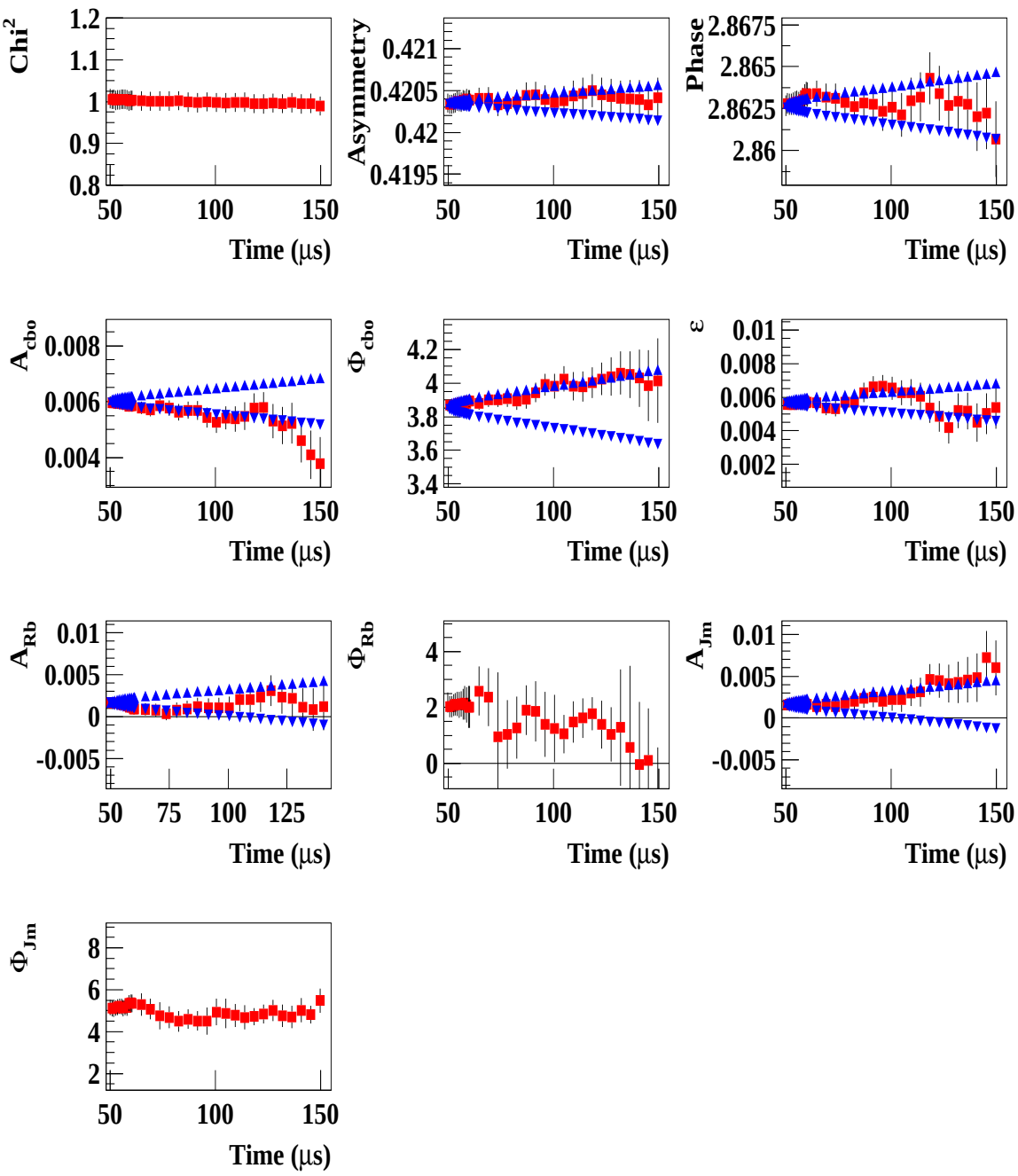

Figure 98 : continued,

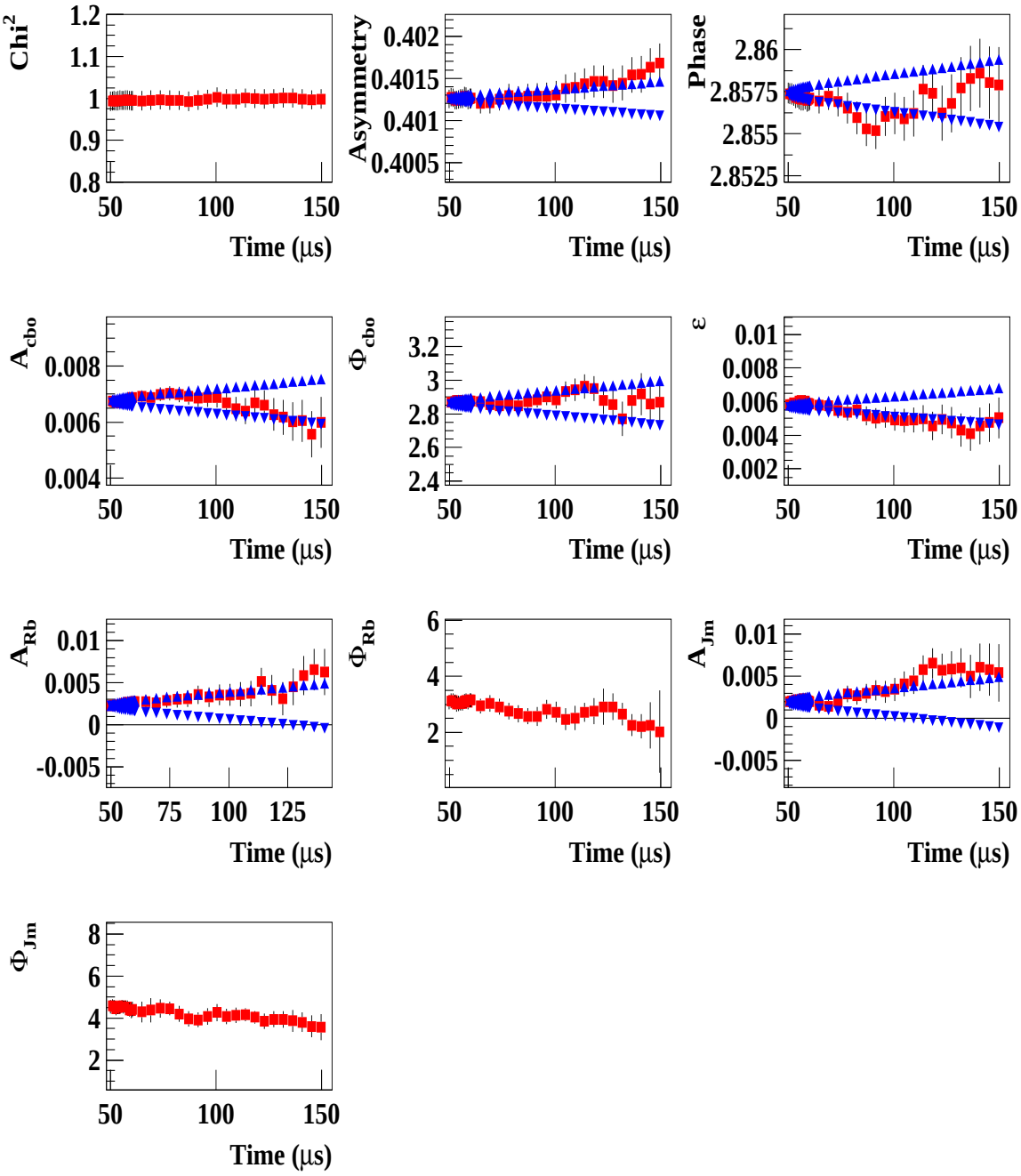

Figure 98 : continued,

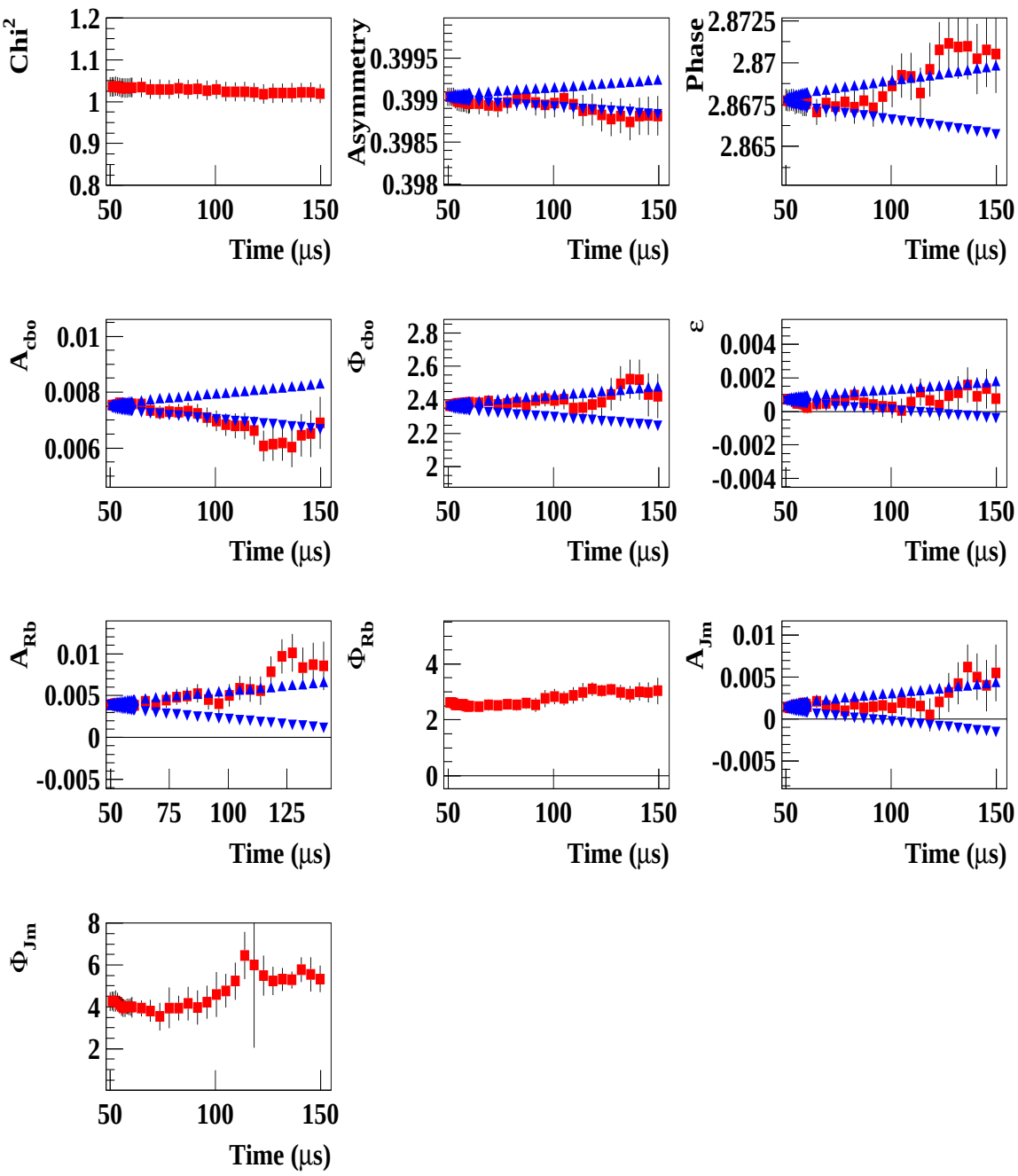

Figure 98 : continued,

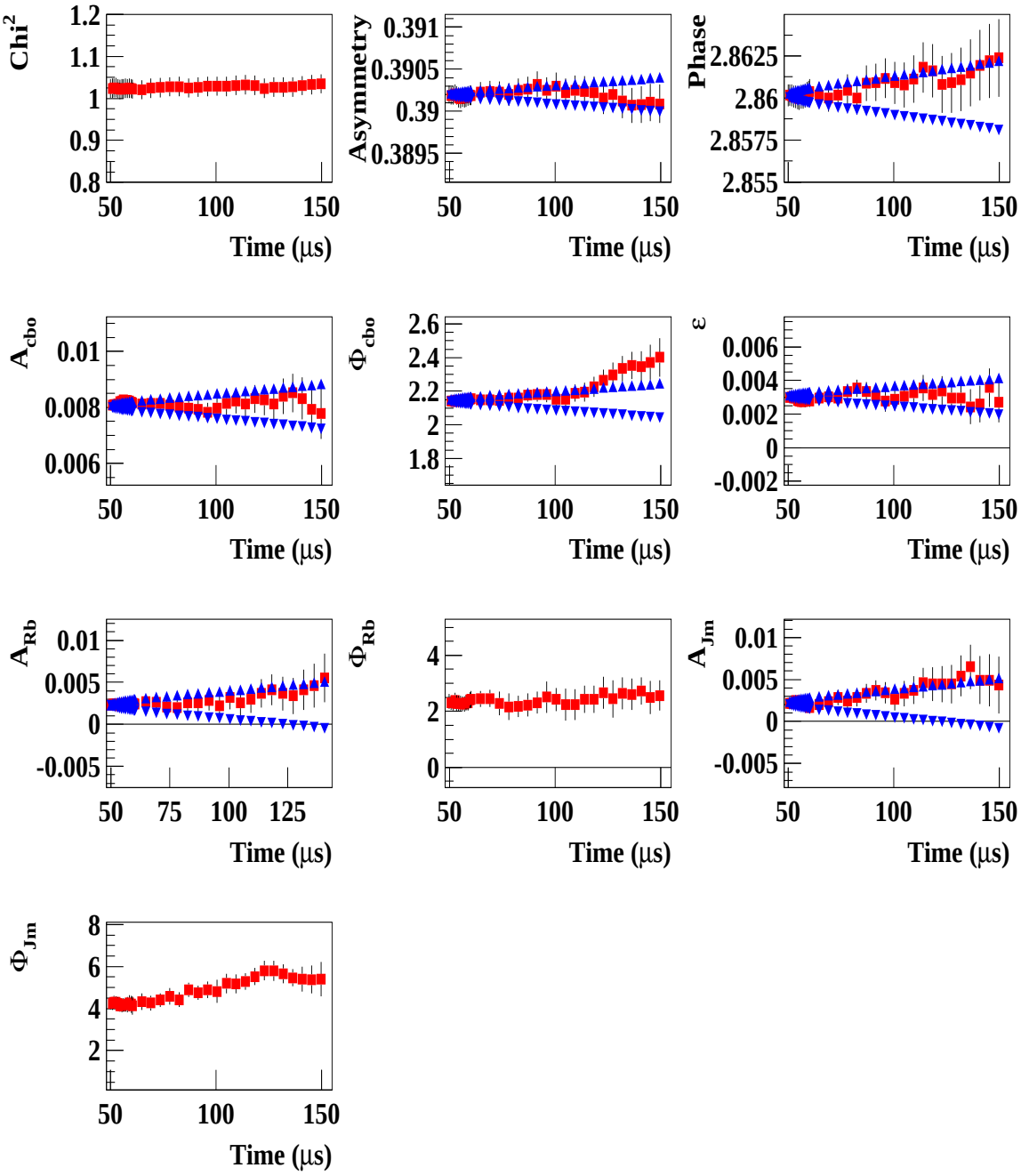

Figure 98 : continued,

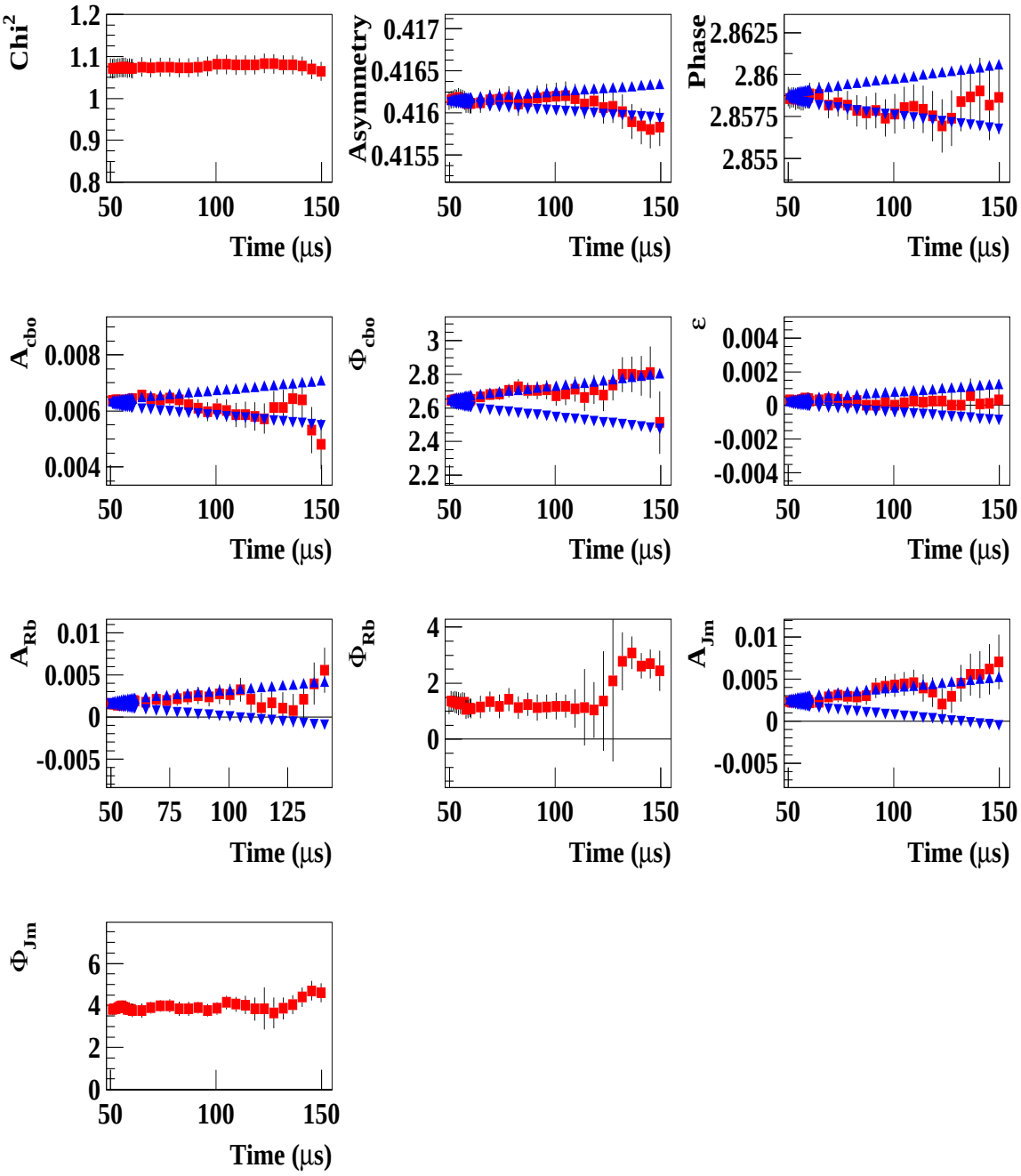

Figure 98 : continued,

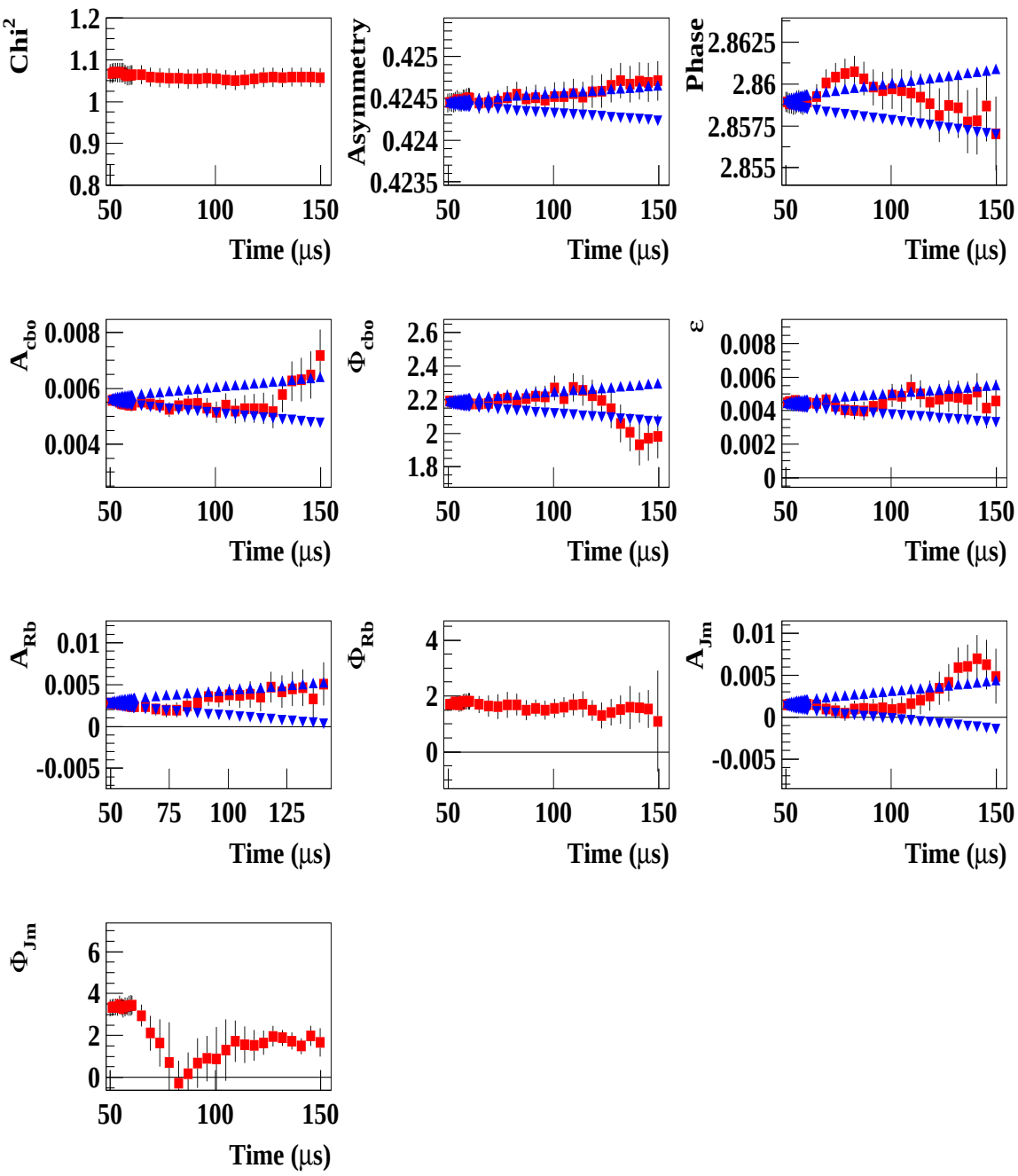

Figure 98 : continued,

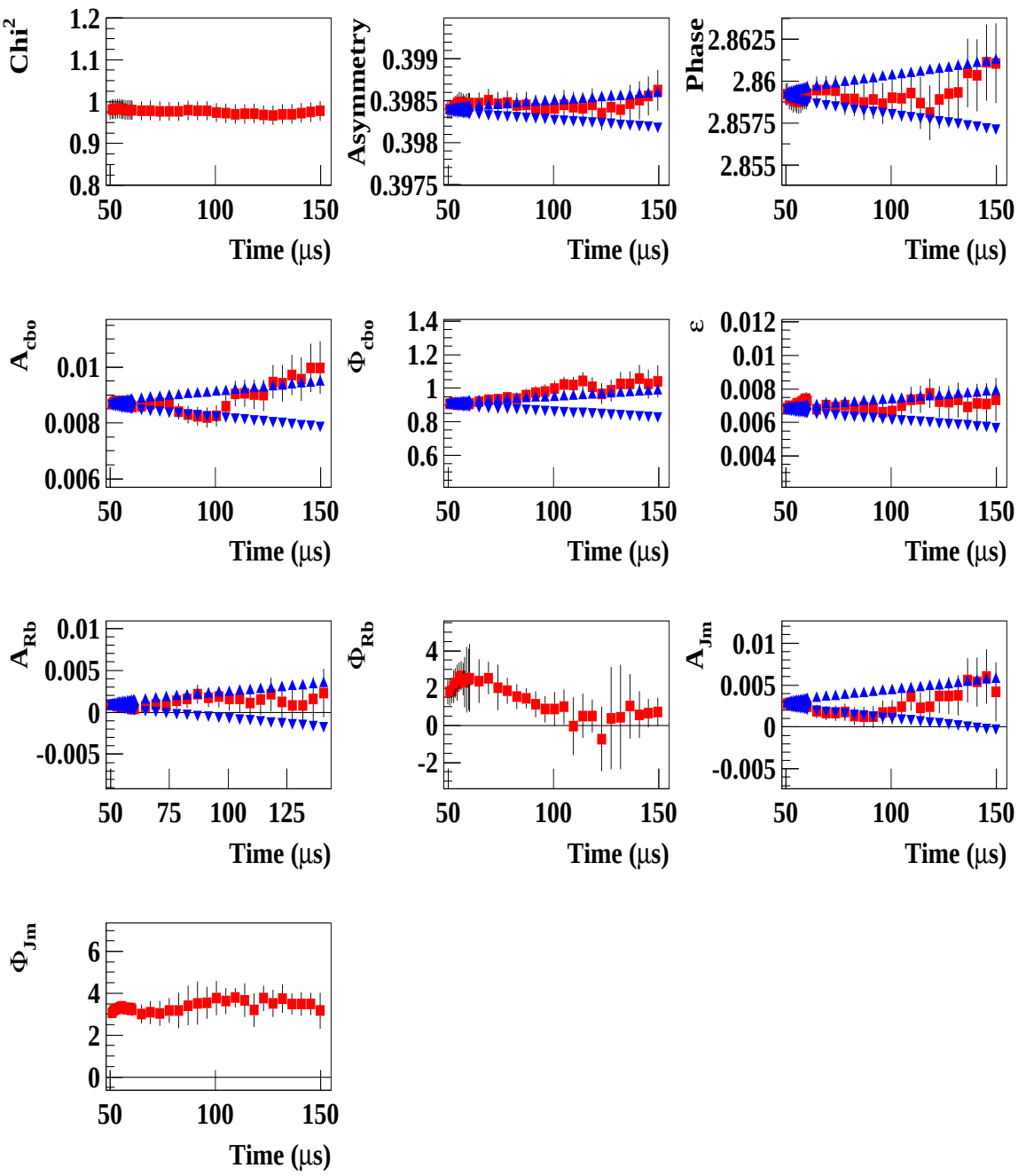

Figure 98 : continued,

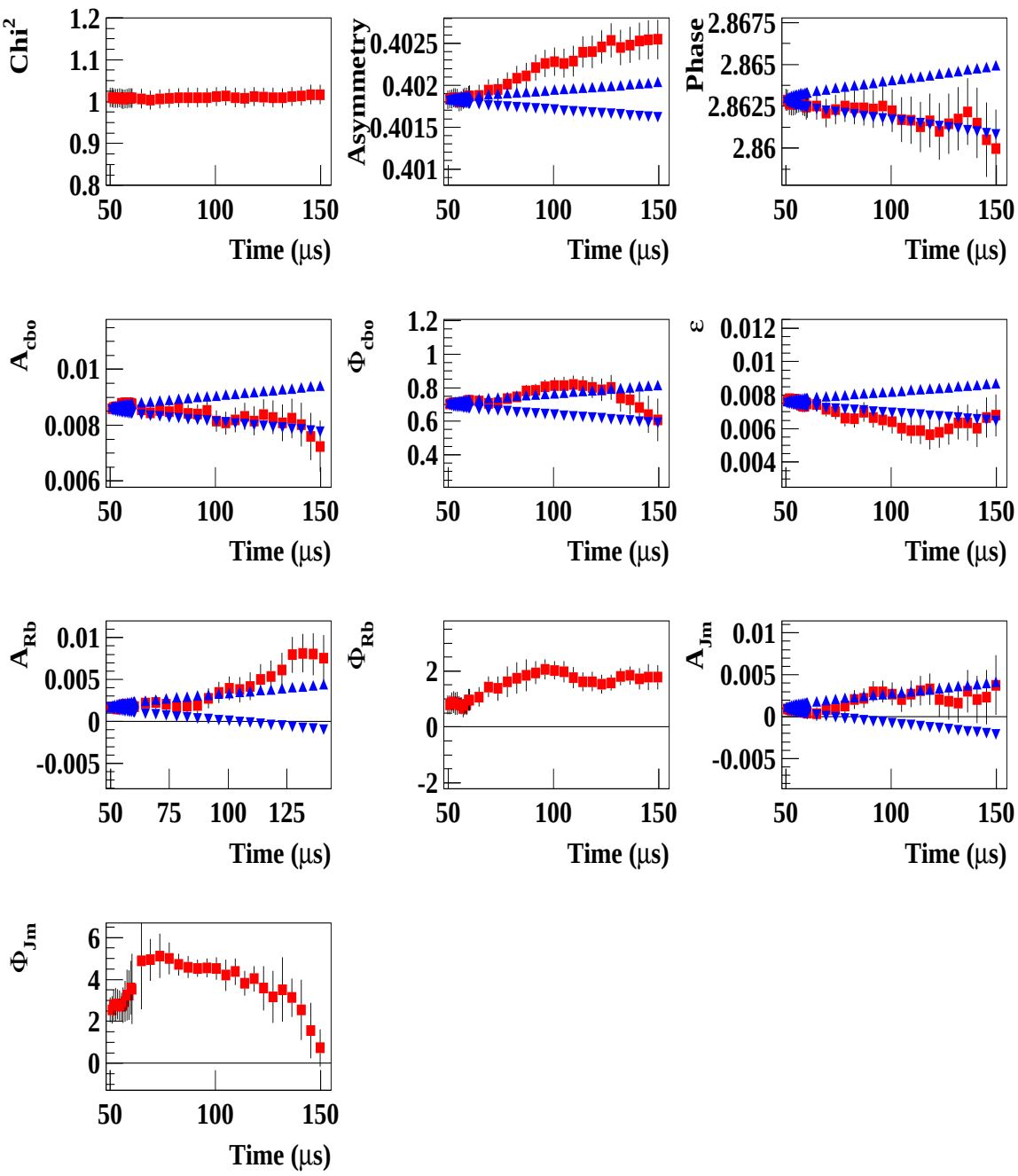

Figure 98 : continued.

7.2.4 Systematics Due to the Uncertainty on the Envelopes

Now it is certain that there are large correlations between the gain type effects and the g-2 phase modulation terms. We also know that the correlation between two of them is via the asymmetry. The other mechanism is if the gain related effects changes the effective lifetime of the envelope. This is very possible since when we look at the fit results of the gain enhanced data (Figure 36), we see the amplitude of both phase and the asymmetry modulations were influenced by the gain dramatically, especially A_{Jm}. These instabilities due to the gain may be recovered in some degree by setting the lifetime of the envelope free so fit can converge to the effective lifetime. To remind you, we use the same experimentally determined envelope for the main CBO and the asymmetry/phase modulations. The effective lifetime is the lifetime in the influence of all other effects. From the previous experiences we know that it is dangerous to fix the parameters correlated with g-2 precession frequency f_a. For that reason, to let the lifetime free for g-2 phase modulation should be justifiable. Since we don't have problem with g-2 asymmetry modulation part, we will concentrate mostly on the envelope of the phase modulation due to CBO. The early studies showed that the A_{Jm} amplitudes in the both halves can be put into Kawall band if the decay lifetime of these effects were changed. In the fits instead of fixing the phase modulation envelope to the experimentally determined CBO envelope, an exponential decay term with free lifetime was introduced. The result of this lifetime comes out to be 25.5±12 μs in the first half and 196±128 μs in the second half. The great difference between two halves can be explain with the shape of the gain differences between two halves. The lifetime of the first half is much shorter than the nominal CBO lifetime ($\approx 120\mu$s) and it is larger in the second half. The sign and the strength of the gain changes are different in both halves as you remember (please refer to the gain section).

Figures 99 and 100 shows the parameter stability in the first and the second halves. The second half was acceptable before but with free lifetime, g-2 phase modulation parameters have much better stability. In the first half there is also improvement. Since the lifetime is very short, the errors on A_{Jm} grows fast and the amplitude is large. The real value at time t can be determined from $A_{Jm}\ e^{-t/25}\mu$s. The behavior of ϕ_{Jm} in the first half is still a mystery.

However there is a great improvement on R stability in the first half eventhough the number has changed by 0.42 ppm and in the second half by 0.16 ppm (Figures 101-102). These numbers are in the same order of the gain systematics determined for the first and the second halves. One may think that assigning free lifetime for the phase modulation may reduce the gain influence on R for the complete physics functional form. Actually this has been tested by fitting the artificially gain enhanced data with free phase modulation lifetime. The gain systematic on R remained unchanged!!

The size of the deep at 80μs (R(t=50μ)-R(t=80μs)) was reduced from 1.92 ppm to 0.82 ppm for the first half and from 0.80 ppm to 0.44 ppm in the second half. In the first half, the R value reduced by 0.42 ppm at 49.9μs and increased by 0.68 ppm around 80 μs when

the lifetime is set free. This means that R is decreased in the higher part and increased in the lower part which reduced the deep amplitude around 80 μs dramatically in the first half.

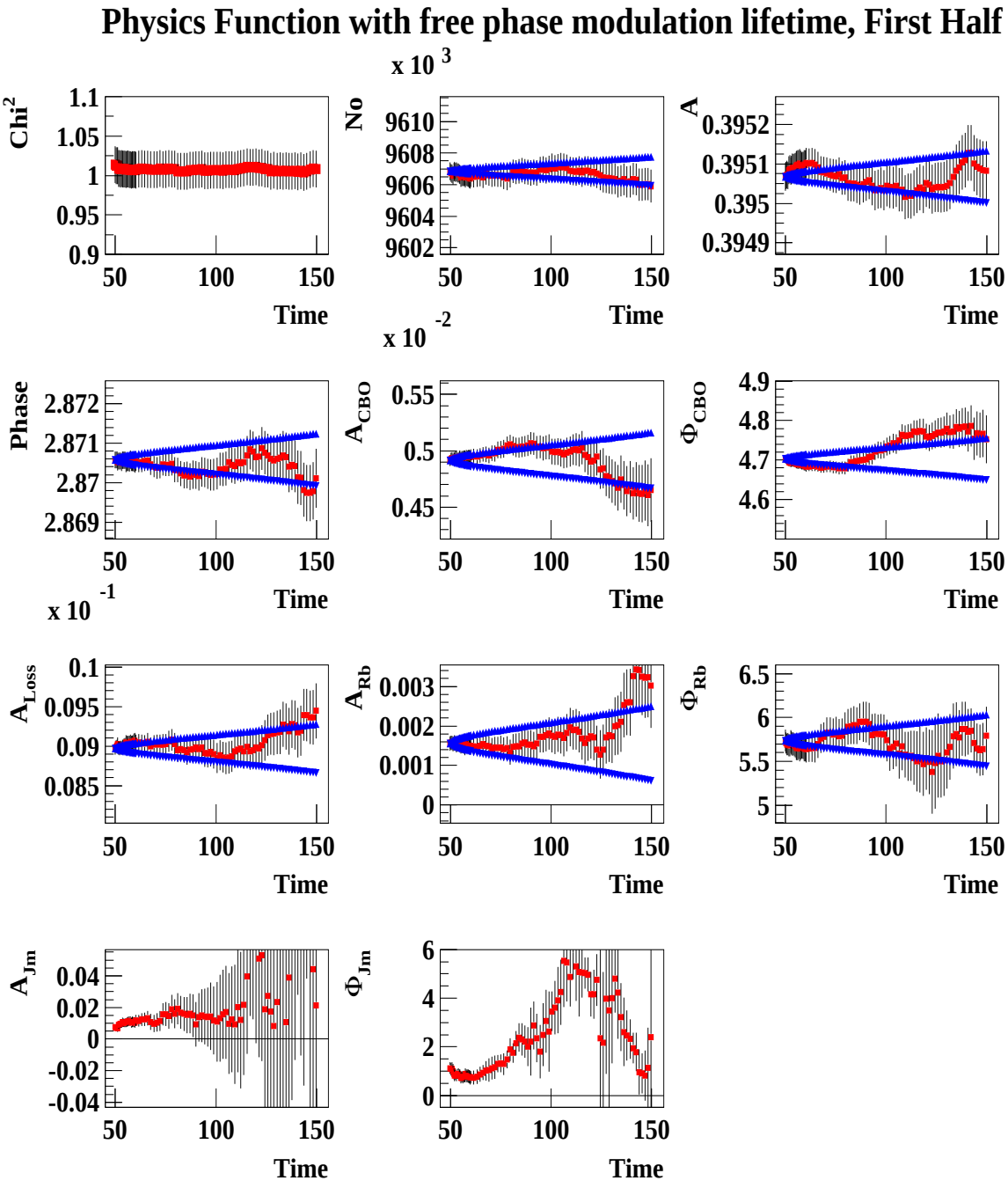

Figure 99 : The parameter stability when the envelope of g-2 phase modulation has different lifetime (25μs exponential) for the first half.

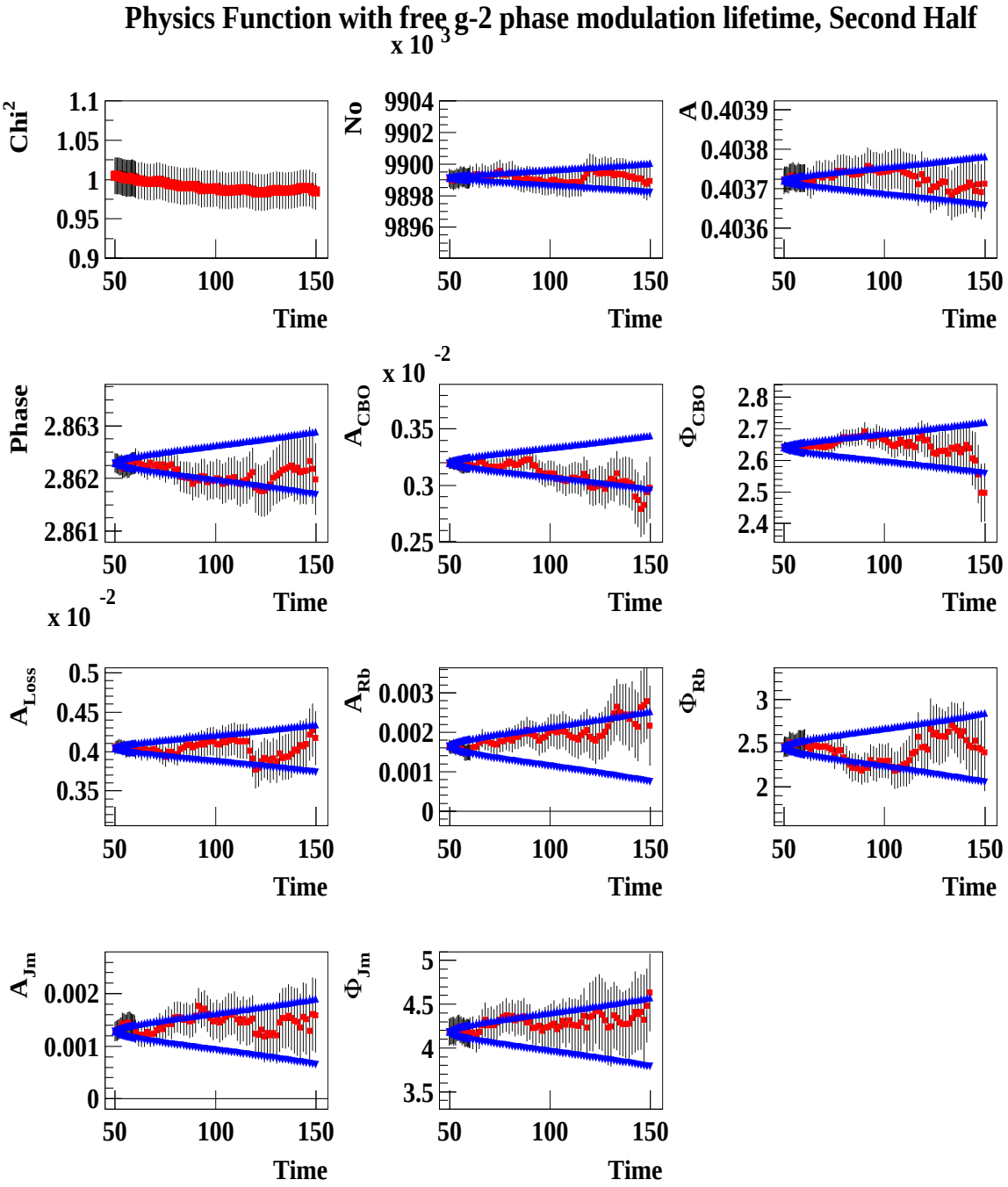

Figure 100 : The parameter stability when the envelope of g-2 phase modulation has different lifetime (196μs exponential) for the second half.

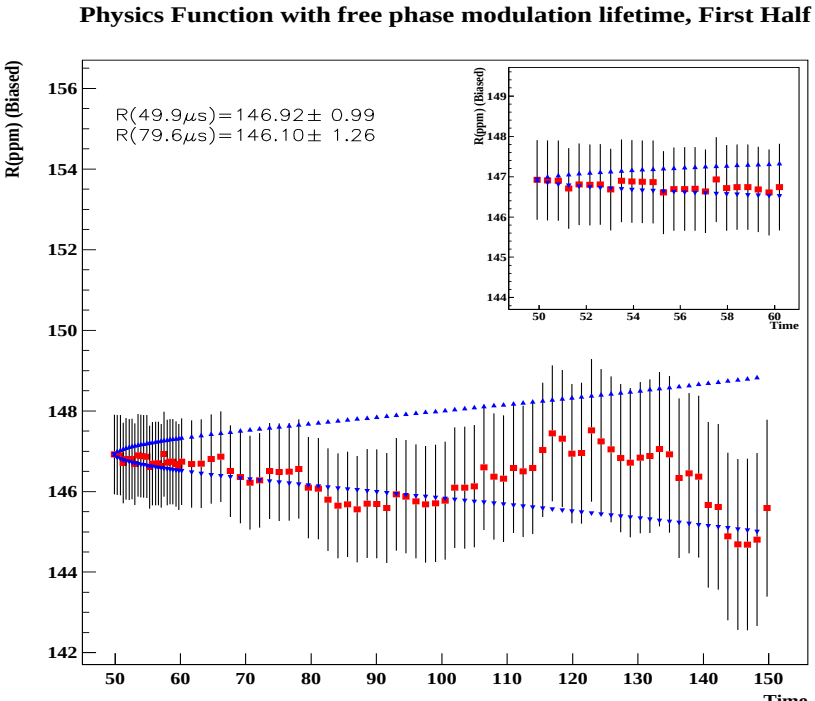

Figure 101 : R vs time in the first half with free g-2 phase modulation lifetime. The result was obtained from the average of 10 random seeds.

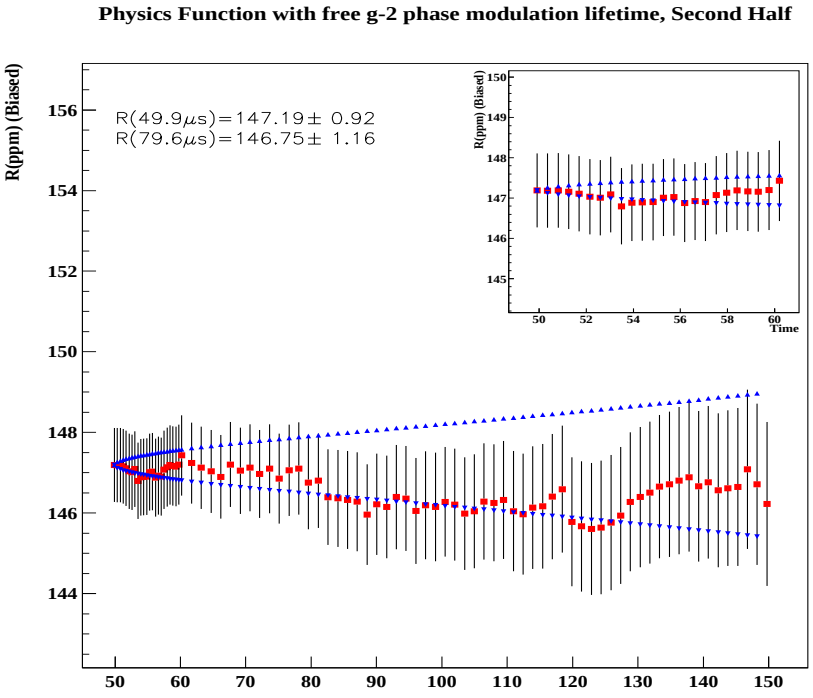

Figure 102 : R vs time in the second half with free g-2 phase modulation lifetime. The result was obtained from the average of 10 random seeds.

In the presence of the large artificial gain changes, the lifetime of the g-2 phase modulation changes dramatically. This was observed from the fits on the artificial gain enhanced

data with and without setting the lifetime of g-2 phase modulation due to CBO free. 7 times larger gain effect than the reality reduced the lifetime of the g-2 phase modulation from ≈100 μs (approximate lifetime of the experimentally determined envelope) to 20 μs level. When the lifetime of the g-2 phase modulation set free in the fits, systematic shift on R was not changed practically. On the other hand the error on R slightly increased ($\approx$ 3%) due to the correlations between R and the new parameter free g-2 phase modulation lifetime.

From the comparison of the R values at 49.9 μs with and without the free lifetime for g-2 phase modulation we will assign **0.29 ppm** systematic due to the uncertainty of the functional form (mainly due to the envelope) from the g-2 phase modulation for the complete physics form. This systematic is uncorrelated with the systematic from the gain since letting the lifetime free does not recover the gain influence on R as we mentioned earlier.

Eventhough the stability of the g-2 asymmetry modulation parameters in the fit are acceptable, we also look at the influence of the free g-2 asymmetry modulation lifetime on 1999 functional form including the g-2 asymmetry modulation. The envelope of g-2 asymmetry modulation was changed to exponential envelope with free lifetime instead of the experimental envelope obtained from the data. The lifetimes were determined from the first and the second halves as 199$\pm$135 μs and 178$\pm$91 μs respectively. The change on R in the average (average of the first and the second halves) was only **0.02 ppm**. This result is very important. It means uncertainty due to the envelope of g-2 asymmetry modulation is very small for the 1999 functional form including g-2 asymmetry modulation due to CBO.

7.2.5 Determining the A_{Jm} and ϕ_{Jm} from the Second Half and Using them in the First Half

In the complete physics function even with the basic form, the parameter stabilities are acceptable in the second half. The problems in the first half mostly rises from the unstable phase modulation parameters especially the phase. When an artificial gain introduced into the data, the most important observation was both g-2 asymmetry and the phase modulation parameters were heavily influenced by the gain. The correct ϕ_{Rb} and ϕ_{Jm} phases (original) were recovered only after the gain influence ended which was around 100 μs. Since the statistics does not allowed us to determine the phases at late times, another approach was necessary to determine the correct phase for the problematic first half. We also know that the amplitude of both asymmetry and the phase modulations are the same through out the ring. The phase difference between the first and the second halves is not exactly π. The reason for it is missing detectors in the first and in the second half are in different locations (detectors 2 and 20). The effect of these could be easily found from the vector sum [14]. If one assumes the amplitudes are the same for the detectors and the fact that detector 2 in the first half and detector 20 in the second half are missing, makes the angle difference between the first and the second halves not 180^0 but 169.5^0. Also the second half amplitude is 8.7% smaller. The ϕ_{Jm} for the second half 4.1031 rad (from the

fit) and from this ϕ_{Jm} for the first half can be found as 6.913 rad. What fit gives for the first half is 7.53 rad. For the amplitude A_{Jm} we will use $1.175710^{-3}/1.087 = 1.081310^{-3}$.

We will fix both the amplitude and the phase of g-2 phase modulation to the value determined from the second half (Figures 103 and 104).

Conclusion from this study is as follows : When the amplitude and the phase of g-2 phase modulation were fixed to the value obtained from using the second half, the R value reduces by 0.59 ppm at 49.9 μs. The asymmetry stability gets worse. The deep at 80 μ disappears.

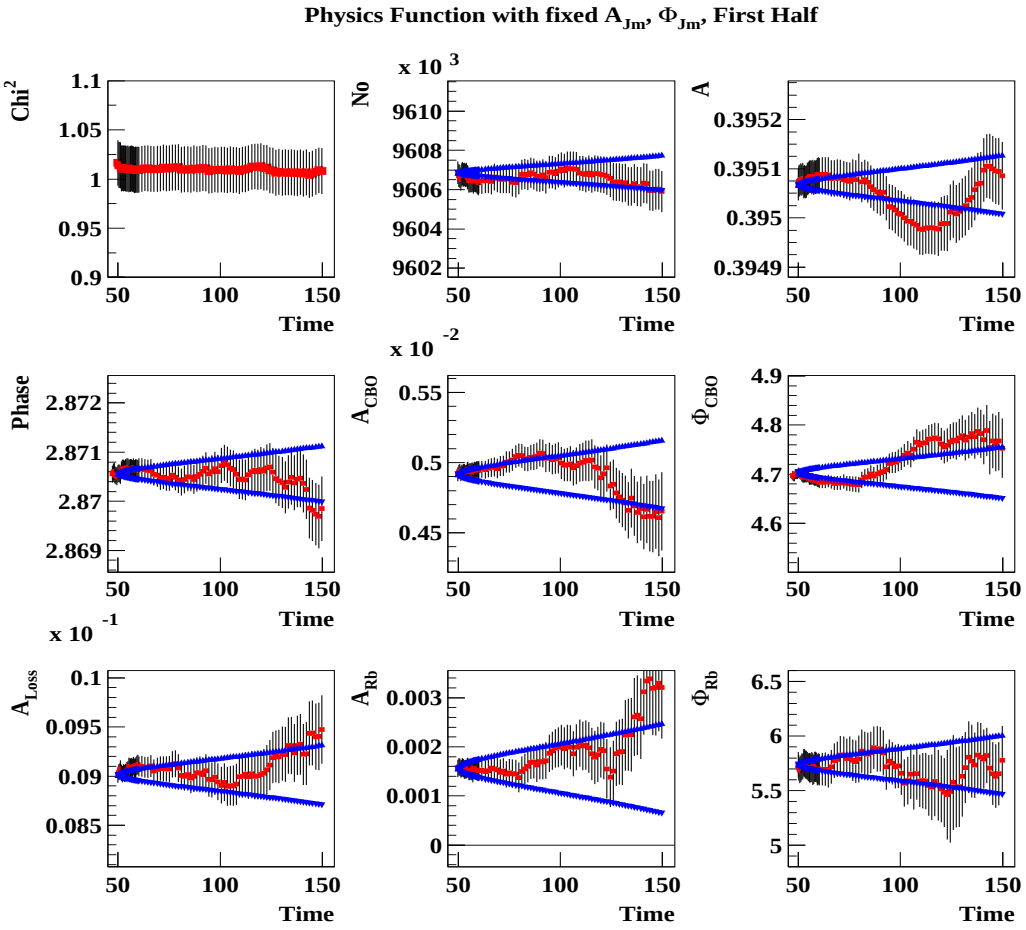

Figure 103 : The parameter stability in the first half when the amplitude and the phase of the g-2 phase modulation were fixed to the value determined from the second half. The result was obtained from the average of 10 random seeds.

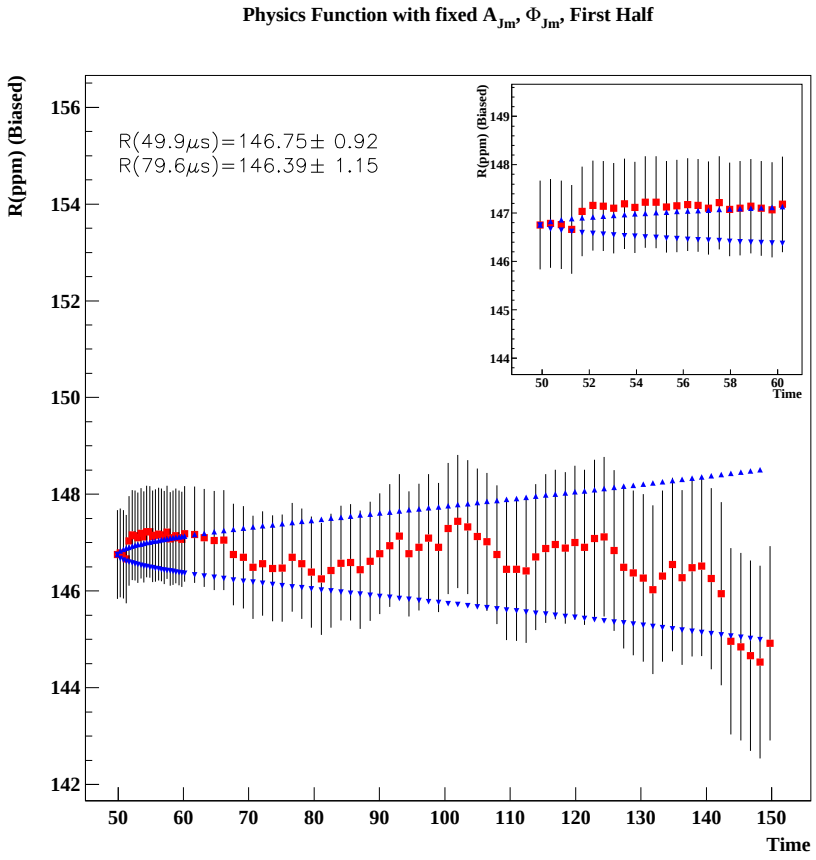

Figure 104 : R vs time in the first half when the amplitude and the phase of the g-2 phase modulation were fixed to the value determined from the second half. The result was obtained from the average of 10 random seeds.

Table 22 gives the comparison of the R values obtained from the various functional forms and treatments.

Table 22: Comparison of the R values for different type of functional forms and cases at 49.9 μs. I: 1999 functional form, II: Including the asymmetry modulation to I, III: the complete physics function. 1: The weighted average of the first and the second half, 2: all detectors together, 3: the average of the individual detectors. The results are in ppm.

Method	I	II	III		
			Physics	Free τ_{Jm}	Fixed A_{Jm}, ϕ_{Jm}
1	147.06±0.61	147.27±0.64	147.35±0.67	147.06±0.67	147.05±0.65
2	147.02±0.61	147.28±0.64	147.34±0.67		
3	147.18±0.61	147.27±0.64	147.35±0.67		

The ≈0.15 ppm difference on the fit results between the detectors together and average of

the individuals for 1999 functional form may be the signature of a systematic effect cannot be handled properly in one of the cases. The discussion of the table as follows : If the complete functional form with free g-2 phase modulation lifetime is used, the resultant R is very close to what we get from 1999 type functional form. This conclusion is the same if one uses the phase and the amplitude information of the g-2 phase modulation from the second half to determine them for the first half and fixes them. There is a maximum 0.33 ppm difference between the fit results from various methods and the treatments. This should be the size of the systematics we are dealing with.

7.2.6 Systematics From Asymmetry and Phase Modulations due to CBO

Our problem is how well we know the reduction factor on both g-2 phase and amplitude modulations when all the detectors are together. This is directly related with the question of how well we know the g-2 asymmetry and the phase modulation amplitudes for individual detectors. Figure 93 shows the average g-2 asymmetry modulation amplitude A_{Rb} is $2.30 \pm 1.26\ 10^{-3}$ and χ^2 to straight line is 39.33/21. This value is unacceptable and corresponds to 2.9σ. This value shows that there are systematics involved on the values for individual detectors not taken into account. However if we look at that picture carefully we will see that the detectors most deviated from the average are detectors 4, 7 and 18. These detectors have large gain influence with funny shapes. When we take them out the average becomes as in Figure 105.

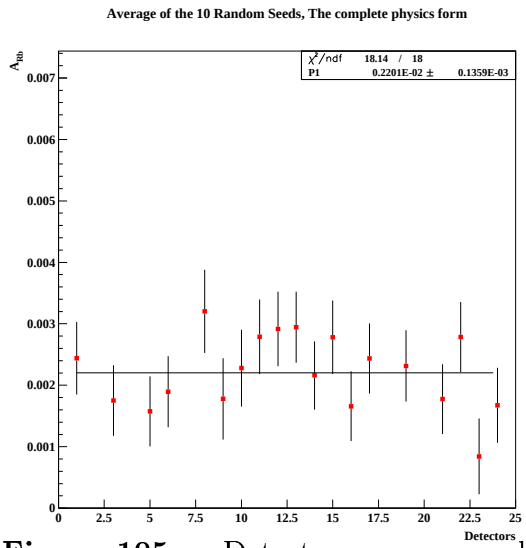

Figure 105 : Detectors versus amplitude of g-2 asymmetry modulation.

In Figure 105 we show the detectors versus amplitude of g-2 asymmetry modulation. Gain problematic (mostly in their shape not in their size) detectors 4,7 and 18 were taken out. Excellent χ^2 is striking. Taking detectors 4,7 and 18 out changed the average only by 0.1×10^{-3}. From this one concludes that the size of the g-2 asymmetry modulation can be precisely determined as long as gain type effects are resolved. In our case we are lucky since the cancellation between detectors 4, 7 and 18 is pretty good. There is no worry about the g-2 phase modulation amplitude since the χ^2 to the straight line is only one sigma away.

The strategy to determine the systematics due to g-2 asymmetry and phase modulations is as follows. Three sets of Monte Carlo data were produced with g-2 asymmetry modulation, g-2 phase modulation and both of them respectively. The amplitudes of those effects introduced into MC were taken from the average fit amplitude of the individual detectors as A_{Rb}=2.2 10^{-3} and A_{Jm}=1.5 10^{-3}. These amplitudes are much larger than the amplitudes determined when the time spectra from the detectors were summed up. The reason for this is the cancellations. Each sets were fitted with three types of functional forms in order to determine the direct correlations between the g-2 phase and amplitude modulations as well as the systematic studies. This is necessary, since in the data, because of the correlations to the other effects (especially to the gain), the direct relations between these parameters can not be determined precisely.
Table 23 shows the parameters introduced in to MC simulations. The initial phases of Rb and Jm effects for MC were taken from the data of all detectors together as ϕ_{Rb}=1.5 rad and ϕ_{Jm}=4.0 rad.

Table 23: MC were produced with the average of the individuals (first column). Second column shows the amplitudes of the related effects determined when the detectors were summed up. The normalization ratio for the systematics were determined in such that A_{Rb} and A_{Jm} known within $\pm$ 1 sigma. For that reason three ratios are given. (column four

	Average of the Individuals (A$\pm\sigma_A$)	Detectors Together (B$\pm\sigma_B$)	Ratio
Parameter			
A_{Rb}	(2.20$\pm$0.13) 10^{-3}	(2.33$\pm$1.3) 10^{-4}	9.4$\pm$5.3
A_{Jm}	(1.49$\pm$0.13) 10^{-3}	(2.48$\pm$1.3) 10^{-4}	6.0$\pm$3.4

Figure 106 shows the parameter stability when both g-2 asymmetry and the phase modulations were introduced into MC but in the fit plain 1999 functional form was used. One can put a limit from the asymmetry stability comparing MC with the data. On the other hand since the asymmetry stability is influenced not only by g-2 asymmetry and the phase modulations but also the gain related effects, it is been preferred not to do this way. The ratios described in the Table 23 are going to be used for that purpose. Large phase pulling on N_0 and CBO related parameters exist in the simulated data. Figure 107 shows the R stability. The systematic shift on R at specific time depends on the initial phase of the related effects. However the MC production phases for these effects were taken from the data therefore it is realistic.

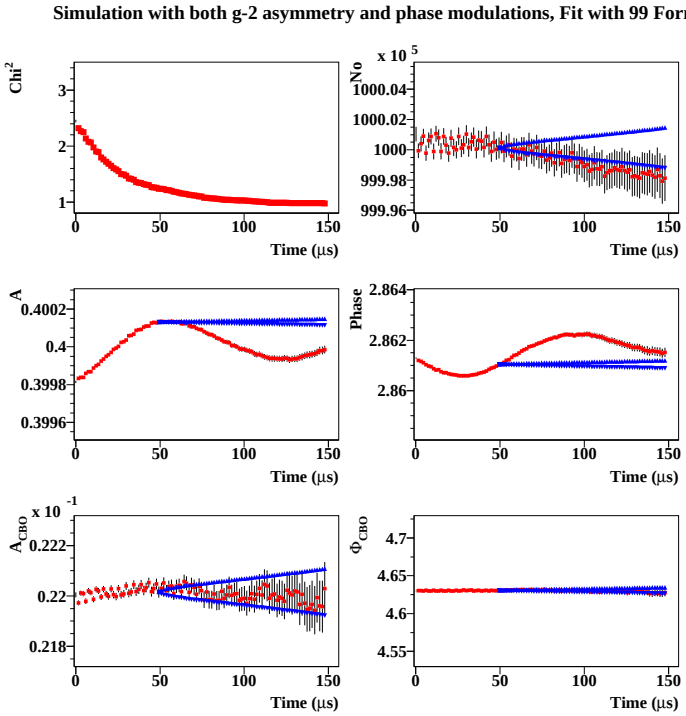

Figure 106 : The parameter stability when both g-2 asymmetry (9.4 times larger than what we have when the detectors were combined) and the phase modulations (6 times larger than what we have when the detectors were combined) were introduced into the MC. For the fit, plain 1999 functional form was used.

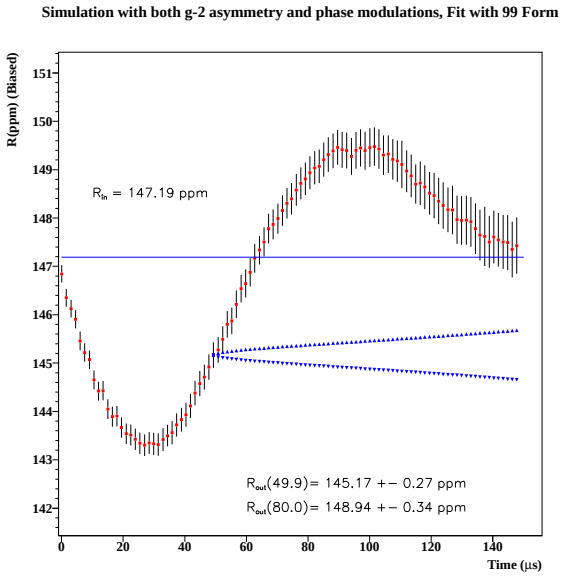

Figure 107 : The stability of R when a MC data, produced with both g-2 phase and asymmetry modulations, fitted to the plain 1999 functional form. The vertical line is the input value of R in the MC. ΔR(49.9μs)=2.02 ppm and half of the peak to peak oscillation is 3.09 ppm.

Figure 108 shows the parameter stability when only g-2 asymmetry modulation was introduced into MC and plain 1999 functional form was used in the fit . The phase pulling at ϕ_{cbo} is mostly vanished. On the other hand the one on A_{cbo} still exist with almost the same intensity. Figure 109 shows the stability on R in this case.

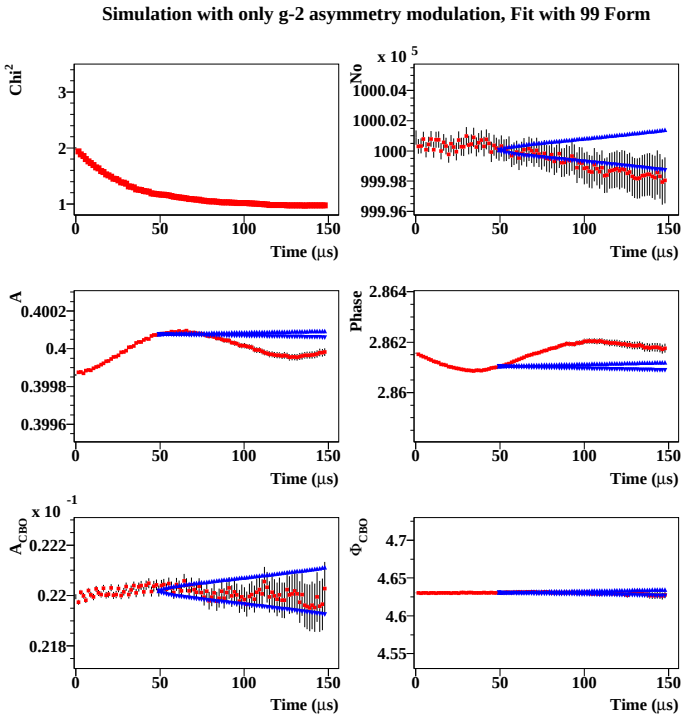

Figure 108 : The parameter stability when g-2 asymmetry modulation was introduced into the MC. For the fit, plain 1999 functional form is used.

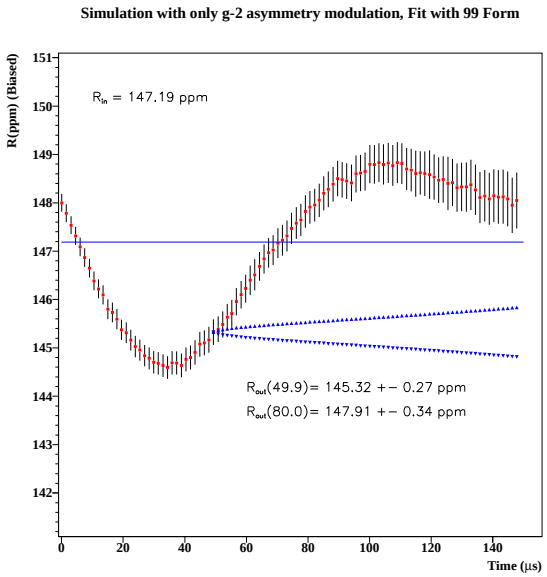

Figure 109 : The stability of R when a MC data, produced with g-2 asymmetry modulation, fitted to the plain 1999 functional form. ΔR(49.9μs)=1.87 ppm and half of the peak to peak oscillation is 2.12 ppm.

Figure 110 shows the parameter stability when only g-2 phase modulation was introduced into MC and plain 1999 functional form was used in the fit . Now the phase pullings on $A_C BO$ and N_0 are reduced dramatically. Figure 111 shows the stability on R in this case.

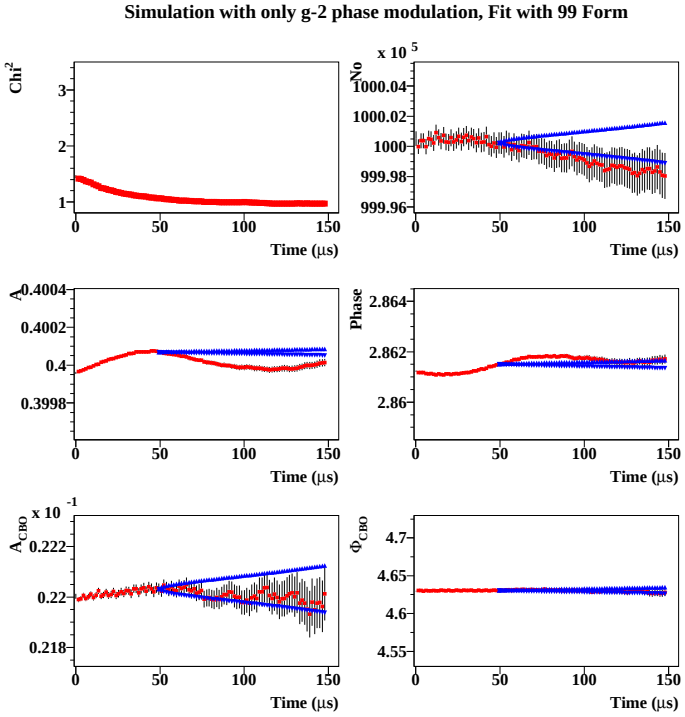

Figure 110 : The parameter stability when g-2 phase modulation was introduced into the MC. For the fit, plain 1999 functional form is used.

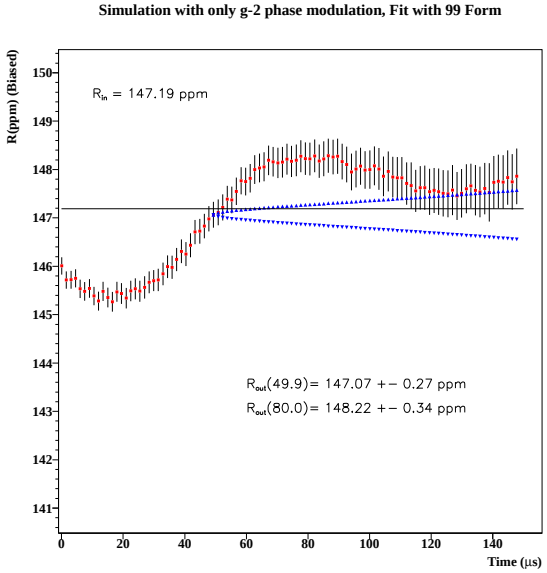

Figure 111 : The stability of R when a MC data, produced with g-2 phase modulation, fitted to the plain 1999 functional form. ΔR(49.9μs).7=0.12 ppm and half of the peak to peak oscillation is 1.51 ppm.

To prove the systematic shift depends strongly on the initial phase of the effects, the initial phases of Rb and Jm terms changed between zero to 2π and corresponding change on R at 50 μs studied. Figures 112 and 113 show this study. In Figure 112 we changed the initial phase of the g-2 asymmetry modulation between zero to 2π. In Figure 113 the same thing was done for the phase of the g-2 phase modulation.

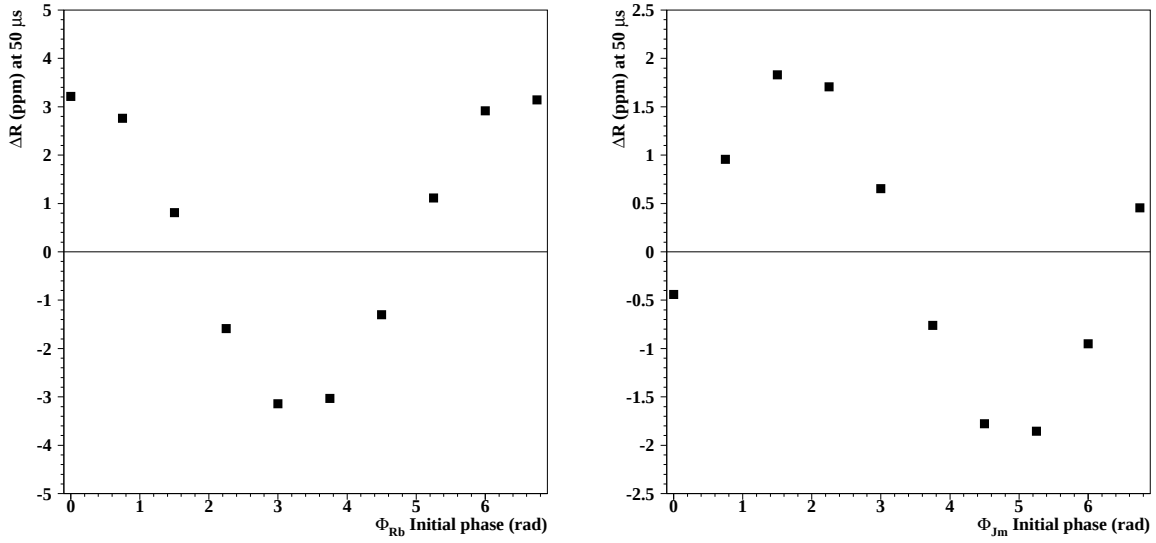

Figure 112 : a-) When the phase of the g-2 asymmetry modulation changes between zero and 2π, the corresponding change on R value at 50 μ. b-)When the phase of the g-2 phase modulation changes between zero and 2π, the corresponding change on R value at 50 μ.

The conclusions from this study are as follows : The initial phase of the effects assigned in the MC make a large difference on the systematic. If we believe the g-2 asymmetry and the phase modulation phases determined by the fits, then we can conclude that most of the systematic is coming from the g-2 asymmetry modulation. However we will follow a conservative approach in here and determine the errors from the half of the peak to peak values of Figure 112 for these effects. Therefore for the 1999 functional form we will assign **0.34 ppm** due to g-2 asymmetry modulation and **0.30 ppm** due to g-2 phase modulation for 1999 functional form using Table 23 for normalizations.

A similar approach will take place for the other types of the functional forms. The next step is the 1999 functional form including the g-2 asymmetry modulation.

Figure 113 shows the parameter stability when both g-2 asymmetry and the phase modulations were introduced into MC but in the fit 1999 functional form including g-2 asymmetry modulation was used. Large phase pulling on N_0 and CBO related parameters are present in the parameters just like in 1999 type functional form. Here g-2 asymmetry modulation can be recovered completely. However probably due to the presence of the g-2

phase modulation in the simulation (we don't fit for it), the stability of the g-2 asymmetry modulation parameters are not very good. The amplitude of g-2 asymmetry modulation is smaller by 10% and the phase of the g-2 phase modulation is smaller by 0.05 rad at 50 μs compared to original input values. Figure 114 shows the R stability.

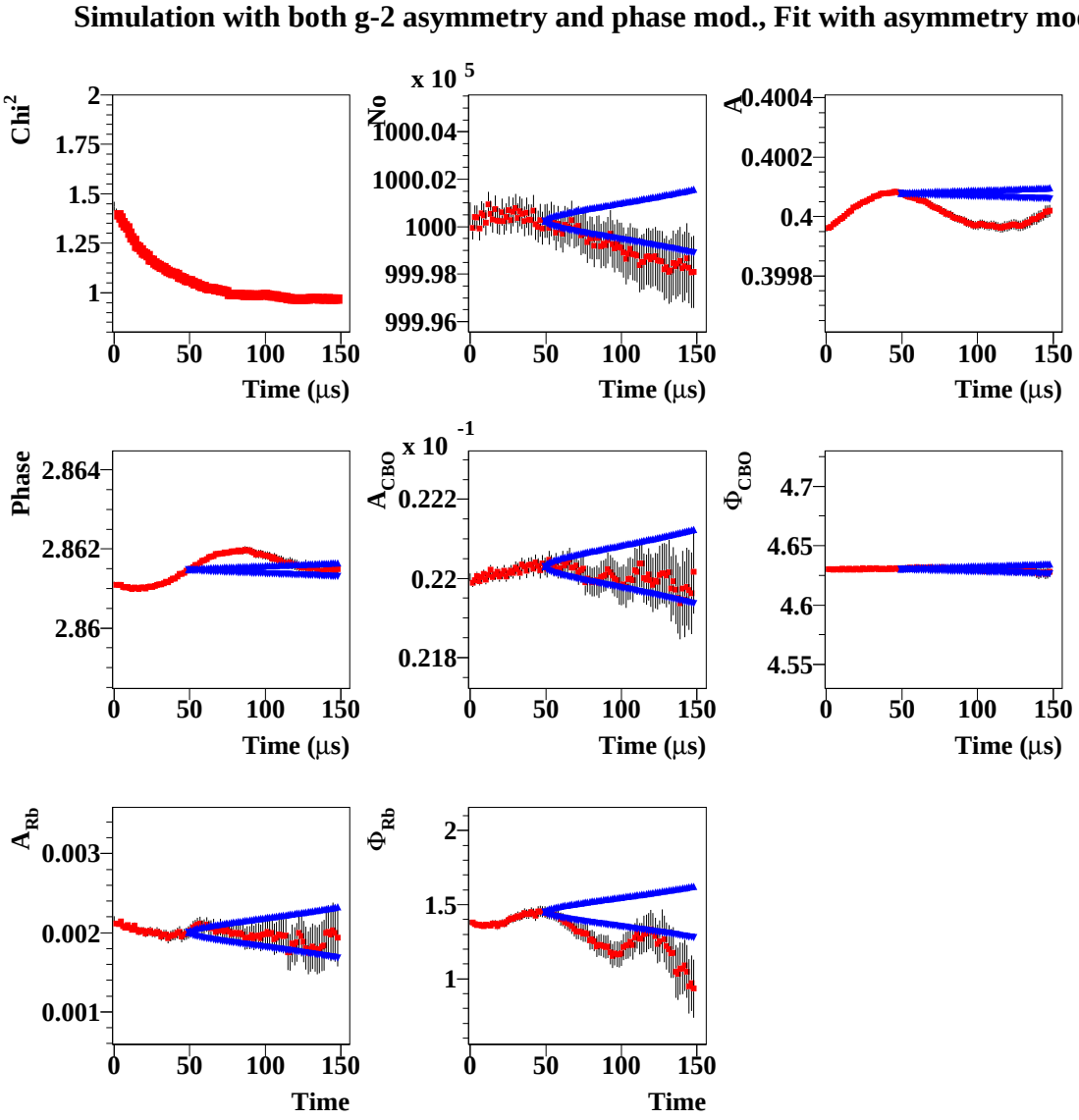

Figure 113 : The parameter stability when both g-2 asymmetry and the phase modulations were introduced into the MC. For the fit, 1999 functional form including g-2 asymmetry modulation was used.

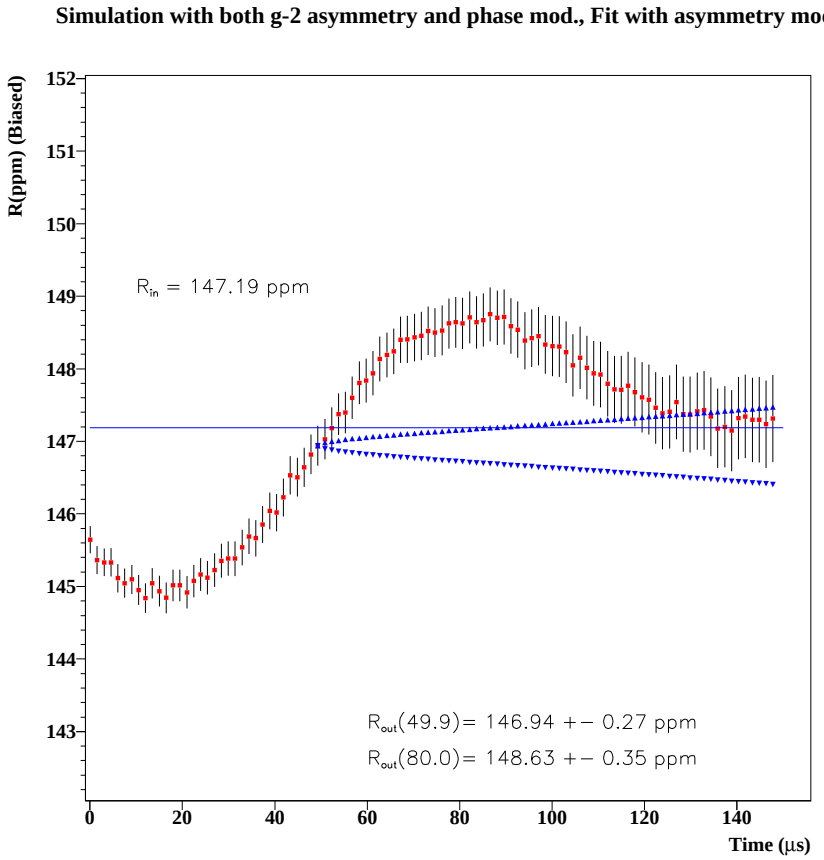

Figure 114 : The stability of R when a MC data, produced with both g-2 phase and asymmetry modulations, fitted to the 1999 functional form including g-2 asymmetry modulation. The vertical line is the input value of R in the MC. ΔR(49.9μs)=0.25 ppm and half of the peak to peak maximum distance is 1.96 ppm.

Figure 115 shows the parameter stability when only g-2 asymmetry modulation was introduced into the MC and 1999 functional form including g-2 asymmetry modulation was used in the fit. The parameter stability is excellent as expected. Figure 116 shows the stability of R in this case.

Figure 117-118 shows the parameter stability when only g-2 phase modulation was introduced into MC and 1999 functional form including g-2 asymmetry modulation was used in the fit. It is interesting to see that some of the fraction of the g-2 phase modulation can be recovered by the g-2 asymmetry modulation. This fraction is approximately %15 in amplitude which is in fair agreement with the correlation coefficient between A_{Jm} and A_{Rb} (Table 20). On the other hand the stability is not good. The determined phase is far away from the input phase of g-2 phase modulation (4 rad). One important conclusion here is the correlations between **Jm** and **Rb** can cause parameter instability!

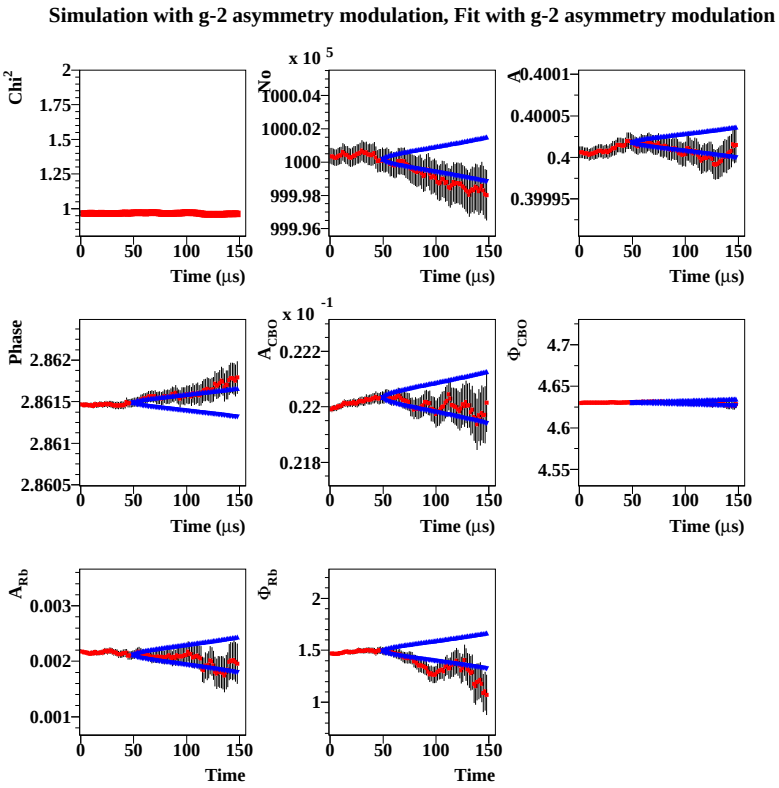

Figure 115 : The parameter stability when g-2 asymmetry modulation was introduced into the MC. For the fit, 1999 functional form including g-2 asymmetry modulation was used.

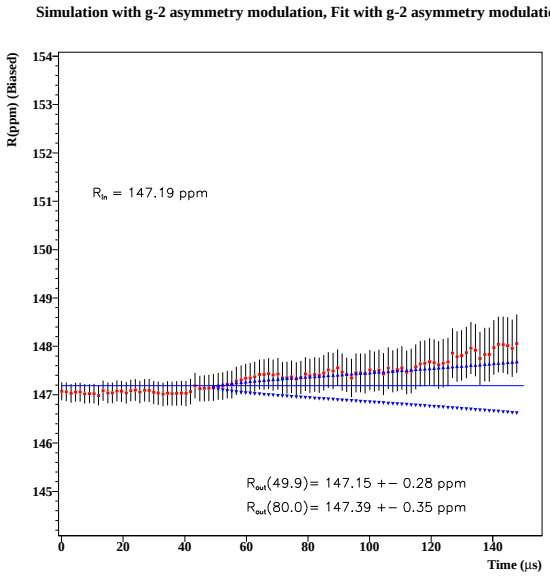

Figure 116 : The stability of R when a MC data, produced with g-2 asymmetry modulation, fitted to the 1999 functional form with g-2 asymmetry modulation.

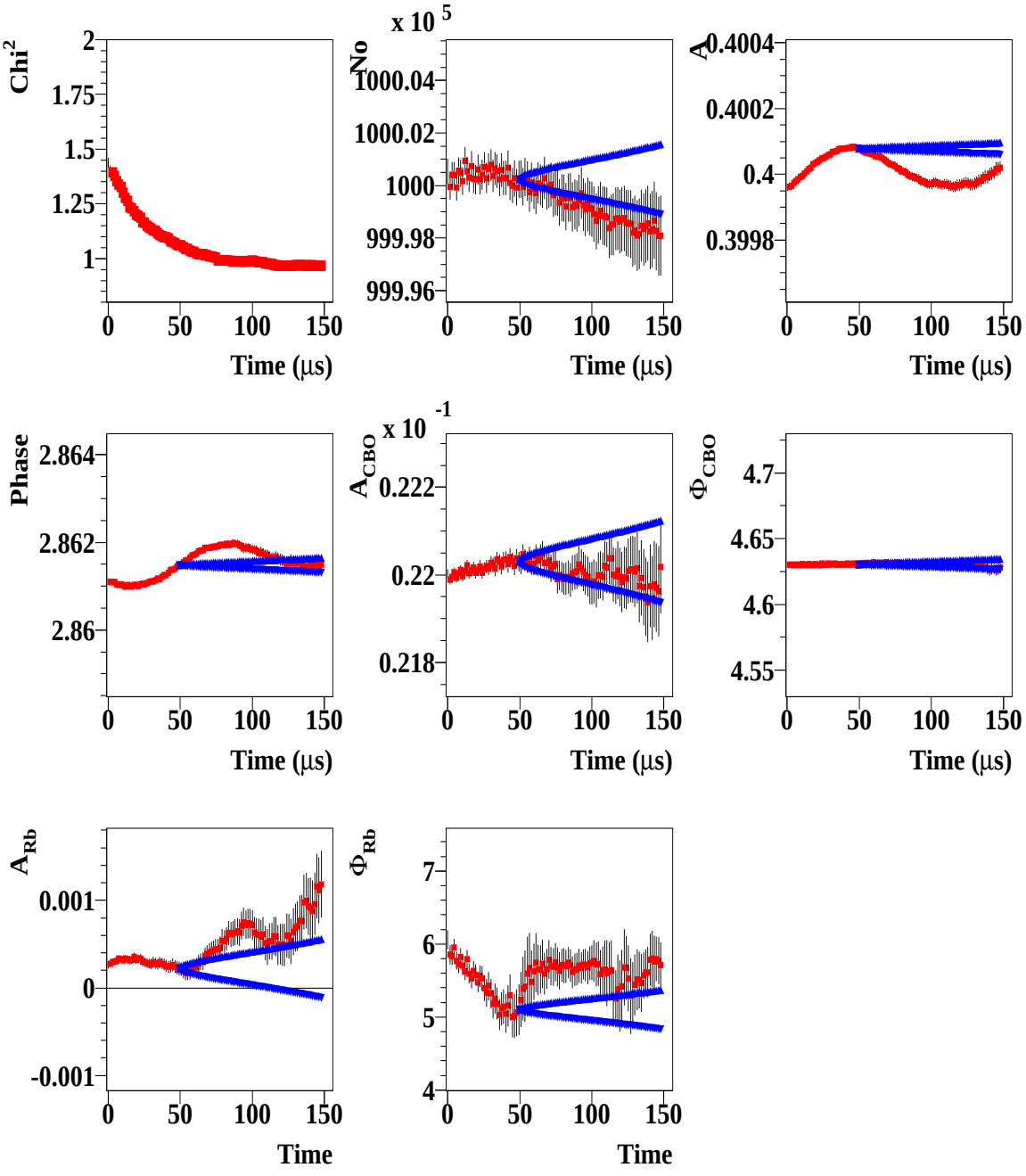

Figure 117 : The parameter stability when g-2 phase modulation was introduced into the MC. For the fit, 1999 functional form including g-2 asymmetry modulation was used.

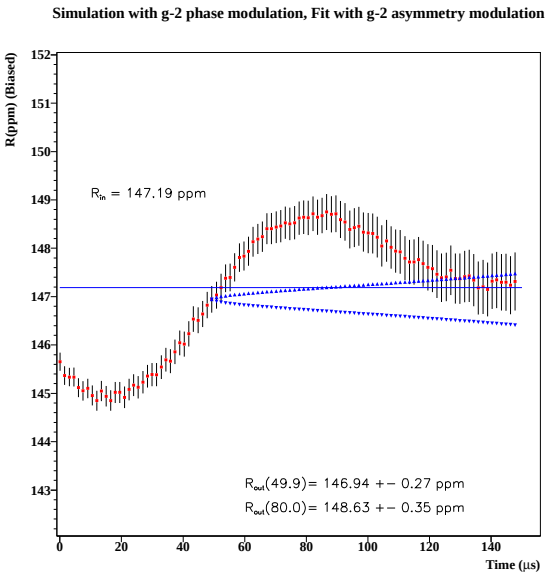

Figure 118 : The stability of R when a MC data, produced with g-2 phase modulation, fitted to the 1999 functional form with g-2 asymmetry modulation. ΔR(49.9μs)=0.25 ppm and maximum deviation from the input value is 1.95 ppm.

Since we now know that g-2 asymmetry modulation can be recovered completely by the 1999 functional form including the systematic due to this part is zero. The g-2 phase modulation is in the simulated data. We don't fit for it. So we should estimate the systematic due to this part. We will do the same thing in the previous study for 1999 form. The generated MC with different phases of the g-2 phase modulation were fitted to the 1999 functional form including the g-2 asymmetry modulation. Figure 119 shows this study. The systematic is slightly less compared to 1999 functional form for this case because 15% of this effect recovered by the g-2 asymmetry modulation itself.

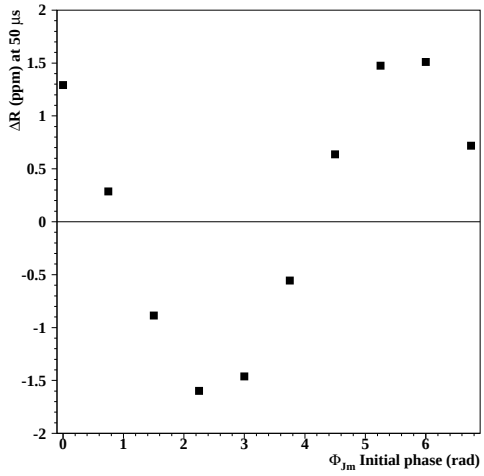

Figure 119 : When the phase of the g-2 phase modulation was changed between zero and 2π, the corresponding change on R value at 50 μ. The fit function is the 1999 function including the g-2 asymmetry modulation.

From this plot we will conclude a conservative **0.26 ppm** systematic error due to not to fit for g-2 phase modulation on the 1999 functional form including the g-2 asymmetry modulation.

The systematics when the complete physics function used for the fits is the next.

Figure 120 shows the parameter stability when both g-2 asymmetry and the phase modulations were introduced into MC and in the fit the complete physics function was used. 100% recovery with the exact input amplitudes in all the parameters are striking. Even though it is ideal case please observe some of the parameters (ϕ_{Rb}) goes outside of the Kawall band. Figure 121 shows the R stability.

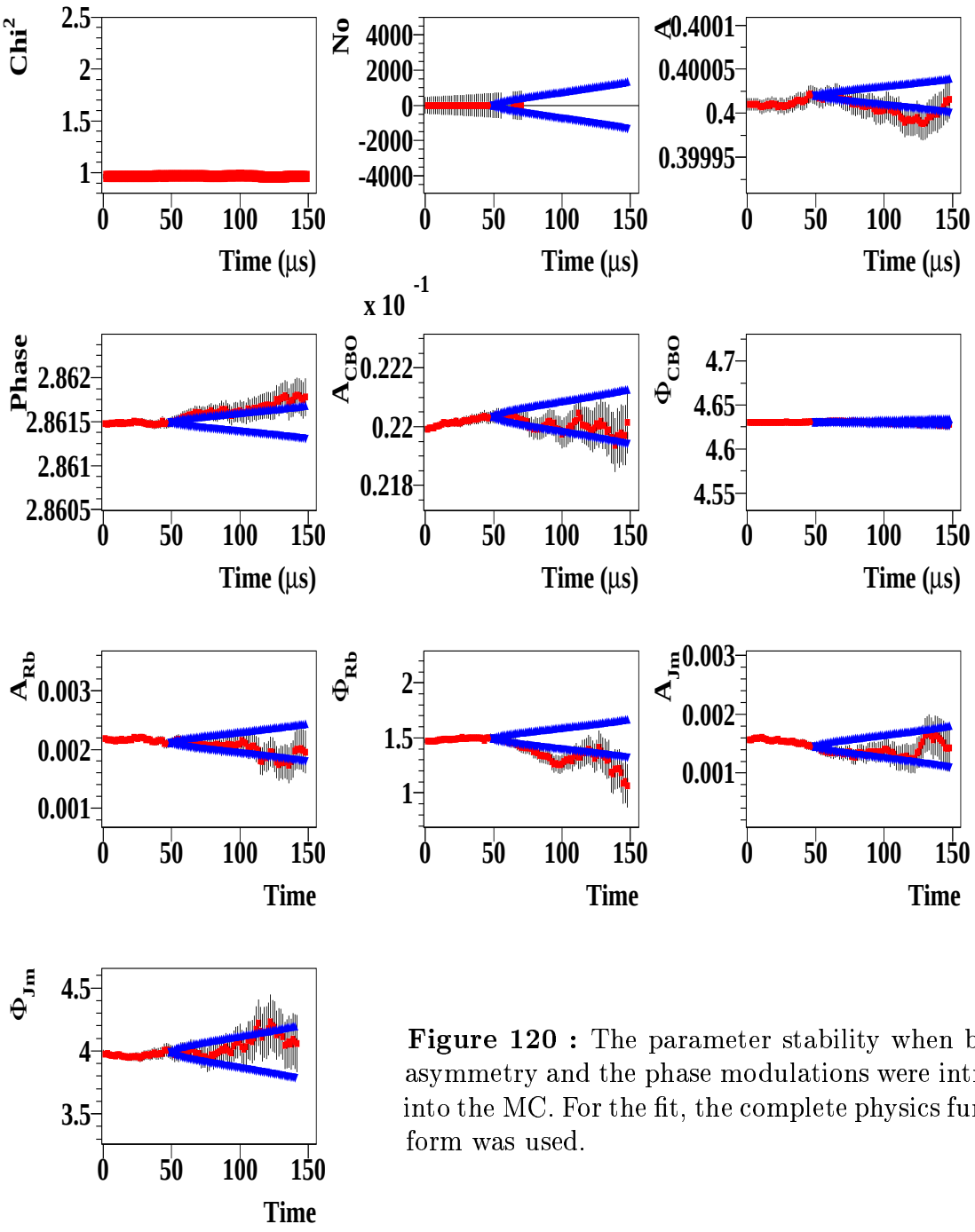

Figure 120 : The parameter stability when both g-2 asymmetry and the phase modulations were introduced into the MC. For the fit, the complete physics functional form was used.

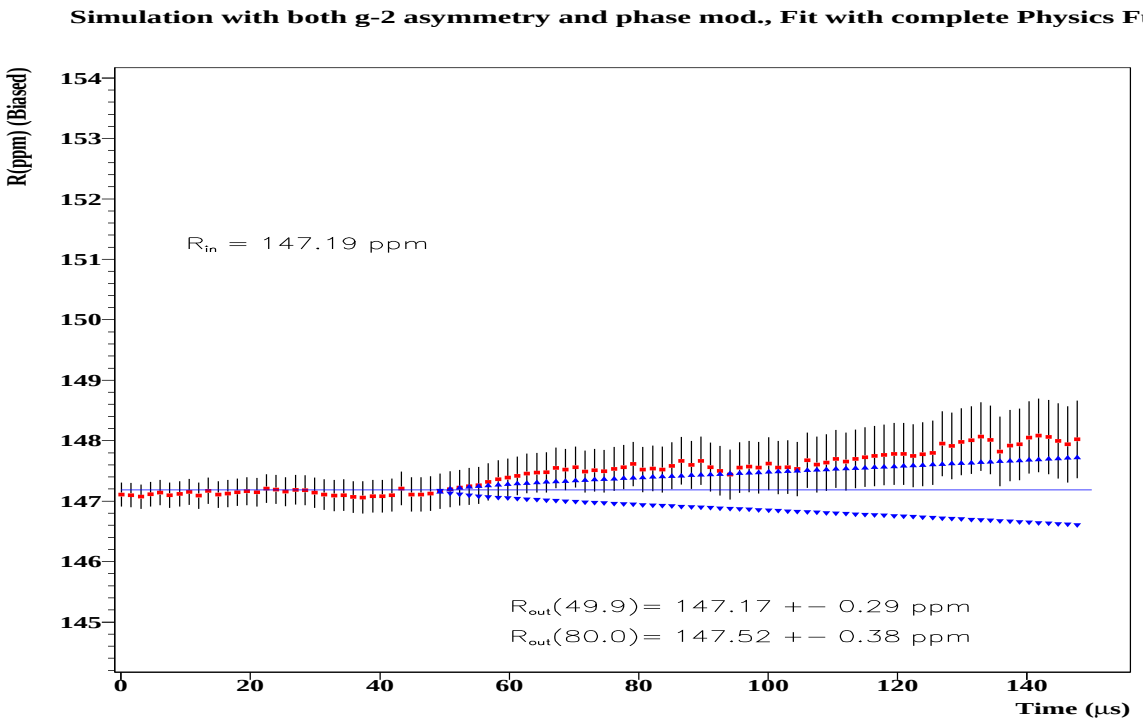

Figure 121 : The stability of R when a MC data, produced with both g-2 phase and asymmetry modulations, fitted with the complete physics form.

Figure 122 shows the parameter stability when only g-2 asymmetry modulation was introduced into MC and the complete physics functional form was used in the fit. It is very encouraging to see that they don't pick up each other. The reason for that explained in detail in reference [**?**]. A_{Rb} recovers exactly what was introduced in the MC for itself. The phase stability of g-2 asymmetry modulation is also good. Figure 123 shows the stability of R in this case.

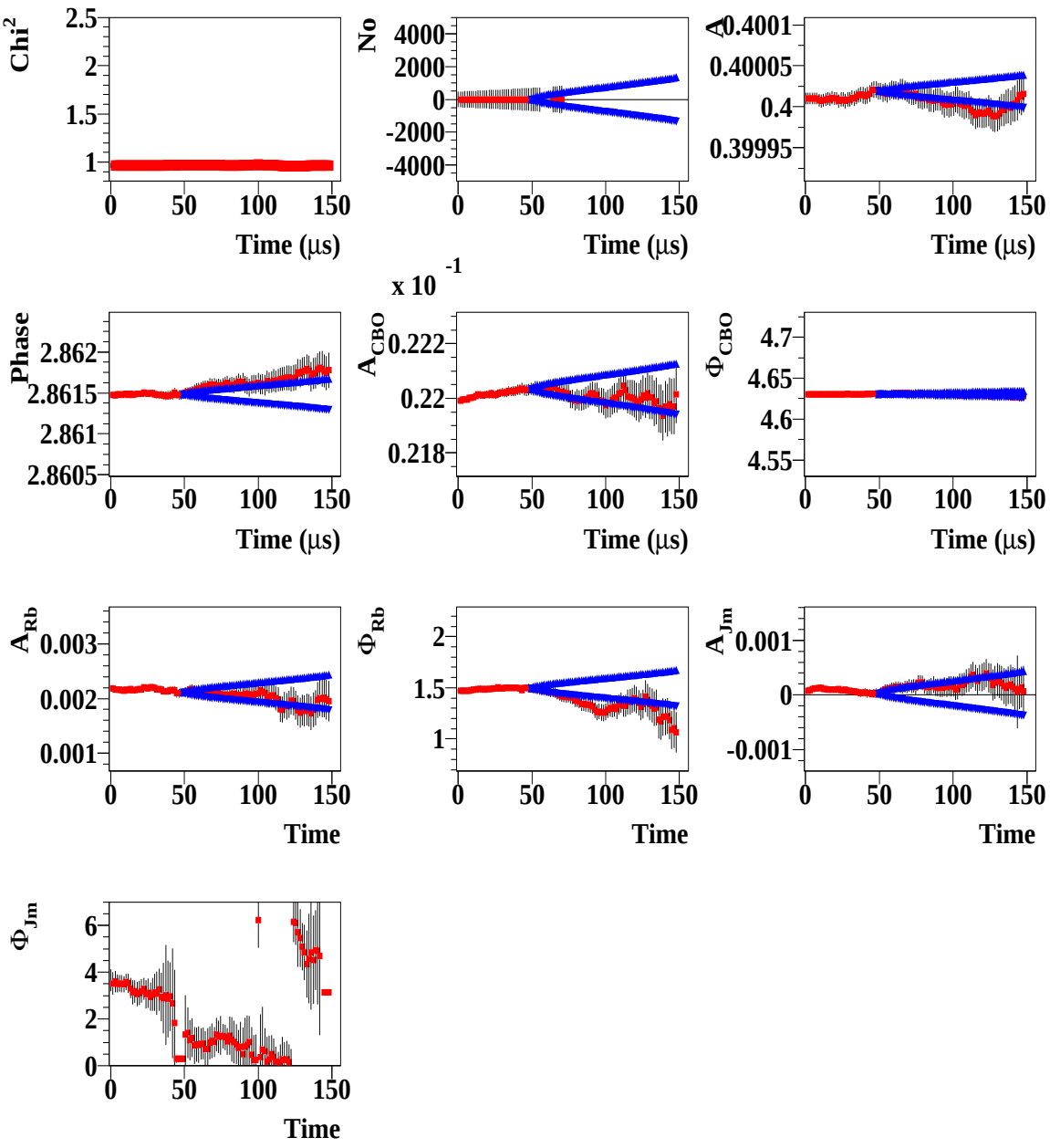

Figure 122 : The parameter stability when only g-2 asymmetry modulation was introduced into the MC. For the fit, the complete physics function was used.

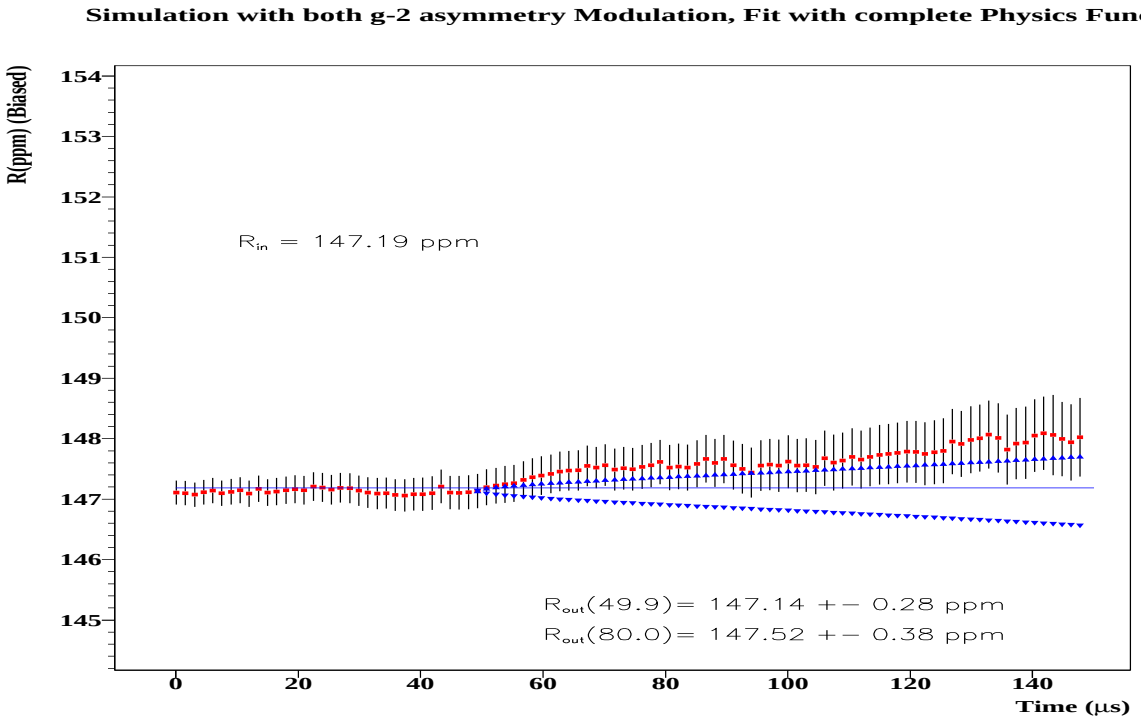

Figure 123 : The stability of R when a MC data, produced with g-2 asymmetry modulation, fitted with the complete physics function.

Figure 124 shows the parameter stability when only g-2 phase modulation was introduced into MC and the complete physics function was used for the fit function. The conclusion from this plot is the same as the previous case. A_{Jm} recovers what was introduced in the MC for itself and stability of g-2 phase modulation parameters are good. Figure 125 shows the stability of R in this case.

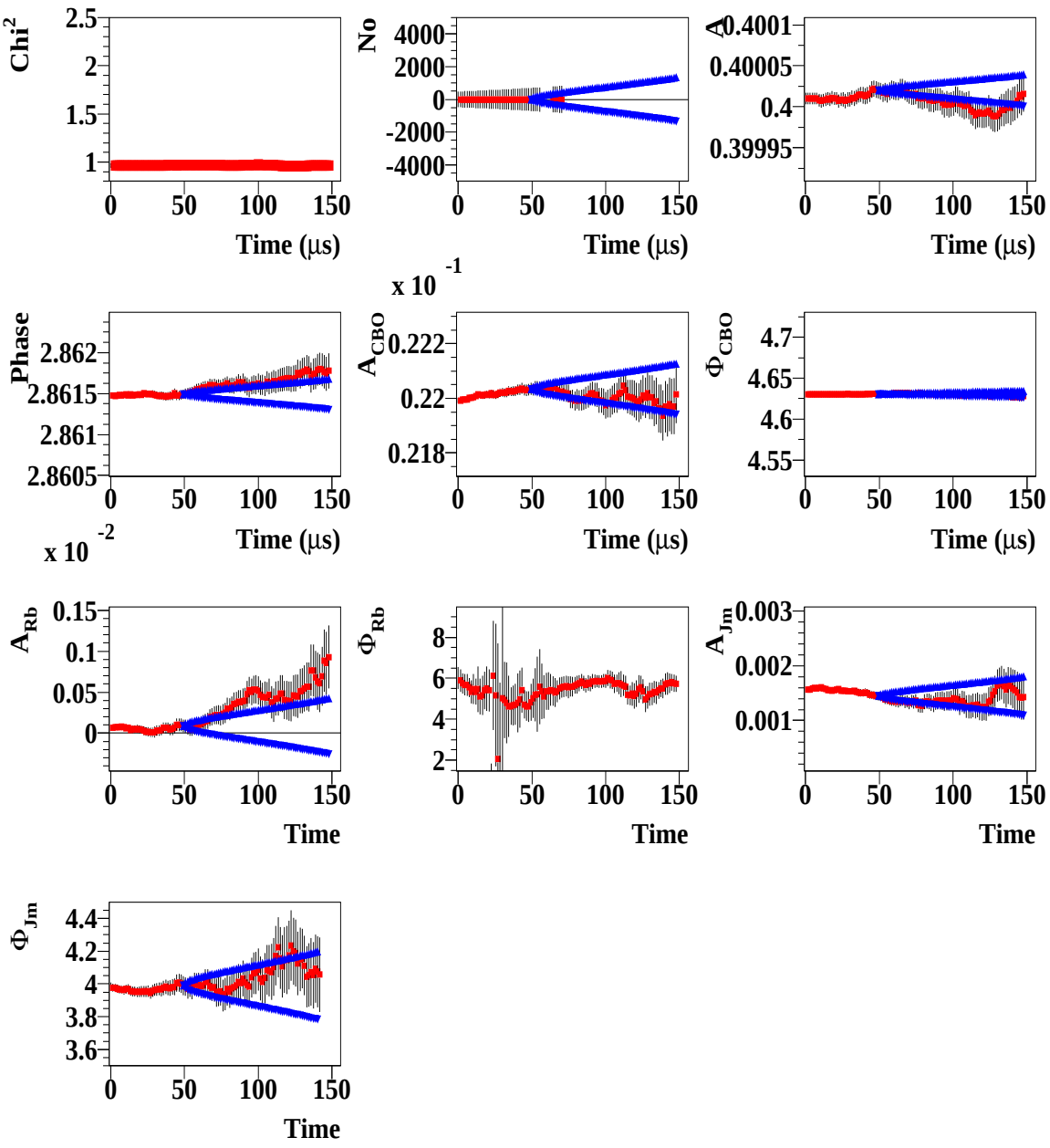

Figure 124 : The parameter stability when only g-2 phase modulation was introduced into the MC. For the fit, the complete physics function was used.

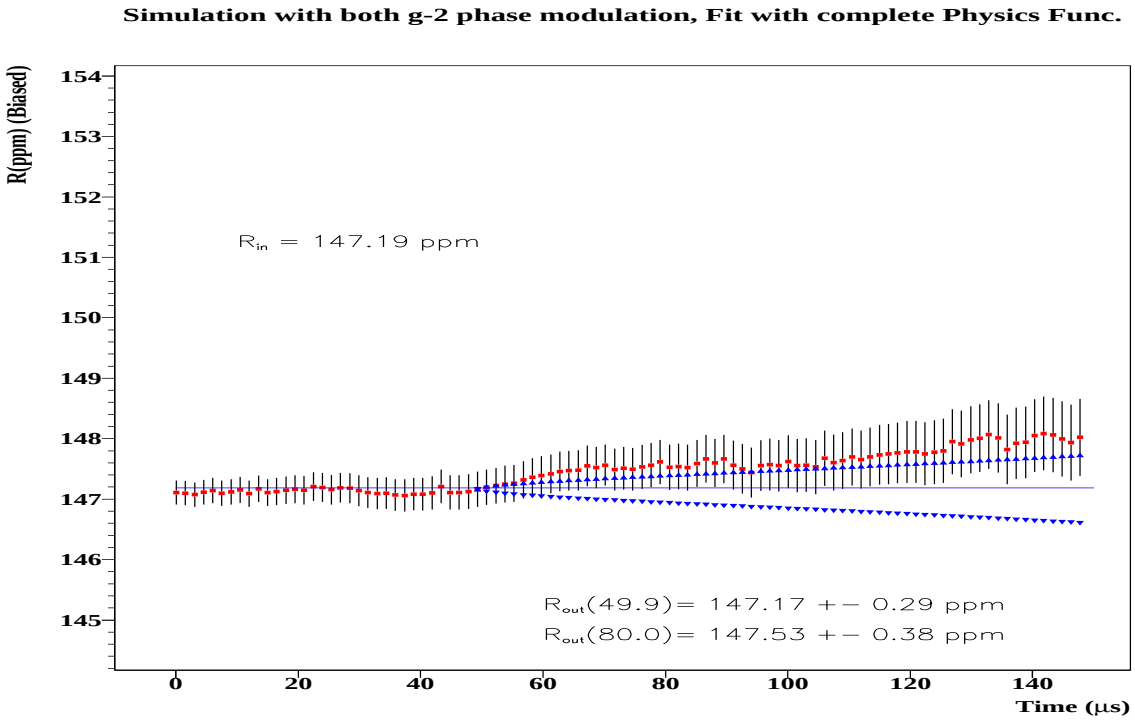

Figure 125 : The stability of R when a MC data, produced with g-2 phase modulation, fitted with the complete physics function.

As a result of this study, we will conclude that the best functional form handles the g-2 asymmetry and the phase modulations is the complete physics function. As expected 1999 functional form is the worst one. Even though one of the effect is not there using the complete physics function does not hurt the R value at all. This is very good because even though it does not remove all the speculations about the amplitude of the g-2 phase modulation, it makes them irrelevant to R. The conservative systematics due to the g-2 asymmetry and the phase modulations are based on the conservative cancellation factor and the conservative phase uncertainty and given in the table below (Table 24).

Table 24: Systematics table due to g-2 asymmetry and phase modulations.

	1999 Form	1999 Form with g-2 Asymmetry Mod.	The Complete Physics Form
σ R	0.34 ppm and 0.30 ppm	0.26 ppm	0 ppm

7.3 Muon Losses and Gaussian Residual Background Correction

Chris and John were provided the muon losses functional form for the 2000 data. Basically after the radial field was changed the muon losses were reduced by order of magnitude.

Hence when the data was combined the losses mostly determined from the data before the radial field was changed. In this analysis integrated average muon losses L(t) was used (Figure 126) with a normalization $A_{\mu L}$.

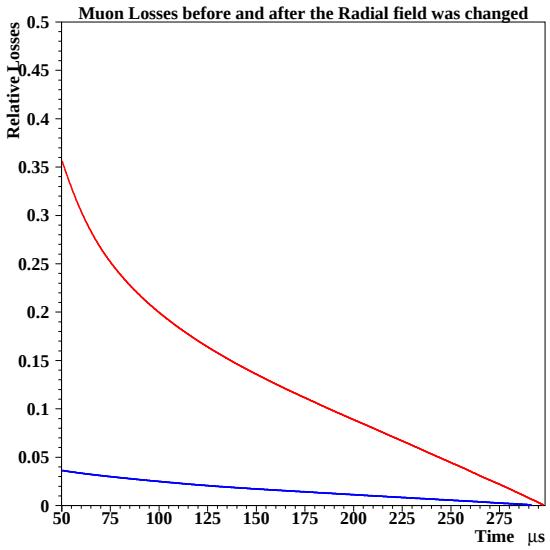

Figure 126 : Relative integrated muon losses before (red) and after (blue) the radial field was changed.

The muon losses before and after the radial field changed were determined from the integration of the original three fold coincidence time spectrum (accidentals subtracted but not loss protons corrected) as follows;

$$L(t_j) \;=\; \int_{t=t_j}^{300} \ell(t)\; e^{t/64.4}\; dt \tag{17}$$

where $0 < t_j < 300\mu$s. Here ℓ is the original coincidence time spectrum and L is the losses function used in the fits. Exponential factor is necessary to compensate the influence of the muon decay on the number of loss muons.

The muon losses functional form is very close to the reality. The first signature was a significant improvement on fit χ^2 after including muon losses into the fits. However small deviations from the shape can increase the χ^2 significantly. To test the accuracy of the muon losses provided by Chris, I used a simple comparison method. The clean detectors with no residual slow effect were added together. These detectors are 1, 10, 17 and 24. In reality detector 17 has a very small residual slow amplitude. However I decided to put it into this group to increase the statistics. The time spectra is fitted to the traditional 1999 functional form at 47μs without muon losses and residual slow term. After the parameters were determined the time spectrum is fitted after 300 μs, where all the slow effects vanish, by fixing all the parameters to the values determined at 47μs

except the acceptance related N_0. Then the DATA/FIT was constructed. Figure 127 shows this study for the data rebinned with g-2 period. The same data was also fitted with Chris's muon losses with the normalization factor $A_{\mu L}$ at 47 μs. The red line shows the $1 + A_{\mu L}\ L(t)$ acceptance term due to the lost muons. The agreement between the data and experimentally determined losses is excellent (at least for these detectors).

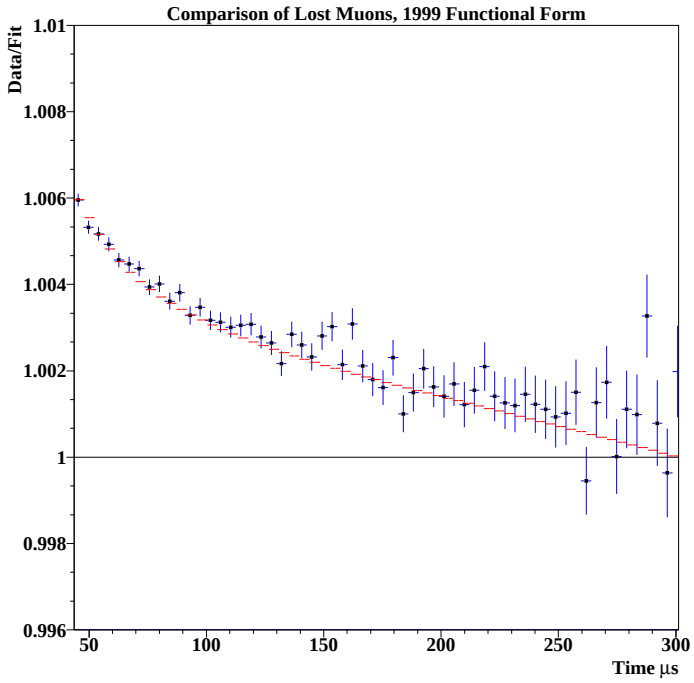

Figure 127 : Comparison of muon losses obtained from the data (blue) and Chris (red). This study was repeated with other functional forms but there is no difference observed.

Since the lost muon functional form is very well agreed with the data, where this residual slow term comes from? When the muon losses were included into the fits the χ^2 reduced from 1.3 to 0.99 for these detectors mentioned above. The correct shape provides acceptable χ^2. However from the early stages of this analysis it was observed that an additional residual slow term component was necessary to achieve an acceptable χ^2. The best parameter stability was obtained with a residual slow function, a Gaussian with $\approx$100 μs lifetime. Figure 128 shows the similar study for the first half detectors. Residual slow term including the muon losses $(1 + \epsilon(t) = (A_{\mu L}\ L(t) + A_r\ e^{-\frac{1}{2}(\frac{t}{\tau_r})^2}))$ is also showed. Obviously only the muon losses itself would not give a good χ^2 and acceptable fit results.

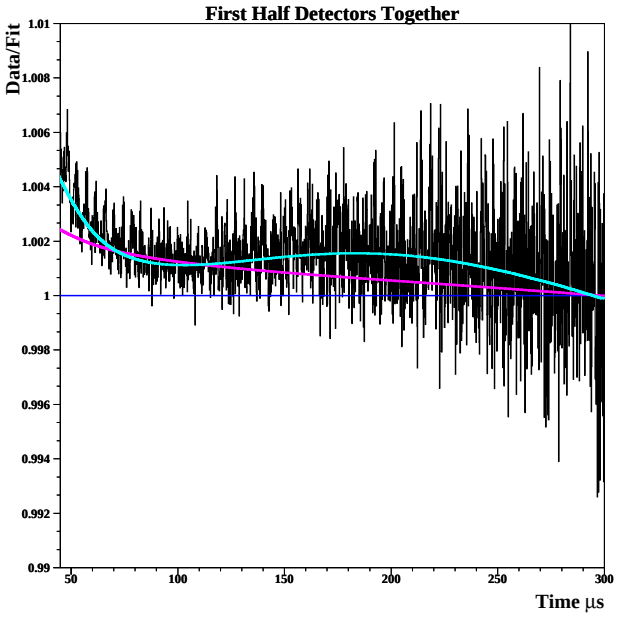

Figure 128 : Residual data (Data/Fit), only acceptance term due to the losses (purple) and after including the residual slow term (turquoise). The fit was performed with 99 functional form.

Figure 129 shows the second half. The second half is much better compared to the first half. On the other hand we still need the Gaussian residual slow term to have better χ^2.

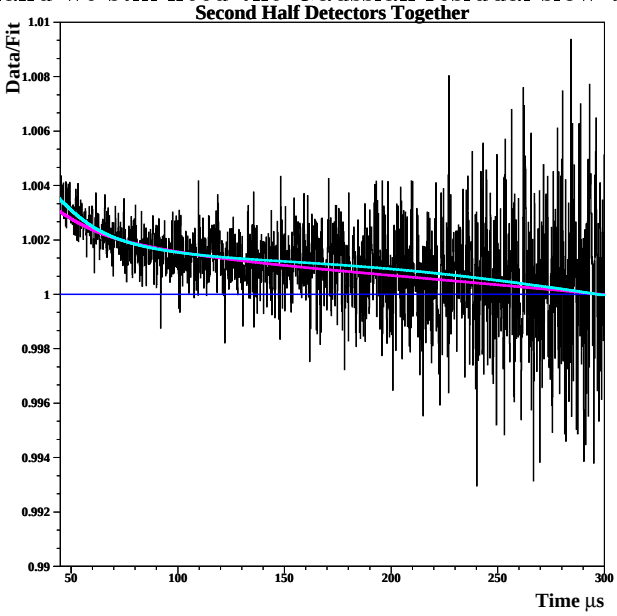

Figure 129 : Residual data (Data/Fit), only acceptance term due to losses (purple) and after including the residual slow term (turquoise) for the second half detectors. The difference between the first and the second half is significant.
On the other hand the gain stability is very different in both halves. Between the first

and the second halves there is a large gain difference which automatically reflects into the amplitude of the Gaussian term. On the other hand the lifetime of the Gaussian term is in both half around 100 μs eventhough the amplitudes are very different?

When the detectors are combined the situation becomes like in Figure 130.

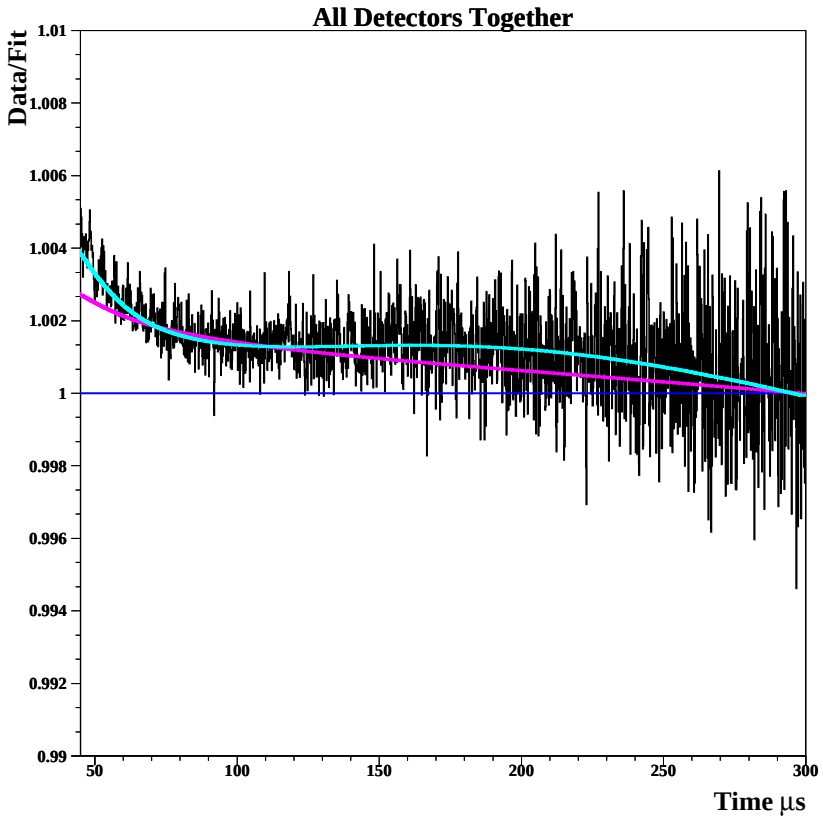

Figure 130 : Residual data (Data/Fit), only acceptance term due to losses (purple) and after including the residual background (turquoise) for all the detectors.

7.3.1 Systematics Due to Muon Losses and Residual Slow Effect

The previous study shows muon losses are quite precise compared with the data. However we will assume 10% uncertainity on the losses due to the lost proton contribution as Chris pointed out. A simulated MC data generated with the realistic muon losses (from the data) were fitted without the muon losses to determine the systematic effect on R. To test the dependence of the shape, the regular losses functional form obtained from the real data (Figure 130, purple) and also including the residual background (Figure 130, turquoise) were embedded into the MC respectively. Then MC data were fitted without any loss or residual background terms. Figure 131 shows the parameter stability when the losses functional form is like experimental losses and Figure 132 shows the same when

the losses functional form is like the complete ϵ term.
Here 99 type functional form was used.

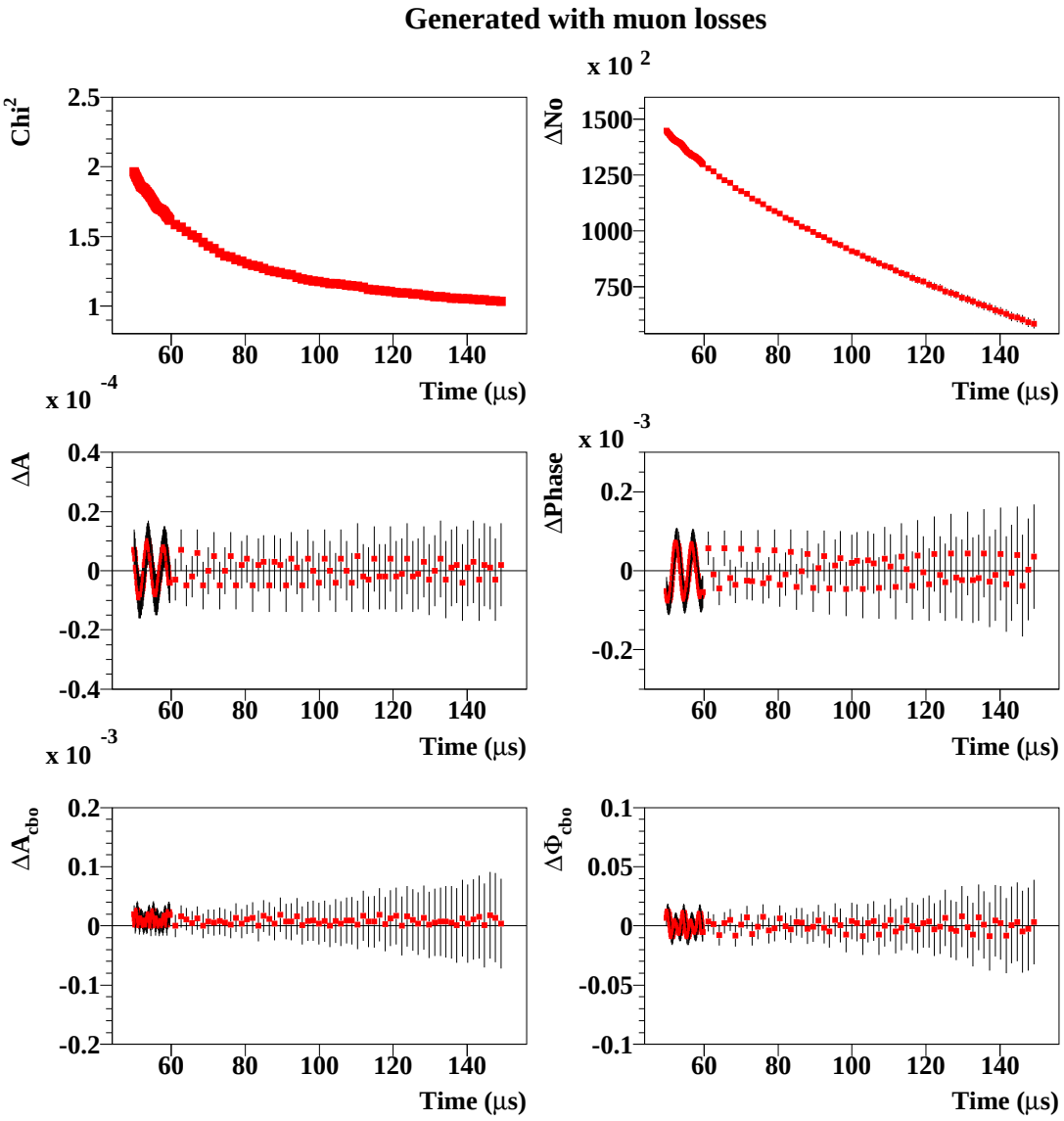

Figure 131 : The MC data was generated with losses and fitted without losses. The size and the shape of the losses were taken from Figure 130 (purple).

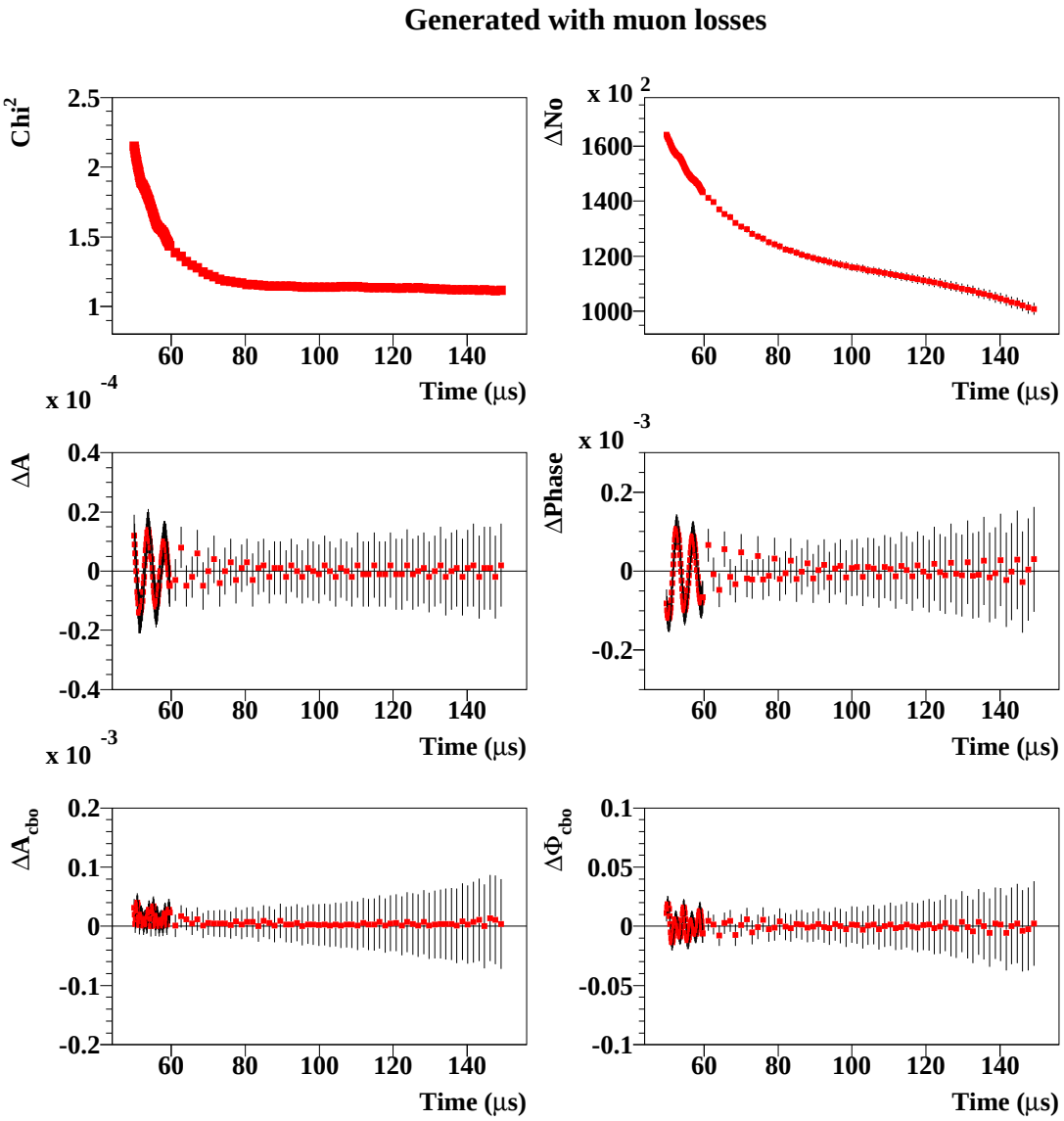

Figure 132 : The MC data was generated with losses plus residual background fitted without losses. The size and the shape of the losses were taken from Figure 130 (turquoise).

Figure 133 and 134 show the stability of R vs start of fit time. As one can see from the plots, lost muons cause phase pulling on R just like the gain effect. The magnitude of the phase pulling is different for two lost muon spectral shapes. This is however mostly due to the input amplitude of muon losses to MC as one sees in Figure 130. It is also strange to see that the phase pulling dies much later in the pure loss functional form.

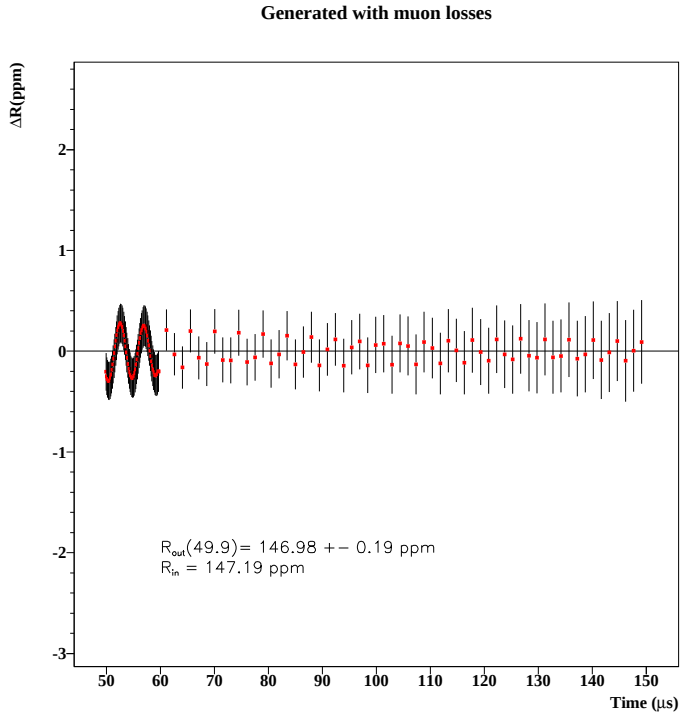

Figure 133 : Systematic due to muon losses for pure loss functional form (Figure 130, purple).

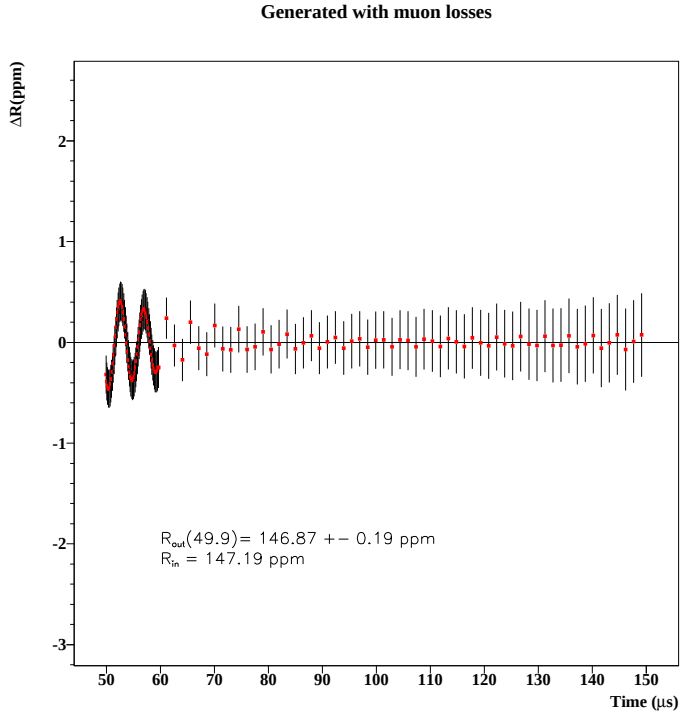

Figure 134 : Systematic due to muon losses for loss functional form including Gaussian residual background (Figure 130, turquoise).

This study repeated also for the other type of functional forms and found to be a small dependence on the functional form for the systematic on R. Table 25 gives the comparison of the results for different functional forms in case we have the muon losses and residual background and we don't fit for them. For that reason these numbers should divided to 10 for 10% uncertainity on residual background and muon losses.

Table 25: Comparison of the systematics due to residual background and muon losses on R in case we don't fit for them. I: 1999 functional form, II: Including the asymmetry modulation to I, III: the complete physics function.

	I	II	III
Only Losses			
Max. peak to peak	0.58 ppm	0.60 ppm	0.63 ppm
@ 50 μs	0.21 ppm	0.29 ppm	0.33 ppm
Losses+Residual Background			
Max. peak to peak	0.87 ppm	0.93 ppm	0.97 ppm
@ 50 μs	0.32 ppm	0.45 ppm	0.33 ppm

To be conservative again we will take 10% of the maximum half peak to peak distances as a systematic error. Hence we assign **0.04** ppm for 1999 functional form, **0.05** ppm for 1999 functional form including g-2 asymmetry modulation and for the complete physics functional form.

8 Final Systematic Table and the Result

The final systematic table is given below for three functional forms we are dealing with in this analysis. I included another 0.1 ppm systematic for the flashlets which I am not going to do that rather I will copy it from Fred's writeup. I is the 1999 functional form, II is 1999 functional form including the g-2 asymmetry modulation, III is the complete physics form.

Table 26: Systematics Table

Effect		Systematics on R (ppm)		
		I	II	III
Quad Voltage Droop		0.01	0.02	0.05
Combination of different n values		0.03	0.04	0.04
Leftover CBO		0.05	0.05	0.05
DCBO and VW		0.01	0.01	0.01
Energy Scale		0.04	0.18	0.37
Bin Width		0.07	0.07	0.07
Pileup (seen)		0.02	0.02	0.07
Pileup (unseen)		0.08	0.08	0.05
Randomization		0.02	0.02	0.02
Muon Losses &				
Residual Slow Effect		0.04	0.05	0.05
Half Ring Effect	Rb	0.34	-	-
	Jm	0.30	0.26	-
Uncertainty on the				
Functional Form		-	0.02	0.29
Others		0.10	0.10	0.10
TOTAL		0.48	0.36	0.50

I will give my final number with the 1999 functional form including the g-2 asymmetry modulation. There are three main systematics relevant to the result R. These are the systematics due to the gain, the half ring effect and the uncertainty on the envelope. Comparing these systematics, this functional form is the best. Not only the systematics but also the way this functional form handles the R vs detectors is also satisfying. The quality of χ^2 on R vs detector for this functional form is 29.33/21 and better than our 1999 result. My final R value is 147.27$\pm$ including 0.64 ppm statistical and 0.36 ppm systematic error. Figure 135 shows R vs fit start time for this functional form.

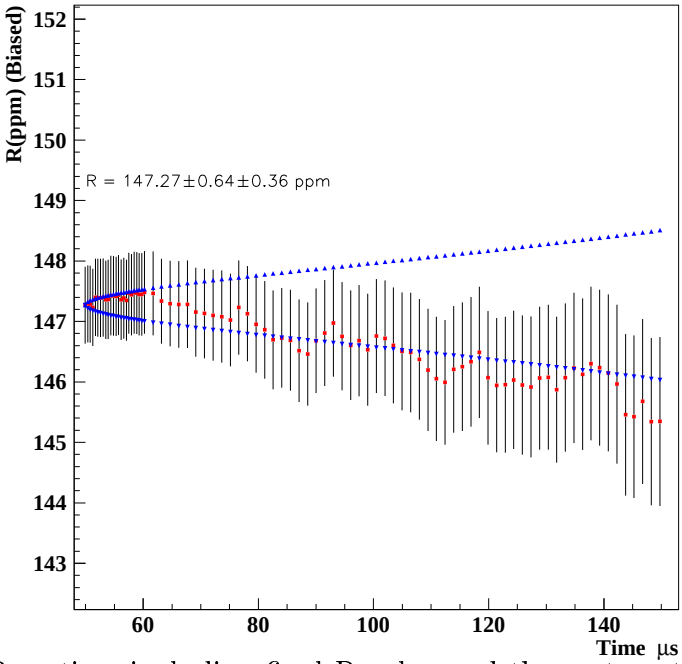

Figure 135 : R vs time including final R value and the systematics.

9 A New Method : Jumping Windows

This method was introduced to the collaboration by Yuri Orlov. This methods is based on splitting the data into the subsets such a way that CBO and related effects cancels. This is possible by strobing the data every time where the time difference between the consecutive sampling poins are equal to the CBO period. For 465.7 kHz CBO frequency this period is 2.147 μs. In order to be able to do this study, the time spectrum has to be properly binned with T_{bin} to make number of subsets integer as $n = \frac{T_{cbo}}{T_{bin}}$. For that reason the data was binned with 153.379 ns to have 14 subsets. Figure 136 shows this procedure schematically.

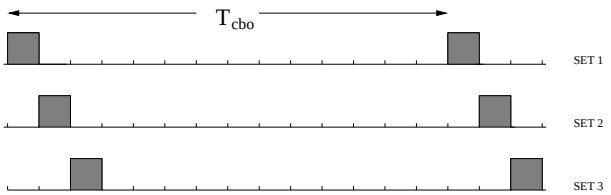

Figure 136 : Strobing of data according to jumping windows method.

Figure 137 shows one of the subsets constructed for Jumping windows study from the data.

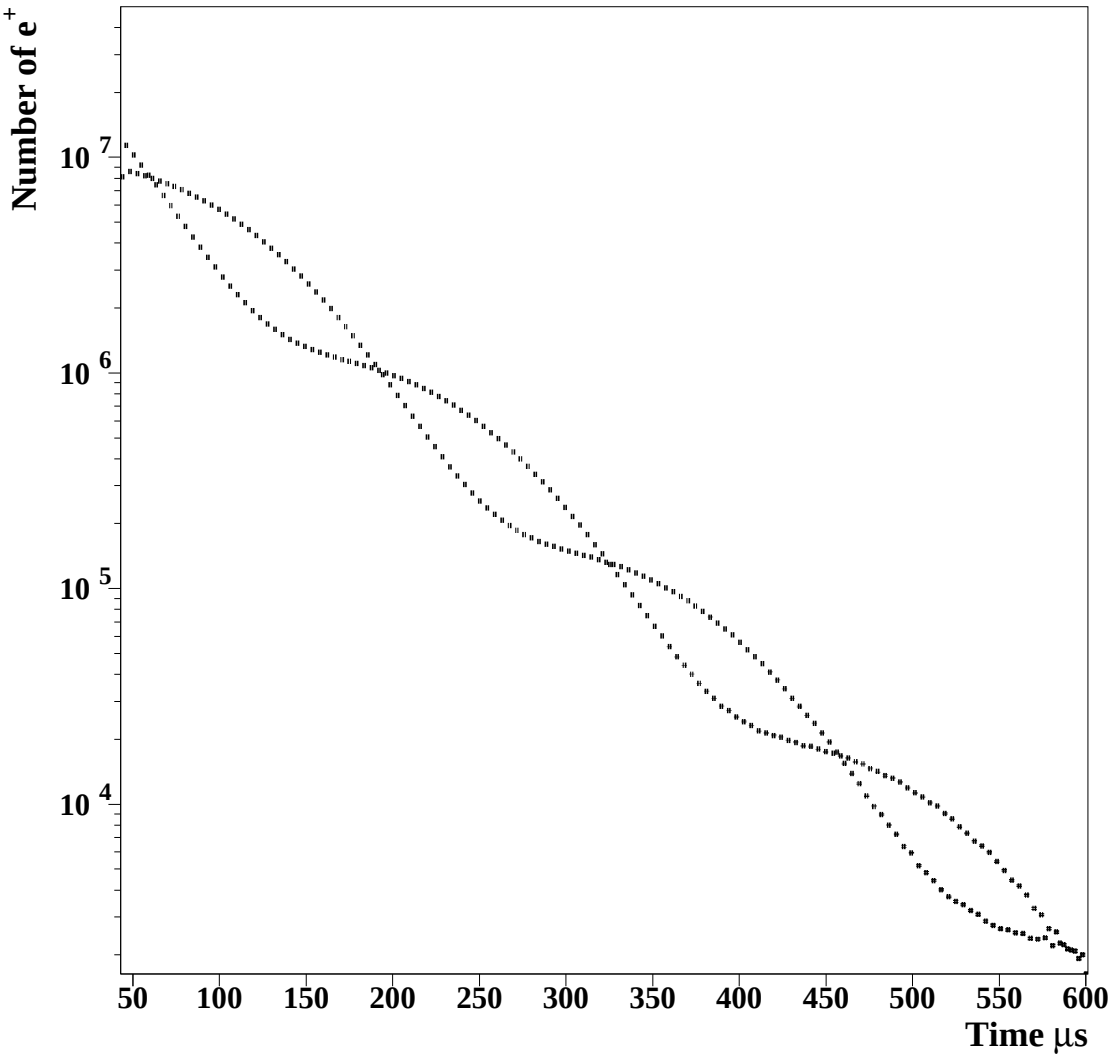

Figure 137 : One of the sets constructed for the Jumping Windows method.
This method was studied with 10 randoms seeds like the other methods. 22 detectors for 14 subsets from 10 random number seeds were fitted to ordinary 5 parameter function including the muon losses and the slow residual component with the following functional form :

$$F(t) = N_0 e^{-t/\tau_\mu} \ [\ 1 \ + \ A \ cos(\ 2\pi f_a t \ + \ \phi_a\ )\ ] \ \left[\ 1 + \ A_l \ L(t) \ + \ A_r \ e^{-\frac{1}{2}(\frac{t}{\tau_r})^2}\ \right] \quad (18)$$

The lifetime of the slow component term were exported from the conventional fit results since the fit for the jumping windows had some difficulties on determining the τ_r lifetime especially for some sets. In any case the fits were also performed with the floating τ_r

lifetime for jumping windows and there was no difference observed on the R value in both cases. However to have stable fits and the same slow component lifetime between the sets, I preferred to fix the τ_r lifetime to the values obtained from the conventional fit results. The fit results from each random number seeds were averaged. The random seed averaged subsets were also averaged taking into account their statistical power. The resultant R values were at given at 50.46 μs which is the average time between the 14 sets for individual detectors on Figure 138.

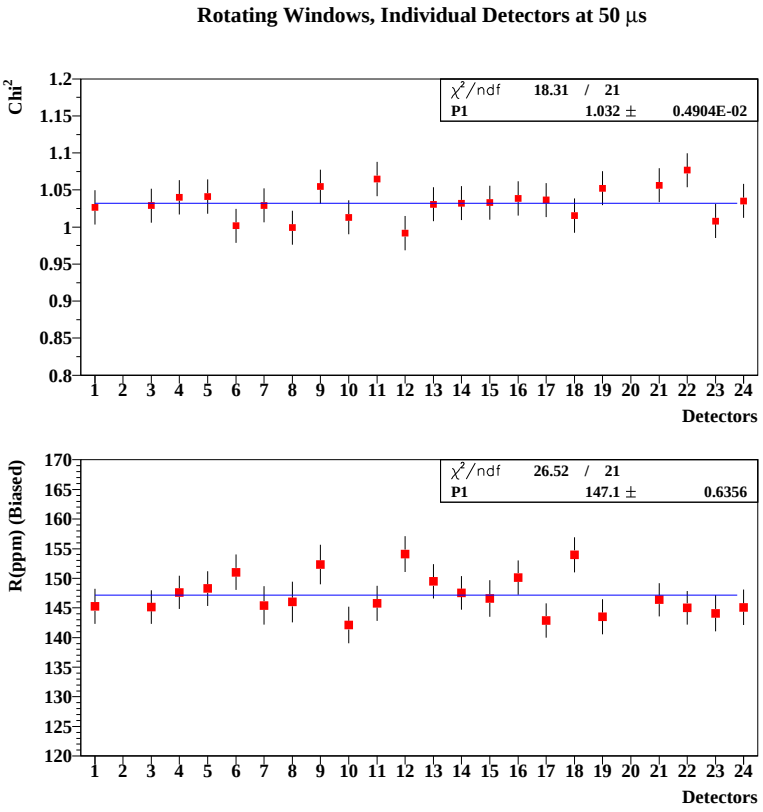

Figure 138 : R vs detectors at 50 μs for Jumping Windows. The average of the 10 random number seeds and error weighted average of the sets were taken.

Most of the systematics were studied by Yannis for this method from mostly Monte Carlo simulations [15]. However we preferred to study the influence of the gain on this method from the real data.

Figure 139 shows the parameter stability when the first half detectors were put together. The muon losses and the parameters for the slow residual effect were determined at the very first point of the fit and they were fixed (both the amplitude and the lifetime) all the time to those values determined.

Figure 140 shows the same for the second half detectors.

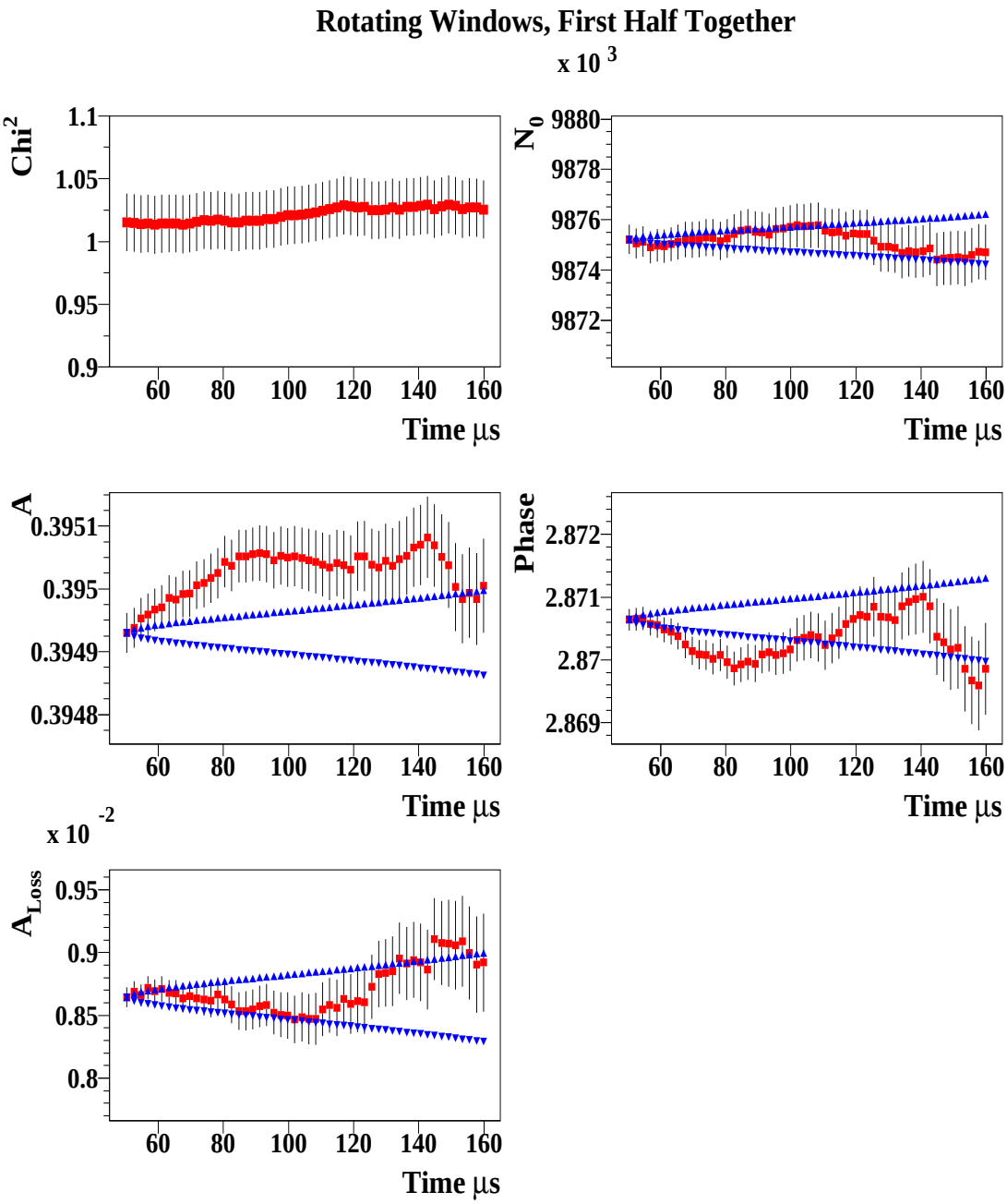

Figure 139 : Parameter stability for the first half on Jumping Windows method.

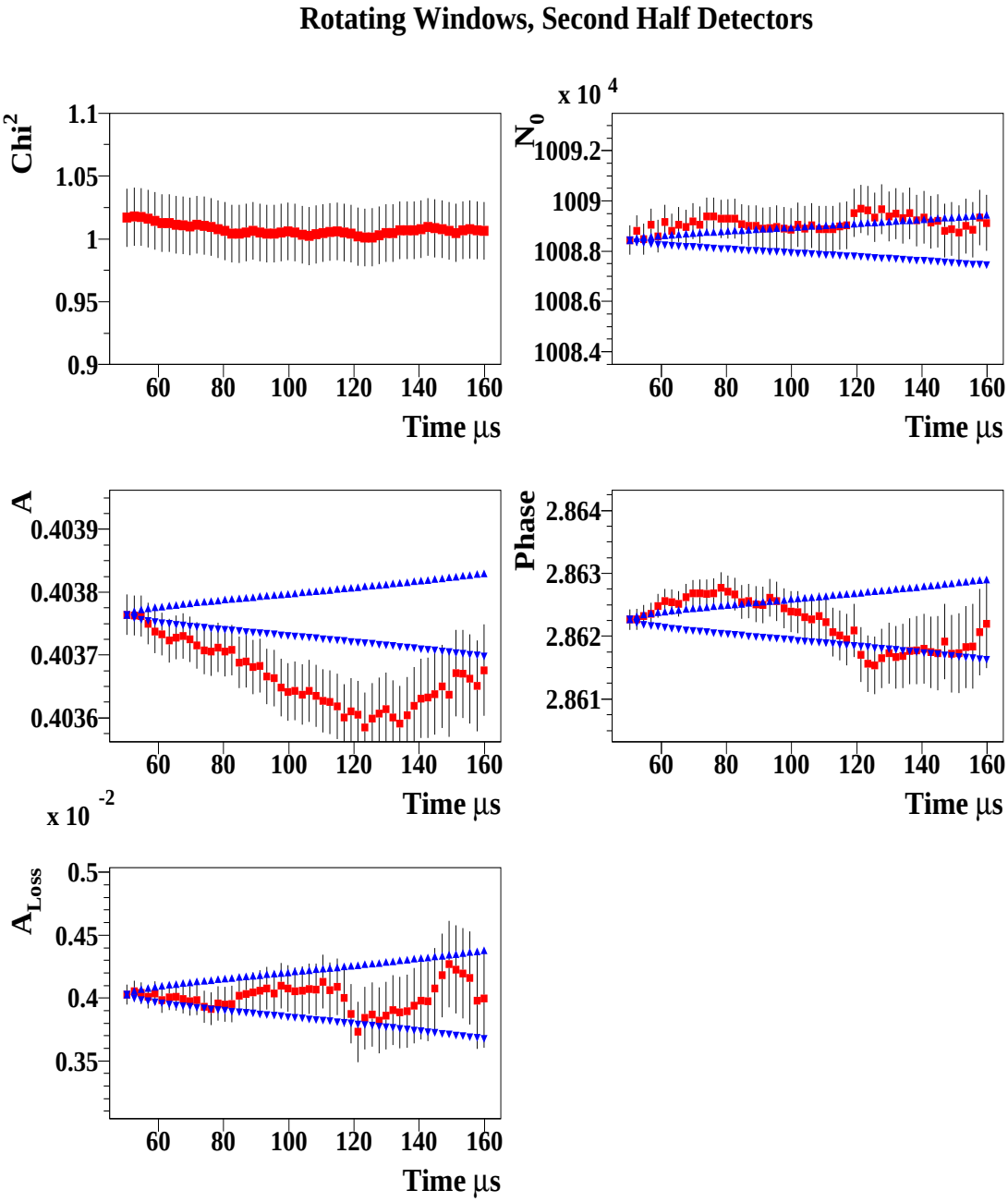

Figure 140 : Parameter stability for the second half on Jumping Windows method. Figures 141 and 142 show the stability of R in the first and in the second halves.

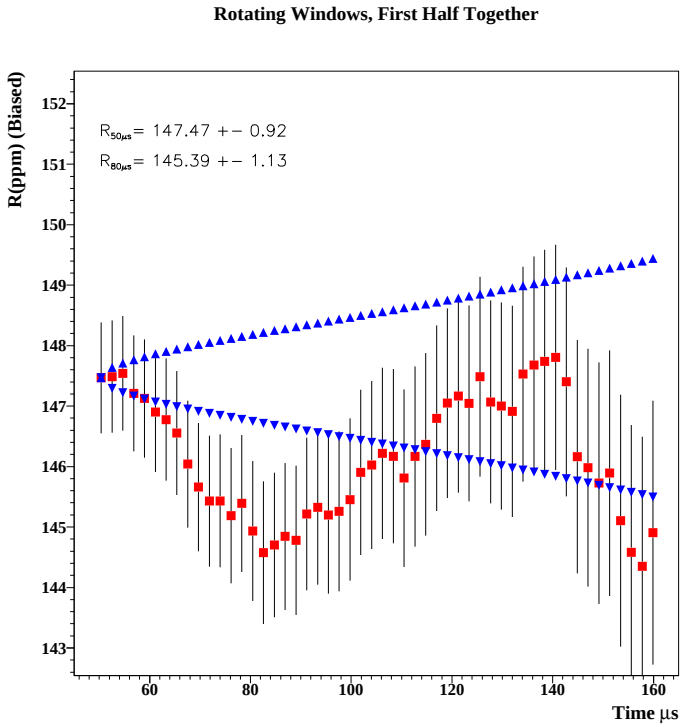

Figure 141 : R vs time for the first half.

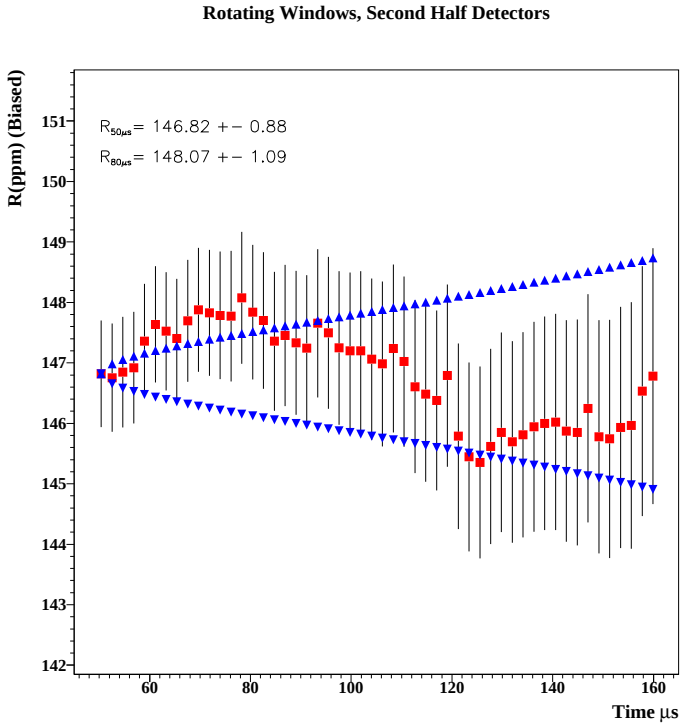

Figure 142 : R vs time for the second half.

Figures 143 and 144 shows the parameter stability when all the detectors were put together.

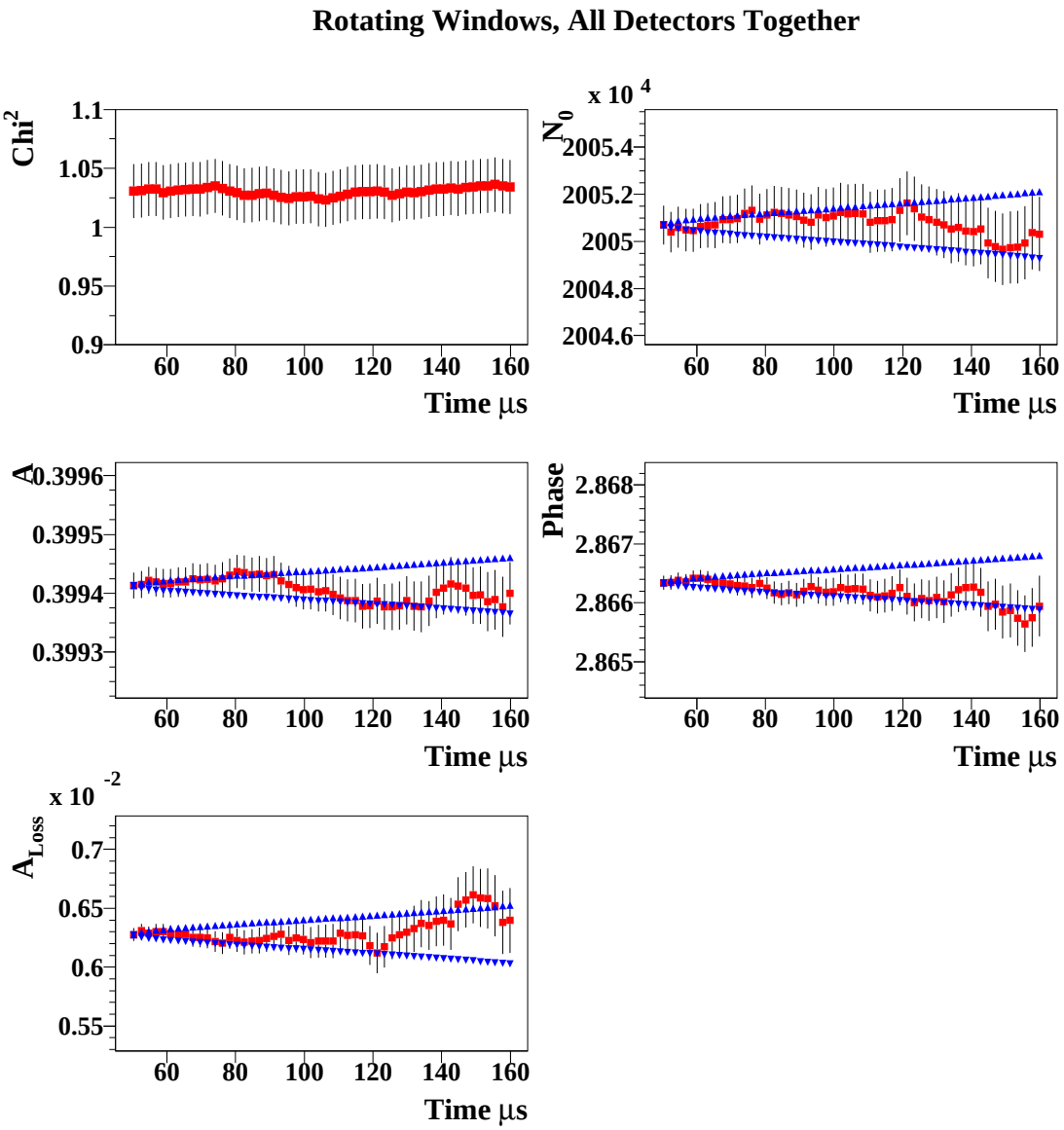

Figure 143 : Parameter stability when all the detectors together for Jumping Windows method.

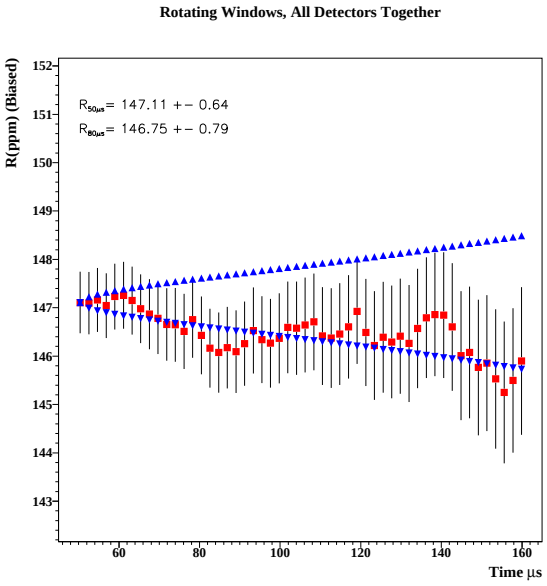

Figure 144 : The stability of R when all the detectors together for Jumping Windows method.

By looking at these results we can conclude that this method gives slightly better quality on fit parameter stability compared to 1999 functional form. The average R value from the individual detectors is amazingly close to the one from the 1999 functional form. For the 1999 functional form R is 147.18 ppm and for this method it is 147.15 ppm at 50 μs. This is extremely important to show that a completely different approaches (probably the systematic influences are also very much different from each other) gave the same result for R value. The half ring effect is reduced but not gone completely. The reason for that is the decay of the half ring effect. The table below gives the comparison of the R value differences between 50 and 80 μs for 1999 and Jumping Windows methods.

Table 27: Comparison of R value differences between 50 and 80 μs for 1999 and Jumping Windows method.

	1999 Form	Jumping Windows
First Half	3.06 ppm	2.08 ppm
Second Half	2.97 ppm	1.25 ppm
Altogether	0.10 ppm	0.36 ppm

As one notices since the size of the half ring effect is close between two halves, cancellation becomes almost becomes almost perfect when the two halves are combined for 1999 functional form. On the other hand for Jumping Windows, the half ring effect becomes unequal in both halves makes the cancellation non-perfect but still very good and acceptable.

As we pointed out before, most of the systematics were studied by Yannis for this method from the simulations. However the influence of the gain changes on R is important to know from the data itself. This is one of the most important systematic we have this year. To do this, the similar procedure is applied for the conventional method described in the section 6.4. was followed. Figure 145 shows the comparison of some fit parameters between the artificially gain enhanced data and the regular data with Jumping windows method. Figure 146 shows the same for R.

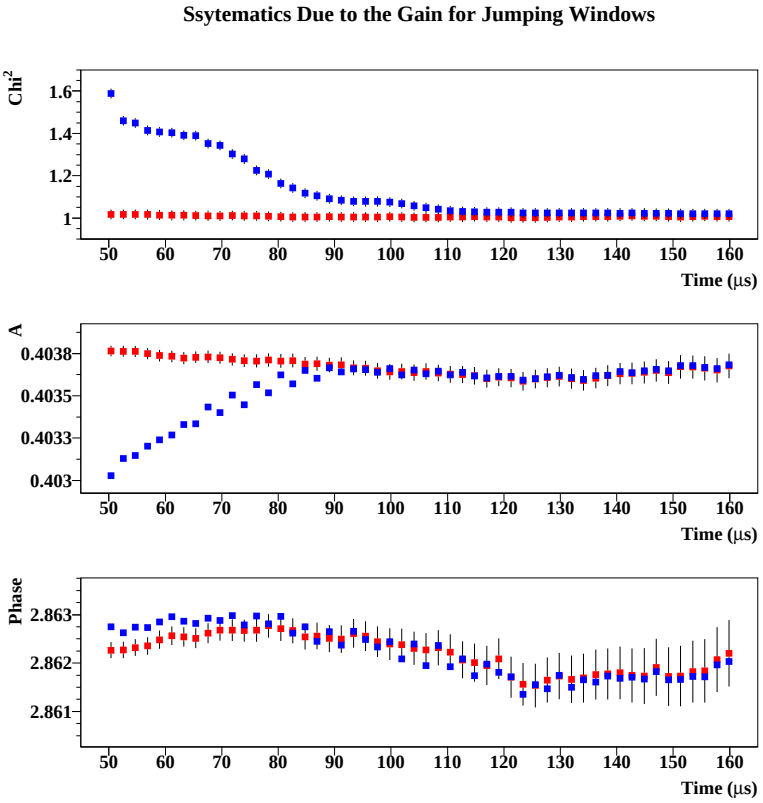

Figure 145 : Comparison of some fit parameters between artificially gain enhanced data and the regular data for Jumping Windows method.

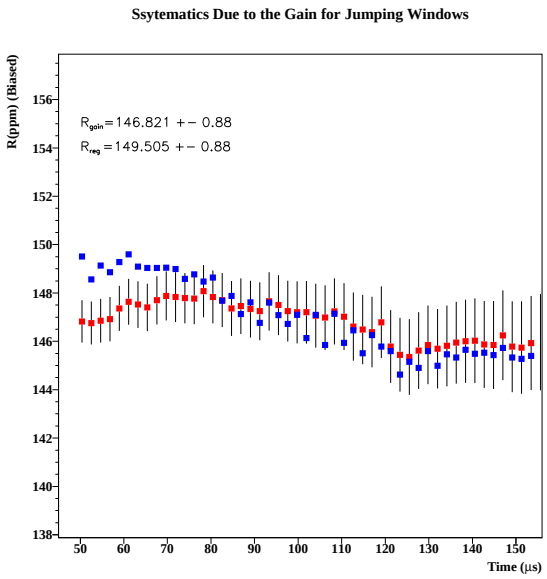

Figure 146 : R value comparison between artificially gain enhanced data and the regular data for Jumping Windows method.

The largest deviation between the gain enhanced data and the regular data is in the first point. The difference is 2.68 ppm. This artificial enhanced gain is 12.6 times larger than the observed gain from the data. For that reason the systematic due to the gain for this functional form is **0.21 ppm.**

This method is more sensitive to the gain effect than the 1999 functional form. 1999 functional form and this method have different sensitivity to the different systematics. However it is very important to have the same result for R from a completely different approach. For that reason this method is boosted up our confidency with our R value.

10 Acknowledgment

I would like to thank to the all the g-2 people who made contributions to my work. Especially the Senior people who support me with their strong letters to obtain my 01 visa like Vernon Hughes, Yuri Orlov, Francis Farley, Lee Roberts, Bill Morse Jim Miller, Gerry Bunce and Yannis Semertzidis. If it wasn't Brenda Kirk's extraordinary work I wouldn't be here and doing this 2000 g-2 ω_a analysis.

Special thanks to Vanya Logashenko not only for the energy dependent dead time and Logashenko coefficients prodives us better pileup subtraction but also for his helps and constructive criticisms in every steps of my analysis. Thanks to Ofer and Ernst for providing us stable and smooth computer power and Ernst again for his run selection, to Ralf, Mario and Huiazhang for useful coffee time discussions. I would like to thank to Bill

Morse for finding me a beautiful place to stay in Bellport, NY and my landlord Bloomfields for being like a family to me.

Finally I thank to Yannis for all of his supports and helps from the day I met him. I have learned the g-2 data analysis from him.

References

[1] Study of the AGS Flashlet Background for 2000 run, V. Druzhinin and G. Fedotovich, BNL Note 375.

[2] The run selection of the 2000 data, Ernst Sichtermann.

[3] The log book summaries, John Paley,

[4] Muon Losses study performed by Chris Polly and John Paley.

[5] Muon Revolution Frequency Distribution from a Partial-Time Fourier Transform of the g-2 Signal in the Muon g-2 Experiment, Yuri Orlov, Cenap S. Ozben, Yannis K. Semertzidis, NIM A 482 (2002) 767-775.

[6] Fast Rotation Analysis, modified CERN method, Alfanso Lam and Rob Carey.

[7] Ph.D. Thesis, Long Duong.

[8] Eliminating Pileup from the g-2 Data, Cenap S. Ozben and Yannis K. Semertzidis, BNL Note 365.

[9] Pileup and Energy Threshold, C.S. Ozben, Y.K. Semertzidis, BNL Note 397.

[10] Correction of CBO phase change due to quad voltage droop, Ralf Prigl and Mario Deile.

[11] The Spectrum of Chi and Systematic Errors Due to Backgrounds in the 2000 Run Data, Y.K. Semertzidis, BNL Note 406.

[12] Expected Fourier Transform Frequencies in the g-2 Spectrum Along with Estimates of Their Lifetimes, Jim Miller.

[13] The low pulse height pile-down effect, Bill Morse, BNL Note 373.

[14] Private communication, Francis Farley.

[15] On the Question of the Functional Form of the 2000 Run Data, Y.K. Semertzidis, BNL Note 403.

Contents